



AALBORG UNIVERSITY
DENMARK

MASTER'S THESIS

M. SC. IN STRUCTURAL AND CIVIL ENGINEERING

**Monotonic Tensile Loading of Suction Bucket Foundation
Model in a Pressure Tank**

Written by
Carolina Andrea Vial Tardio
Elena-Ioana Moldovan

Supervised by
Lars Bo Ibsen
Amin Barari

10th of June 2021



AALBORG UNIVERSITY
STUDENT REPORT

School of Engineering and Science
Department of Civil Engineering

Thomas Manns Vej 23

9220 Aalborg Ø

www.civil.aau.dk

Document type:

Master's thesis

Title:

Monotonic Tensile Loading of Suction
Bucket Foundation Model in a Pres-
sure Tank

Project period:

February 2021 - June 2021

Author:

Carolina Andrea Vial Tardio

Elena-Ioana Moldovan

Supervisor:

Lars Bo Ibsen

Amin Barari

Main report, no. of pages: 58

Appendices, no. of pages: 118

Amin Barari

Lars Bo Ibsen

Elena-Ioana Moldovan

Carolina Andrea Vial Tardio

Preface

This thesis has been prepared for the final project of the M.Sc. Structural and Civil Engineering program in Aalborg University. The report is written during the period of February- June 2021.

We would like to express our gratitude to our professors and supervisors Lars Ibsen Bo, Amin Barari for their advice and guidance throughout the entire project period. We are deeply grateful for the help and guidance PhD student Sorin Grecu has provided throughout the entire project period. His advice has been greatly appreciated. We would also like to acknowledge the help provided by Kim Borup and Tomas Sabaliauskas throughout the testing period in the laboratory. Last, but not at least, we are grateful for the help and support from our friends and families.

Carolina Andrea Vial Tardio
Elena-Ioana Moldovan

10th of June 2021

Abstract

Climate change urges the increased use of renewable energies, and Denmark is known for its potential to harvest wind power. In order to produce more wind, the offshore wind industry is increasing and expanding further in deeper waters. This requires bigger foundations that are more expensive in installation, maintenance and dissembling.

The suction bucket in jacket structures has the potential to be implemented in deeper waters and reduce economical costs.

The loading conditions of the suction bucket in jacket structures requires a 'push-pull' mechanism in which compressive and tensile forces are the dominating forces acting on the foundation system. However, there is not enough knowledge regarding the tensile behaviour of suction buckets. Model testing of foundations in laboratory is an useful tool in generating results and understanding the behaviour of suction bucket foundations when subjected to tensile loading.

The project at hand is focused on understaing the behaviour of suction bucket models subjected to tensile loading. Furthermore, a laboratory equipped with a pressure tank is used for this testing campaign. The density of the soil, pull-out speed and drainage path are the variable used in this tests.

Contents

Preface	iii
Abstract	v
1 Introduction	1
1.1 Background	1
1.1.1 Loading conditions	2
1.1.2 Tensile behaviour	3
1.2 Problem formulation	5
1.3 Purpose of the thesis	5
2 Literature review	7
2.1 Suction buckets in offshore structures	7
2.1.1 Drained capacity/behavior	7
2.1.2 Undrained capacity/behavior	8
2.2 Suction buckets physical model tests in laboratory	9
2.2.1 Stiffness	11
2.2.2 Pore pressures	11
2.2.3 Scaling effects	12

3	Model Testing	15
3.1	Test Setup	16
3.1.1	Soil preparation	18
3.2	Test procedure	20
3.3	Data processing	21
3.3.1	Pressurisation	21
3.3.2	Force processing	22
3.3.3	Excess pore pressure	22
3.3.4	Data normalization	22
3.4	Scaling considerations	23
4	Data Analysis	25
4.1	Pull-out rate of tests with the same density classification	25
4.2	Pull-out rate of tests with same velocity	31
4.2.1	Influence of cyclic load	43
4.3	Pull-out rate by drainage path	45
4.4	Comparison with previous work	47
5	Discussion	53
6	Conclusion and future work	55
	Bibliography	58

A	Test Setup and Procedure	1
A.1	Test Facilities	1
A.1.1	Bucket foundation models	1
A.1.2	Pressure Tank	2
A.1.3	MTS FlexTest Controller	3
A.1.4	Load Cell	4
A.1.5	PP Sensors' Calibration Station	5
A.1.6	Soil vibrators	5
A.1.7	Mini-CPT Equipment	6
A.1.8	Bridge Crane	7
A.2	Test Procedure	7
A.2.1	Soil Preparation	7
A.2.2	Cone Penetration Test	9
A.2.3	Preparing Bucket Foundation Model	15
A.2.4	Installing Foundation Model	17
A.2.5	Attaching hose	19
A.2.6	Sealing the tank	19
A.2.7	Last Adjustments	20
A.2.8	Running the test	20
A.2.9	Clean up	25
B	Cone Penetration Testing	27
B.1	CPTs in High Density Sand	28
B.2	CPTs in Medium Density Sand	32
B.3	CPTs in Low Density Sand	34

B.4	Comparison Densities	36
B.4.1	Tests 150 <i>mm/s</i>	38
C	Test Results	41
C.1	Results in High Density Sand	41
C.1.1	Test D0.05	41
C.1.2	Test D5	46
C.1.3	Test D10	49
C.1.4	Test D20	52
C.1.5	Test D50	55
C.1.6	Test D80	59
C.1.7	Test D100	62
C.1.8	Test D150 with cyclic loading	65
C.1.9	Test D150 without cyclic loading	68
C.1.10	Test D150 Bucket B with cyclic loading	71
C.1.11	Test D150 Bucket B without cyclic loading	73
C.1.12	Test D200	75
C.1.13	Test D300	77
C.1.14	Test D400	80
C.1.15	Test D500	83
C.2	Results in Medium Density Sand	86
C.2.1	Test M0.05	86
C.2.2	Test M10	89
C.2.3	Test M50	91
C.2.4	Test M150-1	94

C.2.5 Test M150-2	97
C.2.6 Test M500	99
C.3 Results in Low Density Sand	103
C.3.1 Test L0.05	103
C.3.2 Test L10	106
C.3.3 Test L50	109
C.3.4 Test L150	112
C.3.5 Test L500	115

Introduction

1.1 Background

Currently, the use of renewable energy is urged by the speeding of climate change worldwide, which has been a consequence of the abundant use of fossil fuels. Renewable energy resources depend on the specific environmental features of a geographic location, and Denmark has been a great site for the generation of wind energy both onshore and offshore.

Although the onshore wind farms are a good resource of wind energy, they face some limitations regarding the landscape, communities, and energy production all year round. The offshore sector represents great advantages for the wind turbine industry development. It can overcome the onshore limitations by permitting more powerful wind turbines, larger wind farms and more open areas without obstructions for wind.

However, due to the offshore development and the increasing demand for offshore wind turbines (OWT), the size of the wind turbines and the water depth installation has been increasing over the years. This growth is accompanied by great challenges such as: more complex design, higher construction prices, more difficult maintenance and dismantling costs. The importance of cost efficient foundations is underlined by Cavazzi & Dutton (2016), where it is described that the cost of the capital expenditure set for foundations is 16 % of its lifetime costs.

To overcome these barriers, different foundation technologies are explored, as seen in Figure 1.1, where is possible to compare the different solutions.

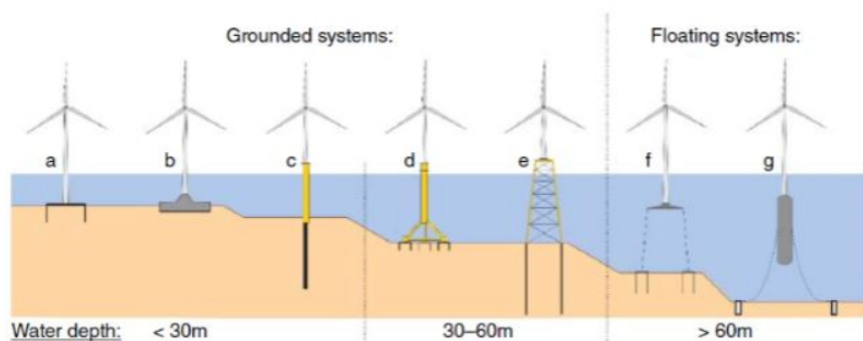


Figure 1.1: a) Suction bucket; b) gravity-based; c) monopile; d) tripod on suction bucket; e) jacket structure; f) tension leg platform; and g) spar buoy floating concept according to Bhattacharya (2019).

While monopile foundation has been used extensively as an OWT foundation due to its practicability, other options need to be explored for the circumstances where a monopile is not a suitable solution. The suction bucket foundation represents a great solution in terms of resistance and cost-efficient design. This type of foundation has two main design approaches: monobucket and jacket structure (Figure 1.2), which can be with three or four buckets.

This project investigates the behaviour of bucket foundations in a jacket structure, which during loading experience a 'push-pull' mechanism in which compressive and tensile capacities are dominating the failure. Earlier experiments have shown that their tensile capacity increases temporarily during a typical storm, thus showing an ability to resist being pulled-out. This can be a positive characteristic in terms of economy, as it could mean the possibility of reducing material in their fabrication. However, there is more need of investigating the behaviour of this foundation in order to improve its design.



Figure 1.2: Suction bucket for jacket structures- (SPTOffshore, 2021)

1.1.1 Loading conditions

Vaitkunaite (2016) explained that offshore structures are subjected to structural, operational and environmental loads. The loads acting on a wind turbine throughout its lifetime are categorized by Damgaard et al. (2014) as following:

- Steady quasi-static loads: from the self-weight of the rotor, nacelle, tower and mean wind;
- Stochastic loads: from the wind turbulence and the irregular sea states;
- Transient loads: from the start, stop and emergency breakdown procedures;
- Cyclic loads: from the rotor frequency 1P generated by mass imbalance in the blades and the 3P frequency due to shadowing effects from the wind each time a blade passes the tower.

Vaitkunaite (2016) described the loading difference between oil platform and offshore wind turbine foundations. Even though the oil platforms are subjected to high horizontal loading, the large self weight of their upper structure results in significant vertical compressive loads on the

1.1 Background

foundation. On the other hand, the lighter weight of the OWT, causes the OWTs to be dominated by an overturning moment.

In jacket foundations the overturning moment of the structure is resisted principally by a 'push-pull' mechanism as explained by Houlsby et al. (2005). Therefore the vertical forces are the ones dominating these multi footed foundations. The compressive and tensile forces are shown in the Figure 1.3.

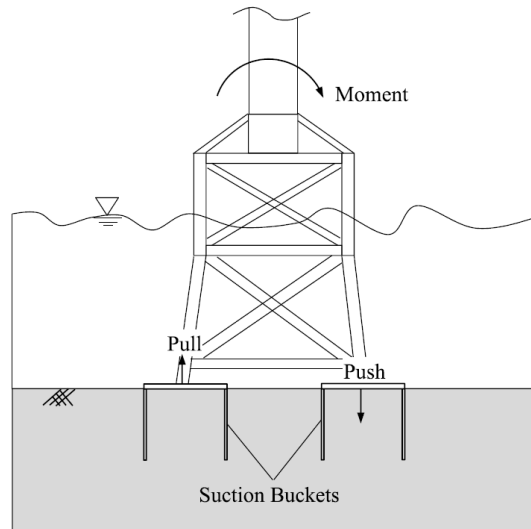


Figure 1.3: Multipod jacket structure OWT (Sun et al., 2020).

The compressive loading response can be understood with the well known behaviour of gravity based foundations. However, there is still not enough knowledge about the tensile response, although this loading is a very important aspect in the design of jacket OWT.

1.1.2 Tensile behaviour

Studies have shown that the suction bucket tensile bearing behaviour is closely influenced by the drainage conditions, as seen in Figure 1.4.

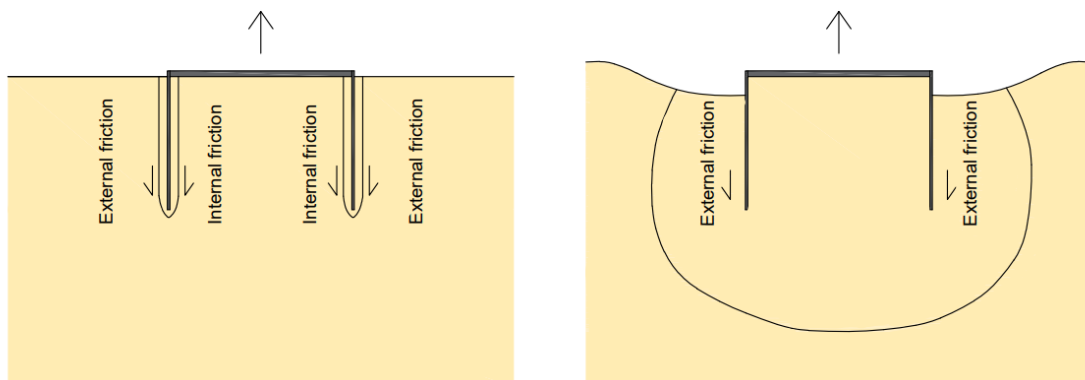


Figure 1.4: Behaviour of suction buckets during pull-out in cohesionless soil (Senders, 2009).

Left figure: drained response, right figure: undrained response.

When the suction bucket is pulled up, a gap in between the soil and the lid is formed, and a drop in pressure under the lid is created. This generates a water flow from the surroundings of the suction bucket towards the gap. This is the pore water seepage flow (Figure 1.5), and its path depends on the bucket's geometry.

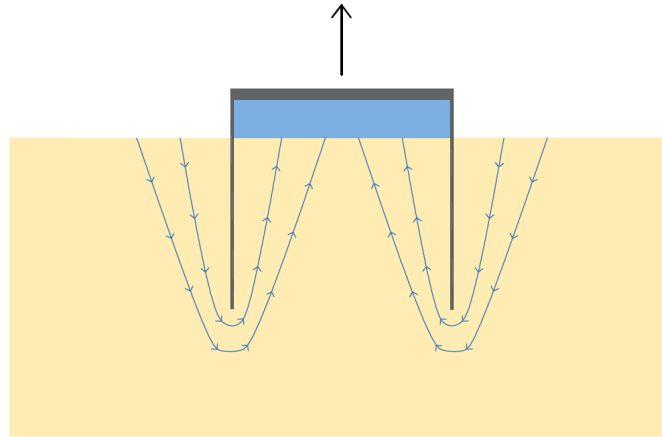


Figure 1.5: Seepage flow during tensile loading in drained response.

At slow loading rates the seepage flow fills the gap slowly and continuously, thus the change of the pore pressure in the soil is negligible, which means that the effective soil stresses are not affected by the seepage flow. This is termed as 'drained' response, and in this case only the internal and external friction are contributing to the tensile capacity. The height of the internal gap in this case is almost the same as the displacement of the suction bucket.

On the other hand, when the load is really high a difference in pressure between the outside and inside of the bucket takes place. This development of differential pressure (suction) restrains the formation of the water filled gap and a soil plug which moves together with the bucket is created. Gütz (2020) explained that this mobilizes the external shear resistance, and the tensile resistance is amplified by suction. This is called 'undrained' response, or as described by Senders (2009) 'reverse end bearing' behaviour. In this case, the plug heave and upward displacement of the bucket have similar height.

Usually, in real life loading conditions, the behaviour of skirted foundations is most likely to be an intermediate response between drained and undrained. This is known as 'partially drained' behaviour. In this case the upward movement of the water gradient prohibits a fully undrained behaviour from taking place. However high loading rates create a certain differential pressure which restrains the behaviour to be treated as drained. Moreover, it is important to understand both the drained and undrained responses of the suction bucket since they represent the lower and upper bound of tensile resistance.

The peak tensile force for each soil drainage condition is going to be different. Figure 1.6 shows that undrained behaviour is most likely to have the highest peak resistance compared with the other two, followed by partially drained response and finally the drained one.

1.2 Problem formulation

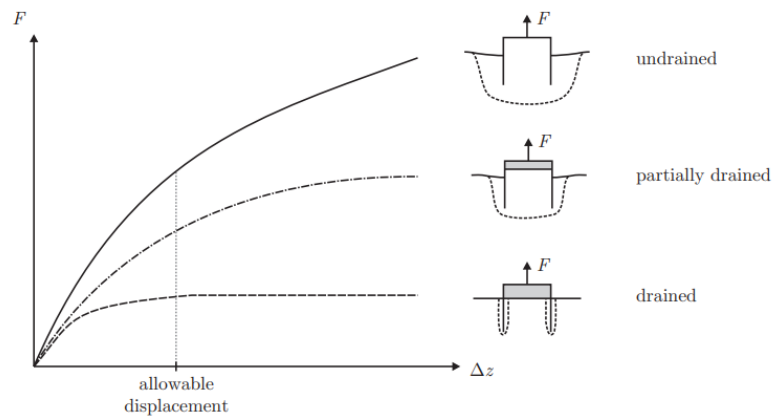


Figure 1.6: Soil failure mechanisms under different drainage conditions during uplift (Gütz, 2020)

According to Kelly et al. (2006b) the transient tensile capacity of suction buckets is controlled by a "complex interaction" between:

- Permeability of the soil;
- Rate of loading;
- Length of the drainage path.

Based on these three parameters, the tensile resistances under the different drainage conditions are analyzed in this project.

1.2 Problem formulation

Based on the loading conditions and response mechanism of the suction buckets in jacket structures, the main forces acting on the foundation are tensile and compressive.

While the compressive behaviour of suction buckets is well understood as a gravity base foundation, the design codes and resources regarding the behaviour of suction buckets under tensile loading are sparse. Therefore, based on the current understanding of this loading type, a question regarding the behaviour of the suction bucket foundations arises:

How do uplift speed, density of soil and drainage path affect the tensile response of suction bucket foundations in a laboratory model testing?

1.3 Purpose of the thesis

The main focus of this project is the understanding of the behaviour of suction bucket under monotonic tensile loading in sand through the conduction of small scale laboratory testing.

To approach this, model testing in the pressure tank is performed with various displacement

rates in different soil densities. Furthermore, two buckets of different skirt lengths are tested with the same pull-out speed in dense soil.

The different displacement rates influence the drainage response. Depending the rate, the water trapped in the pores of the soil is able to dissipate or not, creating a either drained, semi undrained or undrained condition. The skirt length of the bucket is proportional to the drainage path, which also influences the drainage response of the soil.

The density of the soil is one of the variable parameters in this project. Through this it is possible to test in different soil permeabilities, varying the hydraulic conductivity and seepage flow. The two latter ones having a direct influence in the dissipation rate of the pore pressure.

In order to capture this, the data from tests is processed and analysed creating 'Load-Displacement' curves. In addition, the pore pressure development is monitored along the skirt of the bucket in four different levels inside and outside. The responses are recorded and displayed in 'pressure-time' and 'pressure-displacement' graphs.

Furthermore, the importance of applying pressure to the water is to assure that no air bubbles are trapped in the soil, thus simulating a correct pore pressure development. For this purpose, a pressure tank which allows the simulation of 20 m water depth is used.

This testing campaign also considers the application of small compressive pre-cyclic loading. This cyclic load simulates the normal weather conditions that heal the offshore soil which is sheared during installation, before a greater event takes place.

Literature review

2.1 Suction buckets in offshore structures

The present knowledge of suction bucket foundation design comes mainly from the offshore oil and gas sector. Vaitkunaite (2016) explained that the wind and wave structures are significantly lighter, operate in shallower waters, and are subjected to severe cyclic loading and dynamic excitation compared to oil and gas industry. These characteristics result in a different structural behaviours, and as Ibsen et al. (2005) underlined, the horizontal loads and overturning moments are large in proportion the vertical load, unlike in the offshore oil and gas industry, where the vertical load is predominant.

Byrne & Houlsby (2003) explained that foundations with perimeter 'skirts' embed into the sea floor mitigate the effect of scour compared to pile foundations, and these skirted foundations can be either used for a typical jacket structure, or a monopod. Kelly et al. (2006a) underlined that in case of monopod structure, the bucket resists the overturning moment directly, while in the case of multiple foundations cases the overturning moment is resisted through opposing vertical reactions. In case of compressive loading Vaitkunaite (2016) explained that the bucket foundation behaves as a gravity based foundation, and the methodology for bearing capacity and settlement is applicable.

Houlsby et al. (2005b) found that the maximum tensile capacity of caisson foundation in sand depends on the rate of pull-out (in relation to permeability) and the ambient water pressure (which determines whether cavitation occurs).

Thieken et al. (2014) stated that the resistance behaviour of the suction bucket depends on a combination of: geometry of the bucket, pull-out rate and soil permeability.

This section is focused on literature review of the behaviour of axially loaded suction buckets in dense and loose sand.

2.1.1 Drained capacity/behavior

Thieken et al. (2014) explained that during the pull-out phase, a gap occurs between the soil and the bucket lid, and the tensile resistance in perfectly drained conditions depends on the self weight of the bucket and the inner and outer skin friction, as seen in Figure 2.1.

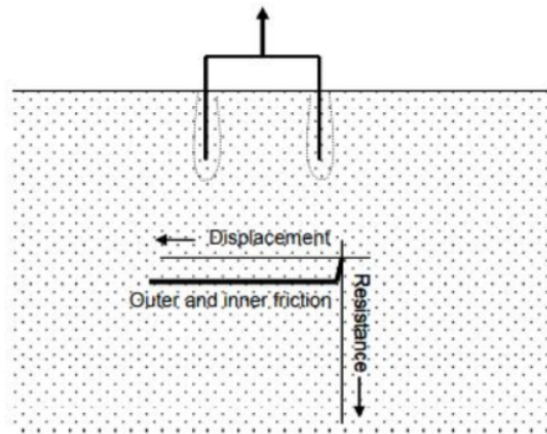


Figure 2.1: Pure frictional resistance (drained) according to Senders (2009)

Houlsby et al. (2005b) mentioned that during slow application of tensile loading, the pore pressures are small, and the tensile capacity can be obtained using a fully drained calculation where the resistance of the caisson is the sum of the inner and outer friction of the bucket skirt.

2.1.2 Undrained capacity/behavior

During perfect undrained condition, Thielen et al. (2014) explained that the suction pressure prevents the formation of gap between the soil and the lid of the bucket. Because of this, a soil plug heave is formed inside the bucket, and due to the occurrence of suction, the soil around the bucket is also affected, and the shear strength of the soil is generated in the surrounding soil. Senders (2009) named this behaviour 'reverse end bearing', seen in Figure 2.2.

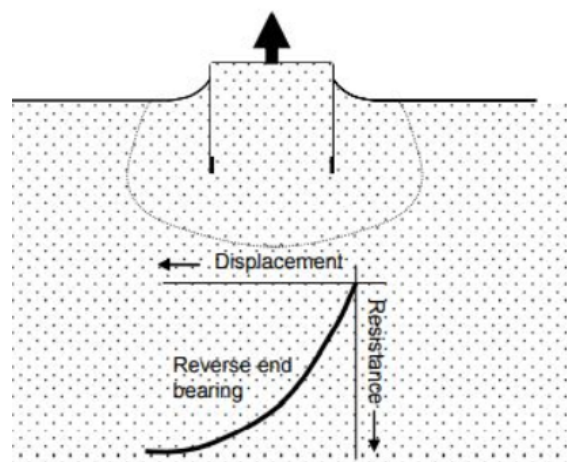


Figure 2.2: Pure reverse end bearing (undrained) according to Senders (2009)

In 'undrained failure', in dilative sand, the negative pore pressure developments "are potentially so large that invariable (except in very deep water) the cavitation mechanism would intervene first" (Houlsby et al., 2005b). To verify this statement, Senders (2009) explained that in a sand profile

2.2 Suction buckets physical model tests in laboratory

with q_c of around 5 MPa and a k value of 0.6, a differential pressure needs to be around 3000 kPa, which can only happen in water depths exceeding 290 m (cavitation criteria). Since this depth is much bigger than the typical installation depth for offshore suction caisson, it can be confirmed that the cavitation is the upper limit of undrained uplift resistance. This means that the prediction of the load displacement curve for reverse end bearing should focus more on the initial behaviour of the load-displacement curve where the cavitation pressure can be reached, rather than on the maximum load.

However, Vaitkunaite (2016) mentioned that during a storm the loads on the foundation would create partial drainage, and the tensile response would be between drained and undrained response, which Senders (2009) named it 'intermediate' response and it can be seen in Figure 2.3.

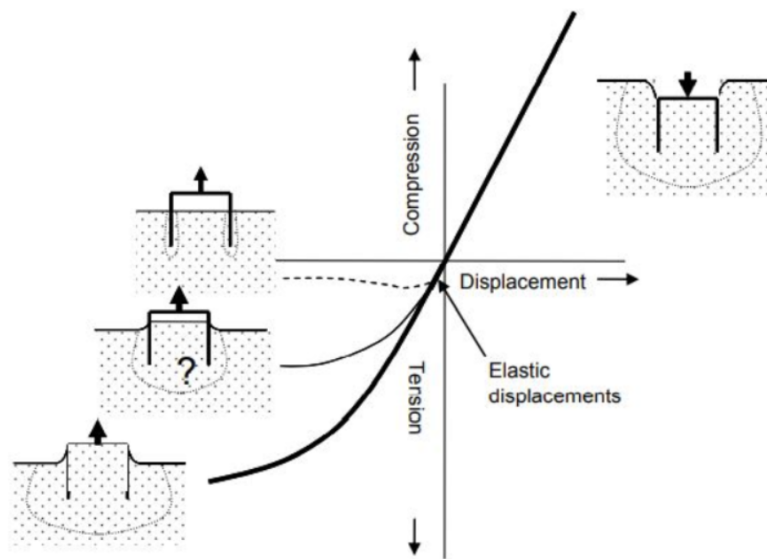


Figure 2.3: Pure reverse end bearing (undrained) according to Senders (2009)

2.2 Suction buckets physical model tests in laboratory

The main focus of this thesis is the physical modelling regarding the axial tensile capacity of the suction bucket in sand. As a basis of the experimental work, it is important to note previous experiments and results regarding this inquiry. Gütz (2020) noted that the physical modelling of the suction bucket can be obtained through prototype, field, laboratory or centrifuge scale. Laboratory tests are an important tool in this research due their reduce cost compared to centrifuge testing or prototype testing. They can provide "high quality measurements of many quantities in numerous tests", and "additional features such as a pressure chamber [...] allow for the simulation of higher water depth" (Gütz, 2020). Various conditions regarding soil preparation, loading magnitudes, geometry of bucket and scaling methods are reviewed in order to produce accurate model parameters for the current testing campaign.

This section directs the attention on suction bucket model tests in sand in laboratory and centrifuge testing. Various conditions regarding soil preparation, loading magnitudes, geometry of bucket and scaling methods are reviewed in order to produce accurate model parameters for the current testing campaign.

Houlsby et al. (2005b) tested a model caisson of 0.28 m diameter and 0.18 m skirt length, in a pressure tank. The tests were performed at atmospheric pressure and atmospheric pressure plus 200 kPa with different pull-out speeds and sands with different permeability. It was noticed that in Redhil sand, cavitation occurs at atmospheric pressure when 100 mm/s are applied, but when the ambient pressure is atmospheric plus 200 kPa, 100 mm/s pull-out is not sufficient to reach cavitation. However, in HP5 sand, which has an estimated permeability of $k = 0.5E - 4$, cavitation is reached at 25 mm/s pull-out speed at atmospheric pressure plus 200 kPa.

Senders (2009) performed centrifuge testing at 100g in silica sand to verify the effect of uplift speed upon the uplift resistance. The tests were performed with either open or closed valve, or with different uplift rates in order to achieve different drainage conditions. According to the performed tests, it was concluded that the total resistance increases with increasing pull-out speed. The friction resistance was calculated by subtracting the differential pressure resistance (measured differential pressure multiplied by caisson area) from the total resistance. During the drained uplift the frictional resistance was at the highest, while the differential pressure was not developed. Furthermore, differential pressure becomes larger with the pull-out speed. The cavitation pressure development was lower than expected (107 kPa instead of 160 kPa), but was consistent throughout testing.

Vaitkune et al. (2016) examined the drainage conditions from drained to undrained by finding the lowest and highest tensile capacity and the change of tensile behaviour between these limits, specifically the change in pore pressures, development of peak resistance and displacements. The soil sample used in this testing campaign in the pressure tank consisted in a 0.6 m of Aalborg University sand No. 1 with a hydraulic conductivity k of $7.4E-5$ m/s and effective soil unit weight γ' of 9.6 kN/m³ at relative density D_R of 85%. The minimum void ratio e_{min} and maximum void ratio e_{max} were 0.549 and 0.858 respectively, the specific grain density d_s 2.64 g/cm³ and the uniformity coefficient U 1.78. The findings of Vaitkune et al. (2016), which were in accordance to Kelly et al. (2006a) suggest a rapid pull out produces a fully undrained behaviour. The peak tensile resistance increased with the pull out rate, but so did the upward displacement. This could face problems regarding the serviceability limit state during the design process. Since the tensile capacity is much higher at higher rates, even if the displacement is set to be only 0.05 D , the pore pressure response should be considered when designing the foundation subjected to tensile loading. Vaitkune et al. (2016) mentions that the pore suction induced by the tensile loading is limited by cavitation, which happens at approximately -100 kPa atmospheric pressure. When testing in the pressure tank at an ambient of atmospheric pressure plus 200 kPa, cavitation should be reached at around $s=-300$ kPa, but the fluctuations could be from imperfections in the saturation of the pipes, air bubbles in the sand and measurement inaccuracies of the pressure transducers Vaitkune et al., 2016.

Gütz (2020) tested various suction bucket geometries in a pressure tank under tensile loading with constant displacement rates. The soil used was silica sand with minimum and maximum void ratios of $e_{min} = 0.553$ and $e_{max} = 0.873$ respectively, an internal friction angle of $\varphi' = 45^\circ$ and dilation angle of $\psi = 20^\circ$. In order to test the scale effects of different bucket geometries, the same displacement rate was tested on different models (low displacement rates which produced drained behaviour). However, the main focus is on a bucket with skirt length, L of 0.5 m and diameter, D of 0.51 m. It is noticed, as seen in Figure 2.4 that higher displacement rates induce higher tensile resistance. The reduction in tensile force is due to continuous extraction of the suction buckets, which is created because of two reasons: frictional resistance diminished with reduction in the skirt length and shortened drainage path by the reduction of the embedment depth. Even though the

2.2 Suction buckets physical model tests in laboratory

higher displacement rates produce higher tensile resistance, they also invoke a higher displacement for the resistance. However, when the normalised displacement $\Delta z/D$ is compared with potential SLS criteria, it is noticed that as long as the displacement criteria is met, the tensile resistance exceeding drained resistance are attainable under partially drained to undrained conditions.

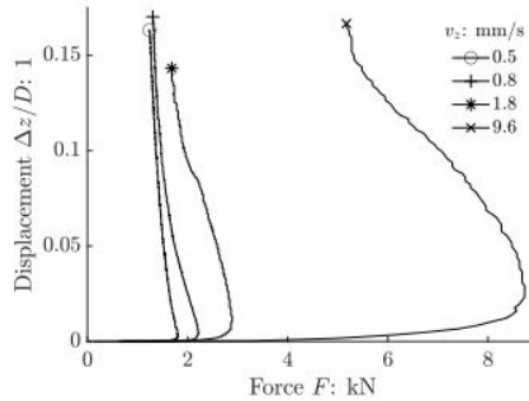


Figure 2.4: Effect of displacement rate on total force according to Gütz (2020)

2.2.1 Stiffness

Vaitkune et al. (2016) explains that the stiffness defines how the tensile load developed in regards to displacement and it was found that there is no clear dependency on displacement rate for initial loading stiffness, and the peak load was reached at higher upward displacements for the higher pull-out rates.

Achmus et al. (2013) found that the initial stiffness of the bucket system is strongly dependent on bucket geometry, relative density of the sand and load eccentricity.

2.2.2 Pore pressures

Vaitkune et al. (2016) found the suction pressure with Equation 2.1, where p_t is the suction applied in the tank, p_{abs} is the measured pressure and p_{atm} is the atmospheric pressure. It further showed that the inner pore pressures are lower than the outer pore pressures, and cavitation was reached at approximately -288 kPa at a pull-out speed of 152 mm/s . Theoretically, cavitation is reached at a suction, s around -300 kPa , but the fluctuations could appear from imperfections in the saturation of the pipes, air bubbles in the sand and measurement inaccuracies of the pressure transducers (Vaitkune et al., 2016).

$$s = p_{abs} - p_{atm} - p_t \quad (2.1)$$

In Vaitkune et al. (2016) the inner transducers showed almost identical measurements at the pull-out rate of 152 mm/s , meaning there was no inner water flow present, which emphasises an undrained behaviour.

2.2.3 Scaling effects

Kelly et al. (2006a) explained that it is "vital" to compare the load-displacement response of caissons at different scales if the model testing is used for predicting the field behaviour. In this study, non-dimensional data from laboratory tests of vertically loaded and moment loaded suction buckets is compared with non-dimensional data from the field tests. It was found that the vertically loaded buckets showed bigger differences between field and laboratory results than the buckets loaded by moment. When comparing field and laboratory tests, in dimensionless terms, the strength and stiffness should be similar in equivalent tests. When considering strength in drained sands, the load is scaled by γR^3 , which is valid when the relative density in the laboratory is lower than the relative density in the field tests, in order to account for the reduction of friction angle with the stress level. This will assure that the bearing capacity factors are similar for both cases. However, this density aspect can be omitted if "the vertical loads [are] only a small fraction of the compressive bearing capacity".

The stiffness resistance depends on the shear modulus G , which in sand is related to the mean confining stress. In order to account for the small stresses in the laboratory environment compared to the field testing, Kelly et al. (2006a) expressed the shear modulus as in Equation 2.2, where A is a dimensionless constant, n is the pressure exponent and σ'_v is a representative effective vertical stress.

$$\frac{G}{p_{atm}} = A \left(\frac{\sigma'_v}{p_{atm}} \right)^n \quad (2.2)$$

In order to avoid the effects of the bucket on the stress magnitude and strain amplitude, a representative stress at a certain depth below the caisson is used to rewrite the shear modulus. This leads further to a non-dimensional expression for cyclic vertical loading in sand (Equation 2.3), where F , is the applied vertical load γ' is the unit weight, z is vertical displacement, f_2 is a dimensionless function, F_m is mean vertical load during testing, and L and D are the skirt length and bucket diameter, respectively.

$$\frac{F}{\gamma' D^3} = \frac{z}{D} \left(\frac{p_{atm}}{D \gamma'} \right)^{1-n} f_2 \left(\frac{F_m}{\gamma' D^3}, \frac{L}{D} \right) \quad (2.3)$$

Depending on the installation method (suction or pushing) the laboratory non dimensional data is plotted and compared to the field non dimensional data, and certain qualitative tendencies can be observed based on data (Figure 2.5). However, there is a need for more test data in order to quantify the accumulated deformations as a function of size, loading amplitude and installation method. Gütz (2020) mentioned that this methods disregards the lack of actual drainage condition and makes it potentially unsuitable for design purposes.

2.2 Suction buckets physical model tests in laboratory

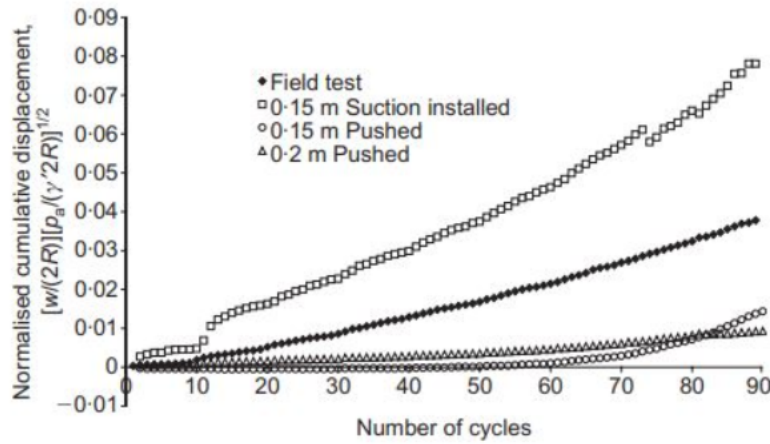


Figure 2.5: Cumulative displacements during vertical loading as a function of cycle number (Kelly et al., 2006a)

Foglia et al. (2013) used non-dimensional groups to express pore pressure quantities Δp developed underneath and around a bucket foundation under lateral loading. In order to capture the interaction between soil, foundation and environmental loading, Δp [Fl^{-2}] is illustrated as a function of the displacement rate, v [IT^{-1}], the soil permeability, k [IT^{-1}], the drainage length, l [I], and the unit weight of the pore fluid, γ_w [Fl^{-3}], as seen in Equation 2.4.

$$\Delta p = f(v, k, l, \gamma_w) \quad (2.4)$$

Since the drainage is assumed to be proportional to the skirt length and diameter, a non-dimensional pore pressure development is expressed as in Equation 2.5, where g is an unknown function, found from the small scale laboratory experiments.

$$\frac{\Delta p}{\gamma_w D} = g \frac{vL}{kD} \quad (2.5)$$

Using this method, the non-dimensional pore pressure behaviour should resemble the behaviour of the prototype if all the terms are expressed correctly.

Vaitkune et al. (2016) explained that the layering, stiffness, strength parameters and hydraulic conductivity as well as loading conditions in offshore sand are more complex than the sand tested in the lab, which can impact the results of the tests. This underlines the importance of scaling and its effects on the data obtained in the laboratory. It was furthermore mentioned that the pore pressure change and distribution during tensile loading are of great interest in this specific testing. Vaitkune et al. (2016) used the non-dimensional scaling proposed by Foglia et al. (2013). This technique can be verified by comparing the non-dimensional patterns of the experiments with different parameters of soil and geometry, as well as FEM analysis.

Gütz (2020) underlined the importance of scaling the most essential physical dimensions in model testing. In the case of tensile loaded suction buckets these are: geometric dimensions,

hydraulic properties and stress state of the soil. However, it was further explained that currently, there is not enough documentation on how to scale properly the model tests to give accurate results for prototypes. In the physical modelling for the performed experiments, Gütz (2020) chose not to scale the results for a desired prototype, but instead to use the measurements and findings of the laboratory testing to develop a sophisticated finite element model (FEM). In order to compare the results and evaluate the effect of the scale qualitatively, the models tested in the lab were exposed to similar loading conditions to each other.

Due to the low stresses in dense cohesionless soil which can affect the shear strength and stiffness of the soil because of the potential for dilation, Gütz (2020) explained that the results cannot be extrapolated directly to an FE model, but can be used for quantification of basic research and validation of FE models (on the condition that the mechanical behaviour of the soil is accounted for accurately).

The reduced scale of the laboratory model leads to a shorter length of the drainage path, which implies more drainage with the same load rate in identical soil. Because of this, the soil's hydraulic conductivity may be decreased or the load rate may be increased for less drainage. To reduce the permeability, finer soils, or more viscous pore fluids can be used. Finer soil implies changing mechanical properties of the soil, which can cause issues when preparing the soil, while a more viscous pore fluid can affect the soil's strength and its applicability depends on the size of the testing facility. For the specific testing, sand with fine particles and higher load rates are used. Since neither displacement rate, nor the load frequency are exactly scaleable, load frequencies of 6 or 12 times higher than expected offshore frequencies of wave loading (about 0.08 Hz) and various displacement rates are used.

Observing the results from the various model tests of suction bucket foundations, a testing campaign where compressive pre-cyclic load is applied prior to the monotonic tensile loading is further investigated. The goal of the testing process is to continue previous investigations of tensile loading capacity of suction bucket foundations and research for other parameters that can have an influence on their behaviour.

Model Testing

A total of 26 tests are performed for this testing campaign. The constant displacement rate, soil density D_r and drainage path are variables to this testing. The first 15 tests are performed in dense soil which is the most encountered soil in offshore Denmark. The purpose of these first tests is to find undrained behaviour by increasing the pull-out rate which affects the drainage behaviour, until similar response of force and excess pore pressure is observed.

After choosing 5 different pull-out rates, the testing is later performed in medium and later loose density. A complete overview of the test configuration of this campaign are found in Table 3.1. It is noted that there are two tests for medium density, M150-1 and M150-2. After performing M150-1, the test M150-2 is made with exact same conditions in order to confirm the correct response of the first one.

In order to understand and evaluate the results of the performed experiments a good understanding of the facilities and methodology of the testing is necessary.

Moreover, since the load cell and pore pressure sensors (PP sensors) measure the entire data during testing, the data needs to be processed in order to apply a filter and thus obtaining the relevant information to analyse the test results.

This chapter is focused on presenting the procedure, equipment and data processing of this testing campaign. A detailed description of the testing facilities and procedure can be found in Appendix A.

Test No.	Test rate [mm/s]	Density classification*	Bucket	Pre-cycling	Test ID
1	0.05	D	A	✓	D 005
2	5	D	A	✓	D 5
3	10	D	A	✓	D 10
4	20	D	A	✓	D 20
5	50	D	A	✓	D 50
6	80	D	A	✓	D 80
7	100	D	A	✓	D 100
8	150	D	A	✓	D 150
9	150	D	A		D 150 (NO PRECYCLING)
10	150	D	B	✓	D 150-B
11	150	D	B		D 150-B (NO PRECYCLING)
12	200	D	A	✓	D 200
13	300	D	A	✓	D 300
14	400	D	A	✓	D 400
15	500	D	A	✓	D 500
16	0.05	M	A	✓	M 005
17	10	M	A	✓	M10
18	50	M	A	✓	M 50
19	150	M	A	✓	M 150-1
20	150	M	A	✓	M 150-2
21	500	M	A	✓	M 500
22	0.05	L	A	✓	L005
23	10	L	A	✓	L 10
24	50	L	A	✓	L 50
25	150	L	A	✓	L 150
26	500	L	A	✓	L 500

Table 3.1: Testing campaign and test ID configuration. Each test ID code starts with density class followed by displacement rate and other details when needed.

* D= dense, M= medium, L= loose.

A more in depth description of the test facilities and procedure can be found in Appendix A.

3.1 Test Setup

Testing takes place in the geotechnical laboratory at Aalborg University using Aalborg sand No.1.

The majority of the tests are performed with a steel suction bucket with skirt length, L of 0.5 m and a diameter, D of 0.5 m (Bucket A). Sensors which measure the pore pressure in the soil are attached to the bucket at different heights in the interior and exterior as seen in Figure 3.1. The bucket is also equipped with two valves on the lid, which are held open during installation process, and closed during the application of cyclic loading and pull-out.

Another suction bucket of skirt length, L of 0.25 m and a diameter, D of 0.5 m (Bucket B) is used for performing two tests used for comparison. For more details regarding Bucket B and

3.1 Test Setup

pictures of the two buckets, refer to Appendix A.1.1.

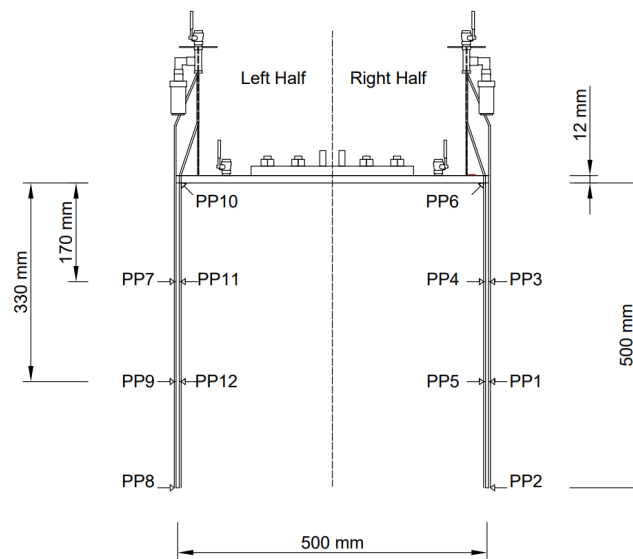


Figure 3.1: Suction bucket A with PP sensors location.

For simplifying the presentation of results, sensors PP1 through PP6 are referred to as the sensors on the right side of the bucket, while sensors PP7 through PP12 are sensors on the left side of bucket.

A steel pressure tank (Figure 3.2 capable of maintain up to 200 *kPa* (safety limit) is used for simulating the loading conditions in 20 meter sea water (*msw*). The dimensions of the tank are approximately 2.10 *m* interior diameter and 2.10 *m* height.

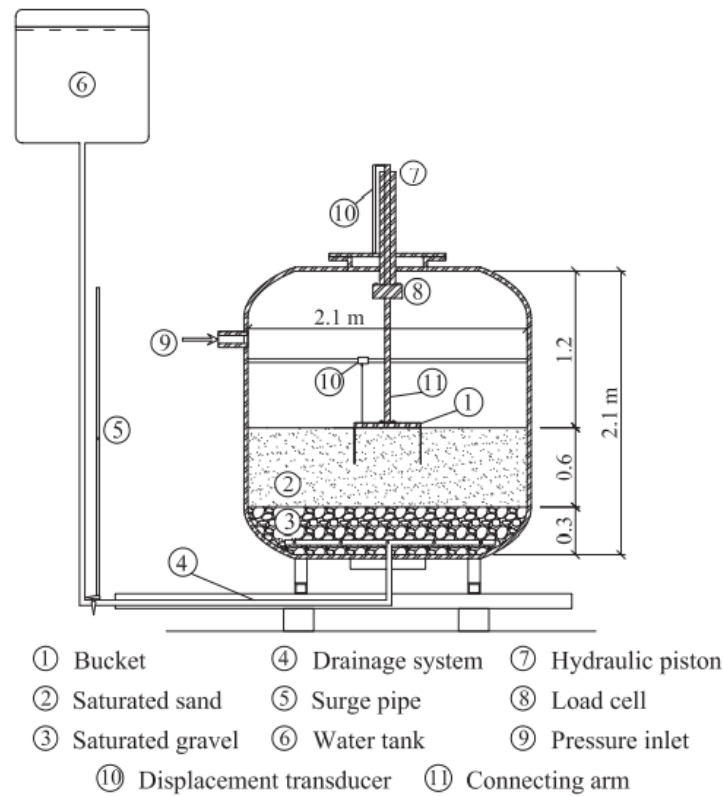


Figure 3.2: Pressure tank (Vaitkunaite, 2016).

The tank contains 0.60 m of Aalborg University Sand No.1 and 0.30 m of gravel at the bottom for ensuring a free water flow from and to the bottom. The sand is retained by a filter layer located in between the sand and the gravel. A valve connected at the bottom allows to both drain and saturate the sand. The saturation is done by applying a water gradient, which comes from a water tank placed approximately 7 m above the pressure tank. For pictures of the equipment see Appendix A.1.2. The control of force and displacement of the tested model is performed by the piston attached on the ceiling of the tank. In order to read and record the data, a load cell is attached to the piston and connected to data acquisition program. A detailed description of the tools and equipment, as well as data configuration is found in Appendix A.

Parameter	Notation	Value
Specific Gravity	G_s	2.640
Minimum Void Ratio	e_{min}	0.549
Maximum Void Ratio	e_{max}	0.858
50% Quantile [mm]	d_{50}	0.140
Uniformity Coefficient	U	1.780

Table 3.2: Characteristics of Aalborg University Sand No. 1 determined by Nielsen (2016).

3.1.1 Soil preparation

To achieve the different density classifications shown in Table 3.1, the soil is prepared through soil vibration with/without previous soil loosening. A more detailed explanation of this procedure is

3.1 Test Setup

explained in Appendix A.2.1.

In order to verify the density of the soil, cone penetration tests (CPTs) are performed before each test. Density is estimated from the measured cone resistance (q_c) using a correlation formula introduced by Ibsen et al. (2009). The formula and its application is explained in Appendix A.2.2.

To verify that the soil density, multiple CPT are carried out for each test, 4 or 8 depending if the test are taken only in one or both sides of the tank. The CPT positions are shown in Figure 3.3, where each side has 4 different radial positions at: 0.19 m, 0.35 m, 0.51 m and 0.81 m.

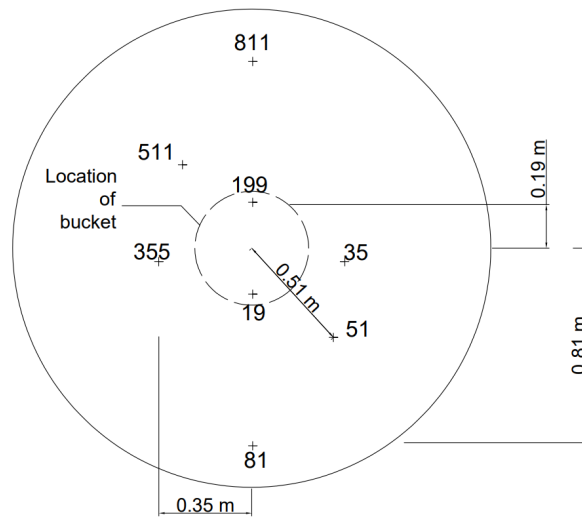


Figure 3.3: CPT locations

The soil density profiles are estimated and D_r value is calculated as the mean value of the whole set of densities for each test. The standard deviation SD is also calculated and used to define the D_r range for each test using Equations 3.1. Density values for each test can be found in Table 3.3.

$$\begin{aligned} \text{Min}(D_r) &= D_r - SD \\ \text{Max}(D_r) &= D_r + SD \end{aligned} \tag{3.1}$$

Where:

$\text{Min}(D_r)$	Minimum D_r value of density range
$\text{Max}(D_r)$	Maximum D_r value of density range

Test No.	Test ID	D_r [%]	SD [%]*	Min(D_r) [%]	Max(D_r) [%]	Range [%]
1	D 005	70.70	4.30	66.40	75.00	8.60
2	D 5	75.24	3.08	72.16	78.32	6.16
3	D 10	79.56	5.35	74.21	84.91	10.70
4	D 20	76.11	6.16	69.95	82.27	12.32
5	D 50	80.59	6.63	73.96	87.22	13.26
6	D 80	78.89	6.93	71.96	85.82	13.86
7	D 100	80.12	8.63	71.49	88.75	17.26
8	D 150	80.10	5.26	74.84	85.36	10.52
9	D 150 (NO PRECYCLING)	82.59	6.77	75.82	89.36	13.54
10	D 150-B	85.74	4.66	81.08	90.40	9.32
11	D 150-B (NO PRECYCLING)	83.48	7.26	76.22	90.74	14.52
12	D 200	77.63	6.80	70.83	84.43	13.60
13	D 300	80.18	5.43	74.75	85.61	10.86
14	D 400	80.25	4.32	75.93	84.57	8.64
15	D 500	75.83	5.57	70.26	81.40	11.14
16	M 005	60.23	7.09	53.14	67.32	14.18
17	M10	58.49	7.38	51.11	65.87	14.76
18	M 50	60.10	9.26	50.84	69.36	18.52
19	M 150-1	67.92	6.75	61.17	74.67	13.50
20	M 150-2	57.32	9.15	48.17	66.47	18.30
21	M 500	66.04	5.47	60.57	71.51	10.94
22	L 005	52.20	9.36	42.84	61.56	18.72
23	L 10	44.13	3.76	40.37	47.89	7.52
24	L 50	45.63	5.84	39.79	51.47	11.68
25	L 150	47.49	5.06	42.43	52.55	10.12
26	L 500	45.21	5.55	39.66	50.76	11.10

Table 3.3: Test densities for each test.

3.2 Test procedure

When soil is prepared and soil density D_r is confirmed with the CPT, the suction bucket model is installed in the tank through mechanical pushing.

Since the testing is carried out with two different buckets, the installation can differ from each other. While Bucket B has a shorter skirt and can be installed in one step, Bucket A requires a two steps installation.

The first part in the installation of Bucket B, the piston is displaced downwards to maximum position with an extension of 25 cm attached. The rate of the first part is 10 mm/s. In the second part of the installation, an extra extension of 20 cm is attached to the piston and the bucket is displaced at a rate of 0.5 mm/s in order to be able to stop manually the installation when the soil touched the lid of the bucket i.e. when the load cell registers an abrupt increase in load and when maybe sand is coming out from the top valves of the bucket.

Since the skirt length of Bucket B is shorter than the skirt length of Bucket A, the installation of Bucket B can be performed in one step. This is also carried out through mechanical pushing of the piston and it is done at a constant rate of 0.5 mm/s.

The tank is closed and sealed and the recording of data is started in the moment when the

3.3 Data processing

pressure of 200 *kPa* is started to be added to the pressure tank.

The next step is to apply a small compressive cyclic load of 5 % of the bearing capacity of the soil is applied in order to create conditions more similar to offshore loading environment, assuming good weather during installation day with small wave loads.

The vertical bearing capacity of the sand is calculated according to Barari et al. (2017), and it is found to be 540 *kN*. The corresponding 5 % is 27 *kN*. The mean value of the load is 13.5 *kN*, but considering the pressurization effect in the load cell, the test is configured to a mean load of 15.1 *kN*, and a maximum of 28.6 *kN*. The compressive cyclic loading is set to a total of 1000 cycles with rate of 0.1 Hz.

This loading starts once the pore pressure reading reaches a stable value. Following the cyclic loading, a monotonic tensile load is applied to the suction bucket.

3.3 Data processing

3.3.1 Pressurisation

Testing in the pressure tank allows to raise the pressure up to 200 *kPa*, thus simulating 20 *msw*.

This application of pressure is found to affect the load cell reading. After conducting a trial test a linear relation in between pressure and load cell reading is found, i.e. the reading signal from the load cell increases linearly with respect to the increase in pressure (refer to Figure 3.4).

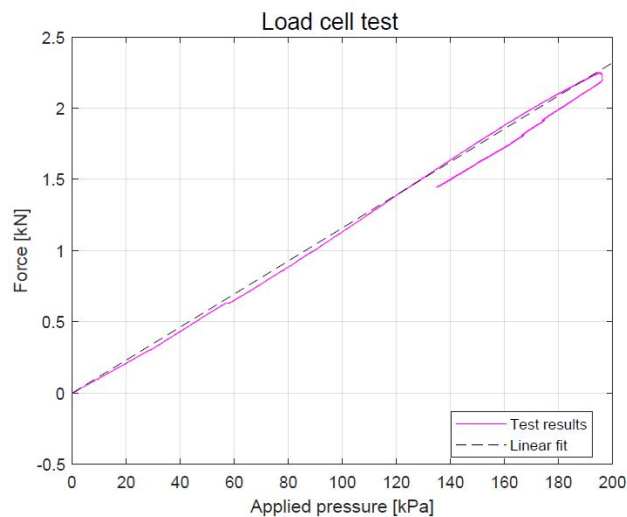


Figure 3.4: Linearized results force vs applied pressure for cell test under pressure

The slope of the line is found to be $n = 0.0116$ and can be used to process the raw data measured by the load cell in all the tests. Furthermore the influence of the 200 *kPa* pressurization on the load

cell is calculated in kN with Equation 3.2.

$$f_{LC} = n \cdot 200 \quad (3.2)$$

3.3.2 Force processing

The raw data regarding the measured force is processed with the Equation 3.3. Here, the effect of pressurization and the submerged weight of the bucket are taken into account.

$$F_f = F_{raw} - w_{sub} - f_{LC} \quad (3.3)$$

Where:

w_{sub}		Submerged weight of the bucket
f_{LC}		Effect of pressure on the LC reading

3.3.3 Excess pore pressure

The PP sensors measure the absolute pressure exerted in them. In order to find the excess pore pressure, all the known pressure components have to be subtracted from the PP readings as shown in Equation 3.4. The pressure components are the atmospheric pressure, hydrostatic pressure and the applied pressure.

$$P_{excess} = P_{measured} - P_{atm} - P_{hyd} - P_{applied} \quad (3.4)$$

Where:

P_{excess}		Excess pore water pressure
$P_{measured}$		Measured PP signal
P_{atm}		Atmospheric pressure (100 kPa)
P_{hyd}		Hydrostatic pressure
$P_{applied}$		Applied pressure during pressurization (≈ 200 kPa)

3.3.4 Data normalization

In order to make the results of this testing campaign directly comparable to other researches, the data in terms of displacement is normalized respect to the bucket diameter. This is done by applying Equation 3.5.

$$u_{z,norm} = \frac{u_{z,abs}}{D} \quad (3.5)$$

3.4 Scaling considerations

Where:

$u_{z,norm}$	Normalized displacement
$u_{z,abs}$	Absolute displacement (measured)

3.4 Scaling considerations

When information between the small scale laboratory testing and field testing is transferred, special attention needs to be directed towards the scaling between the two testing methods. Besides the foundation model differences, the soil properties such as permeability and soil stresses are very different between laboratory and field conditions. The soil stresses in the laboratory are much smaller than the ones found in the field, due to the reduced amount of soil and its weight. It is important therefore to account for these differences with available scaling methods.

Kelly et al. (2006b) used the 1D consolidation theory to derive an equation which presents a way to deduce the behaviour of prototype-scale caissons from model-scale test data. This theory incorporates the parameters which influence the transient capacity of suction buckets (permeability of the soil, rate of loading, length of drainage path). Thus, Equation 3.6 expresses the relationship between prototype-scale caissons and model-scale test data.

$$\frac{k_m}{k_p} = \frac{t_p}{t_m} \left(\frac{D_m}{D_p} \right)^{\frac{3}{2}} \quad (3.6)$$

Where:

k_m, k_p	Permeabilities of model and prototype sand
D_m, D_p	Diameters of model and prototype sand
t_m, t_p	Periods of loading of model and prototype sand

The pre-cyclic loading applied in this testing campaign has a period 0.1 Hz. The scaling method presented by Kelly et al. (2006b) gives insight to design values for prototypes installed in areas with specific conditions (wave period, soil permeability) using the loading and sand permeability of the testing performed in the laboratory.

Data Analysis

After each test is conducted the raw data is processed as indicated in Chapter 3. This chapter addresses the analyses and observations of the tensile capacity and excess pore pressure generated by loading based on different permeabilities of the soil, applied displacement rates and drainage paths. The results presented here focus mainly on the pull-out phase of the test.

Displacements are shown normalized as seen in Subsection 3.3.4. To assure that the analysed data is representative only for when the bucket is still underwater, the data in this chapter is presented and analysed until axial displacement $-0.3D$. This means that for peak tensile resistance occurred after $-0.3D$ displacement are not taken into account, unless it is necessary for comparison purposes (4.3). Figure 4.1 shows the coordinate system used in this project.

Furthermore, all the test results with their complete data are included in Appendix C.

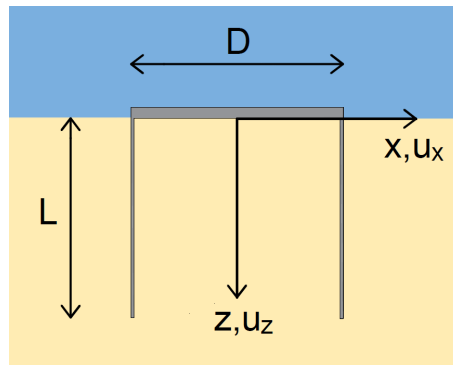


Figure 4.1: Coordinate system.

4.1 Pull-out rate of tests with the same density classification

In this section the analysis is done for each category of density presented in Chapter 3. All pull-out speeds of the tests performed with bucket A are collected for each soil density.

Analyzing the response of the model exposed to varying pull-out speeds is an important step towards understanding the drainage conditions influenced by this. Plots of force vs displacement response are used for the analysis of the tensile peak load and upward displacement and plots of excess PP vs displacement response illustrate the development of suction and other phenomena during the pull out phase.

Drained behaviour is expected to occur at very slow loading rates, which gives sufficient time for the dissipation of differential pressure. In this case, only the inner and outer skin friction resist the upward loading of the suction bucket.

As the pull-out rate is increased, due to the dilative behaviour of the sand and the upward movement of the model foundation, negative excess pore pressure is generated. This creates an increase in effective stresses, thus a higher tensile capacity is formed.

Tests performed in dense sand

The tests performed in the higher densities are shown and analyzed bellow. Figure 4.2 shows the difference in tensile capacity between different pull-out rates in dense sand, while Figure 4.3 shows the difference in the excess pore pressure generated by the different pull-out rates in sensor PP10. Tests in dense sand are carried out with different pull-out speed in order to find undrained behaviour.

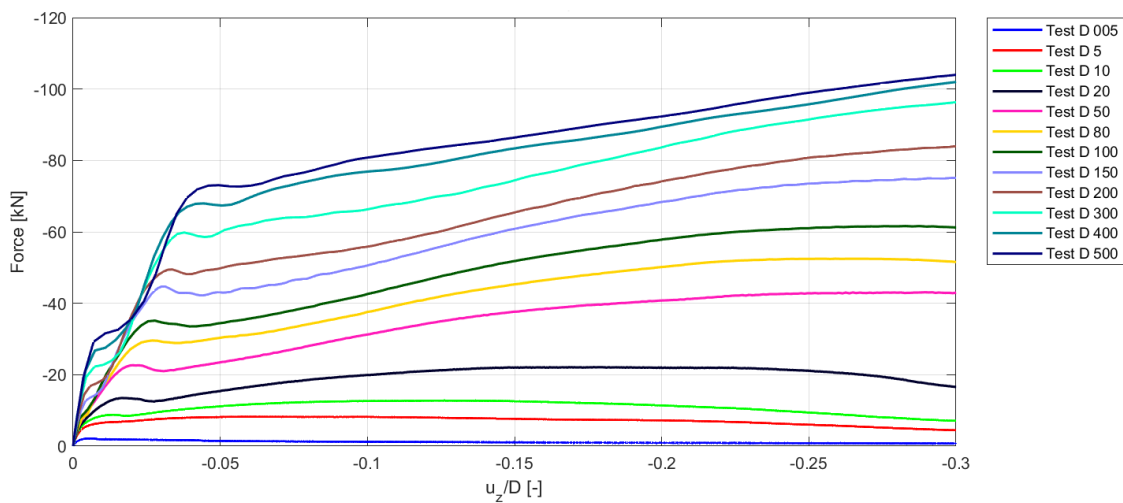


Figure 4.2: Force vs displacement response for all the tests in dense sand during the pull-out phase.

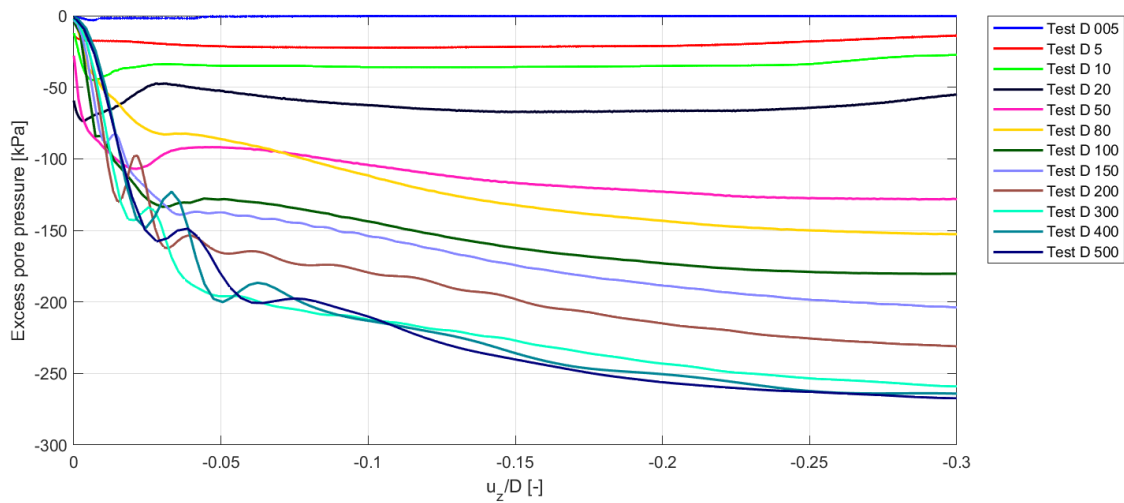


Figure 4.3: Excess PP vs displacement response for all the tests in dense sand during the pull-out phase.

4.1 Pull-out rate of tests with the same density classification

It can be observed a tendency that the tensile capacity and suction measured under the lid increase with the pull-out speed. A similar tendency is noticed with the increase in the required displacement to create the higher tensile capacities. As soon as the response starts approaching the undrained behaviour, a smaller increase in the tensile peak force is observed in between each pull-out rate.

Table 4.1 shows the peak tensile forces recorded until -0.3D in dense sand. From the presented data, a noticeable relationship between the force and the excess pore pressure can be observed in dense sand.

Test No.	Test ID	F_T [kN]	$u_{z,T}$	D_r [%]
1	D 005	-2.16	-0.01D	70.70
2	D 5	-8.24	-0.06D	75.24
3	D 10	-12.80	-0.13D	79.56
4	D 20	-22.13	-0.18D	76.11
5	D 50	-43.09	-0.29D	80.59
6	D 80	-52.48	-0.26D	78.89
7	D 100	-61.63	-0.28D	80.12
8	D 150	-75.11	-0.30D	80.10
12	D 200	-83.94	-0.30D	77.63
13	D 300	-96.22	-0.30D	80.18
14	D 400	-102.00	-0.30D	80.25
15	D 500	-104.10	-0.30D	75.83

Table 4.1: Peak tensile load F_T and vertical displacement at peak tensile load $u_{z,T}$ of tests performed with Bucket A in dense sand with cyclic loading.

The suction recorded underneath the lid seems to represent the behaviour of the measured tensile load, and it appears to be a strong correlation between the force and the generated excess pore pressure. The highest measured negative excess pore pressure is for Test D500, which is -267.5 kPa and it is very similar to the one recorded for Test D400, which is -264.1 kPa. The theoretical suction value for this pressure condition (200 kPa) for reaching cavitation is -300 kPa, which is not reached in the presented tests. However, a similarity between the tensile and suction behaviour is noticed in tests D300 through D500.

It is noted that tests D10 through D500 show an initial peak in the force before the peak tensile capacity is reached. This initial peak is happening around the same displacement as the peak capacity of Test D005. Test D005 shows minor increase in the negative excess pore pressure. The aim of this test was to test a drained response, but the generated suction can be explained due to the fact that the test is performed closing the valves of the lid of the bucket, thus minor suction is generated under the lid.

A second peak before the peak tensile force is reached is recorded in a similar displacement for all tests from D50 to D500, with a tendency to happen at higher displacements with the increase of pull-out rate.

Thoughts regarding these two initial peaks are presented in the next sections of this chapter.

A few pull-out rates are selected after performed the tests in dense sand to continue testing in

different soil densities. Only pull-out rates 0.05, 10, 50, 150 and 500 mm/s are tested in medium and loose sand.

Tests performed in medium density sand

The tests performed in the medium density sand are shown and analyzed bellow.

Figure 4.4 shows the difference in tensile capacity between different pull-out rates in medium density sand, while Figure 4.5 shows the difference in the excess pore pressure generated by the different pull-out rates in sensor PP10.

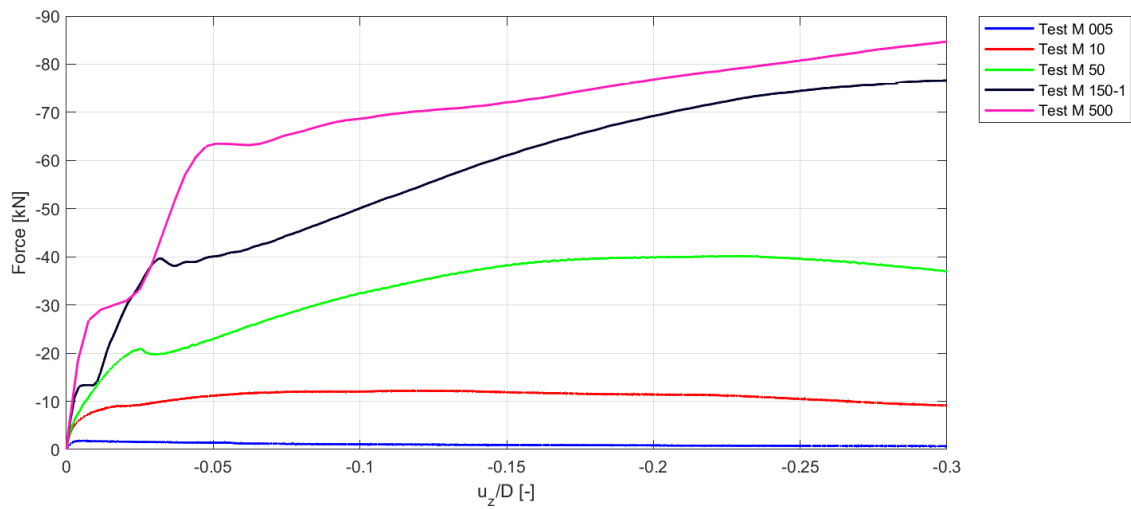


Figure 4.4: Force vs displacement response for all the tests in medium sand during the pull-out phase.

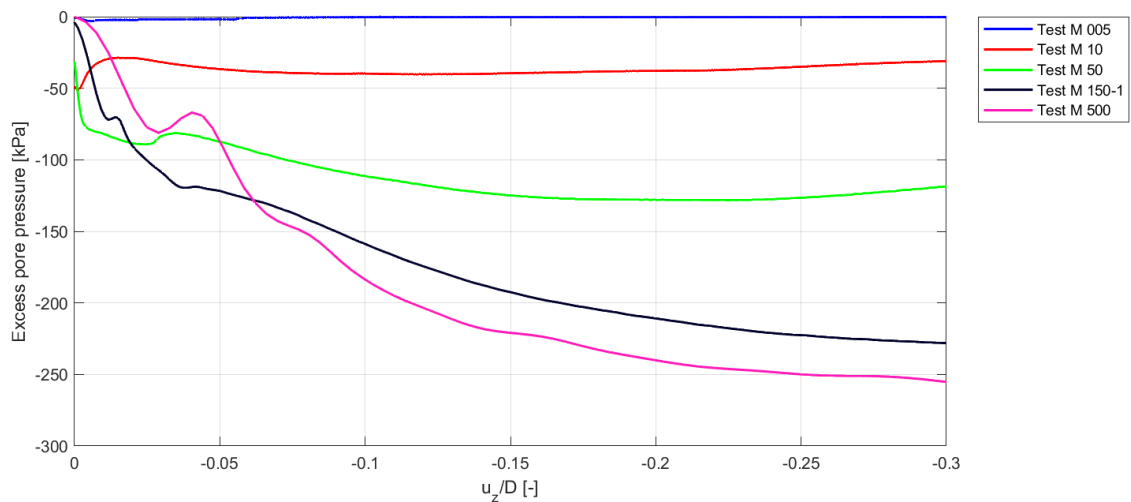


Figure 4.5: Excess PP vs displacement response for all the tests in medium sand during the pull-out phase.

The highest measured negative excess pore pressure is for Test M500, which is -255.2 kPa . In the medium soil, the second highest pull-out rate is 150 mm/s which has a negative excess pore

4.1 Pull-out rate of tests with the same density classification

pressure of -228 kPa . Theoretical cavitation limit is not reached in medium density sand testing.

In the medium density, again the test with rate 0.05 mm/s shows slight development of negative pore pressure probably due to testing with the bucket model with closed lid valves.

Table 4.2 shows the peak tensile forces recorded until $-0.3D$ in medium sand. From the presented data, a noticeable relationship between the force and the excess pore pressure can be observed in medium sand.

Test No.	Test ID	F_T [kN]	$u_{z,T}$	D_r [%]
16	M 005	-1.84	-0.01D	60.23
17	M10	-12.23	-0.12D	58.49
18	M 50	-40.20	-0.22D	60.10
19	M 150-1	-76.62	-0.30D	67.92
21	M 500	-84.69	-0.30D	66.04

Table 4.2: Peak tensile load F_T and vertical displacement at peak tensile load $u_{z,T}$ of tests performed with Bucket A in medium density sand with cyclic loading.

Again initial peaks are observed. Tests M150-1 and M500 show initial peaks which happen at similar displacements as the maximum tensile capacity of test M005. Test M50 however, shows an initial peak which is developed around the same location as the second peak in tests M150-1 and M500.

Tests performed in loose sand

The tests performed with the same pull-out speed as the medium density category are chosen to be analysed in this section.

Figure 4.6 shows the difference in tensile capacity between different pull-out rates in loose sand, while Figure 4.7 shows the difference in the excess pore pressure generated by the different pull-out rates in sensor PP10.

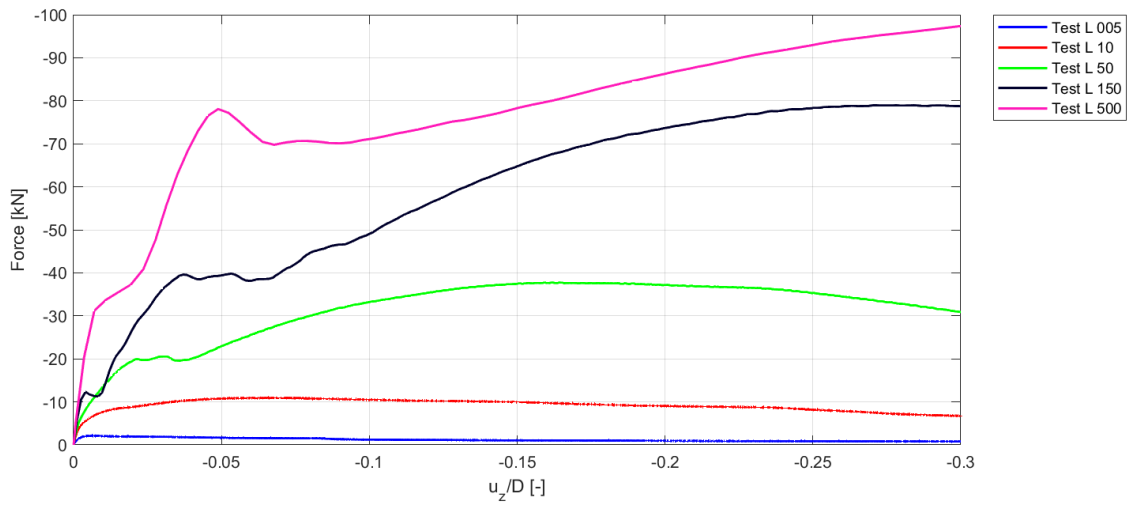


Figure 4.6: Force vs displacement response for all the tests in loose sand during the pull-out phase.

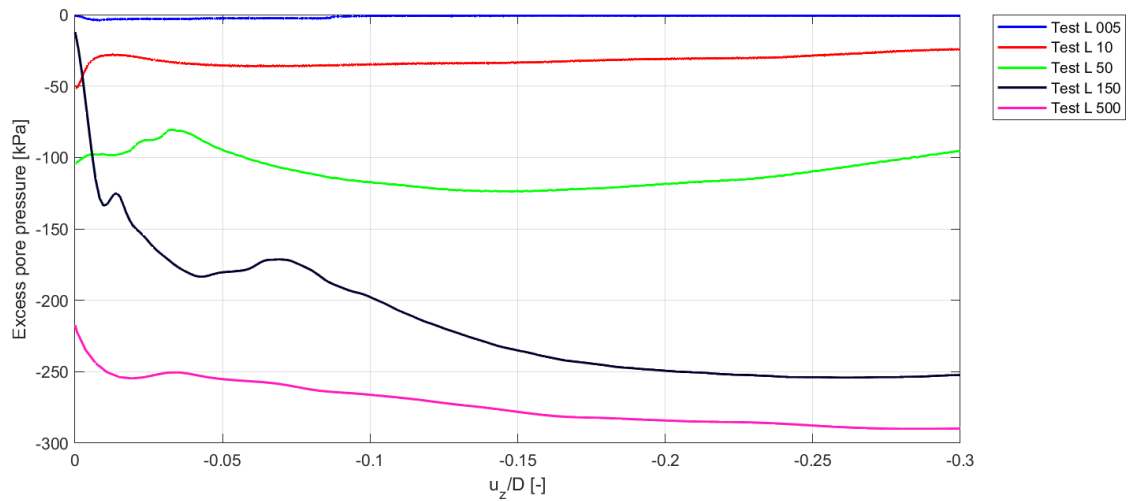


Figure 4.7: Excess PP vs displacement response for all the tests in loose sand during the pull-out phase.

It can be noted from Figure 4.7 that excess pore pressure for Tests L10, L50 and L500 present an initial excess pore pressure different than 0. This is due to the trimming of data from the cyclic loading. However, similar tendencies between force, displacement and excess pore pressure are noticed as in medium and dense soil.

In this case, the highest measured negative pore pressure is recorded for Test L500 with -289 kPa , which is very close to cavitation limit, then followed by L150 with -252.4 kPa . The generated suction for test L500 is higher than the ones recorded in test for dense and medium density sand. This could be due to the application of compressive cyclic load in loose soil, which could provoke a densification of the soil. Further analysis of this effect is taken into account by the observation of the influence of cyclic number on the accumulated displacement and plotting of isochrones which show the excess pore pressure development along the skirt length in specific points in time.

4.2 Pull-out rate of tests with same velocity

Table 4.3 shows the peak tensile forces recorded until $-0.3D$ in loose sand. From the presented data, a noticeable relationship between the force and the excess pore pressure can be observed in loose sand.

Test No.	Test ID	F_T [kN]	$u_{z,T}$	D_r [%]
22	L 005	-2.182	-0.01	52.20
23	L 10	-11.04	-0.06	44.13
24	L 50	-37.74	-0.16	45.63
25	L 150	-78.96	-0.27	47.49
26	L 500	-97.28	-0.30	45.21

Table 4.3: Peak tensile load F_T and vertical displacement at peak tensile load $u_{z,T}$ of tests performed with Bucket A in loose density sand with cyclic loading.

4.2 Pull-out rate of tests with same velocity

In order to compare tests with different seepage flow and hydraulic conductivity conditions, the density of the soils treated as a variable when the pull-out speed stays constant.

In this section results for excess pore pressure versus displacement are presented only from sensor PP10. Results for the rest of the sensors are presented in Appendix C.

For easier reporting of the observations, a few terms are introduced in this section as following:

F_T	Tensile peak capacity of the test in kN
F_{P1}	Initial peak in tensile load of the test in kN
F_{P2}	Second peak in tensile load of the test in kN

Tests performed with displacement rate 0.05 mm/s

In the case of slow tensile loading, a drained response is expected which theoretically shows no negative excess pore pressure development. In this case, the internal and external frictional forces are the only ones expected to influence the tensile capacity of the suction bucket.

It can be observed from Figure 4.8 that the difference in peak tensile capacity F_T between the three different density categories is very small. In the case of slow loading, the tensile capacity does not vary significantly in magnitude and displacement at which it takes place.

When inspecting the initial stiffness it is noticed that tests L005 and D005 have a slightly stiffer response than M005, which is also reflected in their higher peak tensile load respect to M005. The peak is followed by a strain softening throughout the entire duration of the test.

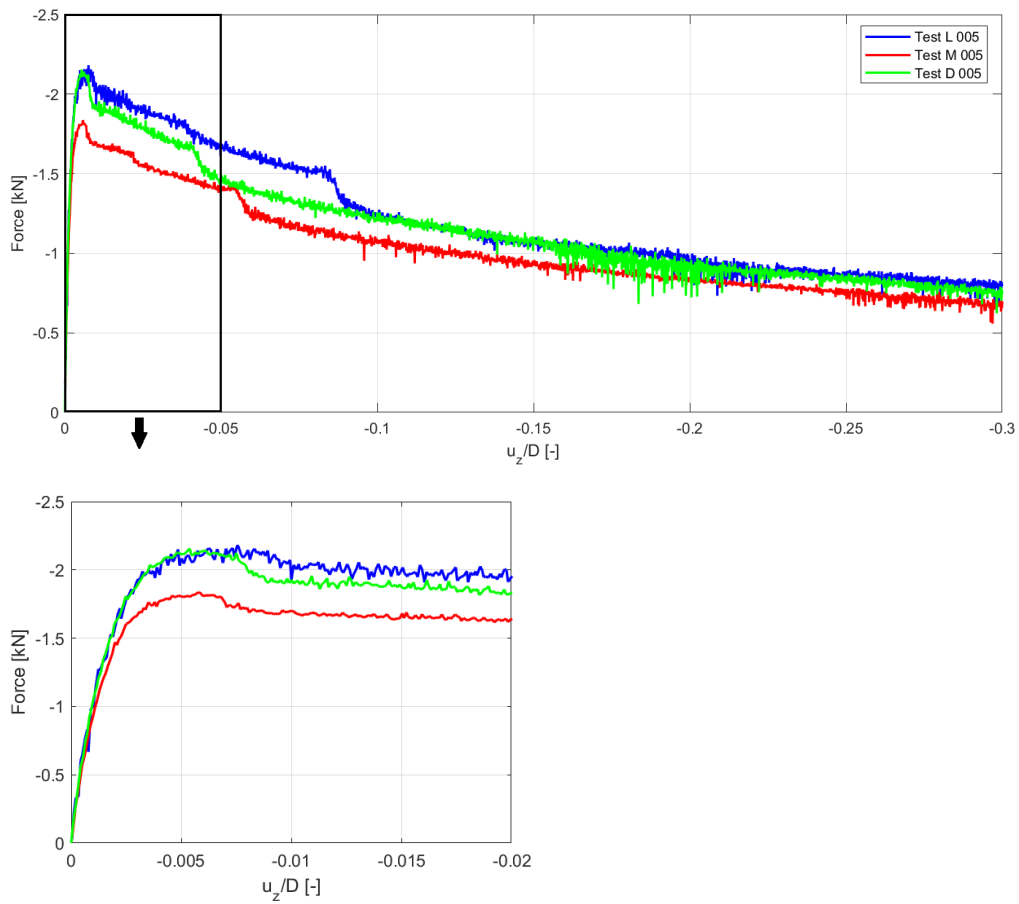


Figure 4.8: Force vs displacement response during pull-out phase for tests of same pull-out speed of 0.05 mm/s made in different soil densities.

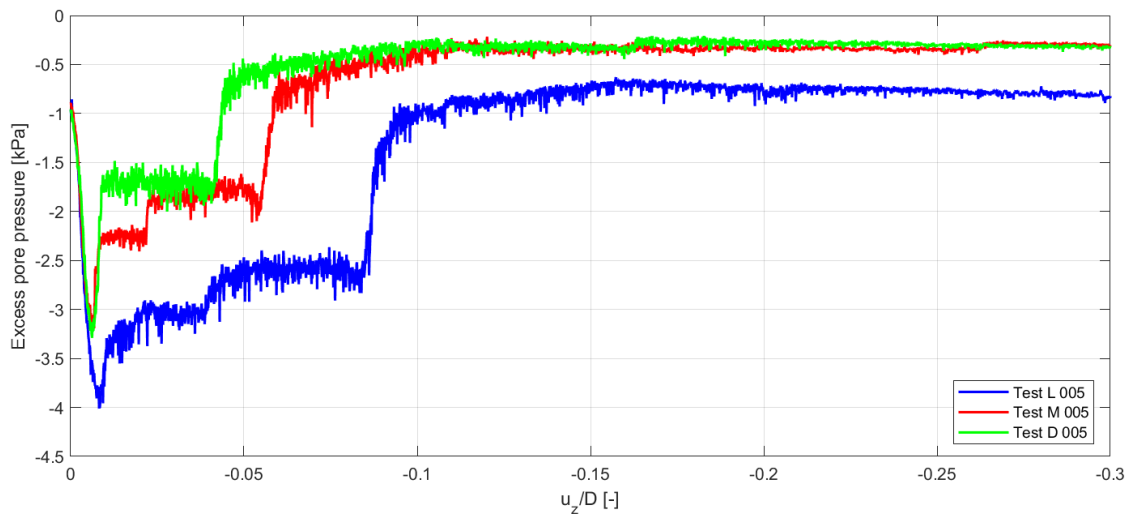


Figure 4.9: Excess PP vs displacement response during pull-out phase for tests of same pull-out speed of 0.05 mm/s made in different soil densities.

4.2 Pull-out rate of tests with same velocity

Figure 4.9 shows the development of excess pore pressure under the lid for the three different density categories. It can be noted that a very small amount of negative excess pore pressure is generated under the lid in the current scenario. This could be due to the closing of the bucket model lid valves after the installation.

Tests performed with displacement rate 10 mm/s

The comparison between different densities with a constant pull-out rate of 10 mm/s is observed in Figures 4.10 and 4.11. In the first part of the tensile loading, a stiffer response of Test D10 is noticed until F_{P1} is developed. The loading experiences a small decrease in capacity, followed by a strain hardening until the peak tensile capacity, F_T of the test is reached.

Test L10 shows a similar behaviour, however, with a peak tensile capacity which seems to be smaller than the ones of tests D10 and M10. Moreover, test L10 experiences a first peak which is less noticeable than in the other two density categories.

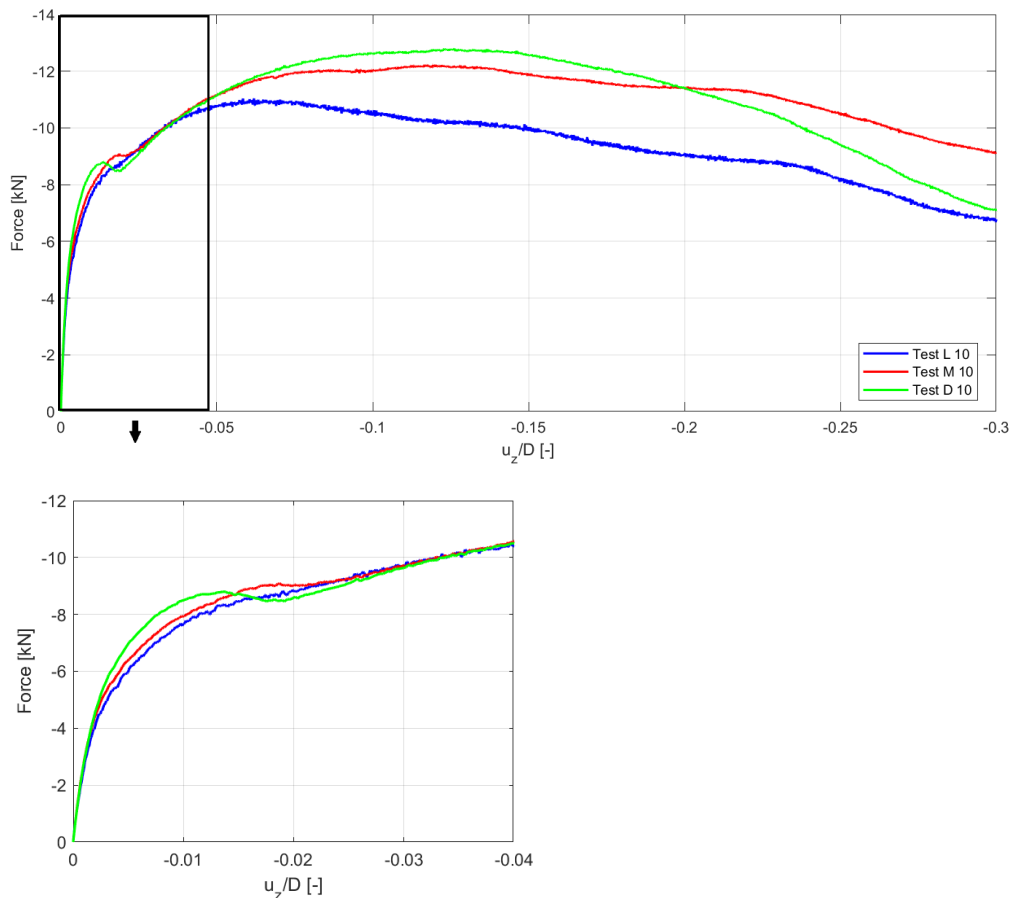


Figure 4.10: Force vs displacement response during pull-out phase for tests of same pull-out speed of 10 mm/s made in different soil densities.

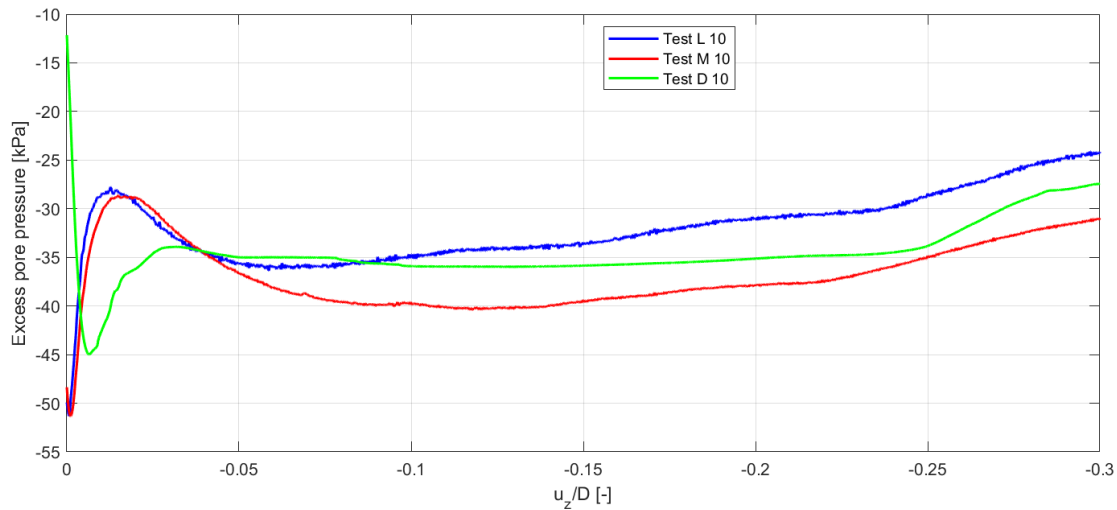


Figure 4.11: Excess PP vs displacement response during pull-out phase for tests of same pull-out speed of 10 mm/s made in different soil densities.

Figure 4.11 shows the data for excess pore pressure development in tests with pull-out rate of 10 mm/s. It is noticed that the excess pore pressure for tests M10 and L10 are start from a lower value, than the ones for D10. This is due to the cutting of the data in the pull-out phase of the test. Between the cyclic loading and the pull-out phase, a short break is taken for the soil to stabilise. The pull-out starts with excess pore pressures measuring zero, however, when the excess pore pressure decreases very rapidly compared to the time passed or displacement travelled, the points are very close to the cutting line, thus showing that the data is measured from a lower value than 0.

Tests performed with displacement rate 50 mm/s

The initial stiffness in tests performed at 50 mm/s is again slightly higher for the dense soil compared to the loose and medium ones. Data presented in 4.12 shows similar behaviour regarding the first peak and tensile capacity as the tests performed with 10 mm/s. A difference is noted in L10, where there are two "initial" peaks close to each other, noted in Table 4.5 with F_{P1} and F_{P2} in the order in which they appear. Moreover, it is noticed a small strain softening after the first peak of the curves, followed by a strain hardening until the tensile capacity of the curves is reached. In this case, the tensile capacities seem to have similar magnitudes, and occur at similar displacements.

In Figure 4.13 it is noticed that the start in excess pore pressure is below zero, but again this is due to data trimming configuration. Only Test L50 when checking the real starting point is found to be -20 kPa (not -100 kPa as shown in the graph due to trimming configuration). In this test, a drop in pressure under the lid, on the left side of the bucket (PP10) is found to happen during the break between the cyclic loading and the pull-out phase. The break between the cyclic loading and the pull-out phase is longer than usual since this test is left to be performed automatically overnight. However, this condition does not seem to affect all the tests left for overnight testing.

4.2 Pull-out rate of tests with same velocity

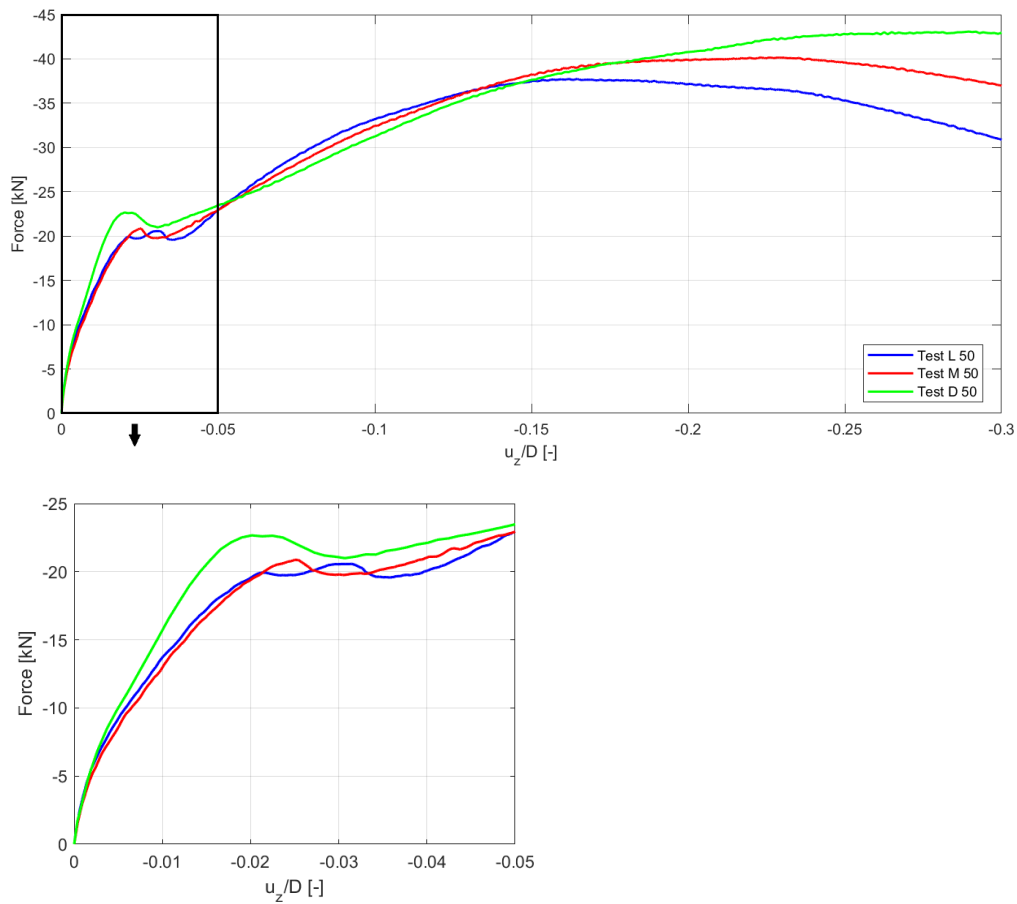


Figure 4.12: Force vs displacement response during pull-out phase for tests of same pull-out speed of 50 mm/s made in different soil densities.

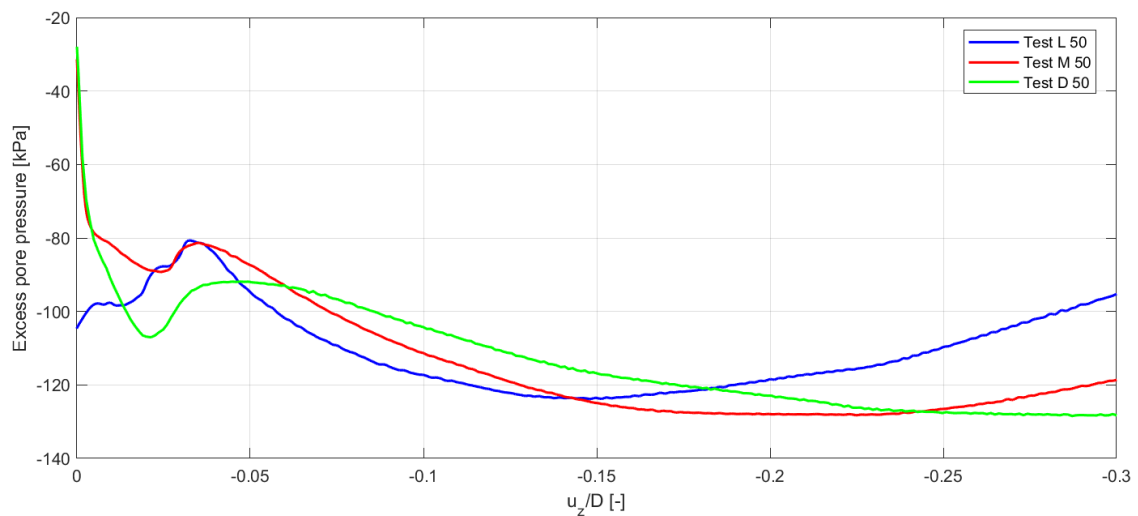


Figure 4.13: Excess PP vs displacement response during pull-out phase for tests of same pull-out speed of 50 mm/s made in different soil densities.

Tests performed with displacement rate 150 mm/s

The first test performed with the rate of 150 mm/s is in dense sand. After performing the same rate test in medium density, it is noticed that the tensile capacity of M150-1 is slightly higher than the test D150. This is unexpected prior to observations from earlier tests. In order to assess the situation the CPT profiles of the two tests is compared in Figures 4.14 and 4.15. D150 has a mean relative density, \bar{D}_r of 80.10 % and a standard deviation, SD of 5.26 %, while Test M150-1 has a mean relative density of 67.92% and a standard deviation of 6.75% as shown in Table 3.3. In Test M150-1 8 CPTs are taken in order to better check the homogeneity of the soil throughout the tank.

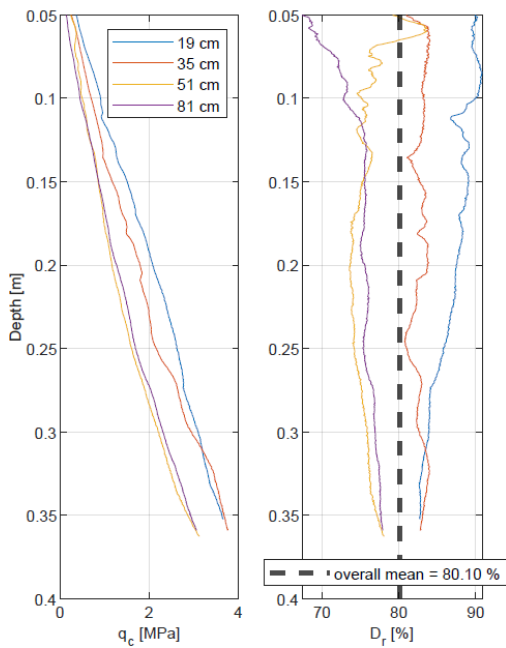


Figure 4.14: CPT results D150.

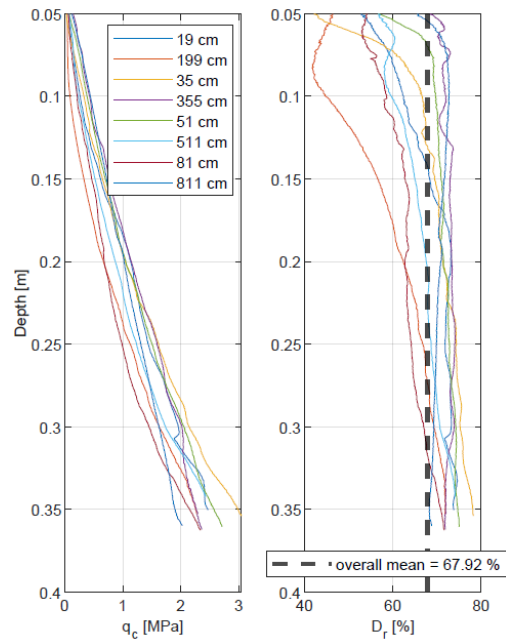


Figure 4.15: CPT results M150-1.

As seen in Figure 4.15 soil of M150 has a higher density in the lower part of the profile, with some values approaching 80 %. Test D150 is less concentrated around the mean, with the 2 CPTs locations further away from the bucket showing profiles almost similar to the majority of the profiles in Test M150-1. This could have an impact on the result of the tensile capacity of the testings.

In order to test this theory, another test with speed 150 mm/s in medium soil is prepared: M150-2. The CPT of the prepared soil for the second test in medium density M150-2 shown a mean relative density, \bar{D}_r of 57.32 and a standard deviation of 9.15 %. Results of this CPT are found in Appendix B.2.

After plotting the results of D150, M150-1 and M150-2, shown in Figure 4.16 it is noticed that the difference between the behaviours of M150-1 and M150-2 are not significant. Therefore, the rest of the results presented in this chapter are shown solely for M150-1.

4.2 Pull-out rate of tests with same velocity

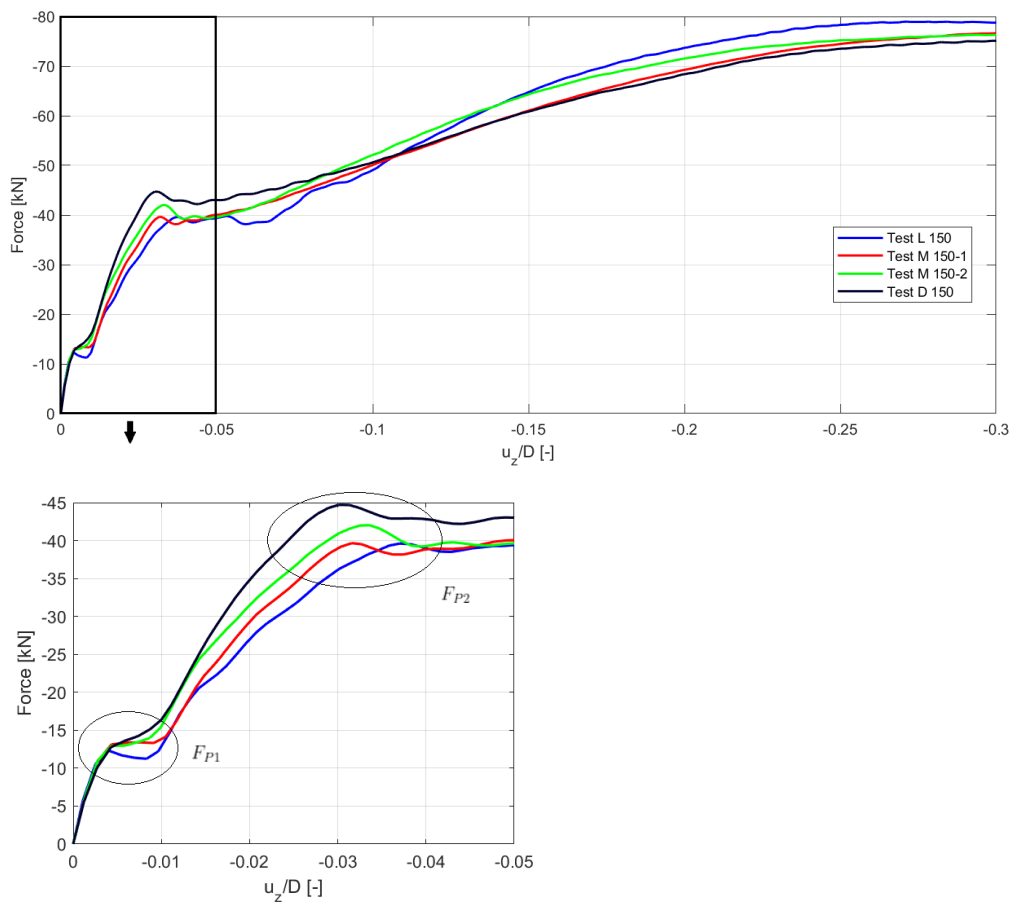


Figure 4.16: Force vs displacement response during pull-out phase for tests of same pull-out speed of 150 mm/s made in different soil densities.

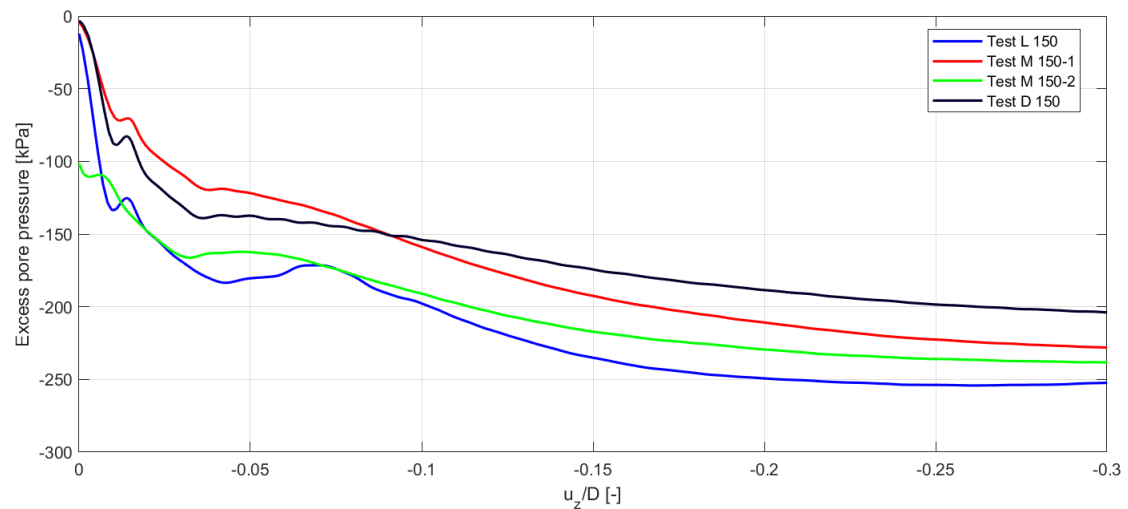


Figure 4.17: Excess PP vs displacement response during pull-out phase for tests of same pull-out speed of 150 mm/s made in different soil densities.

As seen in Figure 4.16, in the case of the pull-out rate of 150 mm/s the behaviour between the three different density categories is quite similar. However, compared to previous pull-out speeds, a second peak, F_{P2} in the tensile force curve is noticed. The initial behaviour of the tests is similar to the previous rates: the initial stiffness shows pretty similar behaviours between the densities, however the stiffness of D150 seems to be slightly lower than the rest of the tests, which could explain the lowest peak tensile capacity of D150.

All tensile force curves present an initial peak followed by a slightly strain softening, and immediately after a strain hardening. In the present case, instead of reaching the peak tensile capacity, the force experiences a second peak, which seems to happen in similar locations between all the four tests. This is followed by a strain hardening until the tensile capacity of the tests is reached.

Tests performed with displacement rate 500 mm/s

Figure 4.18 shows the force vs displacement response during pull-out phase for tests of 500 mm/s . In the case of pull-out rate of 500 mm/s the highest initial stiffness is experienced by Test L500.

A first peak, F_{P1} is formed followed by a strain hardening and a second peak, F_{P2} . After the second peak, the force continues to increase gradually, until the tensile capacity F_T considered at displacement -0.3 .

It can be observed that the initial part of the loading, until F_{P2} the tensile force is higher in the loose soil, than in the dense one. However, at the point where the peak tensile capacity F_T is considered, the magnitude of the forces does not follow a specific trend regarding the density. This could be due to changes in density during cycling prior to the pull-put phase, or from the lack of homogeneity in the loose sand due to its preparation.

Figure 4.20 shows the difference in responses between the excess pore pressures in the three different densities. Contrary to expectations, the test in loose soil is closer to the theoretical value of cavitation, than the test in dense soil. Again, this could be a side effect of the compressive cyclic load applied prior to the pull-out test. Since the frequency and cyclic load are kept at the same values throughout the cyclic testing, in the case of very loose soil it could act as a possible densification process. This further creates conditions for the soil to exhibit a higher negative pore pressure due to dilative tendencies of dense sand.

Since the excess pore pressure data in presented graphs is only shown for PP 10, a better overview of the development of the excess pore pressure is better understood by taking a closer look to isochrones in points of interest.

4.2 Pull-out rate of tests with same velocity

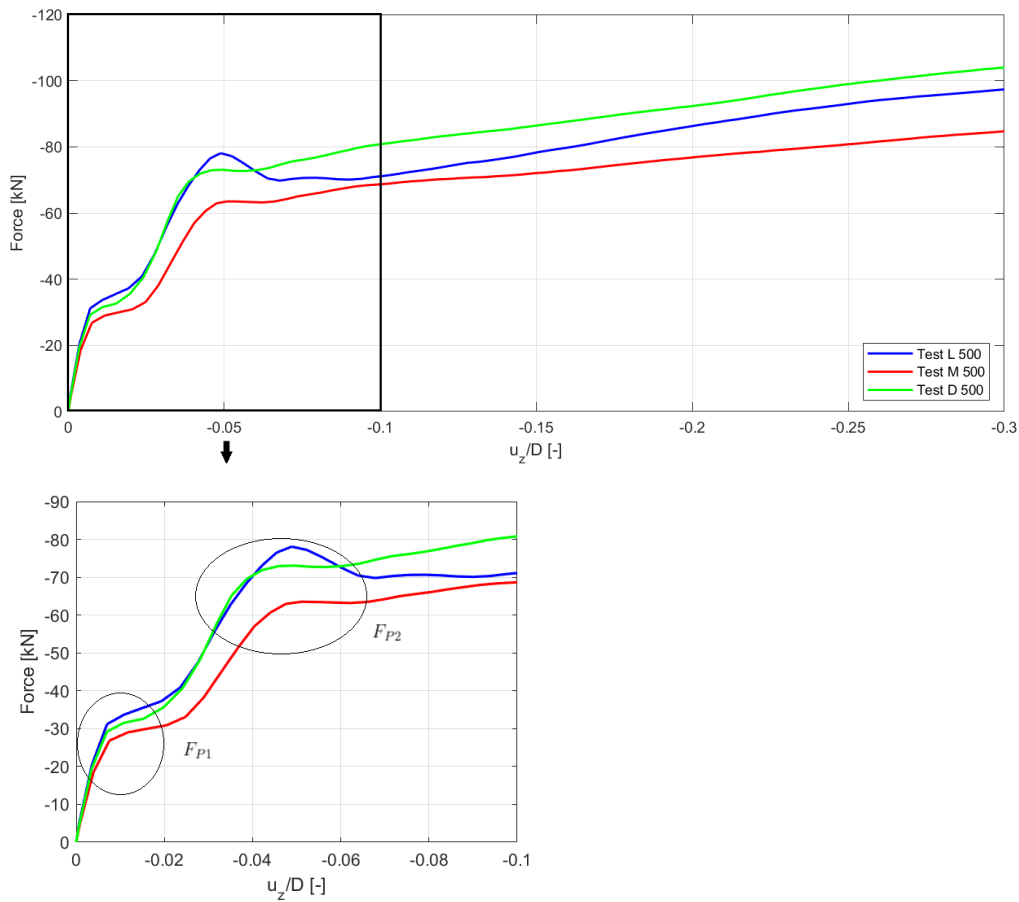


Figure 4.18: Force vs displacement response during pull-out phase for tests of same pull-out speed of 500 mm/s made in different soil densities.

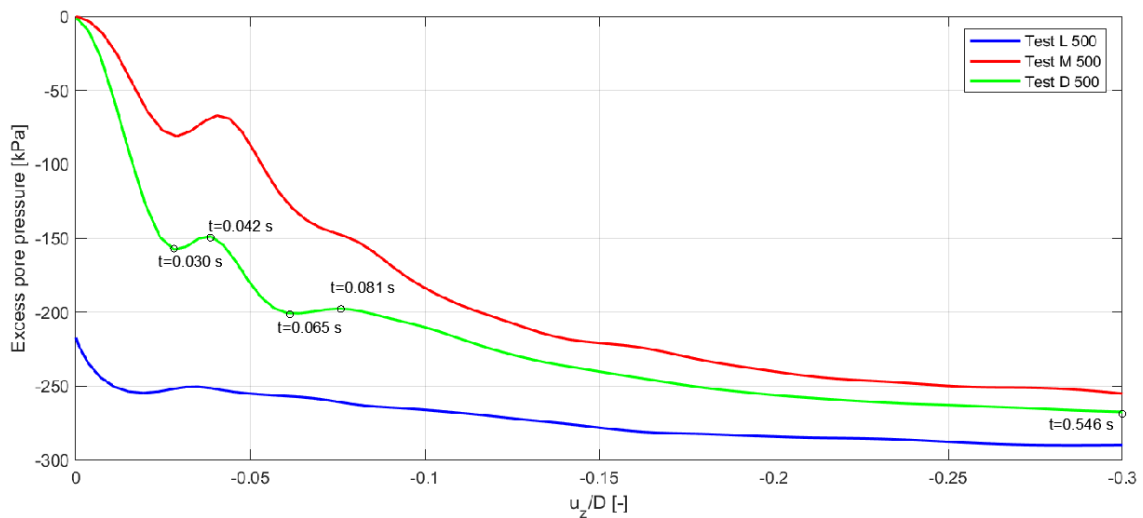


Figure 4.19: Excess PP vs displacement response during pull-out phase for tests of same pull-out speed of 500 mm/s made in different soil densities.

In Figure 4.20 test D500 is chosen to be analyzed with isochrones depending on the critical points of the curve. The first time step, $t=0$ s is chosen in the beginning of the curve to show the initial excess pore pressure in the test. The next time step, $t=0.022$ s is chosen as a point between the origin and the first peak of negative excess pore pressure in order to have a better understanding of the pore pressure development at this point. The third time step, $t=0.030$ s is chosen at the second peak of negative excess pore pressure. Time $t=0.042$ s represents the first decrease in negative pore pressure. Two more extremes are taken into account at $t=0.065$ s and $t=0.081$ s. Lastly, an isochrone equivalent for the peak tensile capacity is considered at $t=0.546$ s. This process is used for plotting the isochrones in order to get a better understanding of the soil behaviour at critical points of the curves. Figure 4.21 introduce the level of the PP sensors and their distribution.

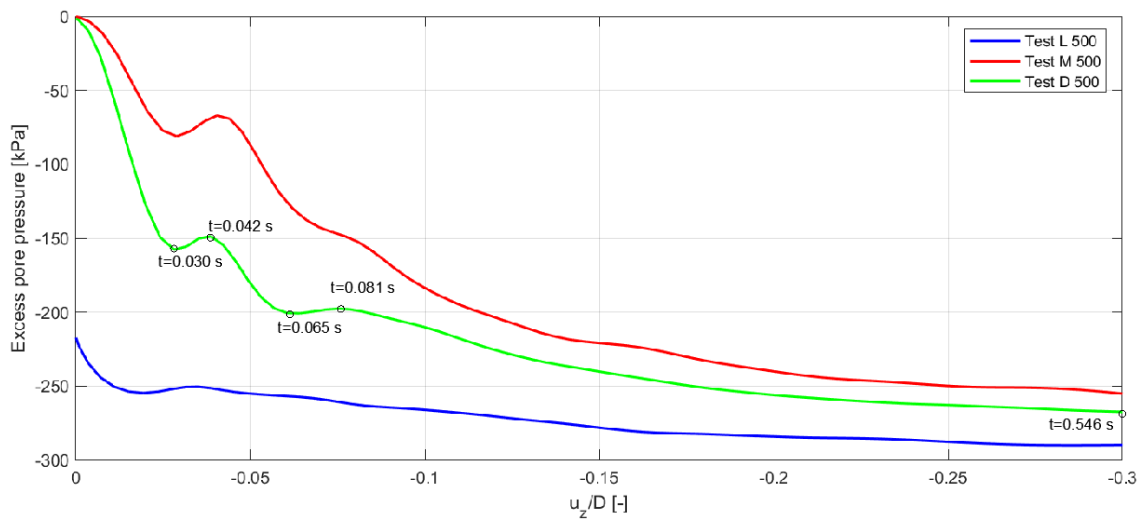


Figure 4.20: Excess PP vs displacement response during pull-out phase for tests of same pull-out speed of 500 mm/s made in different soil densities.

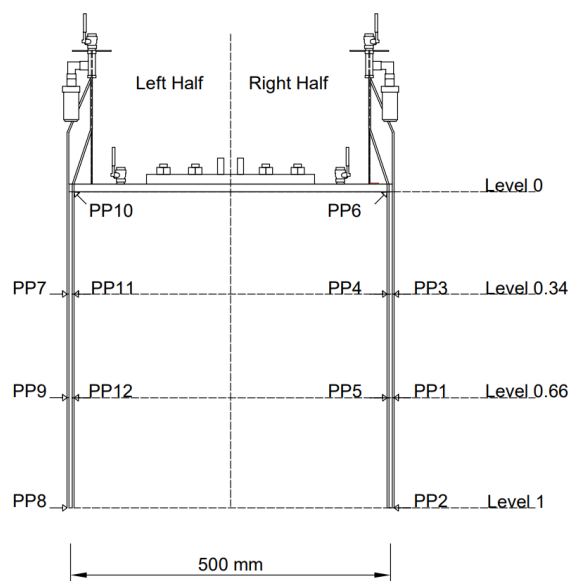


Figure 4.21: Suction Bucket A showing levels.

4.2 Pull-out rate of tests with same velocity

Figures 4.22 and 4.23 show isochrones for Test D500 where the excess pore pressure is plotted along the skirt of the bucket. In the beginning of the loading, the external PPs on the bucket in the levels 0.66 and 1 show little to no change in excess pore pressure. However, the isochrone plotted at time, $t=0.546$ s represents the excess pore pressure reading when the suction is noticeable, especially by sensors at the tip of the skirt. This could be due to the fact that PPs 2 and 8 are right under the bucket and they feel the suction stronger than the external PPs in levels 0.34 and 0.66.

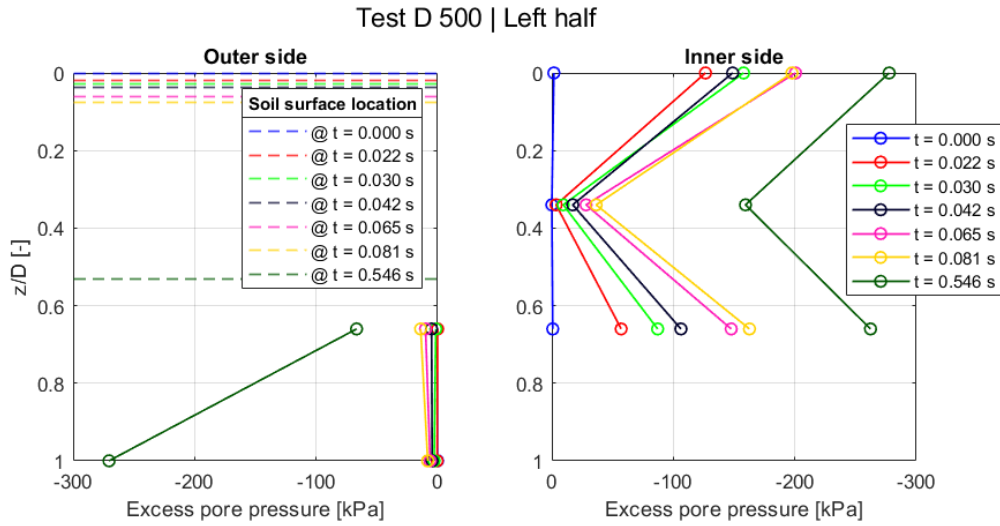


Figure 4.22: Isochrones Test D500 at left side of the bucket.

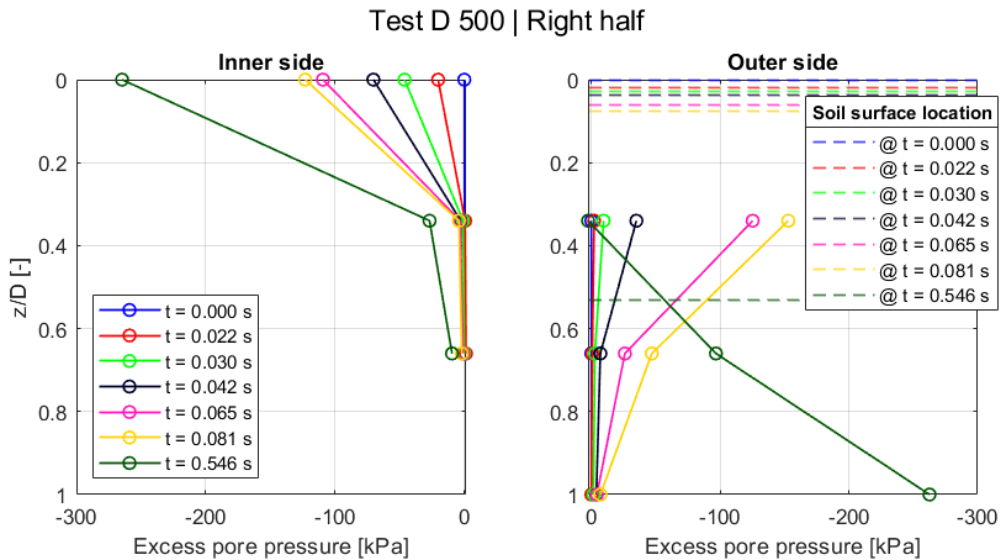


Figure 4.23: Isochrones Test D500 at right side of the bucket.

The first two peaks and their respective drops in negative pore pressure show similar behaviours in the isochrone representation. The excess pore pressure under lid (Level 0) shows a continuous increase in negative excess pore pressure with time (with minor fluctuations at the "valleys" represented in Figure 4.20 on the left side of the bucket). While Level 0.66 shows a similar response in excess pore pressure on the inside of the left half of the bucket, Level 0.34 on the inside and

Level 0.66 inside of the right side show very small development of negative pore pressure, with values being very close to zero on the internal right side of the bucket. In this case, the internal left side of the bucket shows slightly more development of negative excess pore pressure, while the external excess pore pressure on both sides and inside, on level 0.66 on the left side show more negative excess pore pressure.

The reason why the outer side on the left side of D500 cannot be fully represented in all levels is due to missing information from PP7.

Table 4.4 shows the values of the first peak F_{P1} of the tensile force. For tests performed with a speed of 0.05 mm/s the first peak F_{P1} is coincident with the tensile capacity F_T of the test.

Test rate [mm/s]	Dense		Medium		Loose	
	F_{P1} [kN]	$u_{z,P1}$	F_{P1} [kN]	$u_{z,P1}$	F_{P1} [kN]	$u_{z,P1}$
0.05	-2.16	-0.01	-1.84	-0.01	-2.182	-0.01
10	-8.8	-0.01	-9.09	-0.02	-8.59	-0.02
50	-22.66	-0.02	-20.86	-0.03	-19.93	-0.02
150	-13.59	-0.01	-13.13	-0.004	-12.32	-0.004
500	-31.55	-0.01	-29.01	-0.01	-33.7	-0.01

Table 4.4: First peak tensile load, F_{P1} and vertical displacement at first peak tensile load, $u_{z,P1}$.

It is noticeable that the F_{P1} and $u_{z,P1}$ do not show significant change between densities. Moreover, the displacement at which F_{P1} is happening seems to be similar throughout the variation of density and pull-out rate. This similarity between tests regarding the location of F_{P1} and the fact that it happens at the same location with F_t of the tests with 0.05 mm/s speed, could suggest that the first peak of the tests is equivalent to the frictional resistance of the bucket.

Table 4.5 shows the the values of the second peak in the tensile capacities shown in this section. It is observed that the change in F_{P2} and its respective $u_{z,P2}$ do not variate significantly with density. However the generation of the second peak tends to appear in higher speeds.

Furthermore Table 4.5 compares peak tensile capacities, vertical displacement at peak tensile load and densities between tests of same displacement rate and density.

Test rate [mm/s]	Dense		Medium		Loose	
	F_{P2} [kN]	$u_{z,P2}$	F_{P2} [kN]	$u_{z,P2}$	F_{P2} [kN]	$u_{z,P2}$
50	-	-	-	-	-20.56	-0.03
150	-44.7	-0.03	-39.66	-0.03	-39.61	-0.04
500	-72.94	-0.05	-63.52	-0.05	-78.08	-0.05

Table 4.5: Second peak tensile load, F_{P2} and vertical displacement at second peak tensile load, $u_{z,P2}$.

4.2 Pull-out rate of tests with same velocity

Test rate [mm/s]	Dense			Medium			Loose		
	F_T [kN]	$u_{z,T}$	\bar{D}_r [%]	F_T [kN]	$u_{z,T}$	\bar{D}_r [%]	F_T [kN]	$u_{z,T}$	\bar{D}_r [%]
0.05	-2.16	-0.01D	70.70	-1.84	-0.01D	60.23	-2.18	-0.01D	52.20
10.00	-12.80	-0.13D	79.56	-12.23	-0.12D	58.49	-11.04	-0.06D	44.13
50.00	-43.09	-0.29D	80.59	-40.20	-0.22D	60.10	-37.74	-0.16D	45.63
150.00	-75.11	-0.30D	80.10	-76.62 / -76.33	-0.30D	67.92 / 57.32	-78.96	-0.27D	47.49
500.00	-104.10	-0.30D	75.83	-84.69	-0.30D	66.04	-97.28	-0.30D	45.21

Table 4.6: Peak tensile load F_T and vertical displacement at peak tensile load $u_{z,T}$ and D_r comparison of pull-out rate of tests with same velocity.

4.2.1 Influence of cyclic load

The compressive cyclic load applied prior to the tensile pull-out test generated an accumulation of displacement in the soil regardless on its density. The accumulated displacement of all the tests can be found in Table 4.7.

Test ID	$\Delta u_{z,cyc}$	Test ID	$\Delta u_{z,cyc}$	Test ID	$\Delta u_{z,cyc}$
D 005	0.02983D	M 005	0.03449D	L 005	0.03985D
D 5	0.02938D	M 10	0.03553D	L 10	0.05181D
D 10	0.02675D	M 50	0.0425D	L 50	0.04228D
D 20	0.02658D	M 150-1	0.03508D	L 150	0.04945D
D 50	0.02578D	M 150-2	0.03321D	L 500	0.03839D
D 80	0.02718D	M 500	0.0378D		
D 100	0.02804D				
D 150	0.02898D				
D 150-B	0.02735D				
D 200	0.02966D				
D 300	0.03168D				
D 400	0.02846D				
D 500	0.03597D				

Table 4.7: Displacement accumulation after the application of compressive cyclic loading

It is noticeable that there is a tendency of higher displacement accumulation for the tests with lower densities, followed for the test with medium density and finally tests with higher densities. In Figure 4.24 can be found the plots of accumulated displacements for the tests which rates are performed in all densities. Due to technical problems in the lab, a stop in the piston can be seen as a drop in the displacement in Tests D 005 and L 005 in Figure 4.24. This did not affected the final test results.

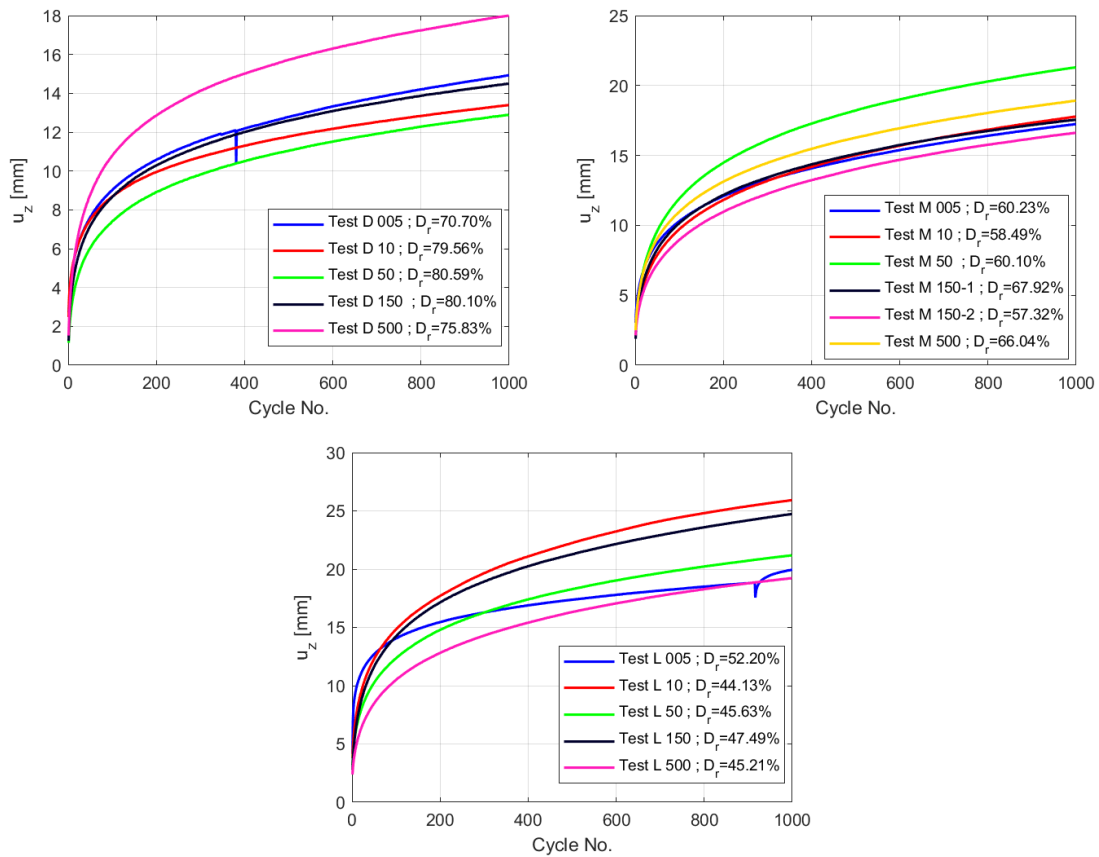


Figure 4.24: Number of cycles vs accumulated displacement.

It is important to note that the cyclic load is force controlled, which means that the piston reaches the programmed force regardless the settlement in the soil. This could be one of the reasons why the soil keeps settling with each cycle. The settlement could be defined as a densification of the soil product of the cyclic loading, but this can not be proved, since no CPT can be done while running the test. However no correlation can be noted in between this cyclic loading effect and the peak tensile capacity results.

Furthermore a development in negative pore pressure is observed when the cyclic load reached its minimum at zero in every cycle. This could indicate the dilation of the soil, followed by a compaction in every cycle. Figure 4.25 illustrates the excess pore pressure development during cyclic load for Tests made with rate 500 mm/s . The compressive cyclic loading comes after a ramp that brings the piston to the mean force. When the cyclic load starts, the piston comes back to zero load and then goes to maximum compressive load, provoking the higher accumulated displacements within the first cycles. The higher initial peaks in the excess pore pressure can be seen as the illustration of this behaviour. A tendency is observed in which the higher responses both negative and positive excess pore pressure, belong to tests performed in dense sand.

4.3 Pull-out rate by drainage path

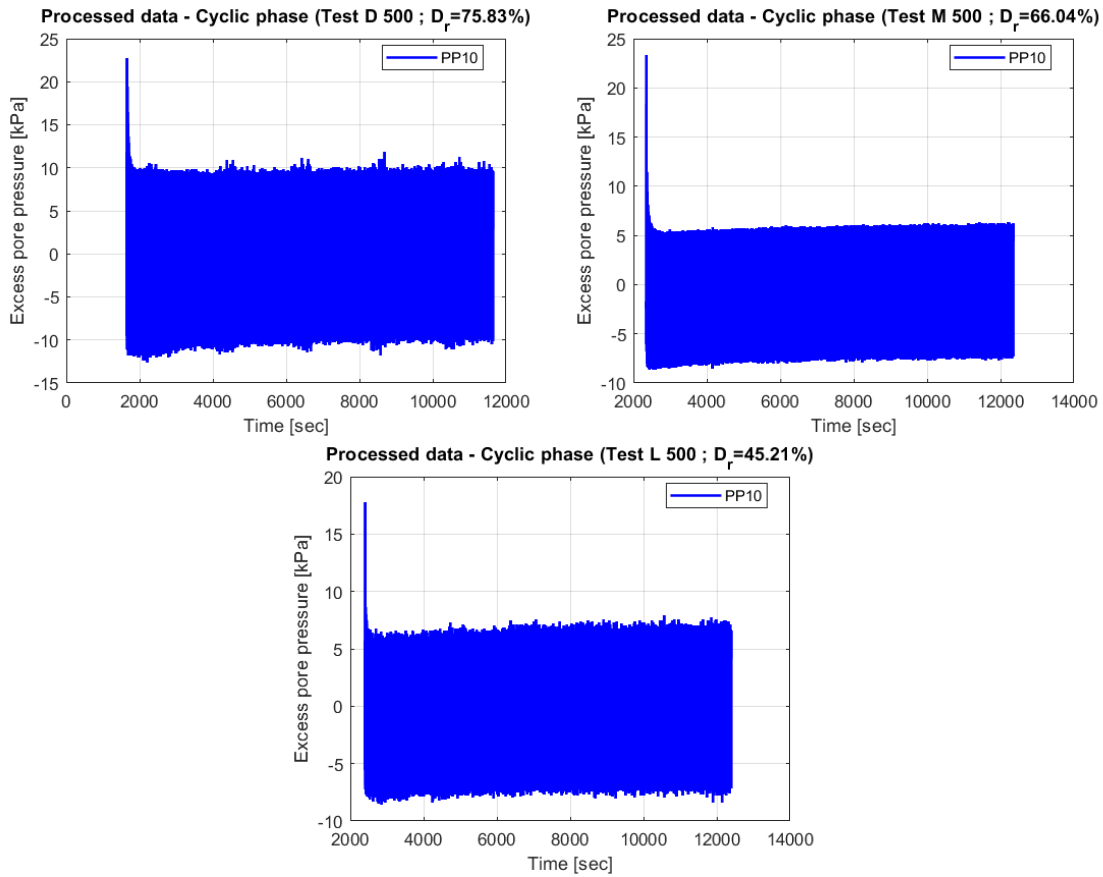


Figure 4.25: Excess PP vs time during cyclic load for tests with displacement rate 500 mm/s .

4.3 Pull-out rate by drainage path

For analysing the drainage path two buckets are tested and later compared: Bucket A and Bucket B. Both buckets have same diameter, but different skirt lengths and therefore different drainage path. For reviewing the geometry of the buckets, refer to Section 3.1. All test in this section are tested in dense sand with a rate of 150 mm/s , with and without cyclic loading before the pull-out test.

Table 4.8 shows the peak tensile load at a maximum of $-0.30D$ displacement and Figure 4.26 shows the plot of the response force vs displacement for all the tests rate 150 mm/s in dense sand during the pull-out phase.

Test No.	Test ID	F_T [kN]	$u_{z,T}$	D_r [%]
8	D 150	-75.11	-0.30D	80.10
9	D 150 (NO PRECYCLING)	-98.28	-0.30D	82.59
10	D 150-B	-85.38	-0.15D	85.74
11	D 150-B (NO PRECYCLING)	-79.51	-0.15D	83.48

Table 4.8: Peak tensile load F_T and vertical displacement at peak tensile load $u_{z,T}$ comparison of pull-out rate by drainage path.

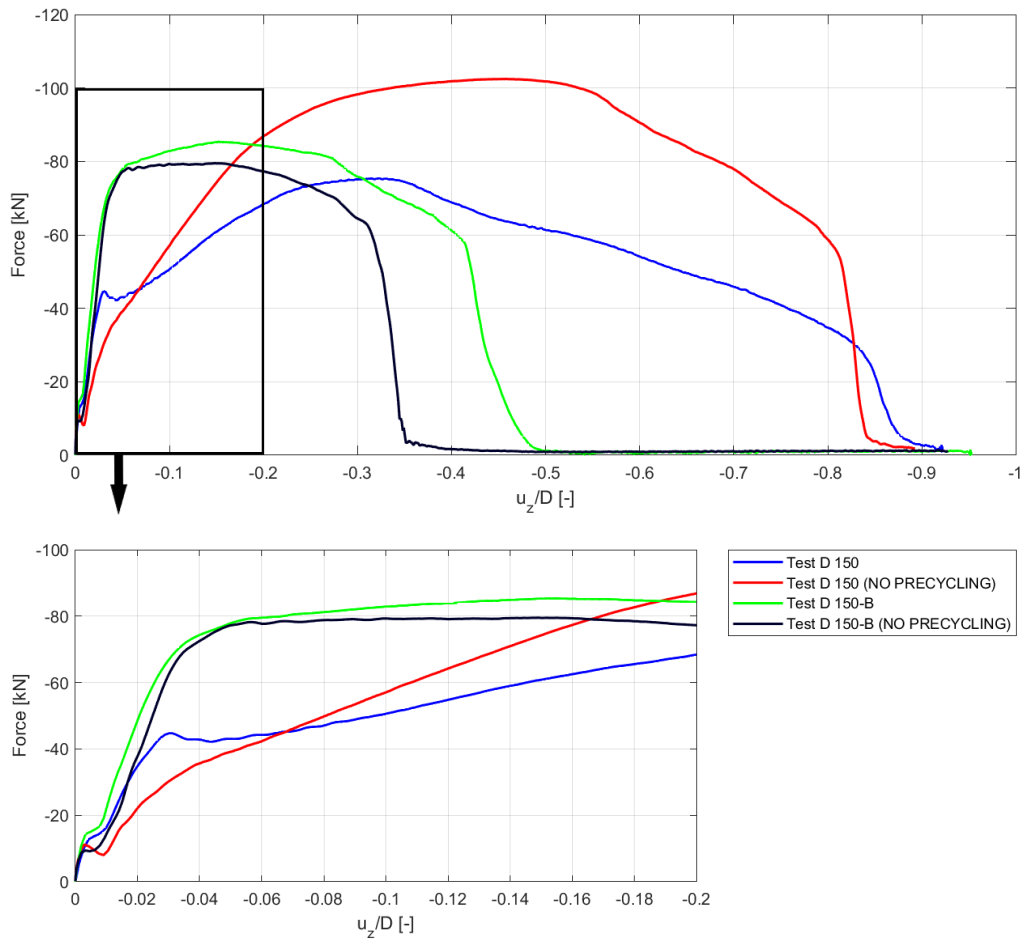


Figure 4.26: Force vs displacement response for all the tests rate 150 mm/s in dense sand during the pull-out phase.

It can be noted that the higher peak tensile load is observed for bucket A without cyclic load (D150 NO PRECYCLING), followed by peak tensile load of bucket B with cyclic load (D150-B), although both peak tensile loads for bucket B are similar. While D150 (NO PRECYCLING) presents the higher peak tensile load, results observed in tests with bucket B could be more favorable in terms of design, since their peak tensile load is present at smaller displacements.

It is also observed that the cyclic loading decreases the peak tensile load for bucket A. It could be that the cyclic load produced dilation of the soil in test D150, loosening the initial density and thus reducing the peak tensile capacity. This is not the case for bucket B where the peak tensile capacity of D150-B is higher than D150-B (NO PRECYCLING), although they are both very similar.

From Figure 4.27 can be observed that tests D150 (NO PRECYCLING) and D150-B have a negative pore pressure development very close to the theoretical cavitation limit of -300 kPa.

4.4 Comparison with previous work

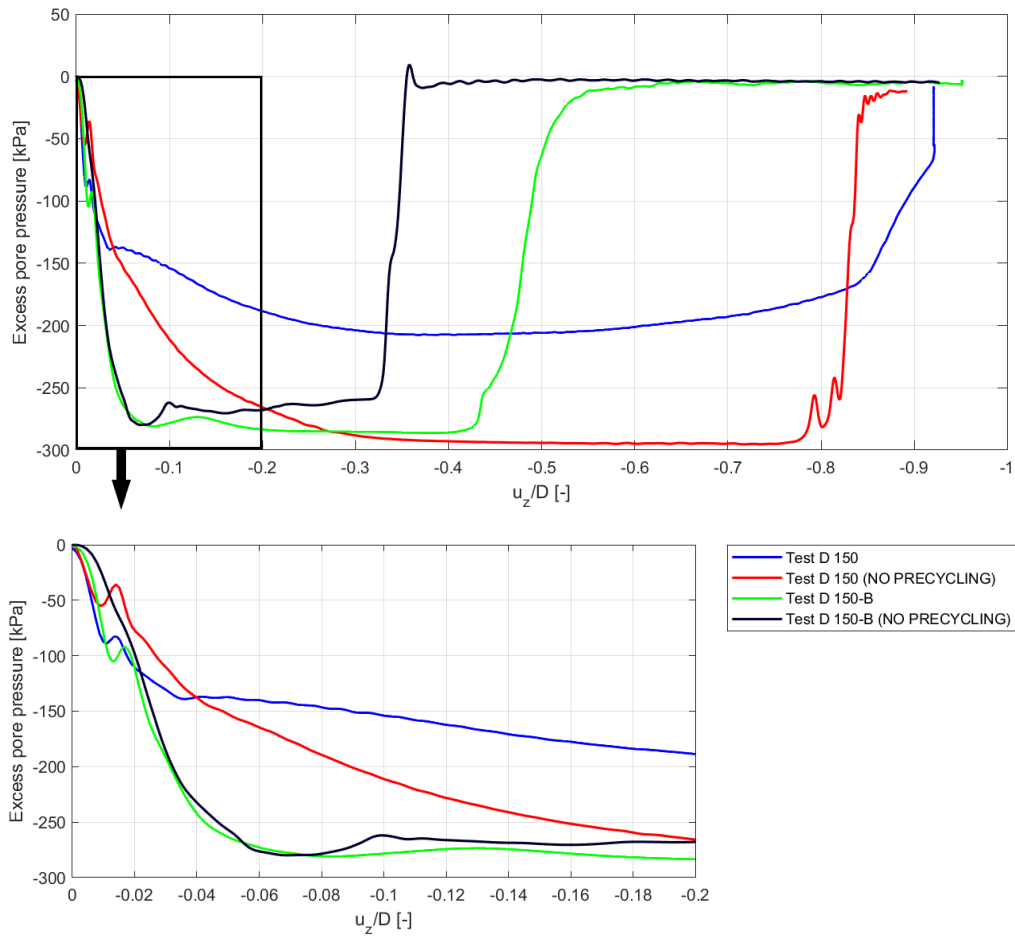


Figure 4.27: Excess PP vs displacement response for all the tests rate 150 mm/s in dense sand during the pull-out phase.

4.4 Comparison with previous work

Results can be further compared to the work done by Vaitkunaite (2016), who tested Bucket B in dense sand in the pressure tank also applying $\approx 200kPa$ without considering pre-cyclic loading.

Firstly, the tests done by Vaitkunaite (2016) are compared to the tests of similar displacement rate done with bucket A in dense sand with pre-cyclic loading, as shown in Figure 4.28. It is important to note that Vaitkunaite (2016) zeroed down the self-weight of the bucket model and displacements, thus results can be directly compared.

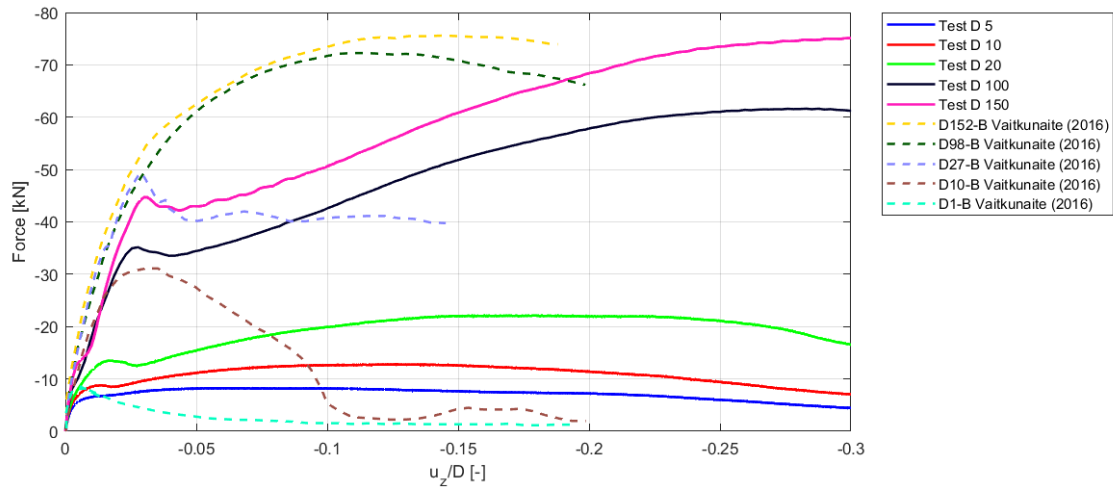


Figure 4.28: Load vs displacement response during the pull-out phase for tests with displacement rates: 1, 10, 27, 47, 98 and 152 mm/s done by Vaitkunaite (2016) and tests D5, D10, D20, D100 and D150 executed in this testing campaign.

Table 4.9 shows the results of peak tensile capacity, displacement at peak tensile capacity and density of tests shown in Figure 4.28. It also collects information of other tests presented by Vaitkunaite (2016), but their plotting is not possible due to missing data.

Results current testing campaign					Vaitkunaite (2016) results				
Test No.	Test ID	F_T [kN]	$u_{z,T}$	D_r [%]	Test ID	Rate [mm/s]	F_T [kN]	$u_{z,T}$	D_r [%]
1	D 005	-2.16	-0.01D	70.70	D 005-B	0.05	-2.70	-0.001D	85.00
2	D 5	-8.24	-0.06D	75.24	D 1-B	1	-8.00	-0.01D	90.00
3	D 10	-12.80	-0.13D	79.56	D 10-B	10	-30.80	-0.03D	90.00
4	D 20	-22.13	-0.18D	76.11	D 22-B	22	-44.10	-0.03D	83.00
-	-	-	-	-	D 27-B	27	-48.80	-0.03D	85.00
5	D 50	-43.09	-0.29D	80.59	D 47-B	47	-65.40	-0.10D	83.00
7	D 100	-61.63	-0.28D	80.12	D 98-B	98	-71.70	-0.12D	82.00
8	D 150	-75.11	-0.30D	80.10	D 152-B	152	-75.20	-0.14D	84.00

Table 4.9: Comparison of results of the current testing campaign with results obtained by Vaitkunaite (2016).

In the tests performed by Vaitkunaite (2016) also show increasing peak tensile capacity with increasing pull-out rate. It can be observed that the increase in peak tensile capacity is higher from D 005 to D 150 (34.77 times) than the increase from D 005-B to D 152-B (27.85 times). Moreover it is also noted in both cases that the peak tensile displacement increases with increasing peak tensile resistance.

Comparing the two testing campaigns, it is observed that the peak tensile loads are higher for results made with Bucket B without pre-cyclic loading, although the peak tensile loads of D150 and D152-B are very close. Vaitkunaite (2016) assumes that the maximum upward displacement allowed for a design case is 0.05D (serviceability limit state SLS), considering this, most of the peak tensile loads of the present testing campaign require higher displacement than the allowed, therefore to respect this limit, the peak to consider should be lower. From the tests performed by Vaitkunaite

4.4 Comparison with previous work

(2016) only D98-B and D152-B exceed this displacement limit, nevertheless, considering a upward displacement of $0.05D$, these peak tensile loads are still the highest of the comparison. SLS is not considered in the scope of this project, but it is only mentioned for comparison purposes.

Vaitkunaite (2016) mentions that PP transducers of test D152-B present almost identical measurement, explaining that the test response should be understood as fully undrained due to no inner water flow present. It is also assumed by Vaitkunaite (2016) that test D152-B reached cavitation although the test did not reach -300 kPa , explaining that deviations from this value can be affected by imperfect saturation of the PP pipes, air bubbles in the sand and measurement accuracy of the PP sensors. Figure 4.29 shows a comparison of the maximum generation of excess pore pressure along the skirt for Tests D152-B, D150 and D500.

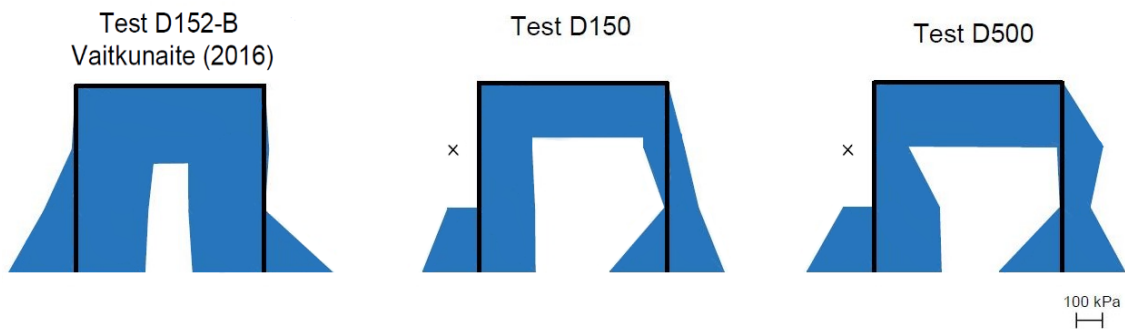


Figure 4.29: Peak excess PP along bucket skirt comparison. Buckets are not up to scale. Where: x represents a non available reading.

From Figure 4.29 can be observed that while Vaitkunaite (2016) considers Test D152-B with a fully undrained response. Neither Test D150 nor the maximum displacement rate test D500 meet these characteristics, since the developed suction is not similar in all the interior PP sensors. Therefore following Vaitkunaite (2016) parameters Tests D150 can not be understood as a fully undrained response.

To further develop this comparison, two other tests are performed as part of the present testing campaign using the same bucket used for Vaitkunaite (2016): bucket B. These are done at a rate of 150 mm/s with and without cyclic loading. In Figure 4.30 the results of these two tests can be compared to the results obtained by Vaitkunaite (2016) with Test D-152-B.

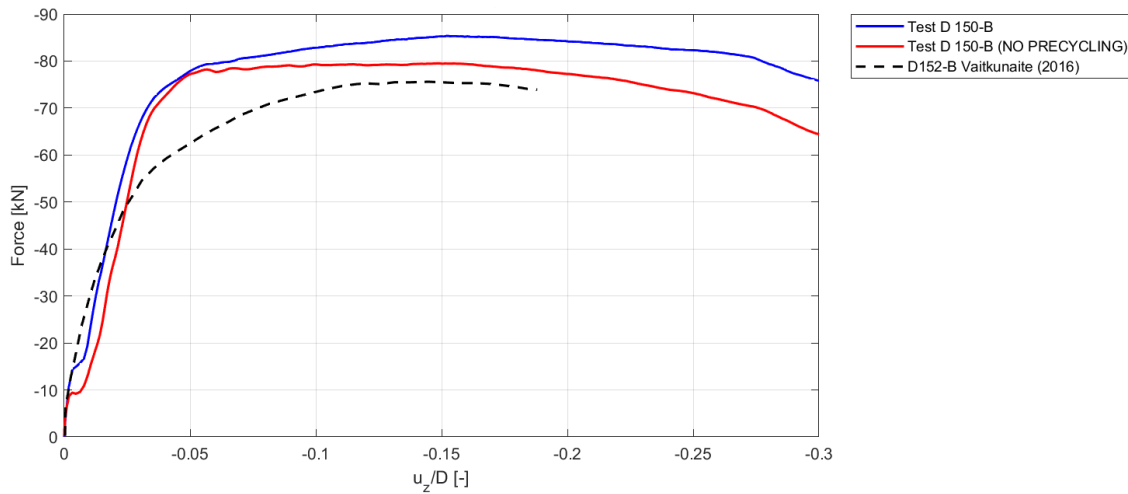


Figure 4.30: Load vs displacement response during the pull-out phase for tests with displacement rates 152 mm/s done by Vaitkunaite (2016) and tests D150-B with pre-cyclic loading and D150-B without pre-cyclic loading executed in this testing campaign.

Table 4.10 shows the results of peak tensile capacity, displacement at peak tensile capacity and density of tests shown in Figure 4.30.

Test No.	Test ID	F_T [kN]	$u_{z,T}$	D_r [%]
10	D 150-B	-85.38	-0.15D	85.74
11	D 150-B (NO PRECYCLING)	-79.51	-0.15D	83.48
-	D 152-B	-75.20	-1.14D	84.00

Table 4.10: Comparison of results of tests in Bucket B with rate 150 mm/s from the current testing campaign and the ones obtained by Vaitkunaite (2016).

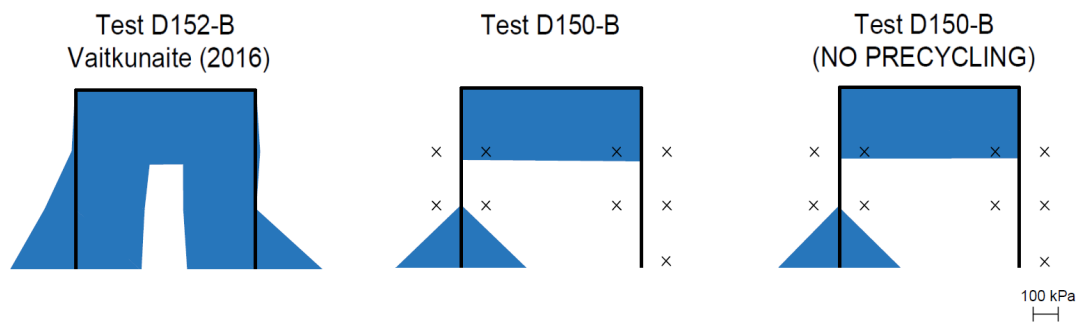


Figure 4.31: Peak excess PP along bucket skirt comparison. Buckets are not up to scale. Where: x represents a non available reading.

Vaitkunaite (2016) states that Test D152-B is assumed to experience cavitation at a higher excess pore pressure than the -300 kPa following the theory. Vaitkunaite (2016) explains that deviations from theoretical value can be influenced by imperfect saturation of the PP pipes in the bucket, air bubbles in the sand and measurement accuracy of PP sensors. Comparing this to the results performed in this testing campaign in Figure 4.31 and having a look to Figure 4.27 which

4.4 Comparison with previous work

shows the excess pore pressure development for Tests D150-B and D150-B (NO PRECYCLING), it could be that following Vaitkunaite (2016) recommendations, cavitation is reached with a small deviation (excess PP are very close to -300 kPa). It can also be observed from Figure 4.31 that a similar excess pore pressure development is experience in the three cases where the information is available regardless of cycling load is applied or not. However due to it was not possible to perform the test with all the PP sensors working in bucket B, no hard statements can be made regarding a full undrained behavior.

Discussion

It was found a tendency of denser soils having a higher peak tensile load and a higher initial stiffness. However, this trend was not present in all of the tests. For example, in the case of the rate of 150 *mm/s* D150, showed opposite behaviour than expected, having the denser soil with a lower peak tensile capacity and lower stiffness than the rest of the tests.

Possible effect of cyclic loading was analysed, but no trend was observed regarding the variations in the peak tensile capacities of the different tests. This analyse showed that the cyclic load provokes some settlements in the soil together with dilation of the sand. It was observed that the amount of accumulated displacement was higher in looser soils. Since no CPTs can be done after the test is started, there is no proof that the soil properties were affected in a different way in between the densities.

More than one peak were found in in the force and excess PP response of each test, except for tests with rate 0.05 *mm/s*, where this peak represented the peak tensile capacity. For the tests with pull-out speed higher than 0.05 *mm/s* the first peak was found to take place at the same point of the displacement in every test and same point of peak tensile capacity for tests with rate 0.05 *mm/s*. These first peaks do not show significant change through the different tests densities regarding their tensile force and displacement at which they take place, but they show a change with changing speed rates. This trend could suggest that the first peak of the tests is equivalent to the frictional resistance of the bucket, which is the higher resistance in the test rate 0.05 *mm/s*, which was meant to be fully drained.

The second peak appeared only at rates which are equal or higher than 50 *mm/s*. The tendency in these peaks is similar in behaviour regarding the fact that they don't depend on the density when experiencing the local peak and the displacement where they take place. These second peaks can be explained for the tests with partial drainage where pore pressure has to be mobilised in the gap between the lid and the soil, after the friction force has occurred. This mobilises the seepage flow and once the gap is filled, the soil plug starts moving together with the bucket. Since it is not possible to see what is happening in the interior of the bucket, it cannot be measured what is happening to the plug. If this behaviour could be explained with this hypothesis, then it could be a good measurement of the plug height.

Previous researches are found to have experienced small peaks previous to the peak tensile resistance. Unfortunately, they do not analyse the phenomenon behind this behaviour.

After performing the tests, it was observed that the failure mechanisms were different with respect to the change in speed. Rate 0.05 was found to have only a frictional failure, where the soil does not experience visible volumetrical strain. The rests of the tests formed what is so called 'a

soil plug' that increases together with the speed rate, until reaching a fully undrained behaviour where the plug, theoretically, is the same height as the distance traveled by the bucket. As explained above, a real measurement of this soil heave is missing, but it can be explained from empirical observations.

Visual proofs of the soil plug can be described since during partial and maybe fully undrained behaviour was observed that after the test was finished, it was observed that a soil plug was lifted with the bucket and in some cases, it was fully separated from the rest of the soil in the tank. In some cases, the soil plug was touched by the hands of the students performing the tests. For the higher rates, after visually verifying that the soil plug was formed, the valves on the lid of the bucket were open, and suction was lost, thus the soil plug falling down.

The difference in densities in the different tests were also observed during installation since in looser soils, water mixed with sand was coming out of the valves, indicating that the bucket is almost touching the mudline. In the opposite scenario, for higher densities, little to almost no sand was observed together with the water coming out of the valves. The reason to monitor the load reading during second installation was very important for denser soils in order to not compress the soil with the pushing of the bucket on the soil surface.

In previous research a fully drained condition was performed with a bucket foundation model with open valves. Thus avoiding any generation of suction and obtaining results in pure drained condition. This approach questioned the nature of the test performed with the pull-out rate of 0.05 mm/s since small negative excess pore pressure was generated and maybe it could even be considered as a mild partially drained behaviour.

The theoretical limit for cavitation at 200 kPa is -300 kPa . There was no tests in this testing campaign which reached the limit of 300 kPa , although some of them were very close. Following Vaitkunaite (2016) statements, it can be that certain laboratory test conditions may impact the limit of cavitation, making it possible to have some of the tests experienced at higher excess pore pressure.

Conclusion and future work

Laboratory utilities can be improved in order to have a better understanding of the phenomenon happening inside and around the bucket when it is subjected to tensile loading. The first suggestion is to implement a transparent bucket where the seepage feeling up the gap in between the soil and the lid and the height of the soil plug can be monitored and measured. Another improvement in the testing conditions could be to adapt pore pressure sensors which can provide readings of the soil around the bucket to have a better understanding of the change in excess pore pressure in a larger volume.

Furthermore according to Kelly et al., 2006b the three parameters that control the transient tensile capacity of suction buckets: permeability of the soil, rate of loading and length of the drainage path. This theory could be improved by investigating the influence of additional parameters:

- Dilatancy;
- Drainage path.

Moreover can be stated that this is only a small part of a bigger research and that more data and testing is needed in order to make stronger conclusions.

Finally can be suggested for future work to perform a similar testing campaign that does not take into account the cyclic loading, or decreasing the limits of the cycles in order to affect the densities of the soil as least as possible.

Bibliography

- Achmus, M., Akdag, C. T. & Thieken, K. (2013). Load-bearing behavior of suction bucket foundations in sand. *Applied Ocean Research*, 43, 157–165. <https://doi.org/10.1016/j.apor.2013.09.001>
- Barari, A. & Ibsen, L. B. (2012). Undrained response of bucket foundations to moment loading. *Applied Ocean Research*, (36), 12–21.
- Barari, A., Ibsen, L. B., Ghalesari, A. T. & Larsen, K. A. (2017). Embedment effects on vertical bearing capacity of offshore bucket foundations on cohesionless soil. *International Journal of Geomechanics*, 17(4), 10.
- Bhattacharya, S. (2019). *Design of foundations for offshore wind turbines*. John Wiley & Sons, Ltd.
- Byrne, B. W. & Houlsby, G. T. (2003). Foundations for offshore wind turbines. *Philosophical Transactions of the Royal Society of London. Series A: Mathematical, Physical and Engineering Sciences*, 361(1813), 2909–2930.
- Cavazzi, S. & Dutton, A. G. (2016). An offshore wind energy geographic information system (owe-gis) for assessment of the uk's offshore wind energy potential. *Renewable Energy*, 87, 212–228.
- Damgaard, M., Zania, V., Andersen, L. V. & Ibsen, L. B. (2014). Effects of soil–structure interaction on real time dynamic response of offshore wind turbines on monopiles. *Engineering Structures*, 75, 388–401.
- Foglia, A., Ibsen, L. B., Nielsen, S. K., Mikalauskas, L. et al. (2013). A preliminary study on bucket foundations under transient lateral loading. *The Twenty-third International Offshore and Polar Engineering Conference*.
- Gütz, P. S. (2020). *Tensile loaded suction bucket foundations for offshore structures in sand* (PhD Thesis). Leibniz University Hannover. Hannover, Germany.
- Houlsby, G. T., Ibsen, L. B. & Byrne, B. W. (2005). Suction caissons for wind turbines. *Frontiers in Offshore Geotechnics I: Proceedings of the First International Symposium in Frontiers in Offshore Geotechnics (ISFOG), Perth, Australia*, 75–93.
- Houlsby, G. T., Kelly, R. B. & Byrne, B. W. (2005b). The tensile capacity of suction caissons in sand under rapid loading. *Proceedings of the international symposium on frontiers in offshore geomechanics, Perth*, 405–410.
- Ibsen, L. B., Barari, A. & Larsen, K. A. (2012). Modified vertical bearing capacity for circular foundations in sand using reduced friction angle. *Ocean Engineering*, 47(4), 1–6.
- Ibsen, L. B., Hanson, M., Hjort, T. & Thaarup, M. (2009). *MC-parameter calibration of Baskarp sand no. 15* (DCE Technical Reports No. 62). Department of Civil Engineering, Aalborg University. Aalborg, Denmark.
- Ibsen, L. B., Liingaard, M. & Nielsen, S. A. (2005). Bucket foundation, a status. *Proceedings of the Copenhagen Offshore Wind*, 26–28.

- Kelly, R. B., Houlsby, G. T. & Byrne, B. W. (2006a). A comparison of field and laboratory tests of caisson foundations in sand and clay. *Géotechnique*, 56(9), 617–626.
- Kelly, R. B., Houlsby, G. T. & Byrne, B. W. (2006b). Transient vertical loading of model suction caissons in a pressure chamber. *Géotechnique*, 56(10), 665–675.
- Nielsen, S. D. (2016). *Transient monotonic and cyclic load effects on mono bucket foundations* (PhD Thesis). Aalborg University. Aalborg, Denmark.
- Senders, M. (2009). *Suction caissons in sand as tripod foundations for offshore wind turbines* (PhD Thesis). The University of Western Australia. Perth, Australia.
- SPTOffshore. (2021). *Wind turbine generator (wtg) foundations* [<https://www.sptoffshore.com/wind-turbine-generator-wtg-foundations/>].
- Sun, L., Qi, Y., Feng, X. & Liu, Z. (2020). Tensile capacity of offshore bucket foundations in clay. *Ocean Engineering*, 197, 106893.
- Terzaghi, K. (1943). *Theoretical soil mechanics*. John Wiley; Sons, Inc.
- Thieken, K., Achmus, M. & Schröder, C. (2014). On the behavior of suction buckets in sand under tensile loads. *Computers and Geotechnics*, (60), 88–100.
- Vaitkunaite, E. (2016). *Physical modelling of bucket foundations subjected to axial loading* (PhD Thesis). Aalborg University. Aalborg, Denmark.
- Vaitkune, E., Nielsen, B. N. & Ibsen, L. B. (2016). Bucket foundation response under various displacement rates. *International Journal of Offshore and Polar Engineering*, 26(2), 116–124.

APPENDIX A

Test Setup and Procedure

Aalborg University's Geotechnical Laboratory accommodates a series of equipment that made possible to conduct each test with the required conditions to satisfy the research. Besides the above, a procedure is stipulated in order to carry out the experiments with a certain protocol, thus making sure that all of them are conducted in the same way.

The following sections present a detailed description of the test facilities and procedures used during the laboratory work.

A.1 Test Facilities

In this Section the main equipment and tools available for carrying out the tests are going to be described.

A.1.1 Bucket foundation models

Most of the tests are performed with a bucket foundation model A (Bucket A) of diameter $D = 0.50$ m and skirt $L = 0.50$ m, which is the chosen dimension for this investigation and it is shown in Figure A.1. A shorter one, Bucket B illustrated in Figure A.2, is used later on, since it has been used before by Vaitkunaite (2016) and results can be used for comparison and study. The dimensions of the last one are $D = 0.50$ m and skirt $L = 0.25$ m.

In order to measure data during each test, pore pressure (PP) sensors in are attached to the tanks as shown in Figure A.3. Bucket A has them in two sides of the skirt, inside and outside of the bucket, and in three different heights: at the lid, in the middle and at the bottom. Due to the reduced time for performing tests in Bucket B, only three PP sensors are adapted to this bucket: two right under the lid and one on outside the skirt, at the bottom.



Figure A.1: Bucket A with PP sensors attached to the piston.



Figure A.2: Bucket B with PP sensors attached to the piston.



Figure A.3: PP sensors attached to Bucket A.

A.1.2 Pressure Tank

The pressure tank illustrated in Figure A.4 is used for testing the tensile capacity of the bucket foundations. This large steel container with cylindrical shape is able maintain up to 200 kPa , limit set for safety reasons, which is equivalent to 20 msw once is sealed, thus simulating a offshore condition. The dimensions of the tank are approximately 2.10 m interior diameter and 2.10 m height.

The tank contains 0.60 m of Aalborg University Sand No.1 and 0.30 m of gravel at the bottom for ensuring a free water flow from and to the bottom. The sand is retained by a filter layer located in between the sand and the gravel. This is a geotextile membrane that allows water to flow through it without draining the sand. A valve connected at the bottom allows to both drain and saturate the sand. The saturation is done by applying a water gradient, which comes from a water tank placed approximately 20 m above the pressure tank.



Figure A.4: Tank with piston installed at the top and Bucket B attached to the piston inside.



Figure A.5: Closed tank entrance.

The piston shown in Figure A.4, which is installed on top of the tank makes possible the displacement of the different equipment inside the tank up and down in vertical direction and the application of force.

A.1.3 MTS FlexTest Controller

MTS FlexTest Controller (Figure A.6) allows to control the force and motion precisely, thus to control the tests accurately. This hardware makes it is possible to control the piston (displacement or force control), calibrate and configure the equipment, create test procedures as desired, and acquire, control and save the data.

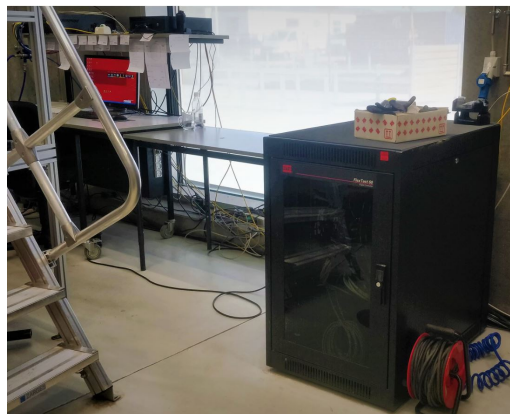


Figure A.6: MTS FlexTest.

Part of the units is a data acquisition hardware with different channels to connect the signal of the equipment for the chosen test. This project uses 16 signals: load cell, 12 PP sensors, Cone Penetration Test (CPT) equipment, PP calibration station and an extra PP sensor measuring the pressure inside the tank, this last one used only for checking purposes only.

MTS also counts with different software applications, and three of them are used in this project. The main one is the Station Manager shown in Figure A.7, which has many features, such as starting the pump and controlling the piston from the "Station Controls" pane. The piston is configured to move through a range of 0.52 m, the limits are set to be -0.26 m and 0.26 m. It is also possible to see the reading of the connected signals in real time, zero them down, calibrate them, etc. This program is used mainly before and after running a test (test preparation and cleaning up).

Testing operation is also possible from the above described application, but in this project the MTS Multipurpose Elite is the software used to configure and save the tests procedure both tensile and CPT. In this application it is possible to control the system on how to perform the test adding different functions that send different orders such as: how much force or displacement to apply, configure cycles, rates, when to record the data, when and where saving the data, etc. The described above is defined by a "spaghetti code". The tests are saved as files and stored to use them with the same configuration when needed.

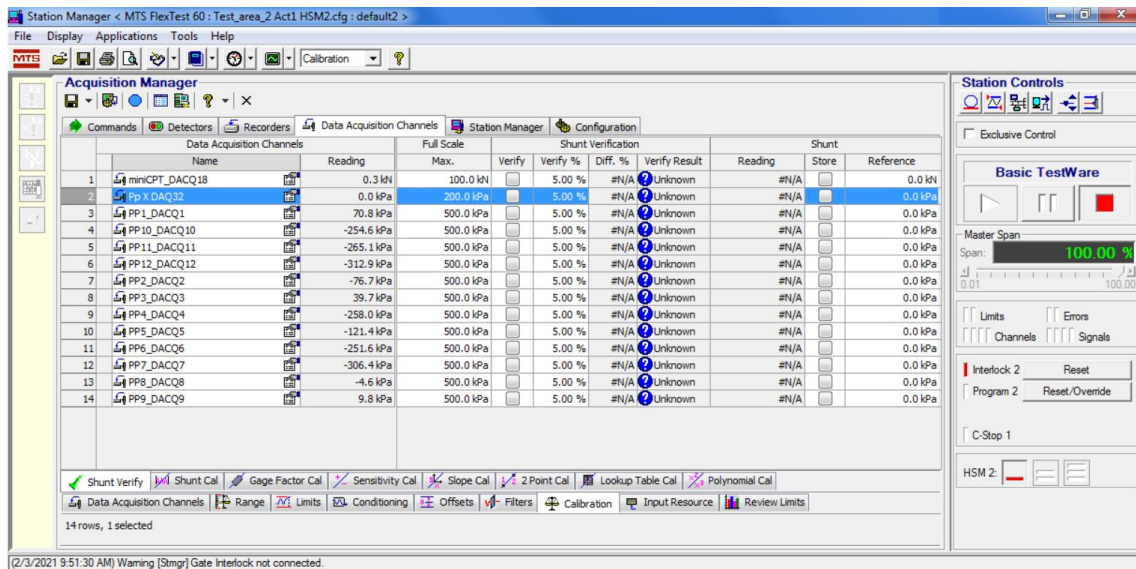


Figure A.7: MTS Station Manager, data acquisition channel view.

A third application is used, the MTS Data Display, where different view panes are configured in order to display different group of data and graphs, allowing a better overview of the different processes.

A.1.4 Load Cell

The load cell is a force transducer that makes it possible to measure the force both in tension and compression during the tests. It is illustrated in Figure A.8 together with a part of the piston and one of the extension bars used in this project when the length of the piston is not enough for the desired displacement.

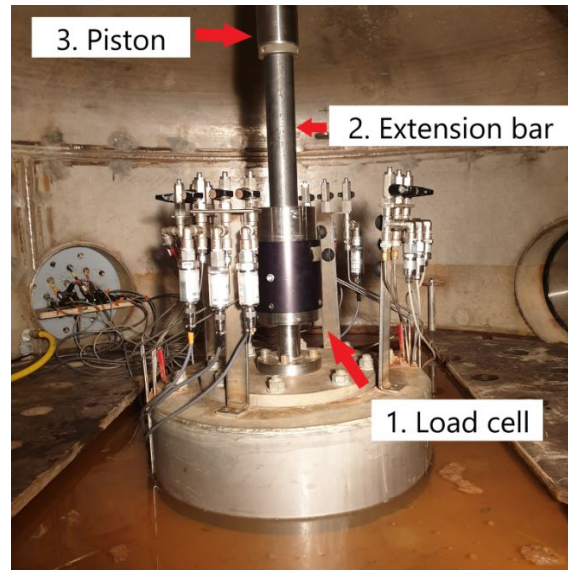


Figure A.8: Bucket A installation. 1. Load cell 2. Extension Bar 3. Piston.

A.1.5 PP Sensors' Calibration Station

In order for the MTS Station Manager to show a correct PP signal, it is necessary to find the calibration factor of each one of the PP sensor. A PP calibration station is used, as shown in Figure A.9 where each PP sensor is connected and pressure can be applied manually. The right calibration factor is introduced in the MTS Station Manager and a proof of the right reading is that both 1. MTS Station Manager and 2. Real pressure display show the same reading as in Figure A.9.

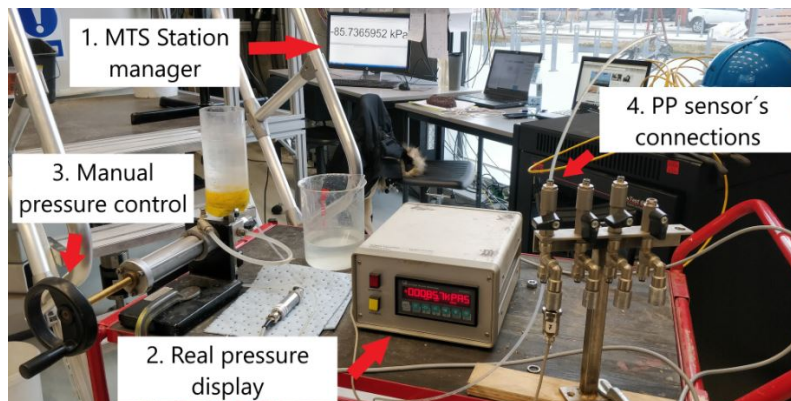


Figure A.9: PP sensor's calibration station.

A.1.6 Soil vibrators

This research covers different tests not only with different rates, but with different soil relative densities D_r . For the densification of the soil, vibrators (Figure A.10) are used to rearrange the particles of soil, placing them closer to each other by introducing the rods in the soil with a determined pattern following the tank boards orifices.



Figure A.10: Soil vibrator.

A.1.7 Mini-CPT Equipment

In order to verify the desired soil density D_r before each test, CPTs are conducted inside the tank with a mini-CPT cone penetrometer, measuring the cone resistance q_c along the depth of the sand with the device shown in Figure A.11. The soil density is derived later on from these results.



Figure A.11: Mini-CPT cone penetrometer.

To install this device, two of the metal extensions, length 0.25 m and 0.05 m , are attached to the piston inside the tank, to assure that the piston can reach the desired depth at the bottom without damaging the geotextile membrane under the sand as mentioned in Subsection A.1.4. These extensions are followed by a beam of length almost the perimeter of the tank, which is attached perpendicular to the extensions. The total installation is completed by attaching the cone penetrometer in one side of the beam and a "fake" cone penetrometer, that looks exactly as the original, in the other side of the beam. The function of the fake cone penetrometer is to provide a counterbalance in the other free end of the beam.

A.1.8 Bridge Crane

As some of the materials and equipment are very heavy, they can not be manipulated or carried by people and therefore these are maneuvered with a crane.

The geotechnical laboratory counts with a bridge or overhead crane (Figure A.12) in a installation with runways close to the ceiling, which can move horizontally (in two directions) and vertically (up-down) while being operated by a remote control.



Figure A.12: Bridge crane.

The crane weight capacity is approximately 100 kg. Some of the regular tasks operated by the crane are: lifting, lowering and moving the bucket foundation and tank's lid.

A.2 Test Procedure

In this section, a test manual is described, detailing the procedure that leads to the experiments performed for this project. It is important before starting anything to start the pump from the MTS Station Manager, so the piston can be controlled. When starting the pump MTS Station Manager has to be in displacement control mode for safety reasons.

A.2.1 Soil Preparation

Soil preparation includes two steps: loosening and densification.

Two different soil loosening approaches are tested:

1. Draining out totally the water of the tank through the draining system located at the bottom of the tank and then applying the water gradient saturating the sand again.
2. Applying a stronger water pressure by introducing a metal pipe attached to a hose through the orifices of the boards all the way to the bottom and moving around in order to loosen up as much as possible.

It is found that the first approach is not loosening up the soil homogeneously. It looses the top part and leaves the bottom compacted, therefore the gradient approach is used only at the beginning of testing and not longer used for the upcoming tests. The second approach of loosening with the

hose is used instead, but the amount of rounds around the board depends on the state of the soil before testing and the soil state needed for the test that is being prepared.



Figure A.13: Sand surface disturbed after second loosening approach: applying water pressure with a hose.

Regarding soil densification, two vibrators are used simultaneously operated by two persons inside the tank. This is done by pushing down the rods through the orifices of the boards in certain pattern. The amount and speed of vibration depends also on the state of the soil before testing and on the one needed later. Table A.2.1 indicates the necessary amount of loosening and vibrations in order to get a more homogeneous vibration profile and reach the desired density range.

D_r Last test	Required D_r	No. Loosening Rounds	No. Vibration Rounds
Dense	Dense	0	3
Dense	Medium	1	1
Medium	Medium	1	1 (quick immersion)
Medium	Loose	2	1 (quick immersion)
Loose	Loose	1	1 (quick immersion)
Loose	Dense	1	6

To go from loose to dense there is still need for one loosening, due to the soil looking very uneven after performing a test in low density, therefore one loosening round leaves the soil smoother.



Figure A.14: Vibration of soil inside pressure tank.

A.2.2 Cone Penetration Test

After loosening and/or vibrating the soil D_r has to be checked that is in the correct range. CPTs are performed in different locations to assure that the soil conditions meet the established in approximately the whole ratio of the tank.

The different steps and aspects to consider until obtaining the density profile of the soil are described bellow.

Calibration and check of mini-CPT cone

The first time using the cone penetrometer, it has to be calibrated. This is done by placing it in the floor pointing up as shown in Figure A.11 and making sure that it is connected to one of the channels.

A plastic cap is placed covering the tip, to protect the cone during this process, and then the reading signal is zeroed down from the MTS Station Manager by pressing "Auto Offset", which is found in the Properties of the Data Acquisition Channel as shown in Figure A.15. The reading is checked by placing an element of known weight on top of it as illustrated in Figure A.16. A 10 kg (0.098 kN) element is used in this case.

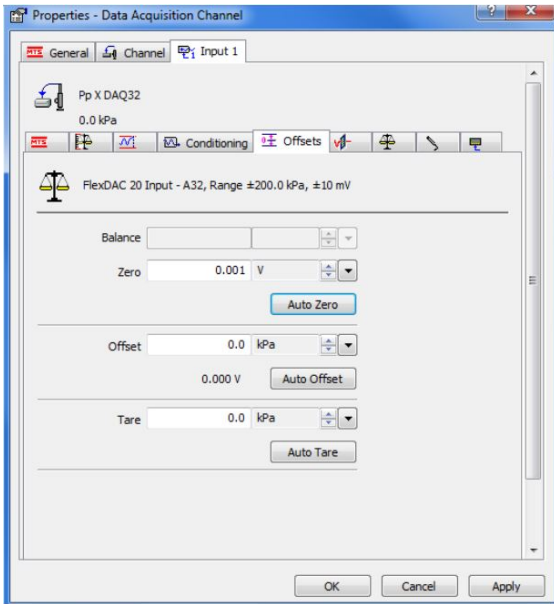


Figure A.15: MTS Station Manager - Properties of one of the data acquisition channels, where the reading can be zeroed down by clicking in "Auto Offset".

Figure A.16: Cone penetrometer calibration by checking reading of 0.098 kN element.

The signal reading is calibrated by finding the scale factor. The formula used to find it is shown in Equation A.1, thus the scale factor is calculated dividing the weight of the element by the non calibrated signal reading, displayed in the MTS Station Manager.

$$m_{elem} = SF \times \text{Signal}_{MTS} \tag{A.1}$$

Where:

m_{elem}	Known weight of an element in <i>kN</i>
SF	Scale factor
Signal_{MTS}	Reading signal displayed in MTS in <i>kN</i>

Once the scale factor is found, it is added to the reading channel in the Properties of the Data Acquisition Channel as shown in Figure A.17.

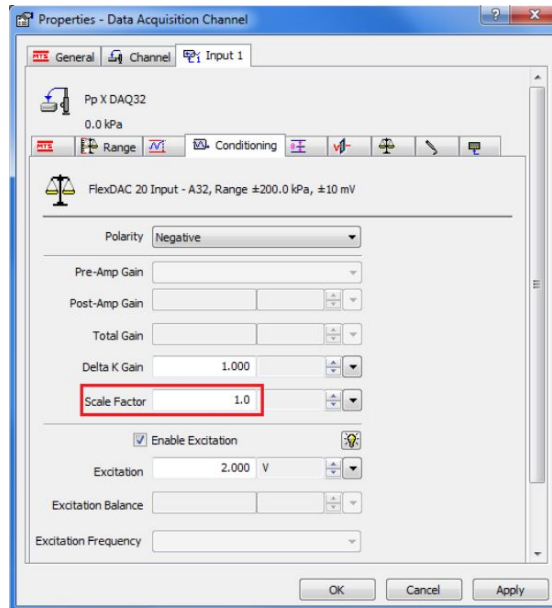


Figure A.17: MTS Station Manager - Properties of one of the data acquisition channels, where the scale factor can be added.

Every time before using the mini-CPT equipment, the reading has to be checked as described above: zeroing it down and placing an element of known weight on the cone. If the reading is not accurate, then a new scale factor has to be found and the whole process of calibration has to be done again.

Installation inside Pressure Tank

The pressure tank needs the right appliances for installing the cone penetrometer. Two metal extensions of 0.25 m and 0.05 m are first attached to the piston inside the tank, providing the necessary depth to reach almost the entire sand layer. These extensions are followed by a horizontal beam, in which the cone penetrometer and its fake version, for counterbalance, are installed as shown in Figure A.18.



Figure A.18: CPT being performed.

The test is performed in four radial positions from the center of the tank: at 0.19 m , 0.35 m , 0.51 m and 0.81 m in different angles, avoiding that vibration holes are coincident with the cone path, thus preventing to measure loose soil pockets that are not representative of the general soil condition. The right position is found manually by rotating the beam counterclockwise, ensuring that it will not detach. When the right position is found, from the MTS Station Manager the piston is moved down until just the cone is inside the sand. The test is now ready to be performed.

Running CPT

The test is configured and started from the MTS Multipurpose Elite Software. The configuration used in this project is shown in Figure A.19.

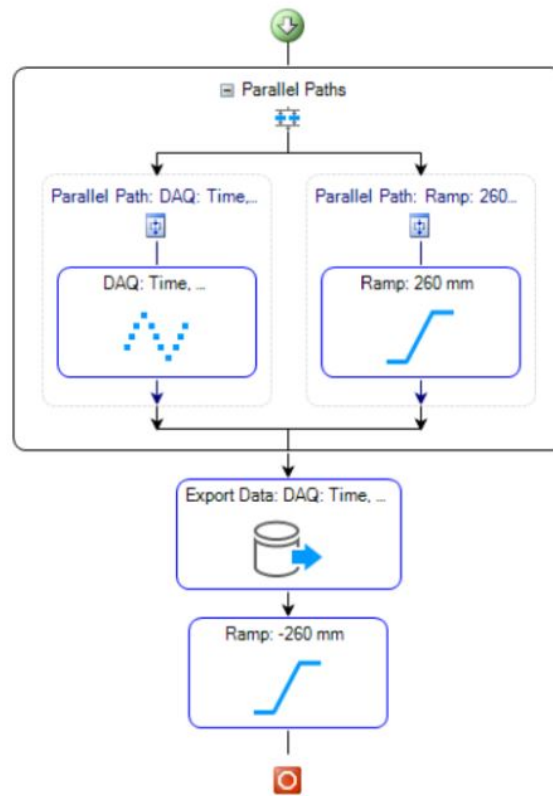


Figure A.19: CPT test configuration.

The test configuration is set to start with a parallel path, which means that there are two processes running at the same time: displacement control of the piston, from -0.26 m and 0.26 m as described in Subsection A.1.3, and the data acquisition, which records the measurements the readings. Later on in the configuration, the data is exported to the folder chosen prior to the test run. The last step is the final ramp, which allows the piston to comeback to initial position.

Estimating Relative Density of the Soil

Although CPT measures q_c , this data is used to calculate D_r with Equation A.2. This is a formula introduced by Ibsen, Hanson et al. (2009) to determine Aalborg University Sand No.1's D_r from a CPT using a mini-CPT cone.

$$D_r = 5.14 \left(\frac{\sigma'_{v0}}{q_c^{0.75}} \right)^{-0.42} \tag{A.2}$$

Where:

σ'_{v0}	Vertical effective stress in <i>MPa</i>
q_c	Cone resistance in <i>MPa</i>
Signal _{MTS}	Reading signal displayed in MTS in <i>kN</i>

The measured q_c data comes in kN , which is converted to MPa using Equation A.3.

$$q_c = \frac{1000 \cdot q_{c,measured}}{A_{cone}} \quad (A.3)$$

Where:

$$\begin{array}{l|l} q_{c,measured} & \text{Measured cone resistance in } kN \\ A_{cone} & \text{Area of the cone in } mm^2 \end{array}$$

$$A_{cone} = \pi r^2 \quad (A.4)$$

Where:

$$r \mid \text{Radius of the cone } 7.5 \text{ mm}$$

Knowing the material properties of the Aalborg University Sand No.1 and that the unit weight of water $\gamma_w = 9.81 \text{ kN/m}^3$, σ'_{vo} can be calculated through an iterative process. The material properties are collected in Table A.1.

Parameter	Notation	Value
Specific Gravity	G_s	2.640
Minimum Void Ratio	e_{min}	0.549
Maximum Void Ratio	e_{max}	0.858
50% Quantile [mm]	d_{50}	0.140
Uniformity Coefficient	U	1.780

Table A.1: Characteristics of Aalborg University Sand No. 1 determined by Nielsen (2016).

Equation A.5 calculates σ'_{vo} in MPa .

$$\sigma'_{vo} = \frac{\gamma' d}{1000} \quad (A.5)$$

Where:

$$\begin{array}{l|l} \gamma' & \text{Effective unit weight of a saturated soil in } kN/m^3 \\ d & \text{Soil depth in } m \end{array}$$

$$\gamma' = \frac{(G_s - 1)}{(1 + e)} \gamma_w \quad (A.6)$$

A.2 Test Procedure

As mentioned above, an iterative process is used to calculate the void ratio e and thus obtaining γ' . The iteration uses Equation A.7 and starts with the guessing $e = e_{min}$. A small tolerance error value is set to find an acceptable e value.

$$D_r = \frac{e_{max} - e}{e_{max} - e_{min}} \quad (A.7)$$

A.2.3 Preparing Bucket Foundation Model

Before the bucket foundation model can be installed, it has to be prepared in order to be able to measure data in an accurate way.

Cleaning Bucket Foundation's Pipes

When the bucket has been used before for testing, it is necessary to check that the pipes, from where the pore water pressure is measured, are clean of sand. This way permits a correct saturation of the sensors and avoids inaccuracies in the measurements.

Cleaning the bucket foundation model's pipes is done one by one with help of an air pistol, by blowing air from the top valve, while covering the part that connects the PP sensor. This sends the air down through the pipe provoking that any sand particle trapped in the pipe is blown out.

Calibrating PP Sensors

Just as the CPT reading signal has to be calibrated in the MTS Station Manager, the reading signal of the PP sensors has to be calibrated as well. The process and equipment are introduced in Subsection A.1.5, the procedure step by step is:

1. Connect a PP sensor
2. Free any air bubble trapped in the system from the superior valve
3. Connect PP sensor to a MTS data acquisition channel
4. Zero PP sensor signal down from the MTS Station Manager by pressing "Auto Offset" found in properties of the corresponding data acquisition channel as illustrated in Figure A.15
5. Zero real pressure display down
6. Apply pressure slowly from the manual pressure control of the calibration station
7. Since the reading in both the real pressure display and MTS Station Manager fluctuates very fast, a good approach to see the instantaneous reading is to take a photo that shows both of them.
8. Calculate the scale factor with Equation A.8
9. Introduce scale factor to the corresponding reading channel in the properties of the data acquisition channel shown in Figure A.17
10. Zero down both readings again
11. Apply pressure manually to check that both readings show the same value

12. Repeat with the next PP sensor

$$P_{real} = SF \times \text{Signal}_{MTS} \quad (\text{A.8})$$

Where:

P_{real}	Real pressure in <i>kPa</i>
SF	Scale factor
Signal_{MTS}	Reading signal displayed in MTS in <i>kPa</i>

A register of the twelve sensors used and installed in the bucket and sensor 13 used to measure and check the pressure inside the tank can be found in Table A.2. There are two types of sensors: the type used in sensors 1, 2, 3, 9, and 13 and the rest of the sensors.

PP Sensor No.	Data Acquisition Channel	Sensor ID	Scale Factor	Excitation Voltage	Range [mV]
1	1	16092509	5528.3	2	100
2	2	16092508	5603	2	100
3	3	16092505	5175.68	2	100
4	4	12116048-001A	17955.45	2	10
5	5	12116048-004A	18147.14	2	10
6	6	12126215-006A	17987.3	2	10
7	7	12126215-003A	21347.52	2	10
8	8	12126215-002A	21428.57	2	10
9	9	16092506	5294.67	2	100
10	10	12126215-008A	18157.99	2	10
11	11	12116048-005A	17995.95	2	10
12	12	12126215-012A	21422.9	2	10
13	13	16092502	5158.3	2	10

Table A.2: Register of pore pressure sensors

Attaching and Saturating PP Sensors

When the PP sensors are calibrated, they can be attached to the bucket as can be seen in Figure A.3. The bucket foundation model is carried with the crane to a barrel filled with water, where it is submerged protecting the PP sensors' connections from the water. Using a fine vacuum tube the sensors' system is saturated by sucking water from the top valve until no air bubbles are carried out, and closing the top valve before the vacuum tube is taken out.



Figure A.20: Bucket foundation model submerged in barrel filled with water for saturation of PP sensors' system.

A.2.4 Installing Foundation Model

The bucket foundation model is carried inside the pressure tank by the crane. A 0.25 m extension is added to the piston and then the load cell is attached and connected to a data acquisition channel. The load cell's reading signal is zeroed down from the MTS Station Manager and then checked by attaching a screw with a nut that helps to hold an element of known weight and then comparing its weight to the reading displayed in the MTS Station Manager.

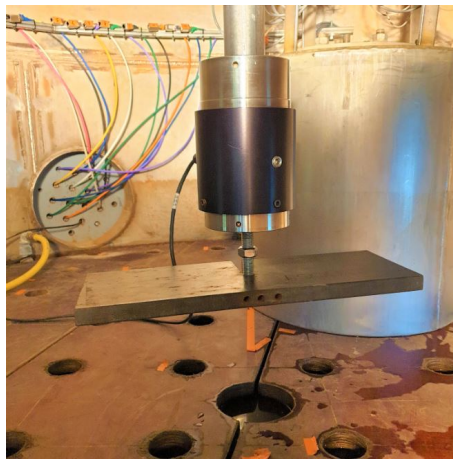


Figure A.21: 10 kg weight element supported by the load cell to check accuracy of reading signal.

Once the reading is proved to be accurate, the load cell leg is attached and the load cell is zeroed down again. The load cell leg is the element that permits attaching the foundation model to the piston system.

The bucket foundation is slid under the leg and the piston is lowered carefully in order to attach the leg to the model. The PP sensors can be now connected to the data acquisition channels. The bucket is lifted and the boards are removed outside the pressure tank.

The installation is configured and started from the MTS Multipurpose Elite Software.

Installation Bucket A

Due to its height, Bucket A can not be fully installed in one run. This installation is performed in two parts. The first one consist in running the test with maximum piston displacement when is only the 0.25 *m* extension added to the piston. Figure A.22 shows the first part of installation completed.



Figure A.22: Bucket A after first part of installation (one piston extension used).

A new extension of 0.20 *m* is added to the piston system in between the load cell and the load cell leg as shown in Figure A.23. The second part of the installation is with manual stop, and observation is needed. The test is stopped when the lid touches the sand, i.e. when the load cell register an abrupt increase in load and when maybe sand is coming out from the top valves of the foundation. When the installation is completed, Figure A.24, the valves of the bucket 's lid can be closed.

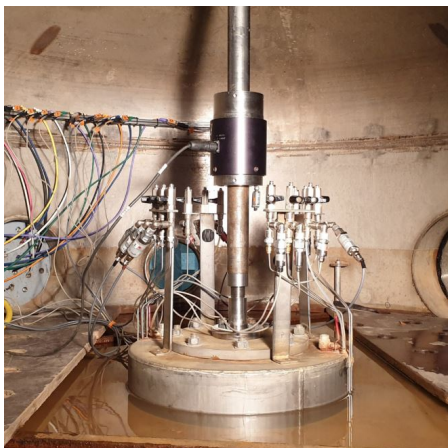


Figure A.23: Bucket A ready to start second part of installation (two piston extensions used).



Figure A.24: Bucket A installation completed.

Installation Bucket B

The skirt of Bucket B is shorter and therefore the installation can be carried out in one step. Only the 0.25 m extension is added to the piston and the test configuration is to be stopped manually when the load cell reading registers an abrupt increase in load and maybe sand is coming out of the valves.

A.2.5 Attaching hose

In order to raise the water level after the pressure tank is sealed, the hose is attached beforehand on the side board in a way that the stream of water disturbs the soil as little as possible.



Figure A.25: Hose attached inside the tank.

A.2.6 Sealing the tank

After checking that all the signal readings are working, the pressure tank is sealed. The lid is lifted and directed to the tank entrance with the crane. Using a pneumatic torque wrench, the lid is secured and the tank is sealed.



Figure A.26: Tank lid carried by the crane.



Figure A.27: Tightening of lid's bolts with pneumatic torque wrench to seal the tank.

A.2.7 Last Adjustments

After checking that all the valves of the tank are closed, except the one connected to the hose, the tank is filled with water as much as possible before reaching the PP sensor's connections and considering that the level of water is lower after pressurization.



Figure A.28: Water raised to a secure distance before the sensor's cable connection. Distance in between sensor and water is drawn as a red line.

A.2.8 Running the test

As mentioned above, the tests are configured and run from MTS Multipurpose Elite, where the piston can be controlled by force or displacement settings based on rate, time or displacement.

In this case, there is only one setting to change when performing a new test: the loading rate in mm/s . It also needs to be considered during the configuration that the chosen frequency of data points has to be higher enough to register a complete test in the case of testing with very high

A.2 Test Procedure

loading rate, when the pull-out test happens very fast.

During the test execution and when needed, the different readings available are controlled from the MTS Data Display, where different view panels are customized to different needs.

The complete test code is illustrated in Figures A.29 and A.30. Both are part of the same code and have been placed side by side for an easy overview.

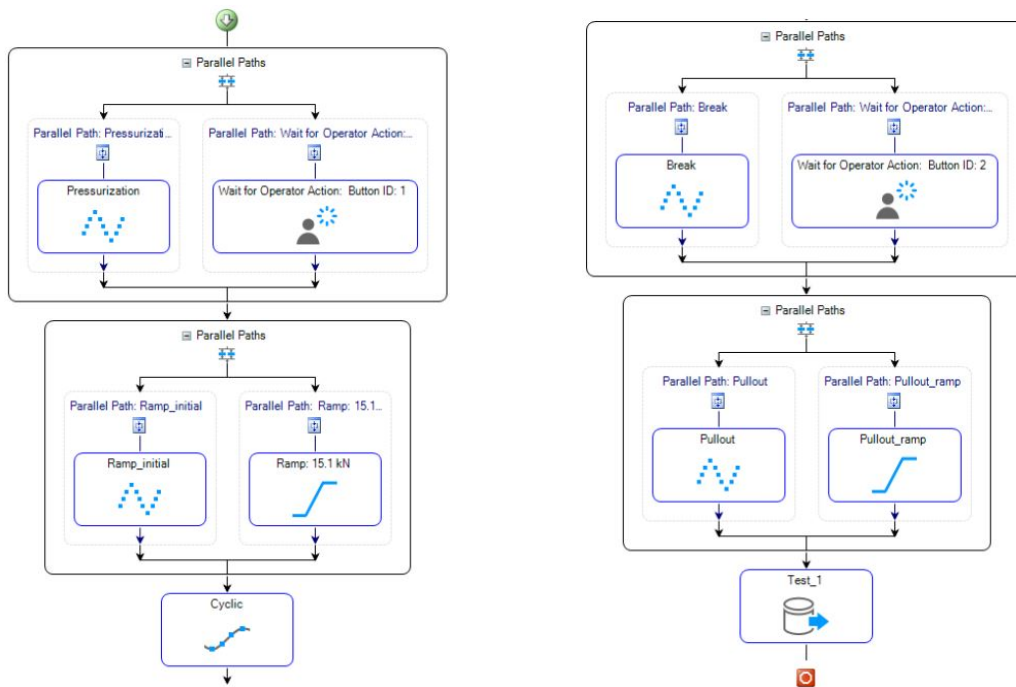


Figure A.29: Main test code: pressurization and cyclic loading. **Figure A.30:** Main test code: pull-out part. It comes right after cyclic loading shown in Figure A.29.

Considerations in test configuration

When installing a bucket foundation the soil is being failed, but in a real offshore scenario of regular waving, the soil starts to heal again with these very small loads. In order to perform the tests as it would occur in real life, assuming a regular day and storm-free installation, it is decided that before the monotonic load, a small cyclic loading of 5 % of the bearing capacity of the soil is applied.

Since the cyclic load is calculated based on the bearing capacity of the soil, it is programmed to act in *Force control* in the configuration. It is important to note that the cyclic load can not be tensile, since a tensile loading would start failing the soil provoking displacements before the actual tensile test, which could affect the results of its tensile capacity.

The readings in MTS software are negative when experiencing tensile forces and positive when exposed to compressive forces. In the very first test of this testing campaign the cyclic loading is configured with a ramp to reach the mean value of the loading, a positive force value, in a way that the peak forces would be equal or greater than 0, avoiding a two-way loading situation. Opposite to

expectation, results showed peaks of cyclic loading bellow 0, i.e. the soil underwent a small tensile loading. This unexpected result is explained by the effect that pressure has on the load cell.

A test is performed to analyze the effect of pressure on the load cell. It consists in pressurizing the tank only with the load pressure installed in the piston. This test is performed only once and its configuration can be found in Figure A.31, where the code tells to acquire the data and export it to the chosen folder.

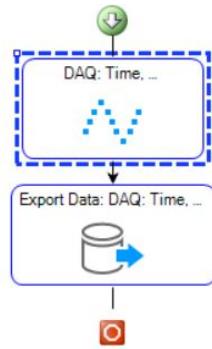


Figure A.31: Code for testing load cell under pressure.

The results are shown in Figure A.32. Looking at the plot force vs pressure, it is possible to observe a linear relation in between them, i.e. the reading signal from the load cell increases linearly with respect to the increase in pressure. The slope of this line is found $n = 0.0116$ and can be used to process the raw data measured by the load cell in all the tests.

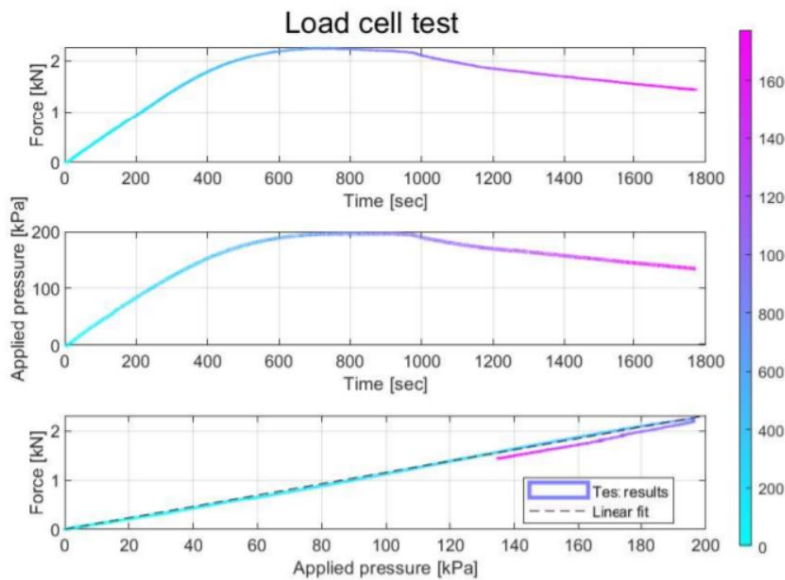


Figure A.32: Results of load cell test under pressure.

Pressurization

The test code starts with the parallel path in Figure A.29 that consists in the recording of the pressure reading inside the tank and a waiting time that tells the system to wait for a manual order

A.2 Test Procedure

to continue the test to the next step.

The pressure gauge attached to the tank is set to 2 *Bar* and after starting the test the pressure valves are opened to let pressure in, while MTS Multipurpose Elite records until the "continue" button is pressed.

The order to start the next part of the test is sent when the pressure inside the tank reaches approximately the 2 *Bar* and the reading signal looks stable in MTS. PP sensor No. 13 is the one assigned to measure the pressure inside the tank, by leaving it suspended in the air during testing.

Cyclic Loading

The next part of the test is configured to be a small cyclic load of 5% of the bearing capacity of the soil, assuming good weather during installation day with small wave loads.

As can be seen in Figure A.29, before the cyclic load is applied, a parallel path starts with data recording and a ramp in which the piston is commanded to act in *Force control* until reaching the mean value of cyclic loading. The mean value is 13.5 *kN*, but considering the effect of pressure in the load cell, the ramp is set to 15.1 *kN*, which is the mean value of the loading after pressurization. After finalizing the ramp, the cyclic loading starts. The code is set to 1000 cycles with rate of 0.1 *Hz*.

The uniaxial vertical bearing capacity of the soil is calculated according to Barari et al. (2017). The formula is presented in Equation A.9, which is a theoretical relationship found by Ibsen, Barari et al. (2012) from adapting the traditional formula for bearing capacity proposed by Terzaghi (1943). The calculation includes a reduced friction angle ϕ_d for the analysis of small-scale physical models as well as a depth factor based on Finite Element Analysis.

$$V_{peak} = \gamma \frac{D}{2} N_\gamma \left(\frac{\pi D^2}{4} \right) + q N_q \left(\frac{\pi D^2}{4} \right) \quad (\text{A.9})$$

Where:

γ	Unit soil weight
D	Bucket diameter
N_γ	Bearing capacity factor
N_q	Bearing capacity factor
q	Overburden pressure

$$q = w \cdot \gamma' \quad (\text{A.10})$$

Where:

w	Vertical settlement at failure
-----	--------------------------------

The bearing capacity factors are calculated according Equations A.11.

$$\begin{aligned}
 N_\gamma &= c_1 \cdot [(N_q - 1) \cos \phi_d]^{c_2} \\
 N_q &= c_3 \cdot e^{c_4 \cdot \pi \cdot \tan \phi_d} \tan^2 \left(45 + \frac{\phi_d}{2} \right)
 \end{aligned}
 \tag{A.11}$$

As stated by Barari & Ibsen (2012), the suction generated during installation prevents detachment between foundation and soil, so the interface soil-foundation behaves entirely bonded. Therefore it is appropriated to assume a rough offshore foundation to prevent detachment between them (Barari et al., 2017).

Coefficient	Circular-Rough
c_1	0.16
c_2	1.33
c_3	0.80
c_4	1.50

Table A.3: Values of coefficients in Equation A.11 for rough circular foundations.

The reduced friction angle is obtained from Equation A.12.

$$\phi_d = 0.214D_r + 22.86
 \tag{A.12}$$

The corrected vertical bearing capacity from Equation A.9 is multiplied with the depth factor d_{cV} calculated with Equation A.13.

$$d_{cV} = 1 + n \frac{L}{D}
 \tag{A.13}$$

Where:

n | Fitting parameter

The parameter n depends on the sand density: loose, medium-dense or dense. As an approximation and in order to avoid conflicts between uncertainties, only one bearing capacity is calculated and all the tests are performed with the same cyclic loading. This calculation is based on a medium density sand for which $n = 2.2$.

The vertical bearing capacity of the sand is found to be 540 kN and its 5% corresponds to 27 kN. The mean value of the load is 13.5 kN, but considering the pressurization effect in the load cell, the test is configured to a mean load of 15.1 kN.

Tensile Load

The tensile test is coded in *Displacement control*, due to the limitations in the piston displacement, thus avoiding choosing a force value that the piston can not meet. The pull-out rate is defined according the condition to be tested. This is the value that is going to be changed from test to test.

Following the path illustrated in Figure A.30, after the cyclic loading, a small break is defined in a parallel path where the system still records the readings. After this short waiting time, another parallel path tells the system to perform the pull-out test while recording the data. The last step of the code is to save the data in local computer for result analysis.

Force Data Processing

After obtaining the test results, the raw force data F_{raw} is processed according to Subsection 3.3.2.

A.2.9 Clean up

Once the test is performed, the pressure valves are closed and the back valve of the tank is opened just a bit, letting pressure and water escape from it. Figures A.33 and A.34 show the valve and its connection to the drainage system. The waiting time for this process is about 20 *min*.

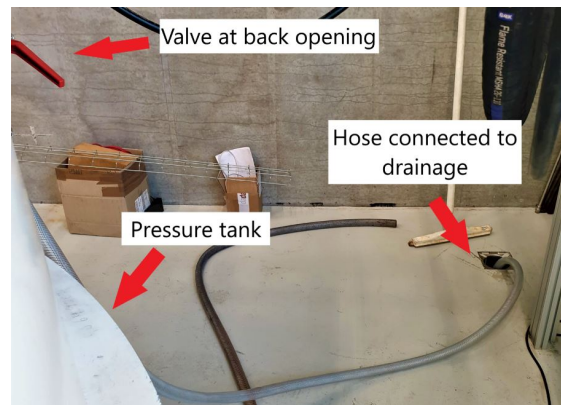


Figure A.33: Valve at the back opening of the tank. **Figure A.34:** Hose attached to back valve and connected to the drainage system.

When extra pressure is gone and the water level is below the tank lid, the tank lid can be opened and thus, the bucket model can be detached, cleaned and taken out of the tank. It is interesting to visualize the failure mechanism of the sand.

A new test can start to be prepared.

APPENDIX B

Cone Penetration Testing

A total of 26 tests are performed as part of this testing campaign. In order to meet the objectives of the present project, the soil is prepared with different densities.

This project is approached in different ways. First, the campaign focuses in encountering undrained behaviour in high density soil, therefore most of the tests are made in dense sand with different pull-out rates.

Secondly, four different pull-out rates are chosen and executed again in medium and low densities. This part of the project is done in order to compare the different pore pressure developments in soils with different permeabilities.

Lastly, one of the four pull-out rates (150 *mm/s*) is chosen to perform tests with Bucket B, which is the one used by Vaitkunaite (2016). This part of the campaign includes also testing without pre-cyclic loading in order to see its effect in the final results. The laboratory facilities are now different to the ones previously used by Vaitkunaite (2016), therefore Bucket B is tested to check if there is an influence of the new equipment on the final result shown in Vaitkunaite (2016).

This is in order to carry out a comparison of the results with in dense sand and perform the same rate in same soil density.

It is very difficult to achieve very homogeneous density profiles in the soil considering the equipment available and the manual procedure of vibration, therefore the soil is classified in a density range where the different density profiles are evaluated as a conjunction belonging to a certain range.

The aim of this chapter is to show the soil results of the CPT performed in the loose, medium and dense soil, thus the reader can have a better understanding of the profile of the different soil densities.

The tests are coded with a letter L, M or D depending if the test correspond to a loose, medium or dense density, followed by a number which represent the pull-out rate. When a second set of CPTs is performed, the code is followed by "-2". The test code ends in "-B" when Bucket B is used.

B.1 CPTs in High Density Sand

A total of fifteen tests are performed in high density sand in order to find untrained behaviour plus extra 150 mm/s rate tests performed in order to compare to the work made by Vaitkunaite (2016).

A high density is reached by vibrating the soil in 3 rounds with relatively slow immersions. After performing the CPTs, the results are considered acceptable for high density, when most of the D_r profiles are approximately in the range of 70% to 90%. The following figures illustrate the high density profiles before each test.

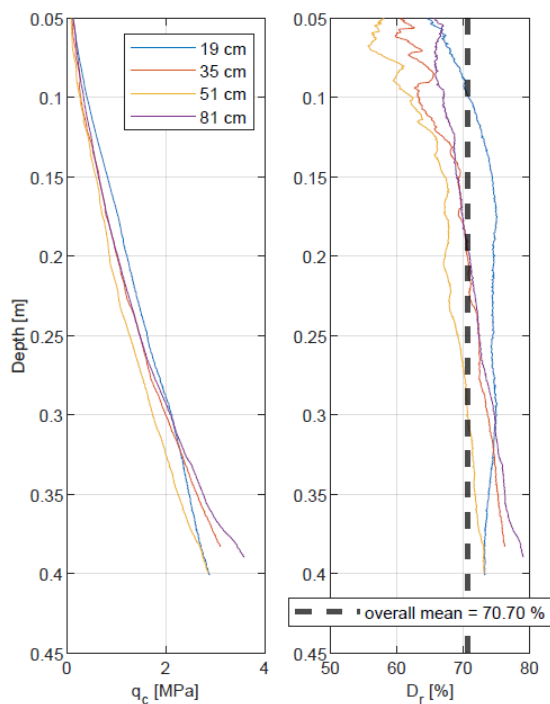


Figure B.1: CPT results D005.

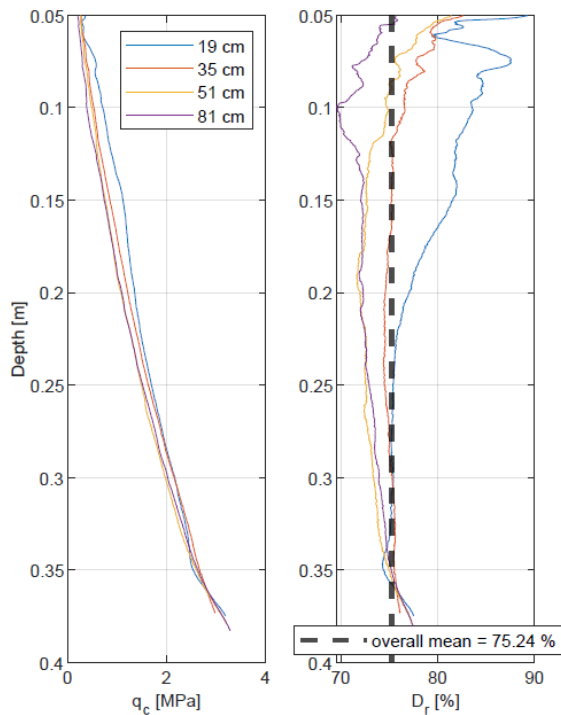


Figure B.2: CPT results D5.

B.1 CPTs in High Density Sand

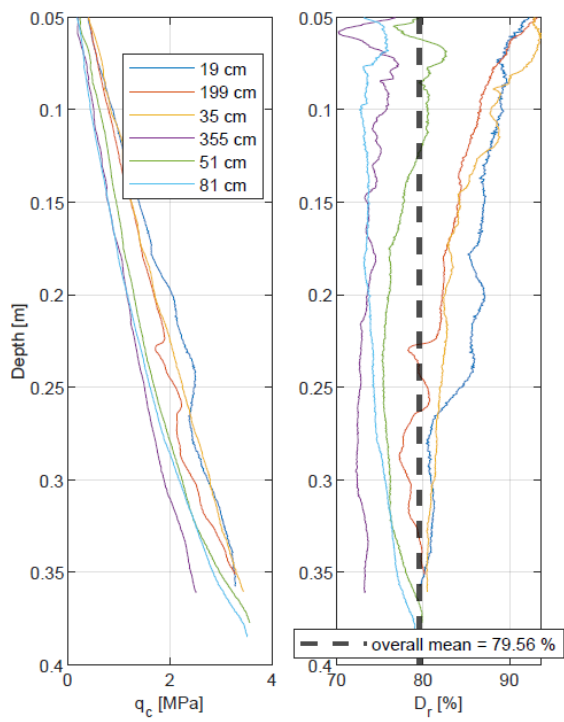


Figure B.3: CPT results D10.

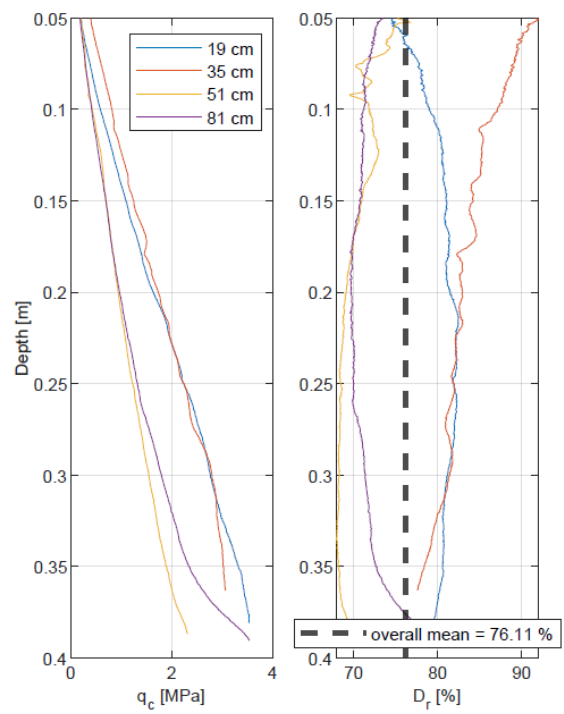


Figure B.4: CPT results D20.

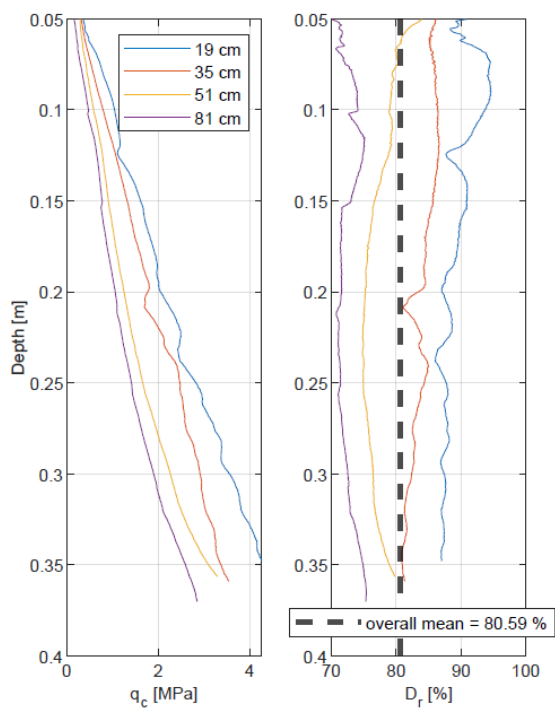


Figure B.5: CPT results D50.

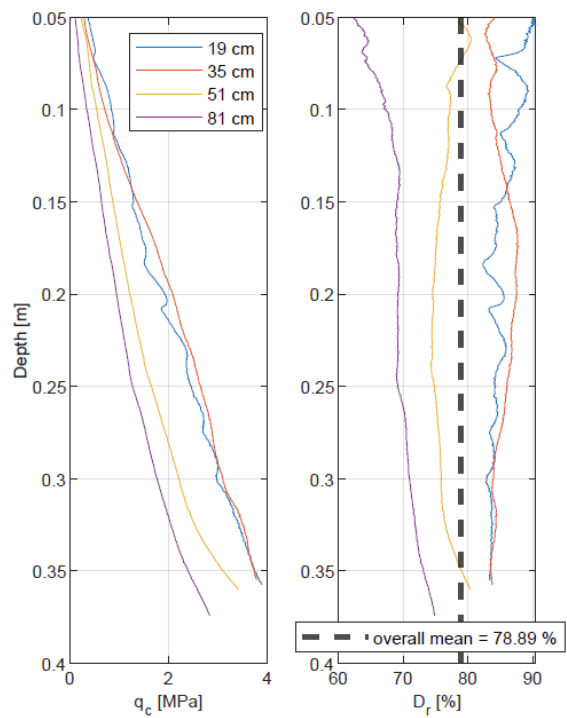


Figure B.6: CPT results D80.

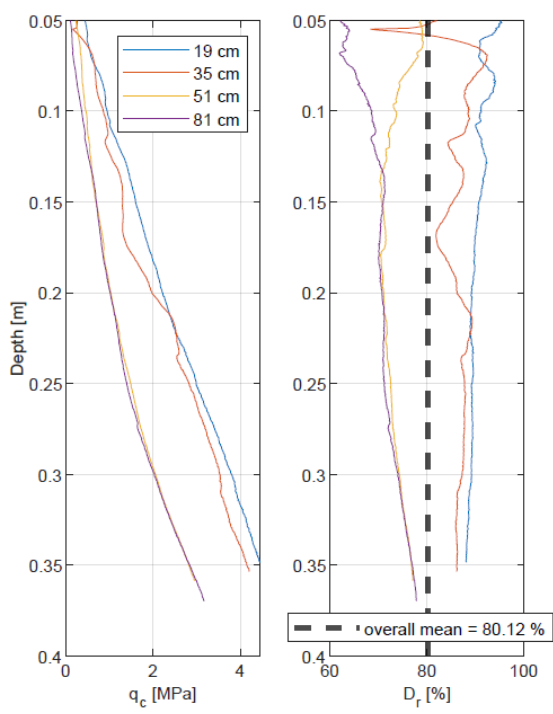


Figure B.7: CPT results D100.

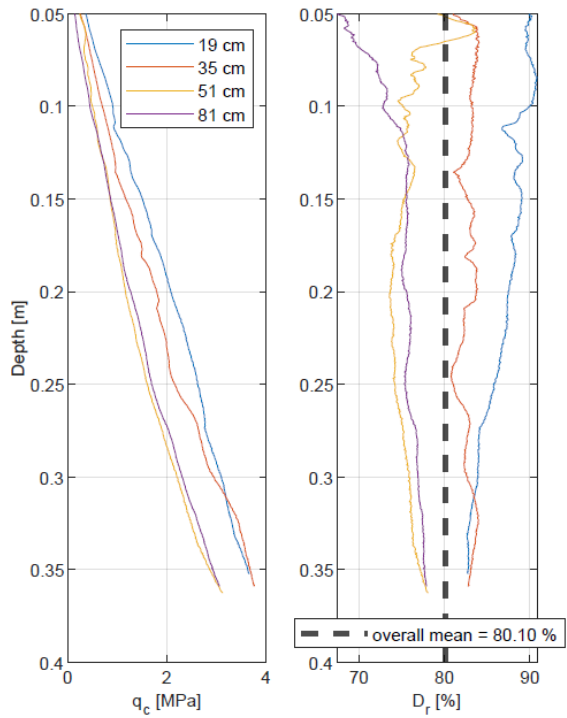


Figure B.8: CPT results D150.

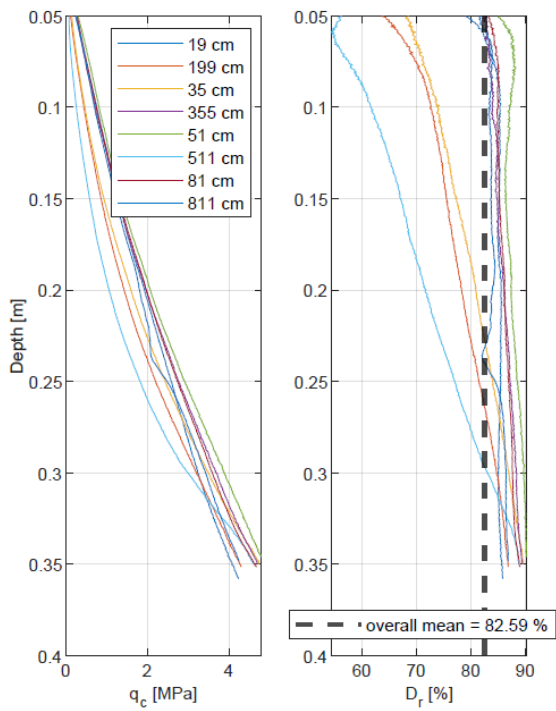


Figure B.9: CPT results D150 without cyclic loading.

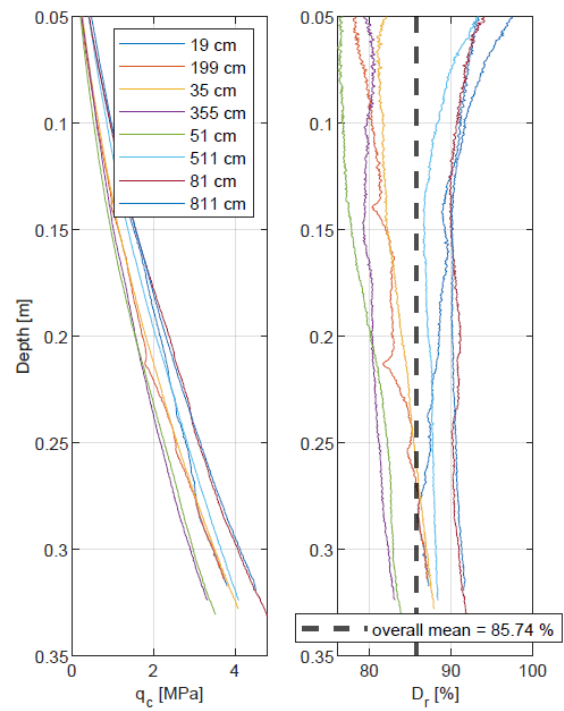


Figure B.10: CPT results D150-B (Bucket B).

B.1 CPTs in High Density Sand

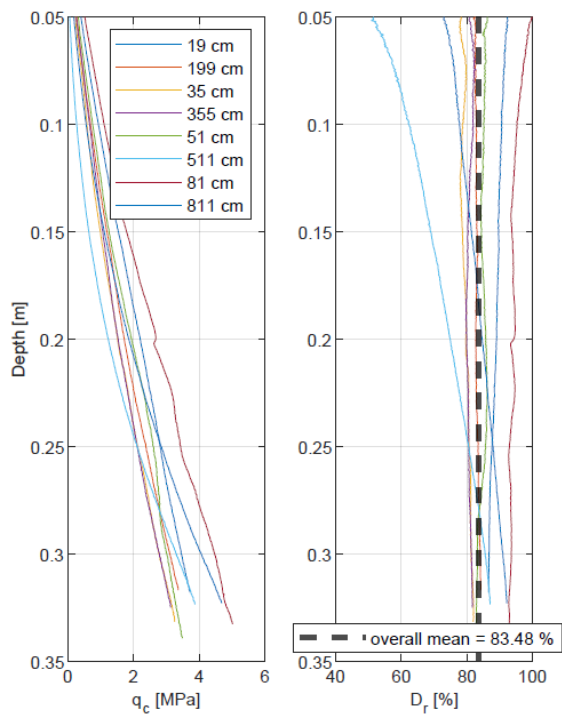


Figure B.11: CPT results D150-B (Bucket B) without cyclic loading.

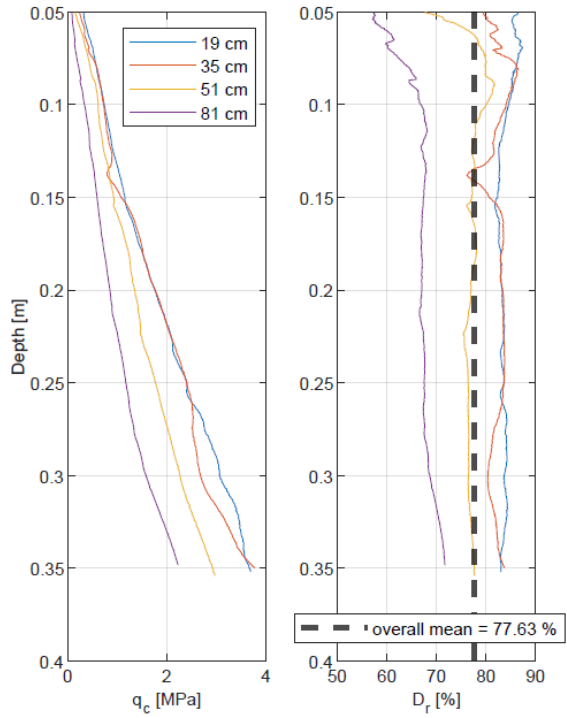


Figure B.12: CPT results D200.

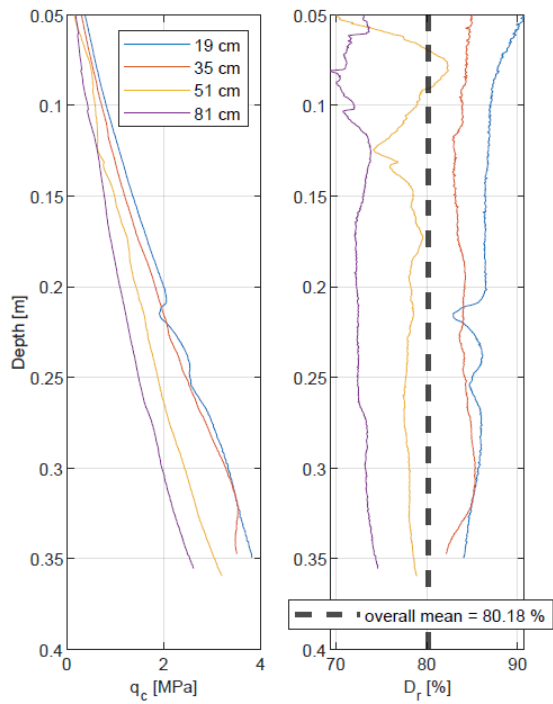


Figure B.13: CPT results D300.

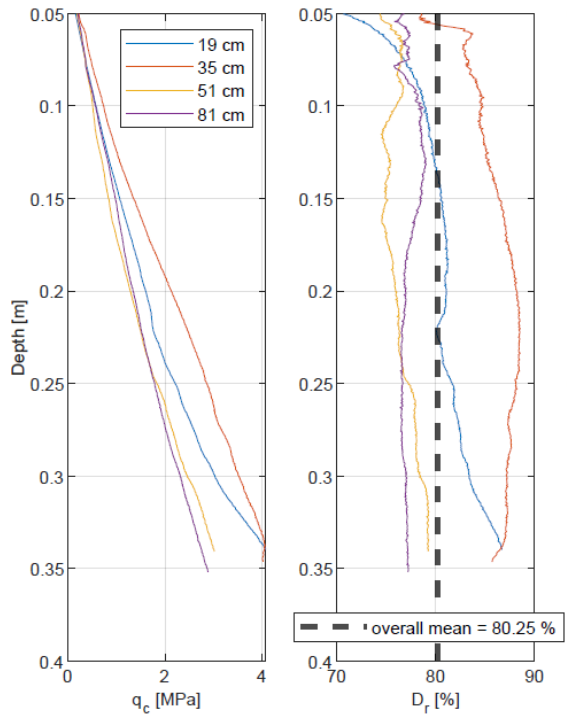


Figure B.14: CPT results D400.

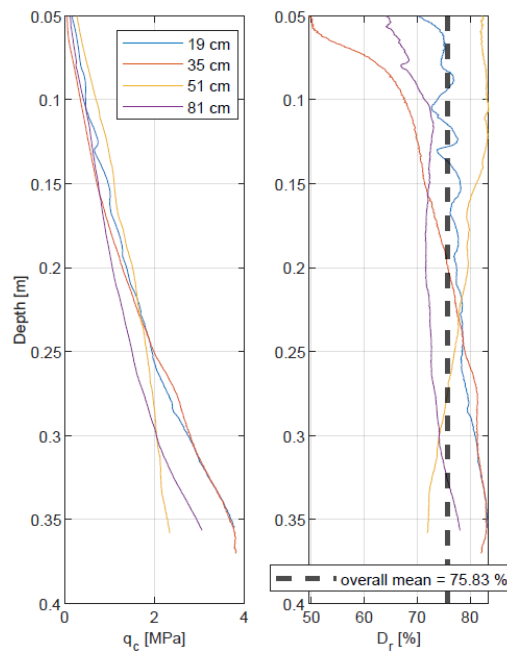


Figure B.15: CPT results D500

B.2 CPTs in Medium Density Sand

A total of six tests are performed in medium density sand: five chosen in order to compare the soil tensile capacities and an extra 150 mm/s test in order to ensure the accuracy of the tensile capacity result observed in this rate.

A medium density is reached by loosening up the soil and vibrating it only once with quick immersions. After performing the CPT, the results are considered acceptable for medium density, when most of the D_r profiles are approximately in the range of 50% to 70%. The following figures illustrate the medium density profiles before each test.

B.2 CPTs in Medium Density Sand

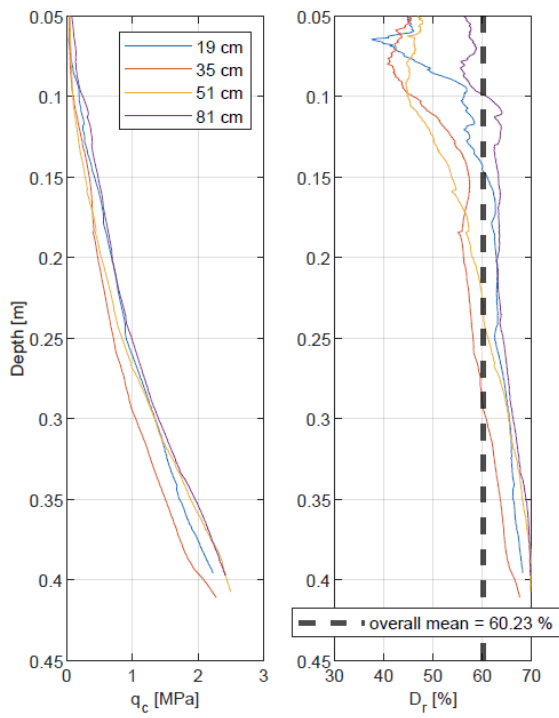


Figure B.16: CPT results M005.

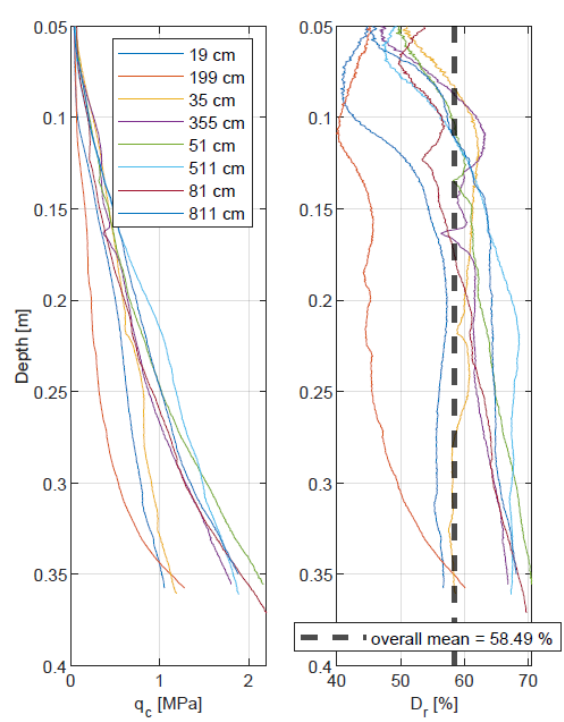


Figure B.17: CPT results M10.

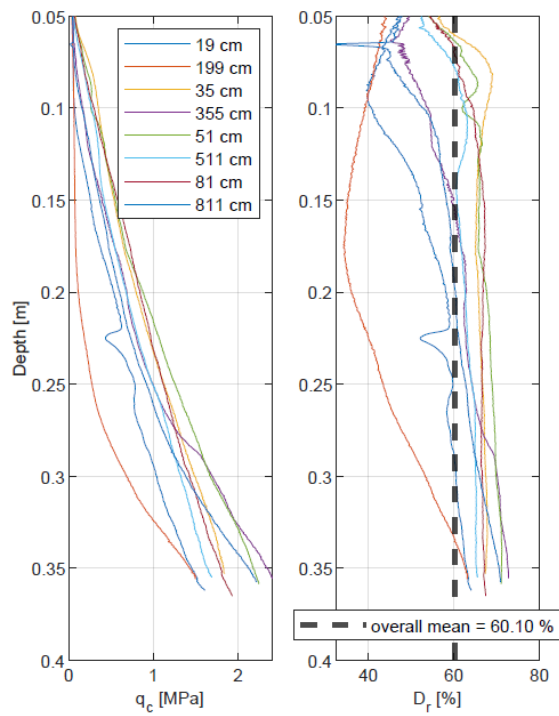


Figure B.18: CPT results M50.

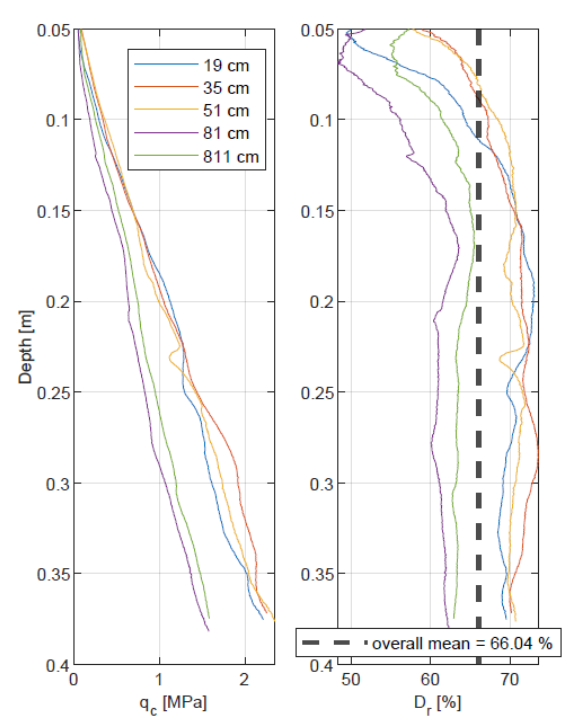


Figure B.19: CPT results M500.

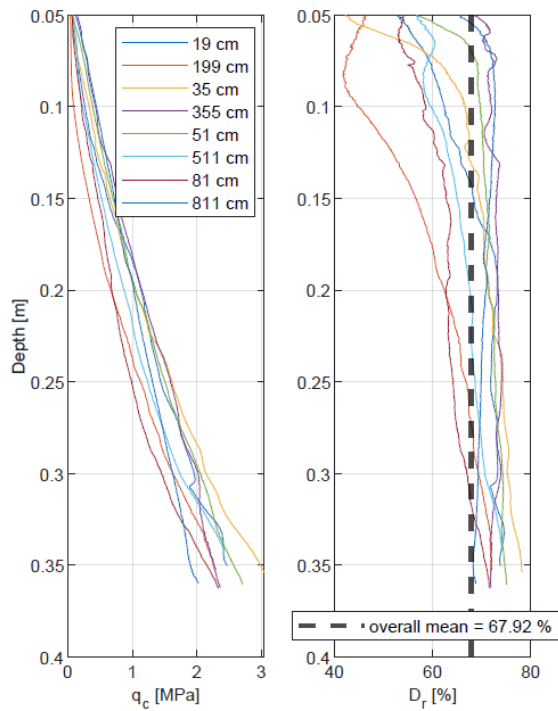


Figure B.20: CPT results M150-1.

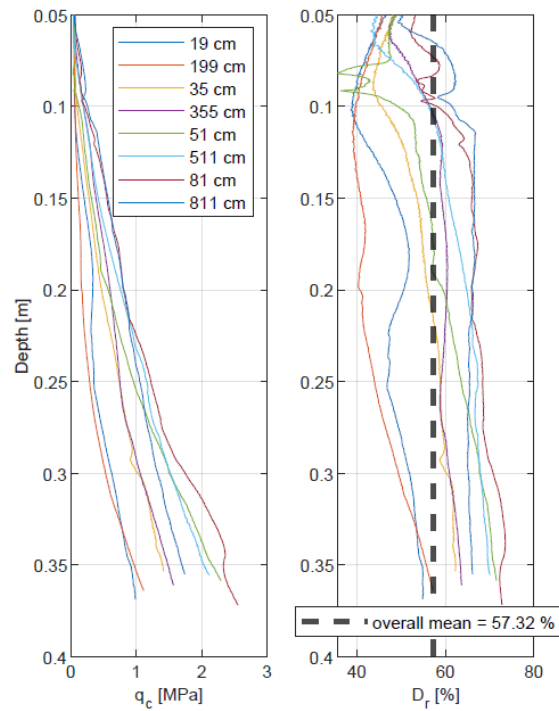


Figure B.21: CPT results M150-2.

B.3 CPTs in Low Density Sand

A total of five tests are performed in low density sand. To assure the above, the soil is loosened up and vibrated only once with quick immersions. After performing the CPTs, the results are considered acceptable for low density, when most of the D_r profiles approximately in the range of 40% to 50%.

The following figures illustrate the low density profiles before each test.

B.3 CPTs in Low Density Sand

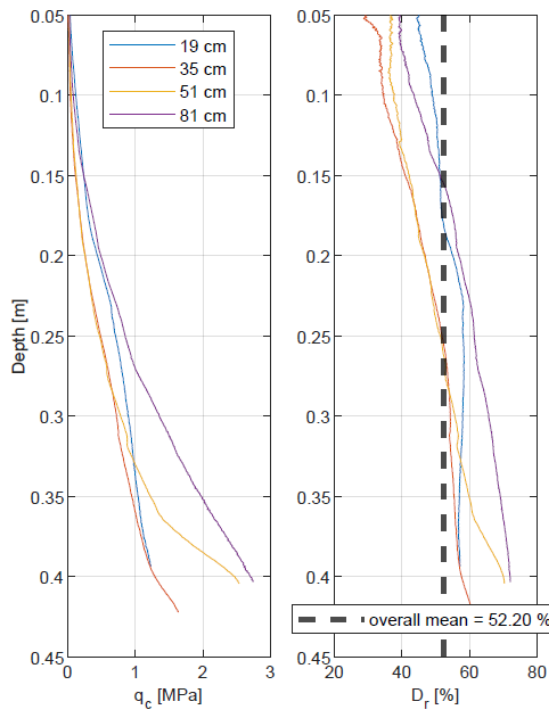


Figure B.22: CPT results L005.

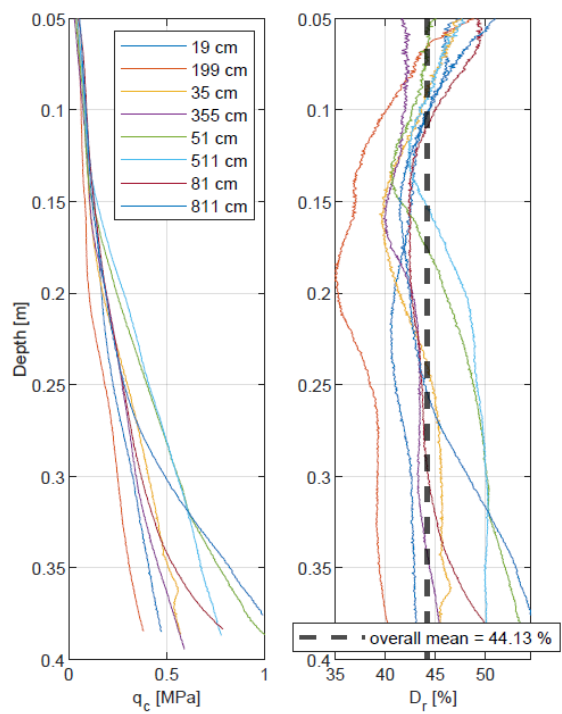


Figure B.23: CPT results L10.

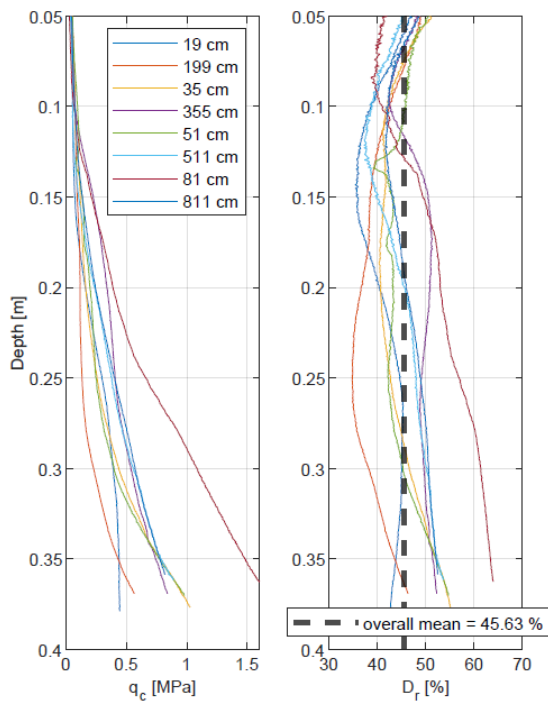


Figure B.24: CPT results L50.

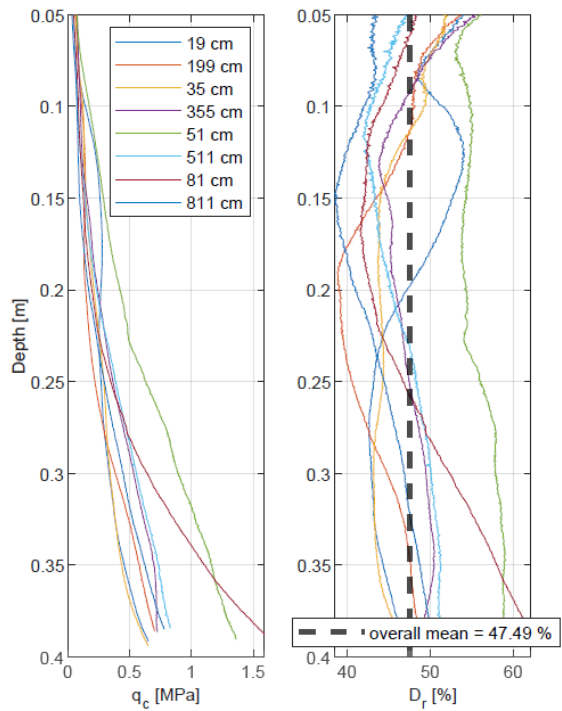


Figure B.25: CPT results L150.

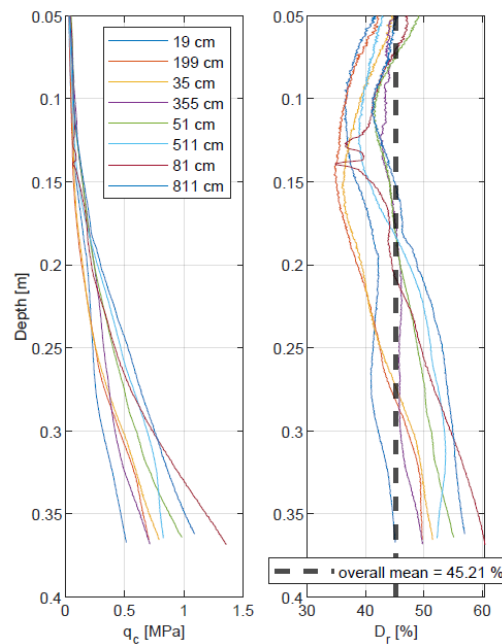


Figure B.26: CPT results L500

B.4 Comparison Densities

It is almost impossible to obtain an homogeneous profile along the depth and in the whole area of sand, therefore dense, medium and low densities can not be defined as only one value. Therefore all the CPTs corresponding to each test are analysed at the same time as described in Section B.1.

In order to show an easy and clear difference in between low, medium and high densities a comparison in one or two of the CPTs' positions (19 *cm* or 35 *cm*) is performed between tests for each pull-out displacement rate. These differences in density contribute to the understanding of the different soil failure behaviours when the pull-out displacement rate is kept constant while changing the permeability of the soil.

With these comparison is assured that the density profiles of each case close to the location of the bucket are different when compared to each other. The distance between the center of the pressure tank to the cone where the CPTs have been taken place is 19 *cm* in Tests 0.05, 10, 50 and 500 *mm/s*. Test 150 *mm/s* is compared at 19 *cm* as well as 35 in order to show the overall density between tests due to density uncertainties.

Below are presented the different density profiles for each pullout speed in low, medium and dense sand.

B.4 Comparison Densities

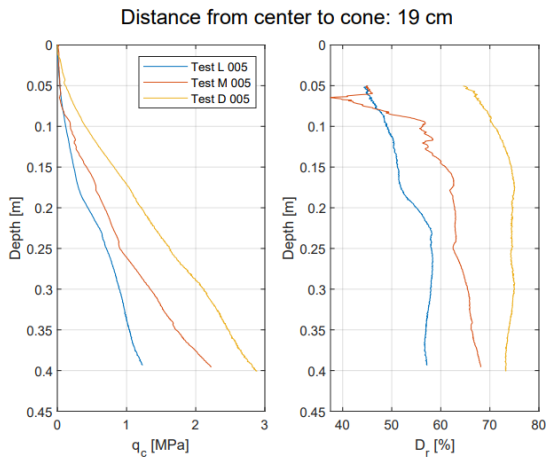


Figure B.27: CPT 19 cm Comparison Tests 005 mm/s.

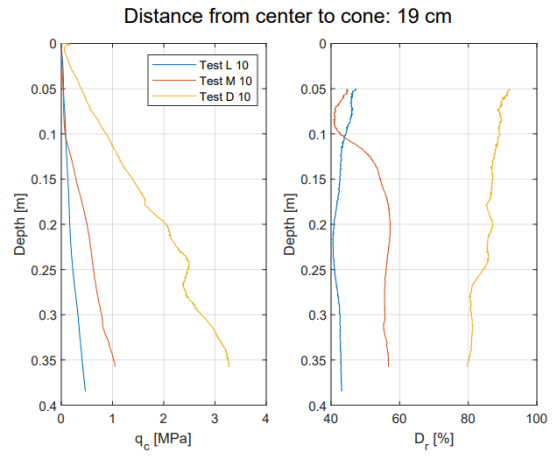


Figure B.28: CPT 19 cm Comparison Tests 10 mm/s.

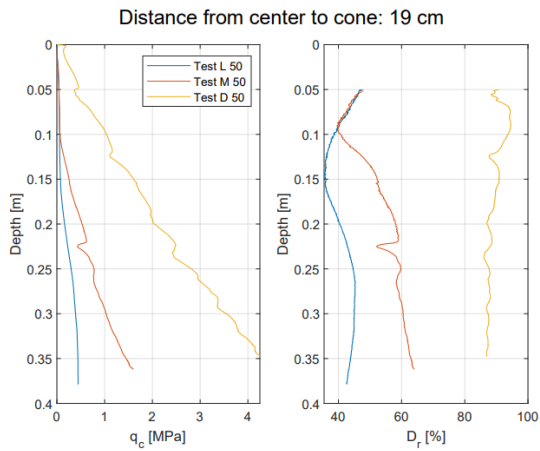


Figure B.29: CPT 19 cm Comparison Tests 50 mm/s.

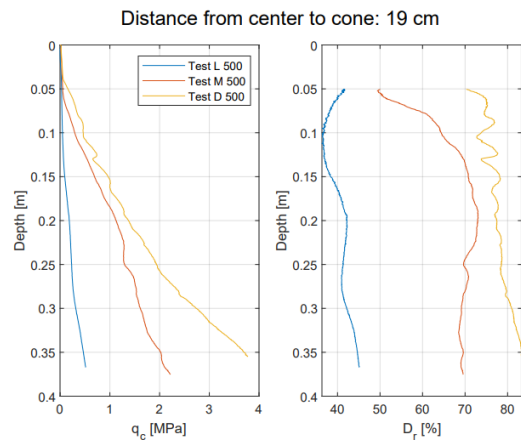


Figure B.30: CPT 19 cm Comparison Tests 500 mm/s.

B.4.1 Tests 150 mm/s

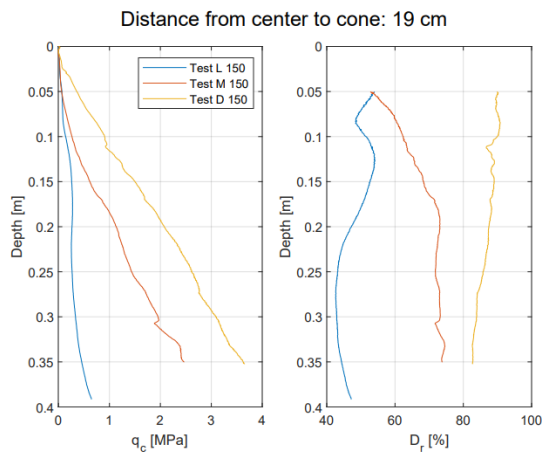


Figure B.31: CPT 19 cm Comparison Tests 150 mm/s considering M150-1

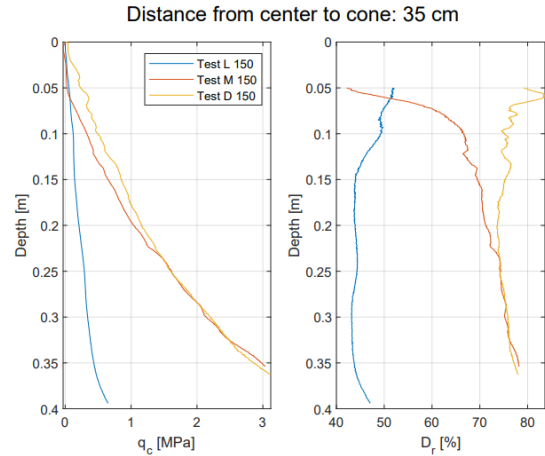


Figure B.32: CPT 35 cm Comparison Tests 150 mm/s considering M150-2

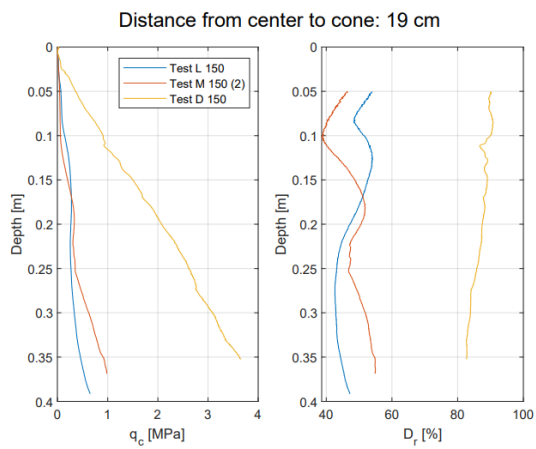


Figure B.33: CPT 19 cm Comparison Tests 150 mm/s considering M150-2

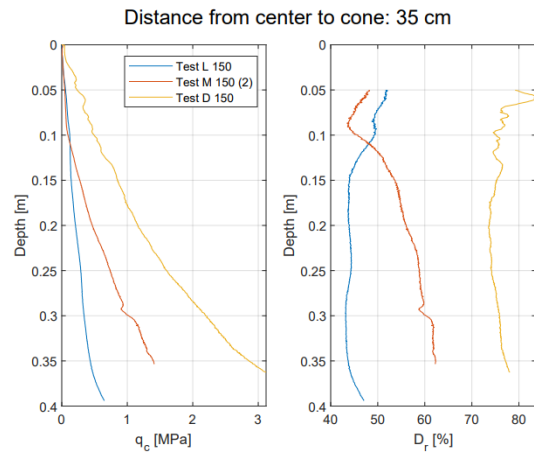


Figure B.34: CPT 35 cm Comparison Tests 150 mm/s considering M150-2

B.4 Comparison Densities

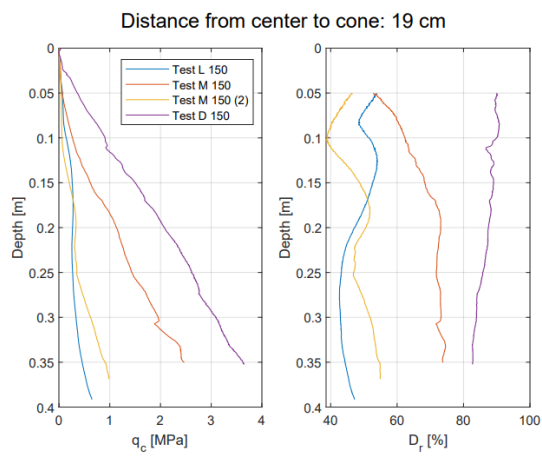


Figure B.35: CPT 19 cm Comparison Tests 150 mm/s considering both M150-1 and M150-2.

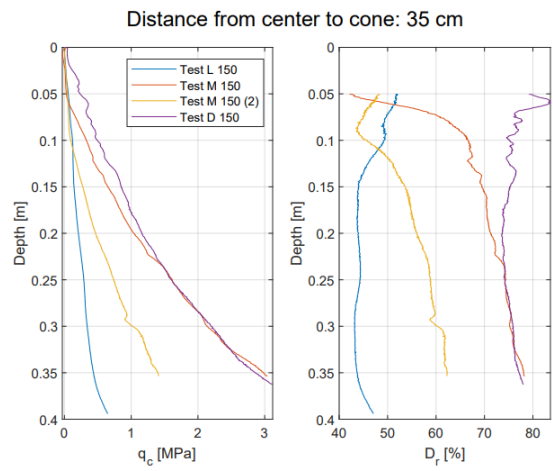


Figure B.36: CPT 35 cm Comparison Tests 150 mm/s considering both M150-1 and M150-2.

APPENDIX C

Test Results

This Appendix presents a complete set of data for all the performed tests in this testing campaign. The missing data in tests D50 to D100 is due to a delay between the command sent to the operating system (e.g. displacement) and the mechanical reaction of the piston. The first moves quicker than the latter, and this lag is not noticeable at low pull-out rates. However, the faster the rate applied, the larger the gap between the target and reality. Since the acquisition manager follows the command displacement, data recording stops before the piston reached the final position. In order to solve this issue, the time for recording the data is increased by a few seconds, which is enough for the piston to reach the target.

C.1 Results in High Density Sand

C.1.1 Test D0.05

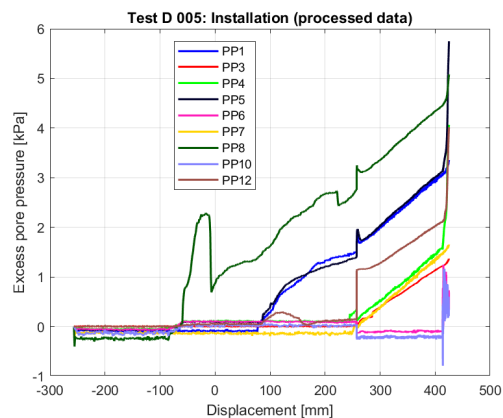


Figure C.1: Excess PP vs displacement for installation in Test D005.

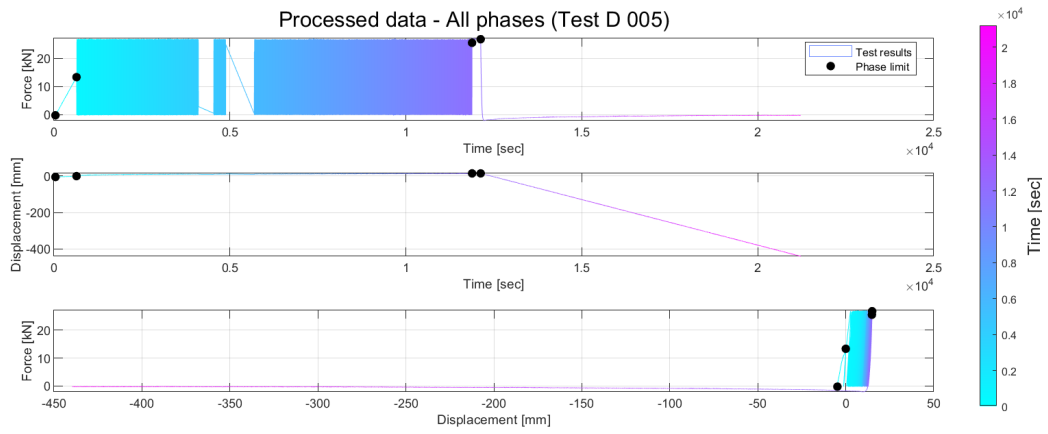


Figure C.2: Force-Time, Disp-Time, Force-Disp in Test D005.

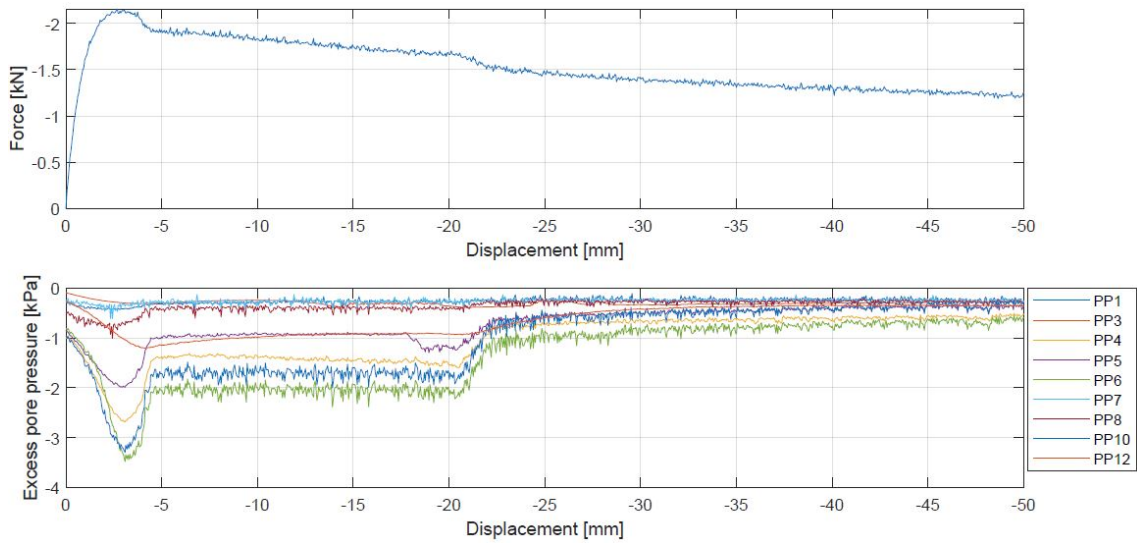


Figure C.3: Force vs displacement and excess PP vs displacement in Test D005.

C.1 Results in High Density Sand

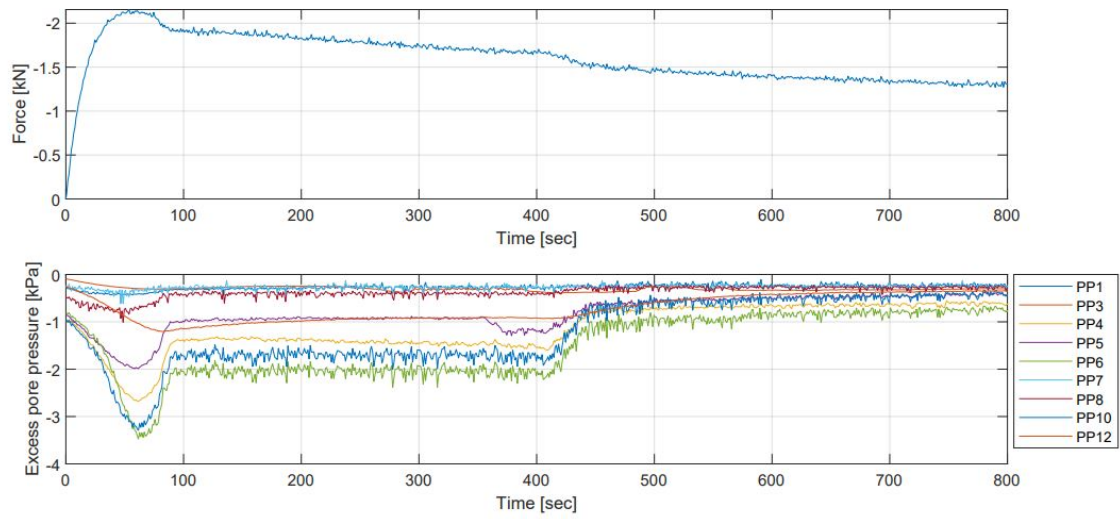


Figure C.4: Force vs time and excess PP vs time in Test D005.

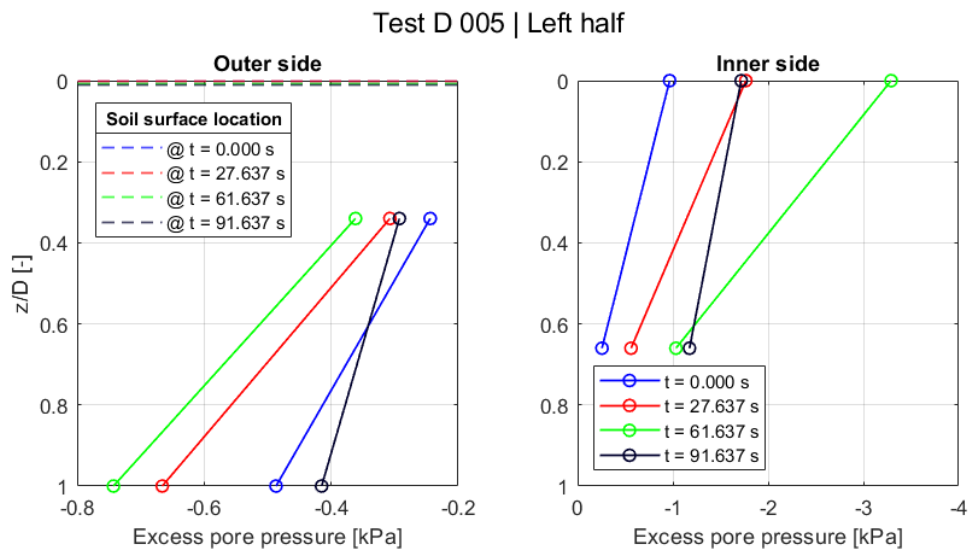


Figure C.5: Force vs time and excess PP vs time in Test D005.

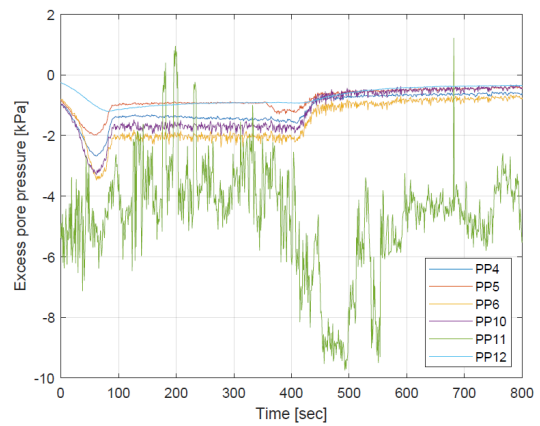
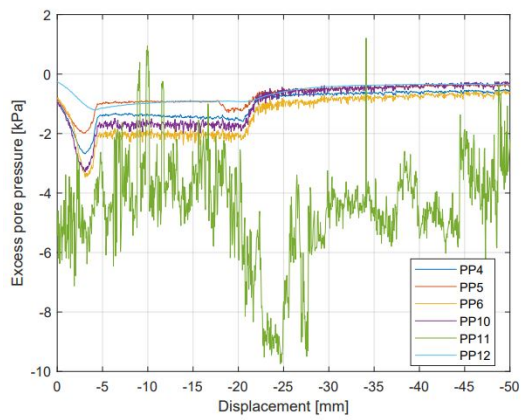
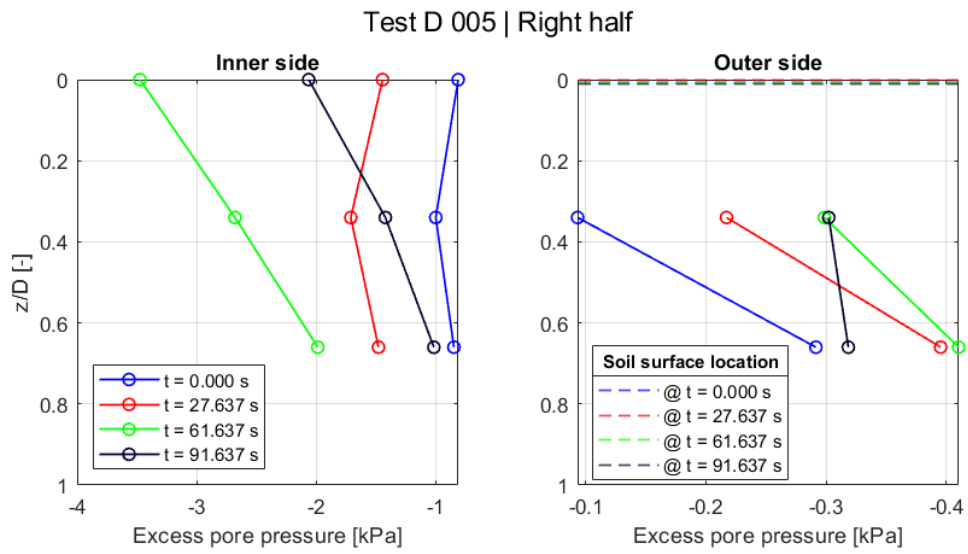


Figure C.7: Internal excess PP vs displacement in Test D005. **Figure C.8:** Internal excess PP vs time in Test D005.

C.1 Results in High Density Sand

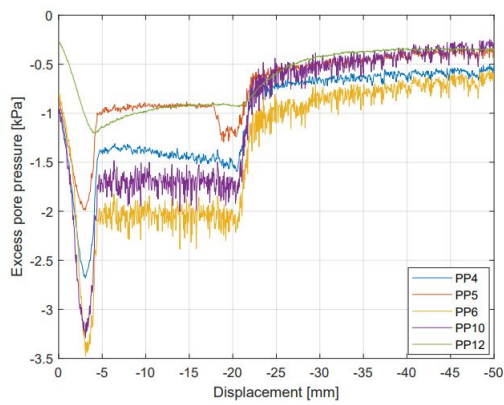


Figure C.9: Internal PP sensors without 11 in Test D005.

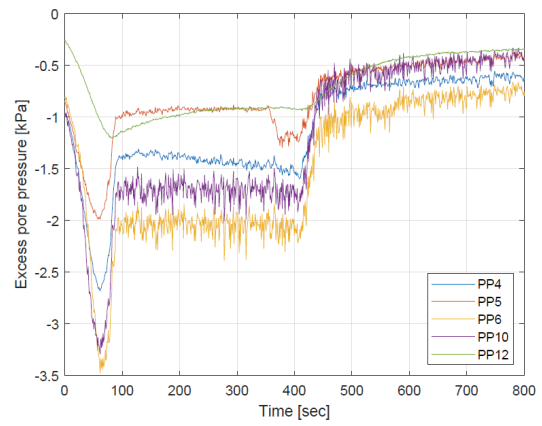


Figure C.10: Internal excess PP vs time in Test D005. PP11 not considered.

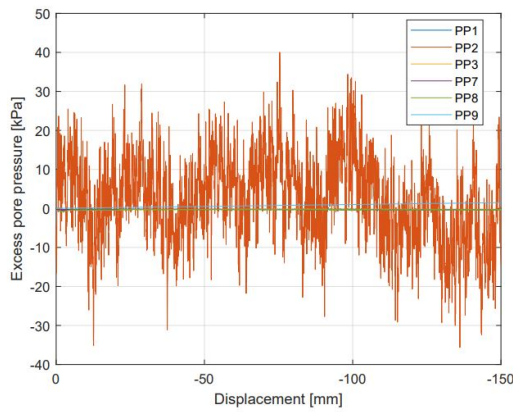


Figure C.11: External excess PP vs displacement in Test D005.

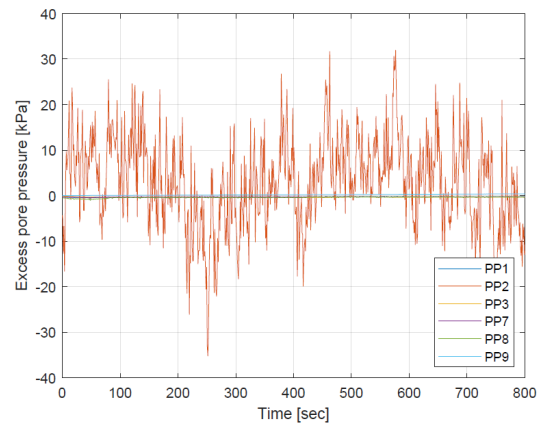


Figure C.12: External excess PP vs time in Test D005.

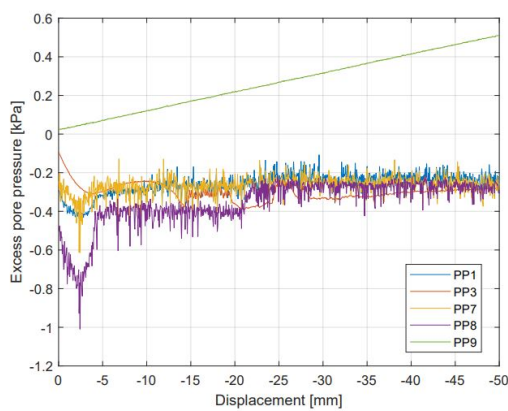


Figure C.13: External sensors without 2 in Test D005.

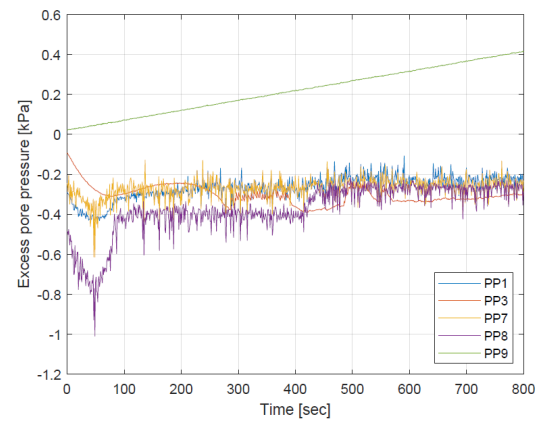


Figure C.14: External excess PP vs time in Test D005. PP2 not considered.

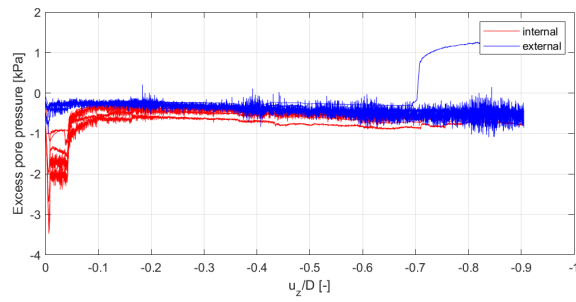


Figure C.15: Internal and external excess PP during D005

C.1.2 Test D5

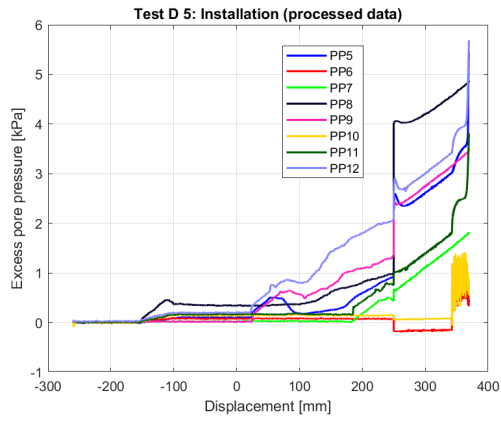


Figure C.16: Excess PP vs displacement for installation in Test D5.

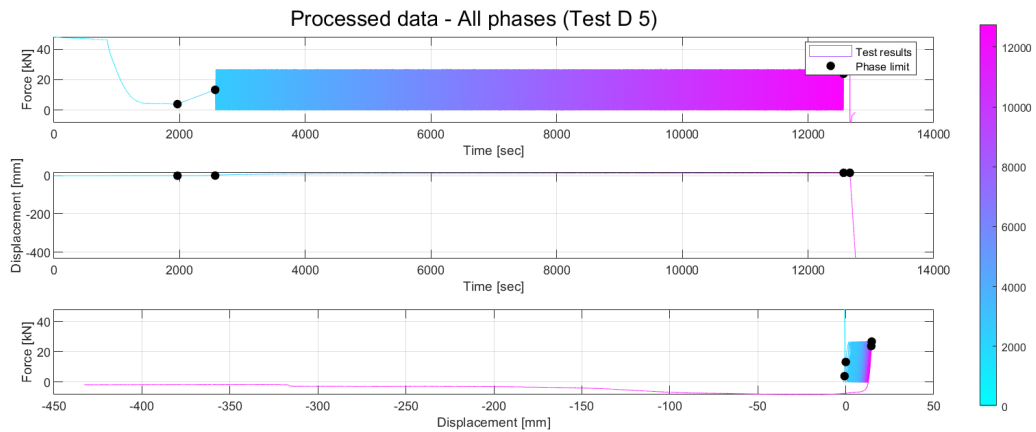


Figure C.17: Force-Time, Disp-Time, Force-Disp in Test D5.

C.1 Results in High Density Sand

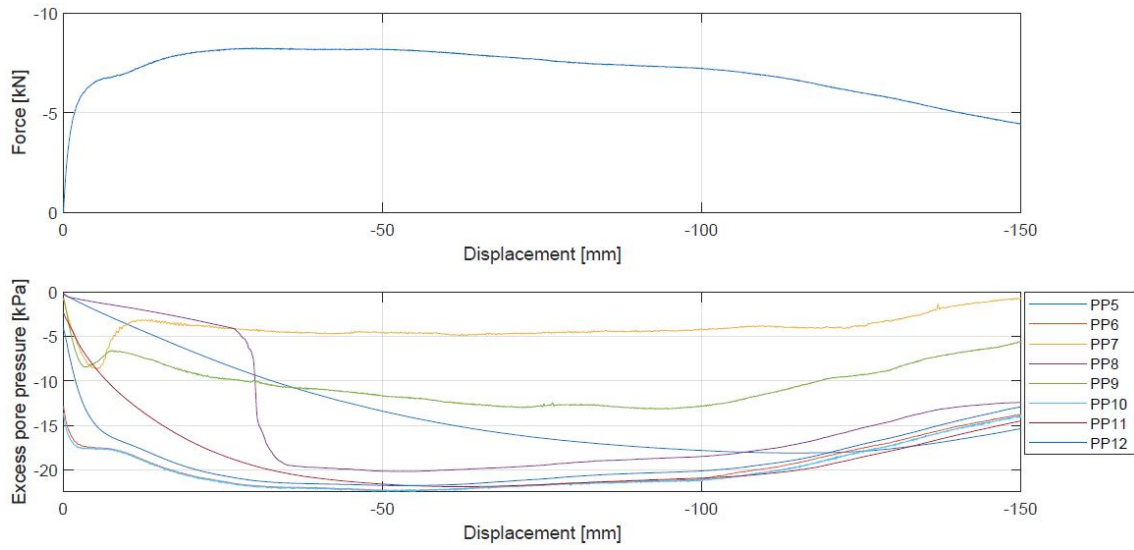


Figure C.18: Force vs displacement and excess PP vs displacement in Test D5.

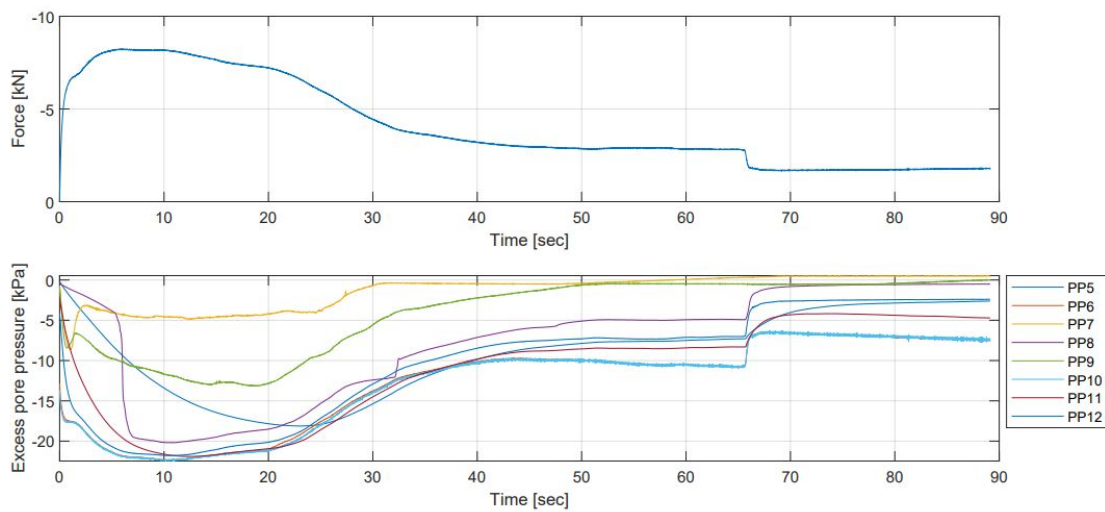


Figure C.19: Force vs time and excess PP vs time in Test D5.

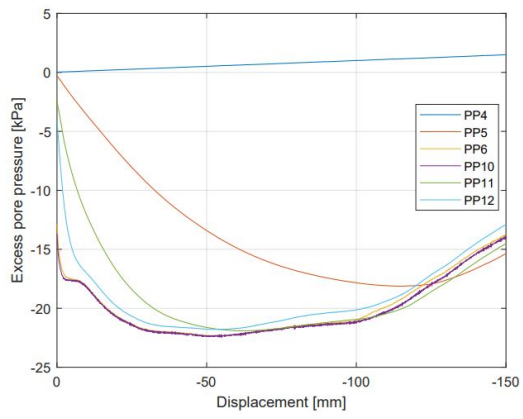


Figure C.20: Internal excess PP vs displacement in Test D5.

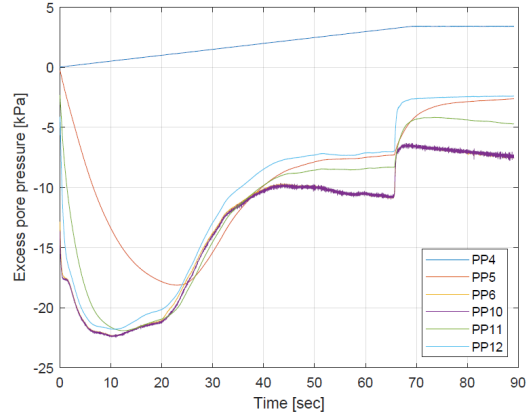


Figure C.21: Internal excess PP vs time in Test D5.

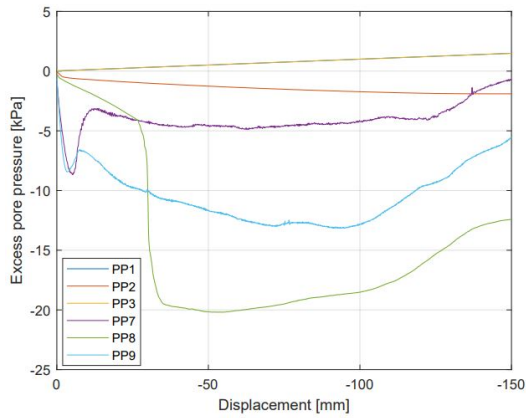


Figure C.22: External excess PP vs displacement in Test D5.

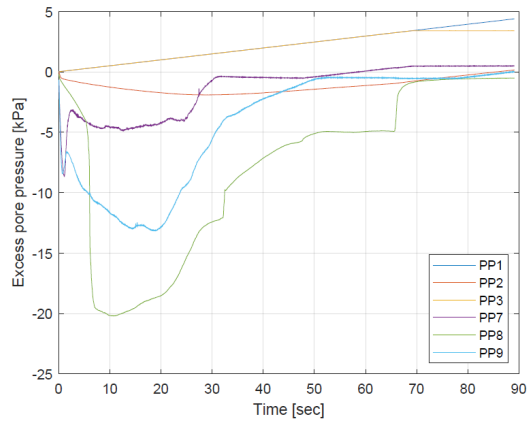


Figure C.23: External excess PP vs time in Test D5.

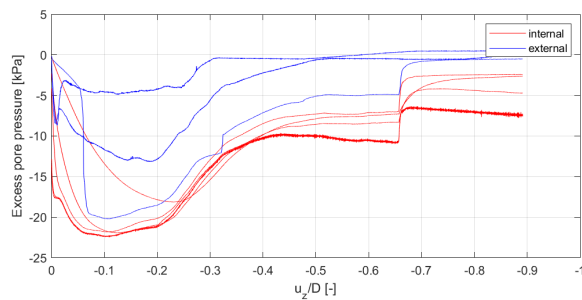


Figure C.24: Internal and external excess PP during D5

C.1.3 Test D10

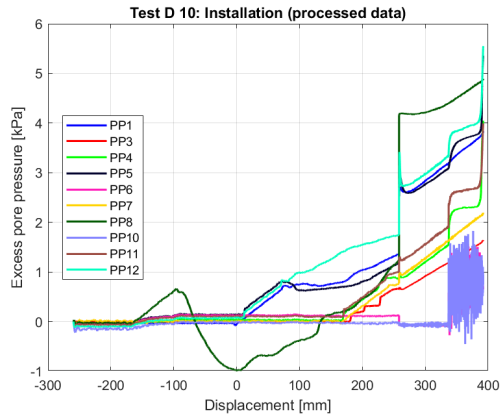


Figure C.25: Excess PP vs displacement for installation in Test D10.

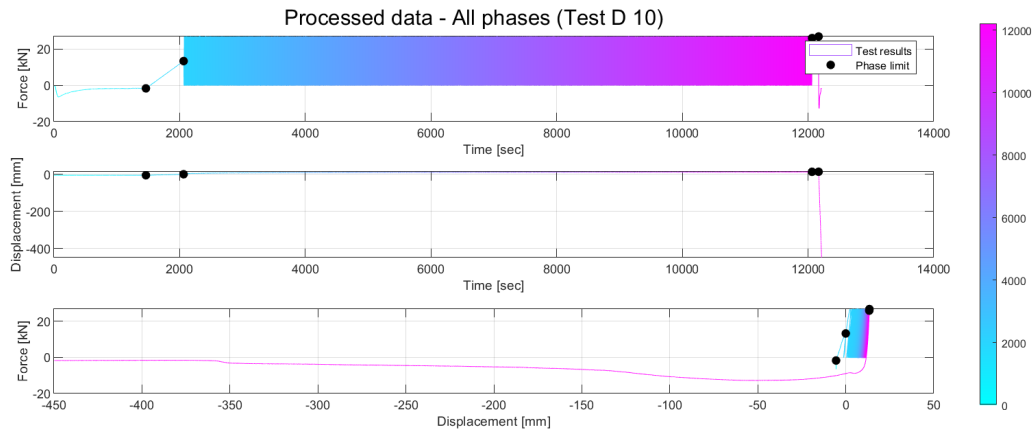


Figure C.26: Force-Time, Disp-Time, Force-Disp in Test D10.

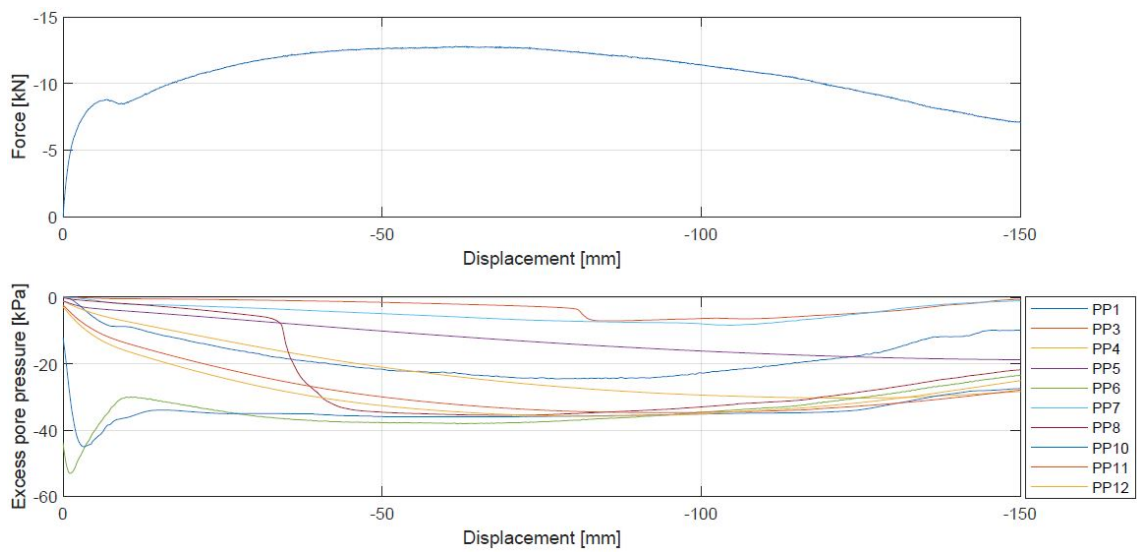


Figure C.27: Force vs displacement and excess PP vs displacement in Test D10.

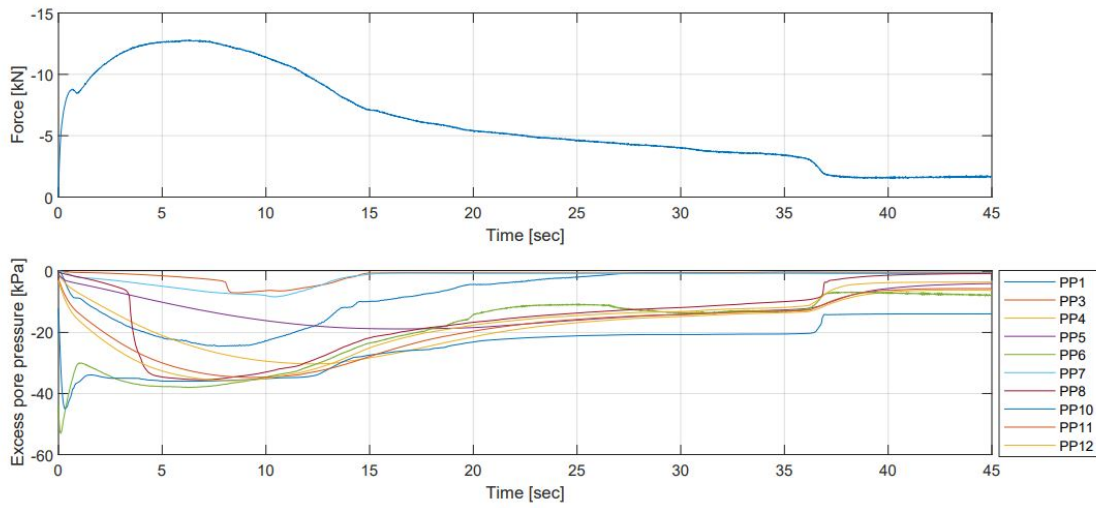


Figure C.28: Force vs time and excess PP vs time in Test D10.

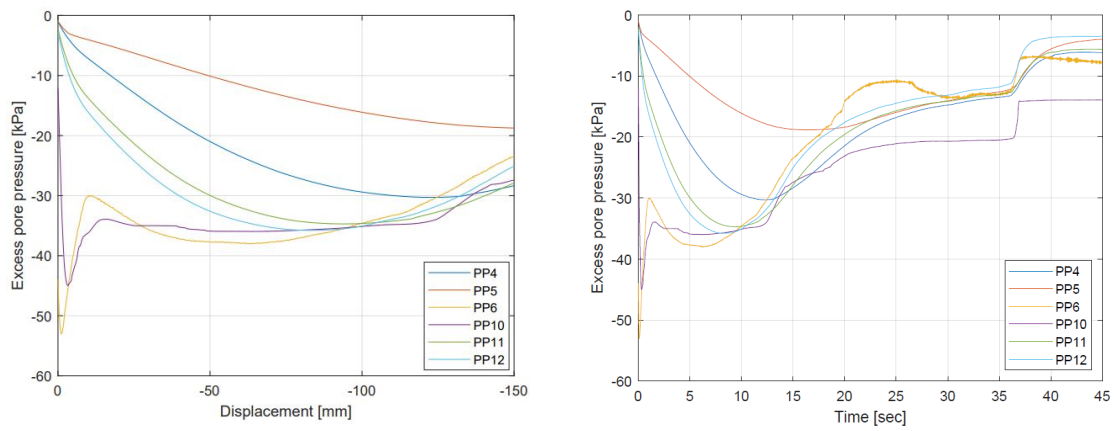


Figure C.29: Internal excess PP vs displacement in Test D10.

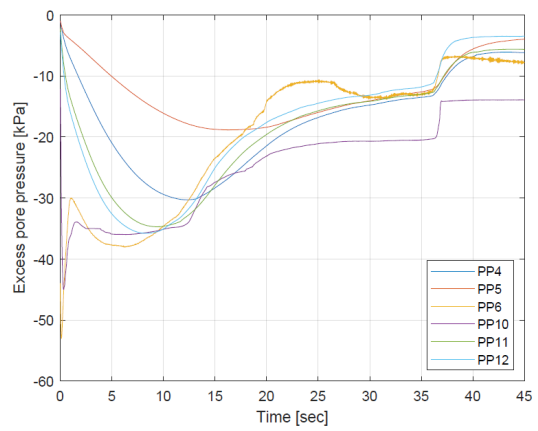


Figure C.30: Internal excess PP vs time in Test D10.

C.1 Results in High Density Sand

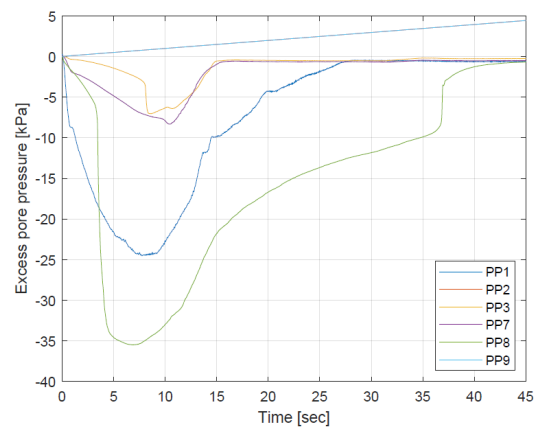
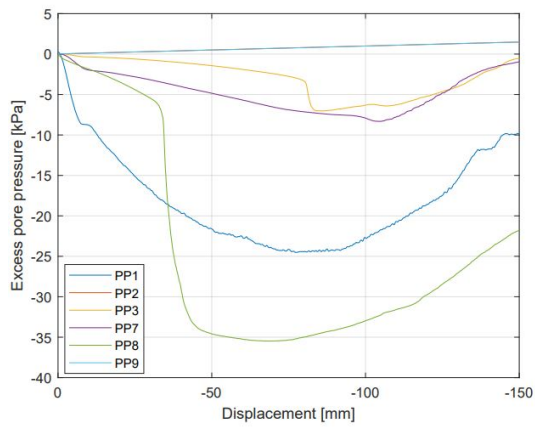


Figure C.31: External excess PP vs displacement in Test D10. **Figure C.32:** External excess PP vs time in Test D10.

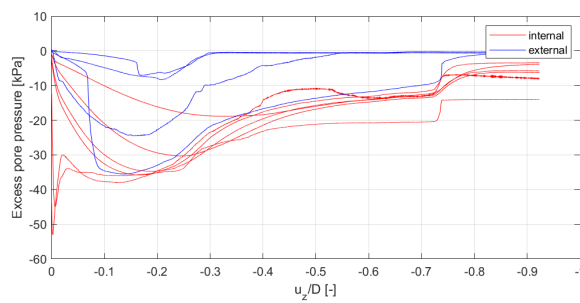


Figure C.33: Internal and external excess PP during D10

Test D 10 | Left half

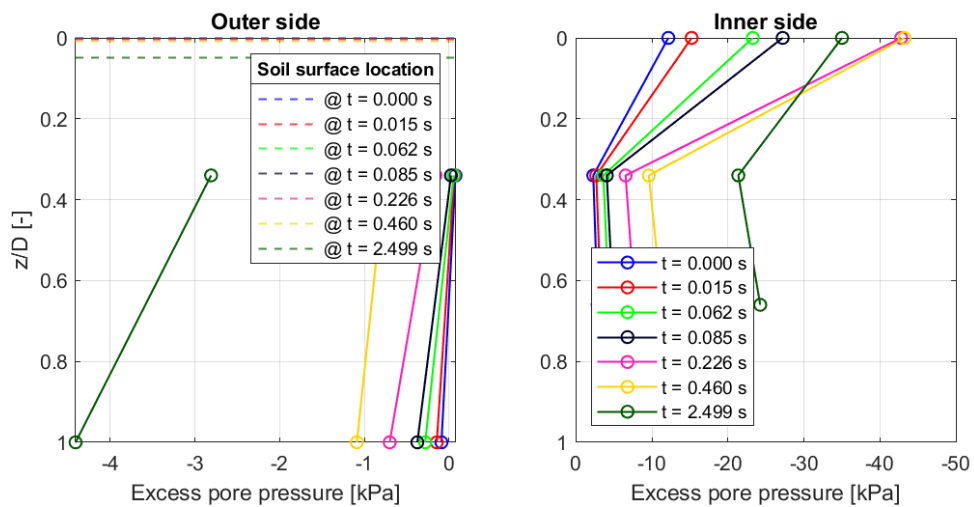


Figure C.34: Force vs time and excess PP vs time in Test D10.

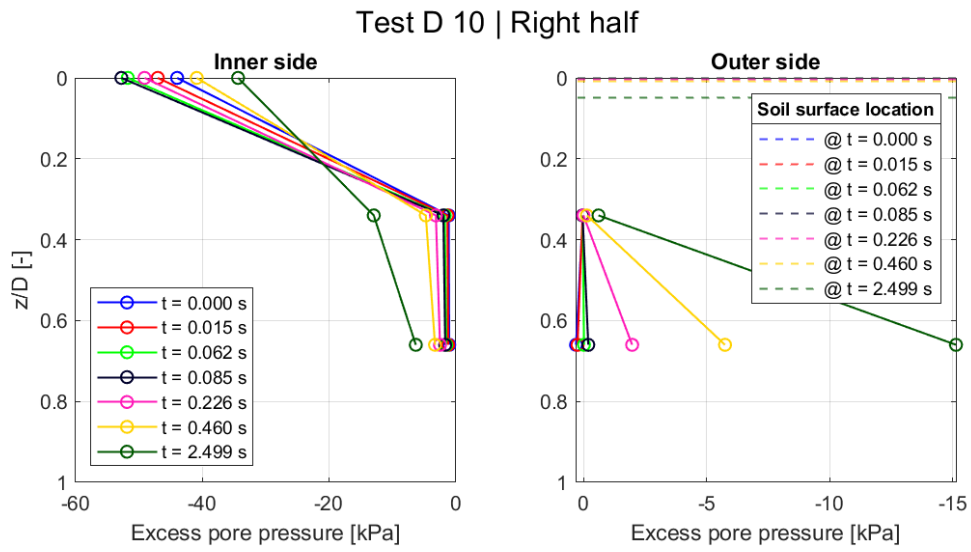


Figure C.35: Force vs time and excess PP vs time in Test D10.

C.1.4 Test D20

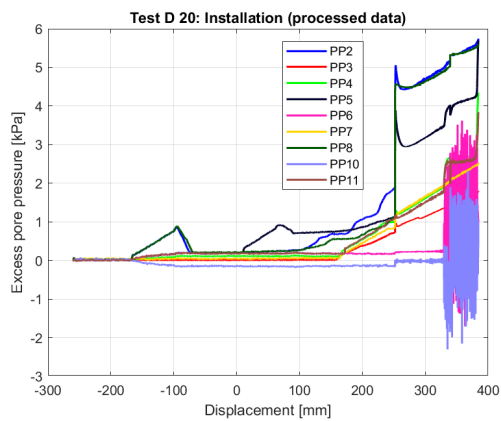


Figure C.36: Excess PP vs displacement for installation in Test D20.

C.1 Results in High Density Sand

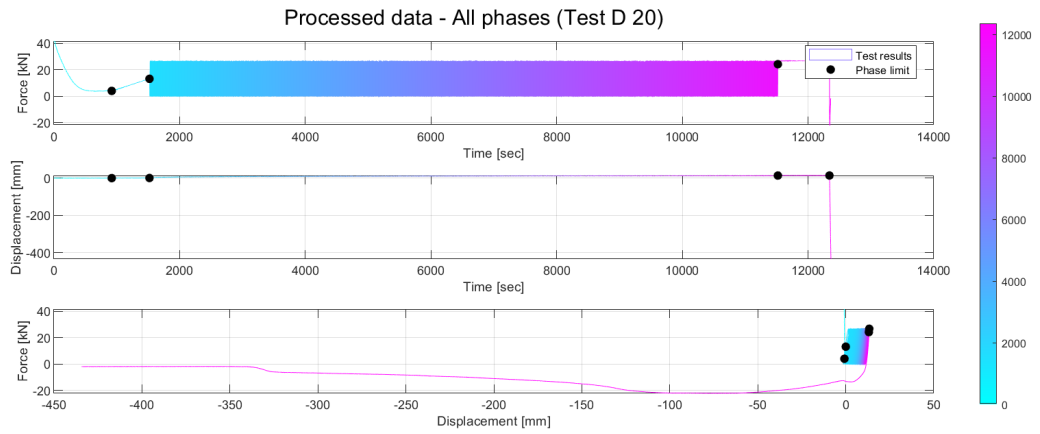


Figure C.37: Force-Time, Disp-Time, Force-Disp in Test D20.

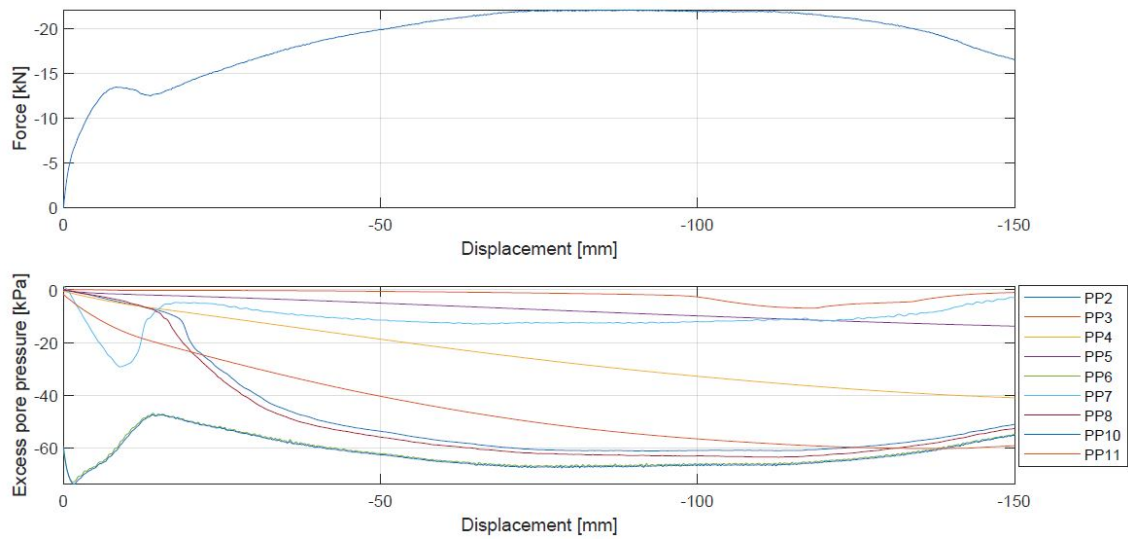


Figure C.38: Force vs displacement and excess PP vs displacement in Test D20.

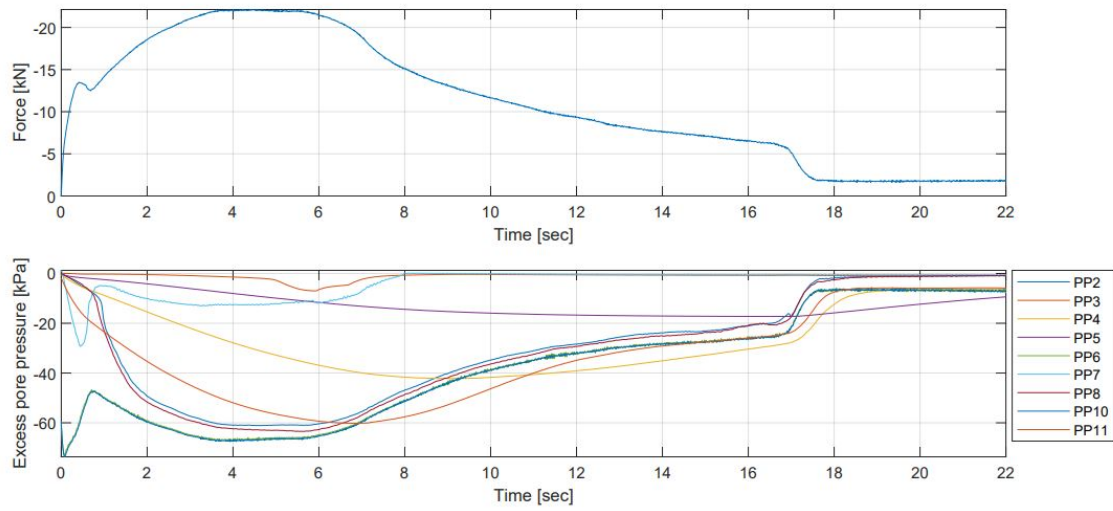


Figure C.39: Force vs time and excess PP vs time in Test D20.

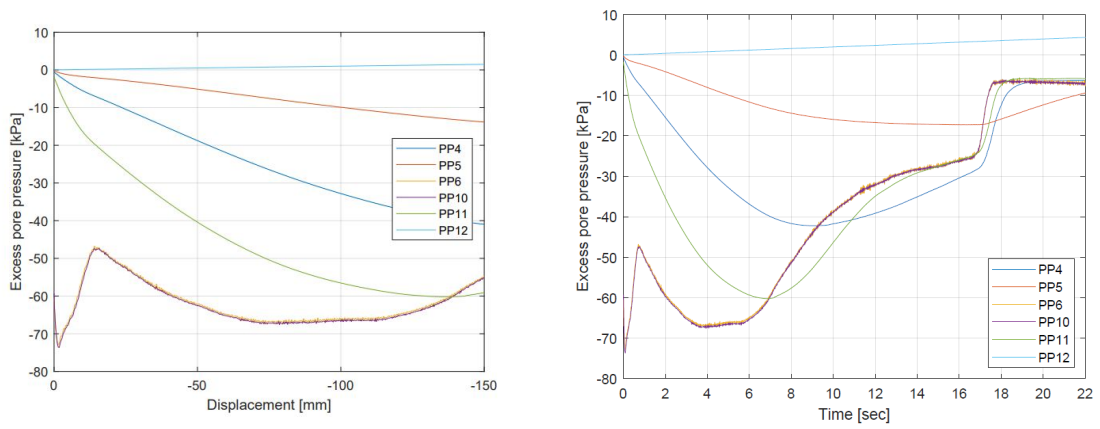


Figure C.40: Internal excess PP vs displacement in Test D20. Figure C.41: Internal excess PP vs time in Test D20.

C.1 Results in High Density Sand

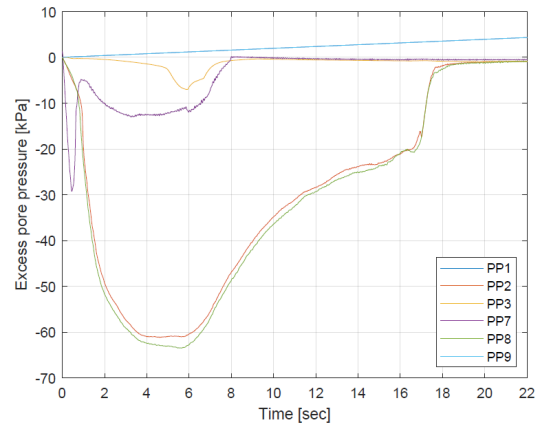
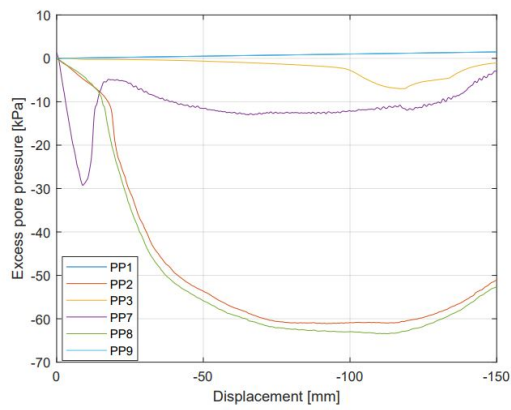


Figure C.42: External excess PP vs displacement in Test D20. **Figure C.43:** External excess PP vs time in Test D20.

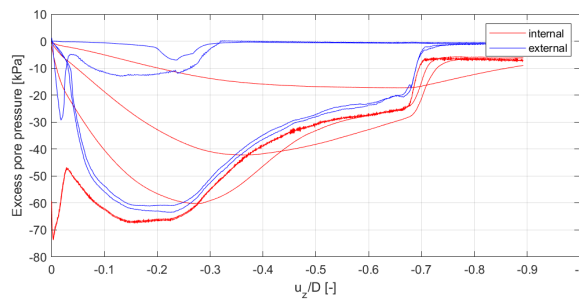


Figure C.44: Internal and external excess PP during D20

C.1.5 Test D50

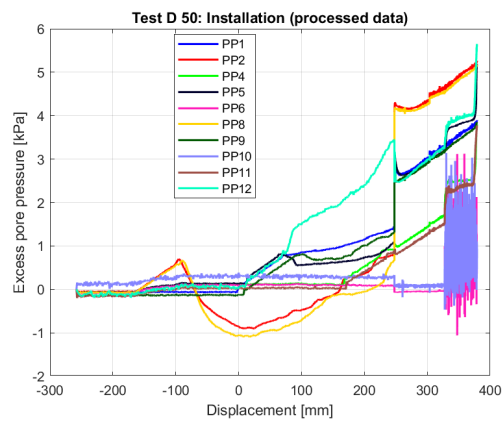


Figure C.45: Excess PP vs displacement for installation in Test D50.

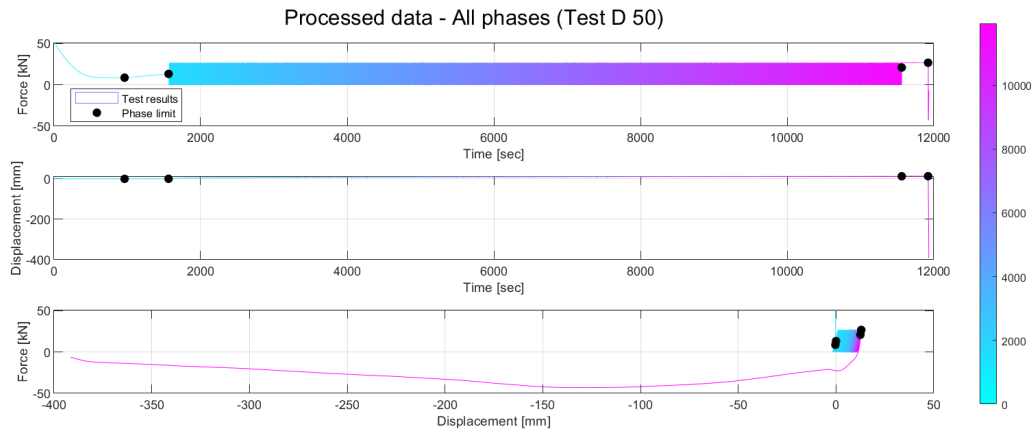


Figure C.46: Force-Time, Disp-Time, Force-Disp in Test D50.

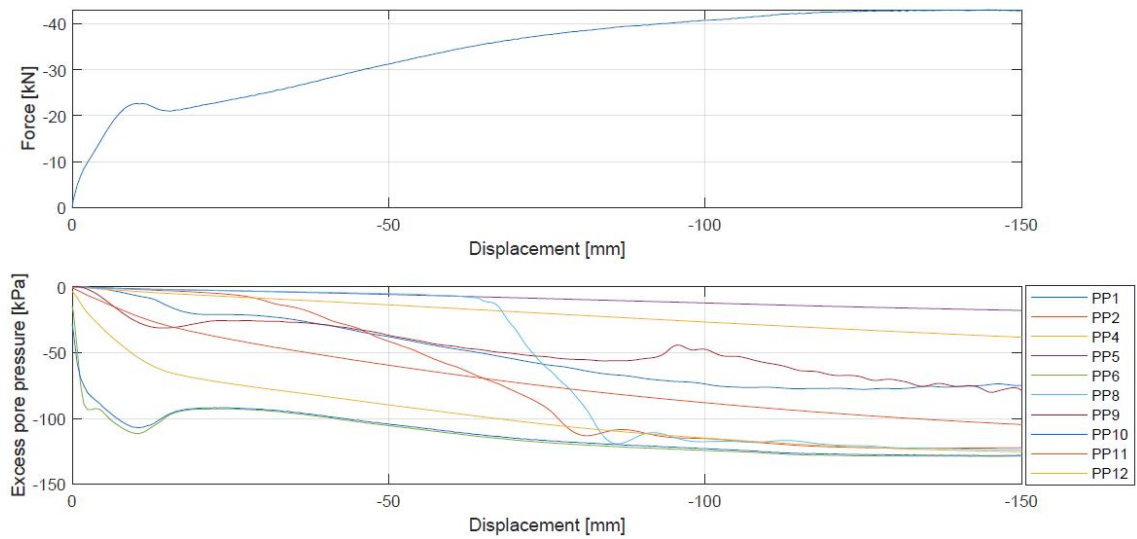


Figure C.47: Force vs displacement and excess PP vs displacement in Test D50.

C.1 Results in High Density Sand

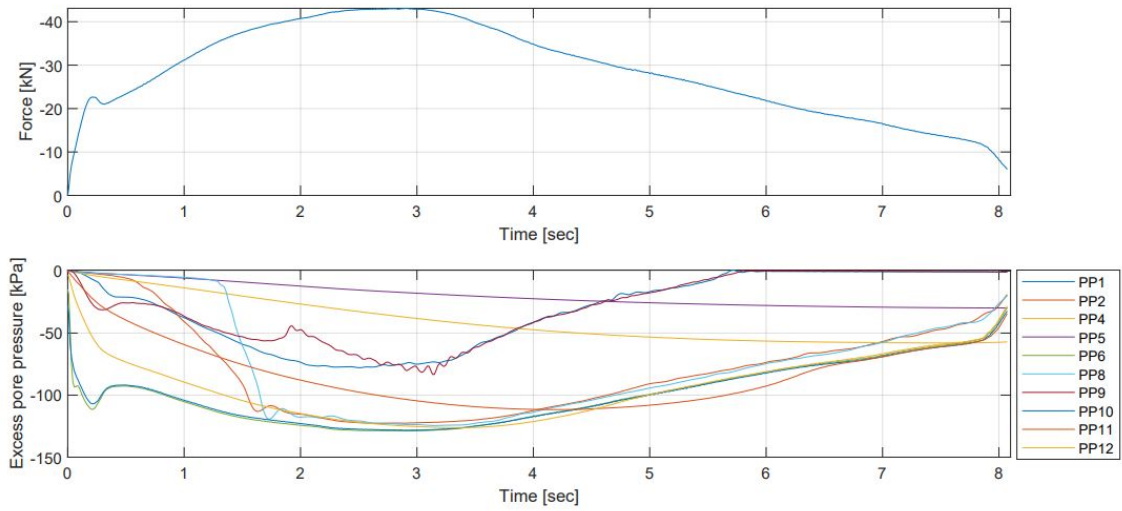


Figure C.48: Force vs time and excess PP vs time in Test D50.

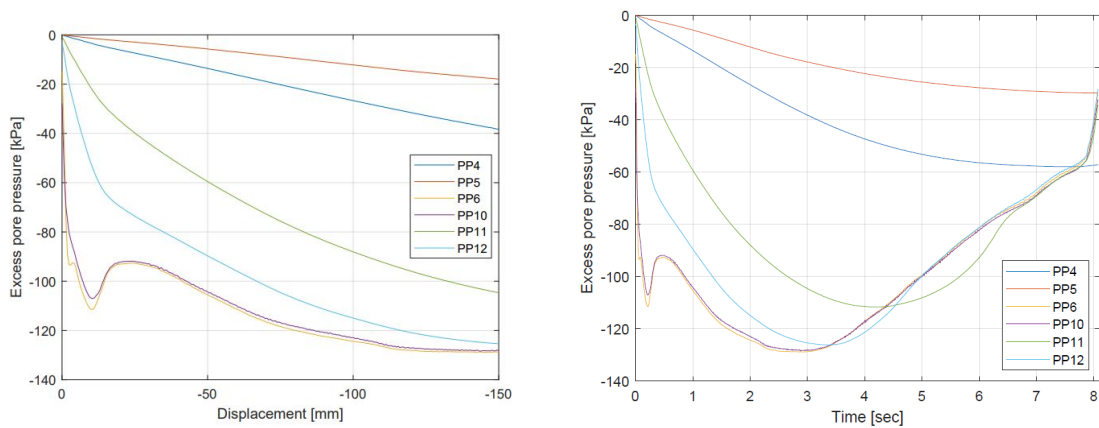


Figure C.49: Internal excess PP vs displacement in Test D50.

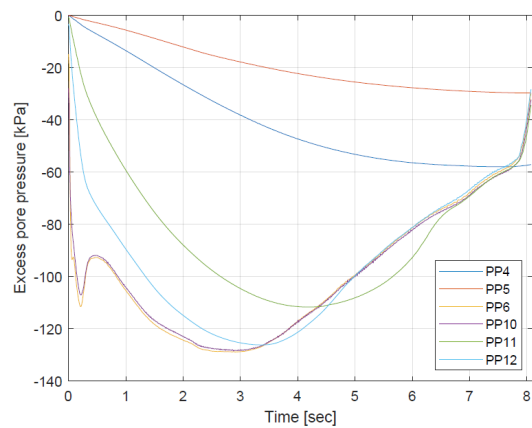


Figure C.50: Internal excess PP vs time in Test D50.

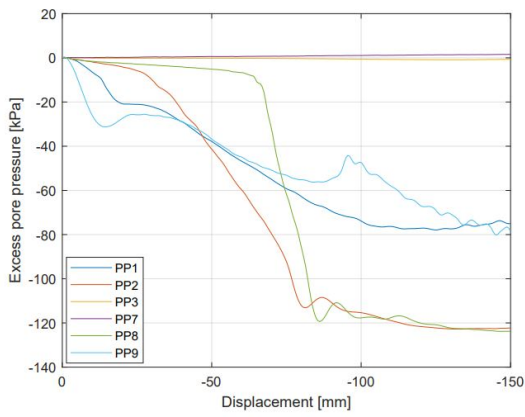


Figure C.51: External excess PP vs displacement in Test D50.

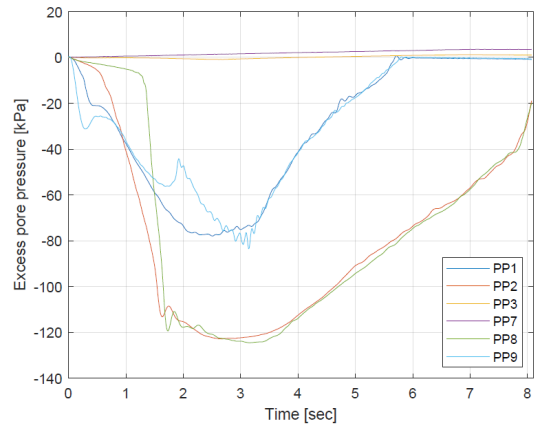


Figure C.52: External excess PP vs time in Test D50.

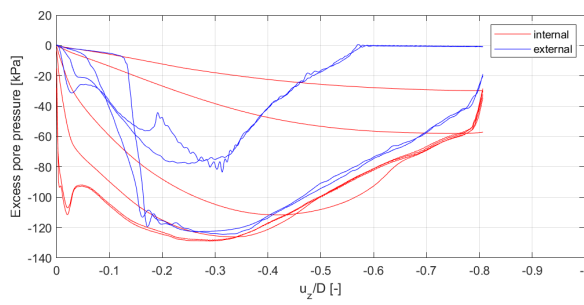


Figure C.53: Internal and external excess PP during D50

Test D 50 | Left half

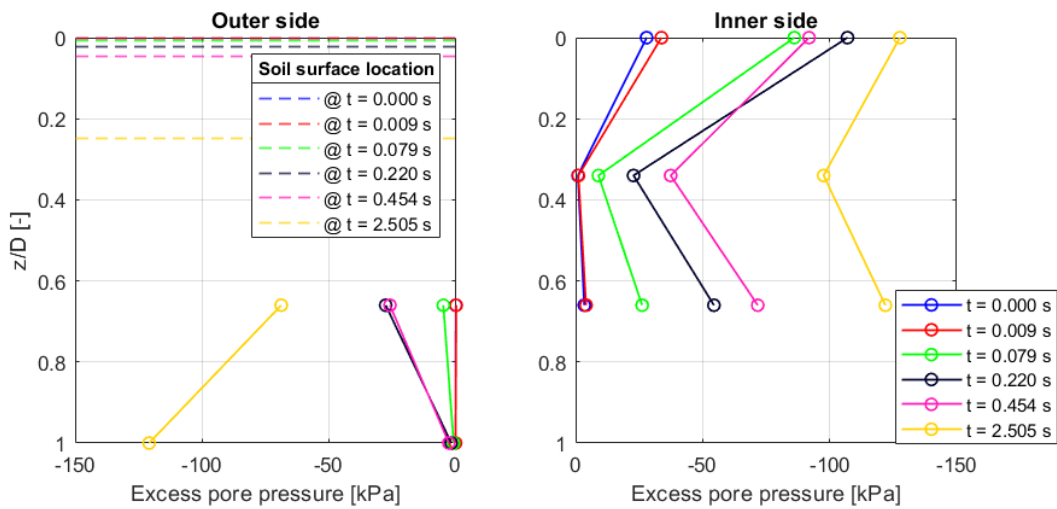


Figure C.54: Force vs time and excess PP vs time in Test D50.

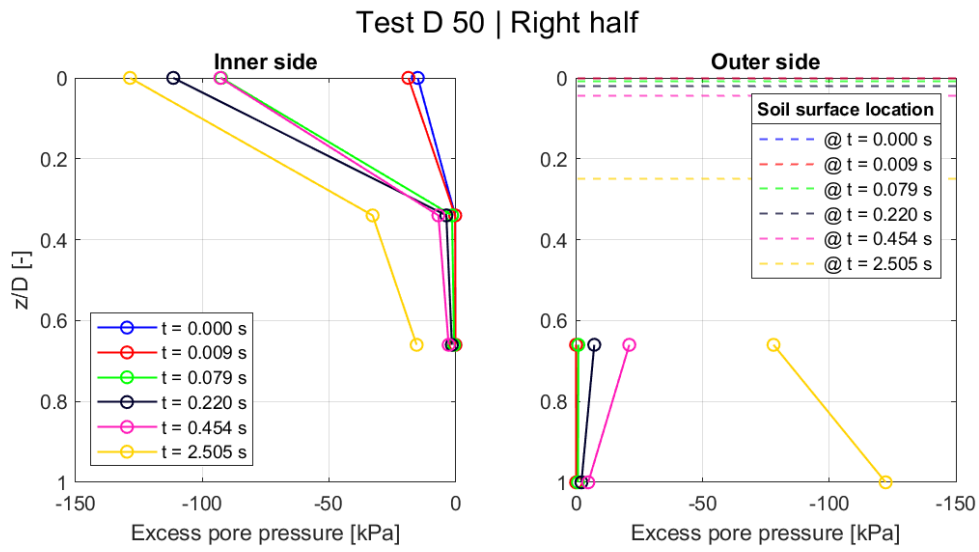


Figure C.55: Force vs time and excess PP vs time in Test D50.

C.1.6 Test D80

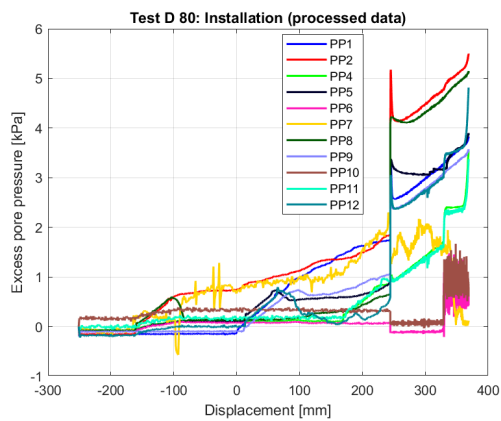


Figure C.56: Excess PP vs displacement for installation in Test D80.

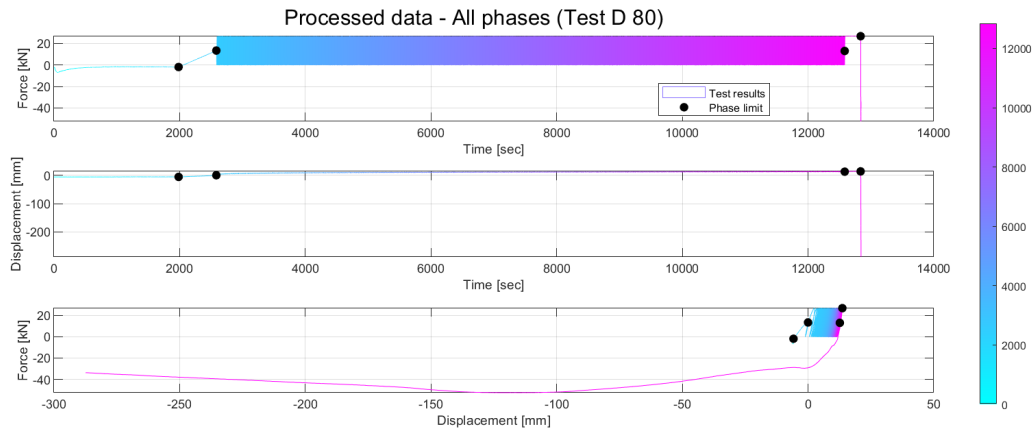


Figure C.57: Force-Time, Disp-Time, Force-Disp in Test D80.

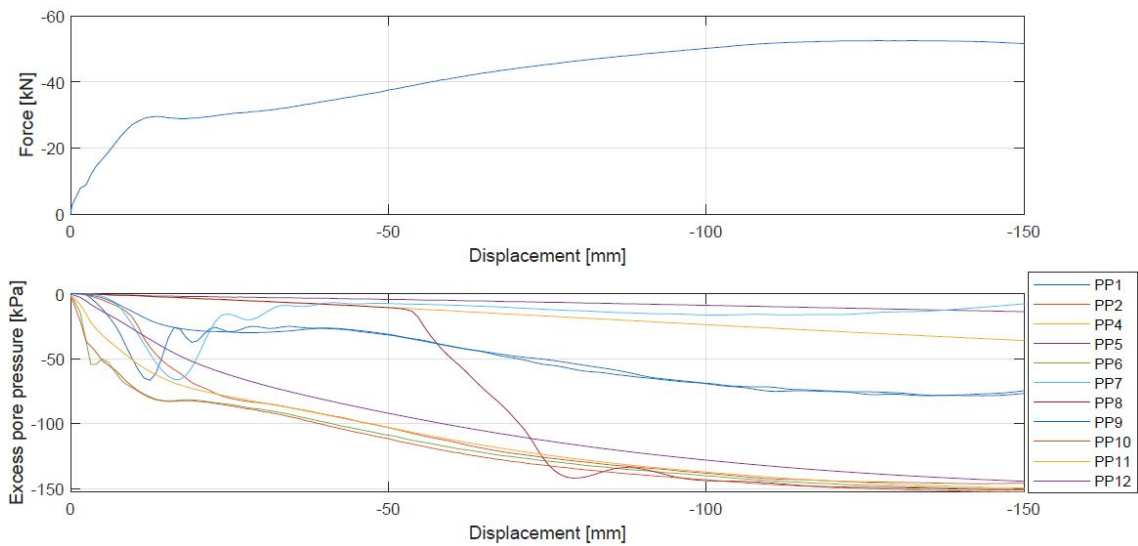


Figure C.58: Force vs displacement and excess PP vs displacement in Test D80.

C.1 Results in High Density Sand

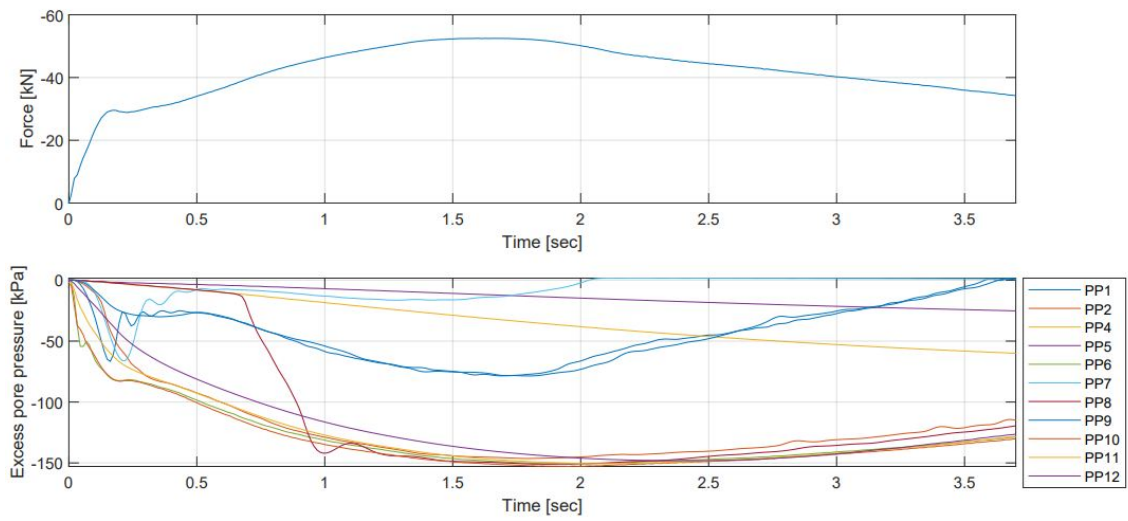


Figure C.59: Force vs time and excess PP vs time in Test D80.

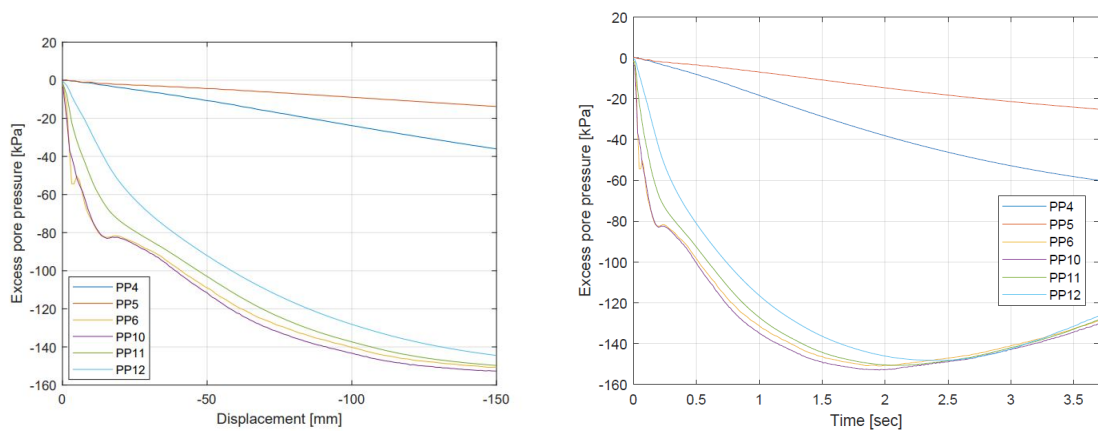


Figure C.60: Internal excess PP vs displacement in Test D80.

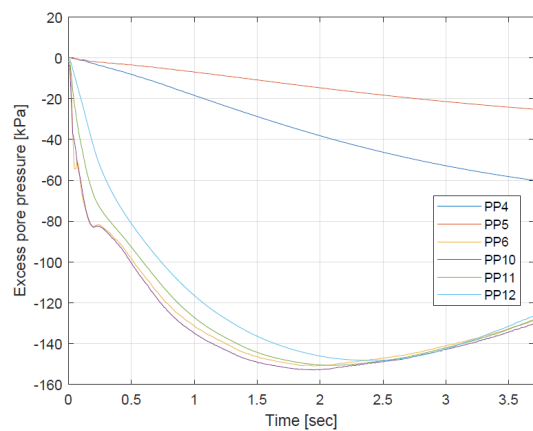


Figure C.61: Internal excess PP vs time in Test D80.

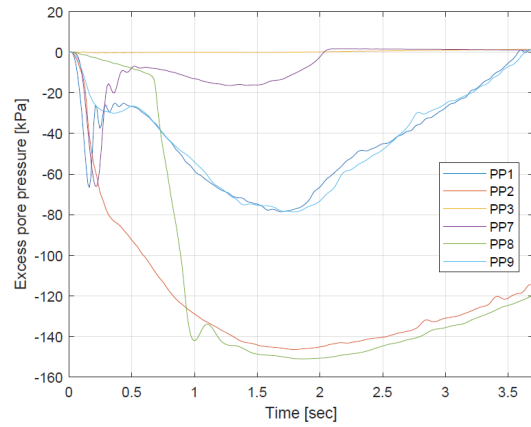
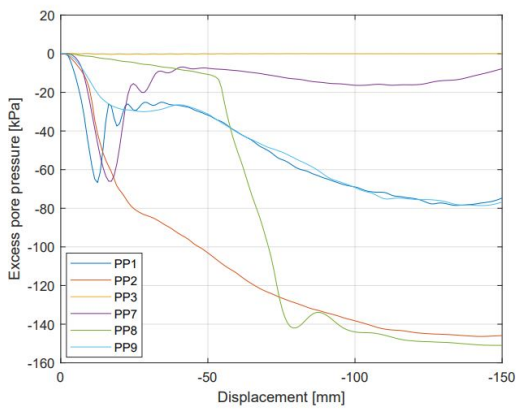


Figure C.62: External excess PP vs displacement in Test D80. **Figure C.63:** External excess PP vs time in Test D80.

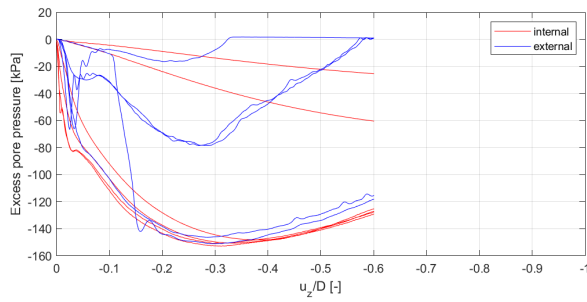


Figure C.64: Internal and external excess PP during D80

C.1.7 Test D100

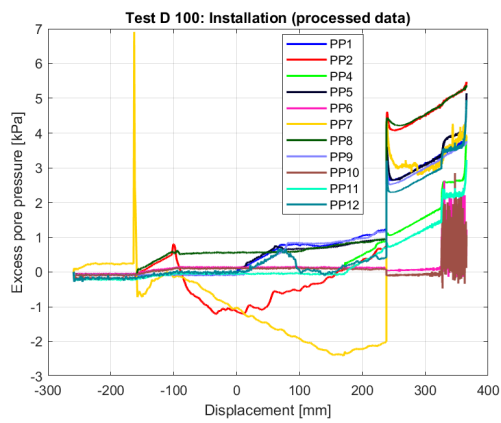


Figure C.65: Excess PP vs displacement for installation in Test D100.

C.1 Results in High Density Sand

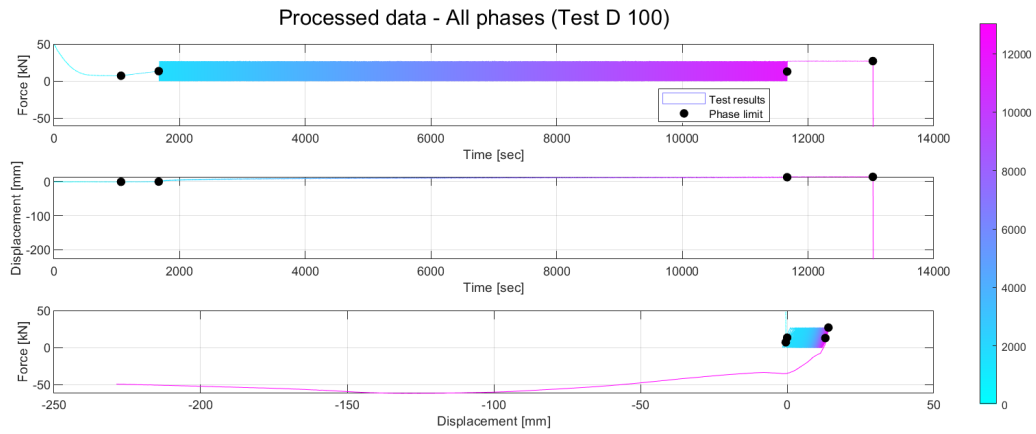


Figure C.66: Force-Time, Disp-Time, Force-Disp in Test D100.

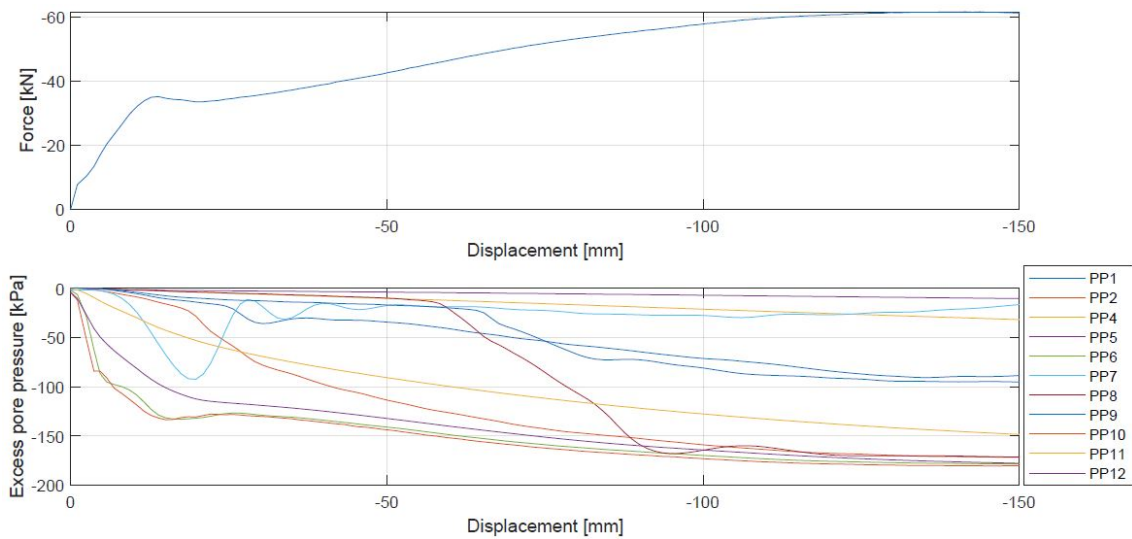


Figure C.67: Force vs displacement and excess PP vs displacement in Test D100.

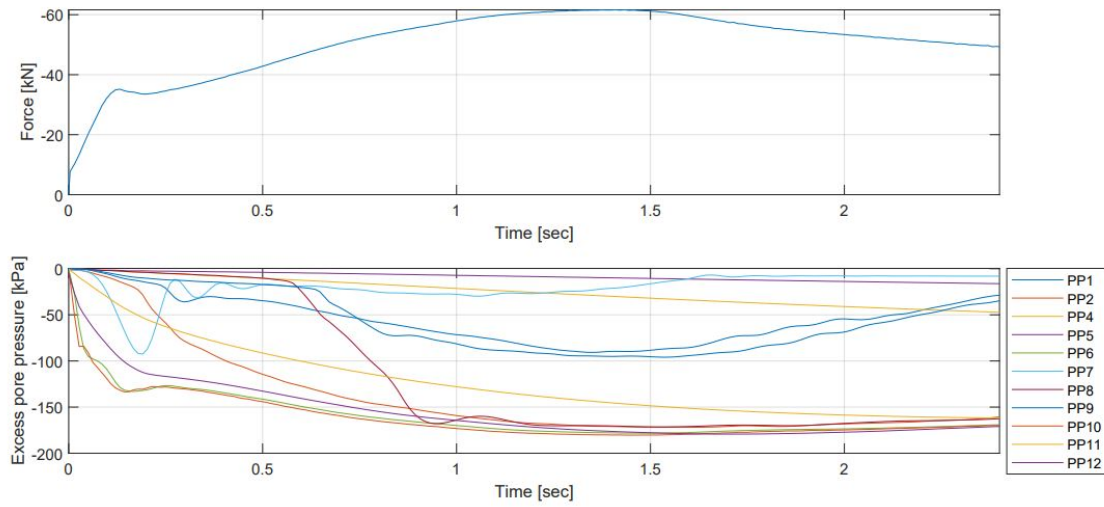


Figure C.68: Force vs time and excess PP vs time in Test D100.

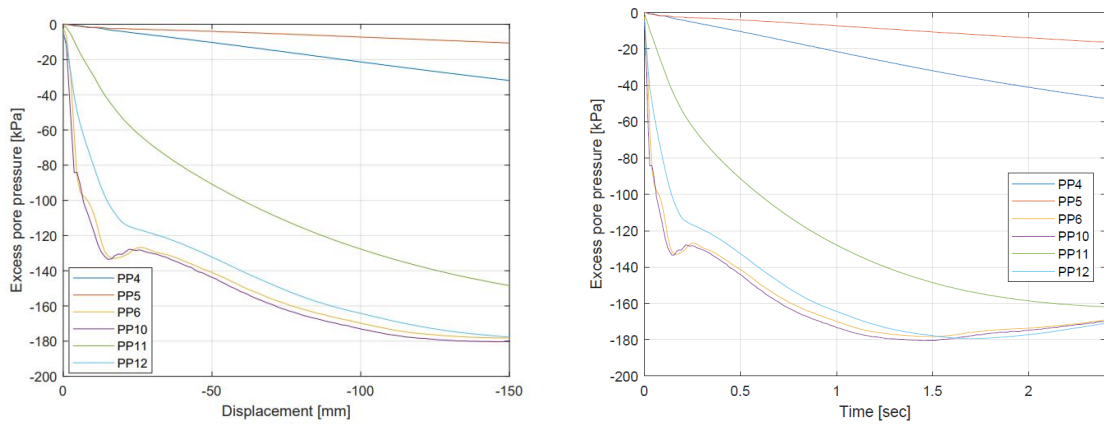


Figure C.69: Internal excess PP vs displacement in Test D100. Figure C.70: Internal excess PP vs time in Test D100.

C.1 Results in High Density Sand

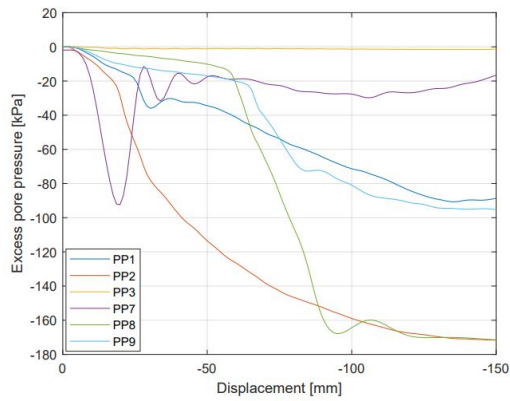


Figure C.71: External excess PP vs displacement in Test D100.

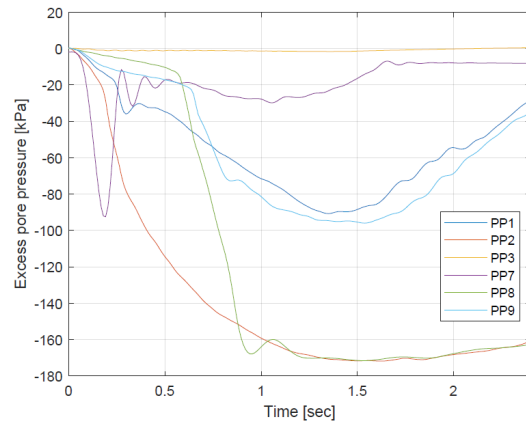


Figure C.72: External excess PP vs time in Test D100.

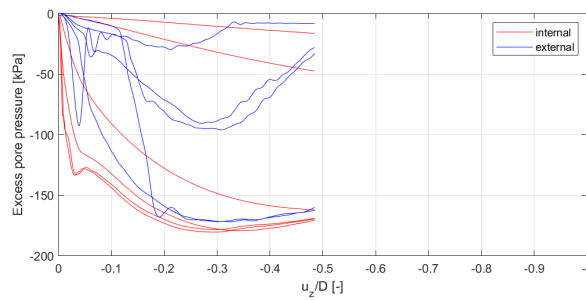


Figure C.73: Internal and external excess PP during D100

C.1.8 Test D150 with cyclic loading

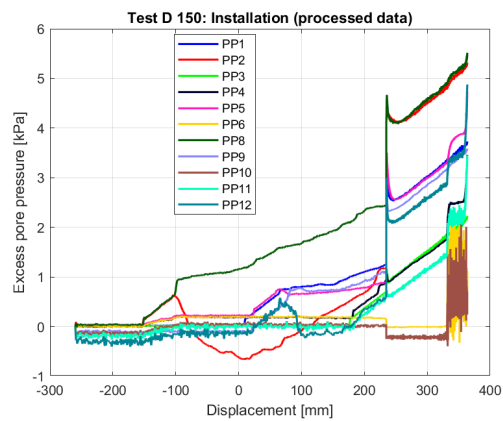


Figure C.74: Excess PP vs displacement for installation in Test D150.

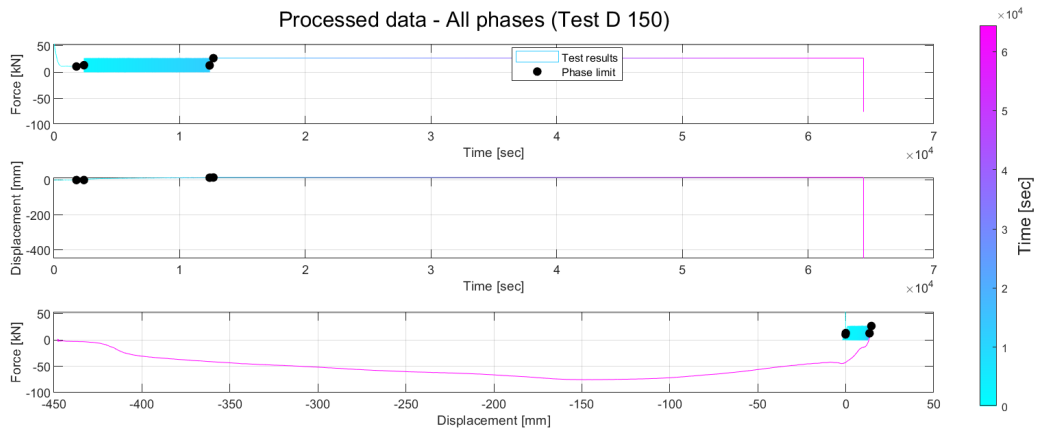


Figure C.75: Force-Time, Disp-Time, Force-Disp in Test D50.

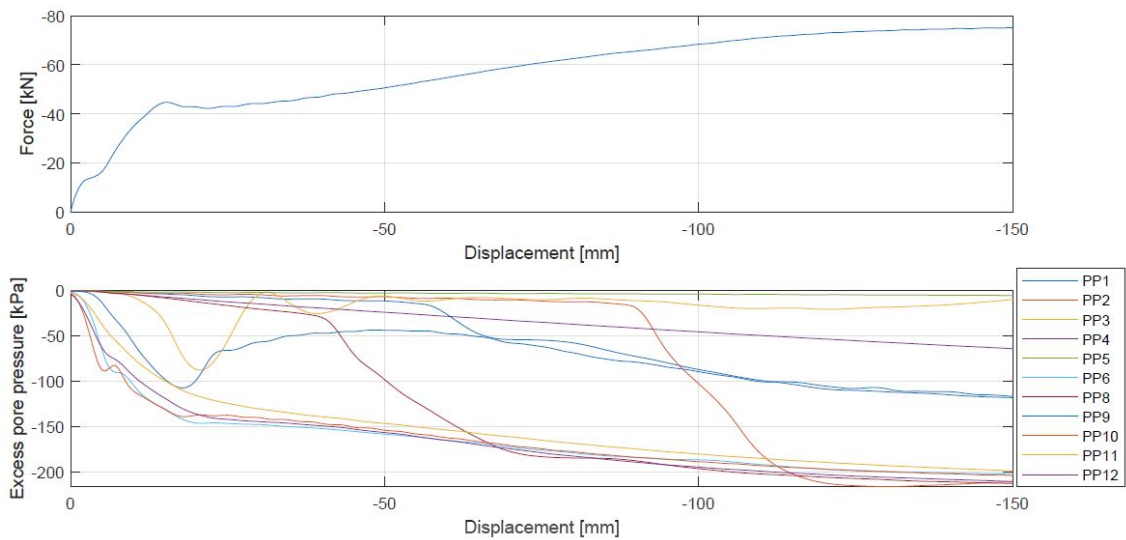


Figure C.76: Force vs displacement and excess PP vs displacement in Test D150.

C.1 Results in High Density Sand

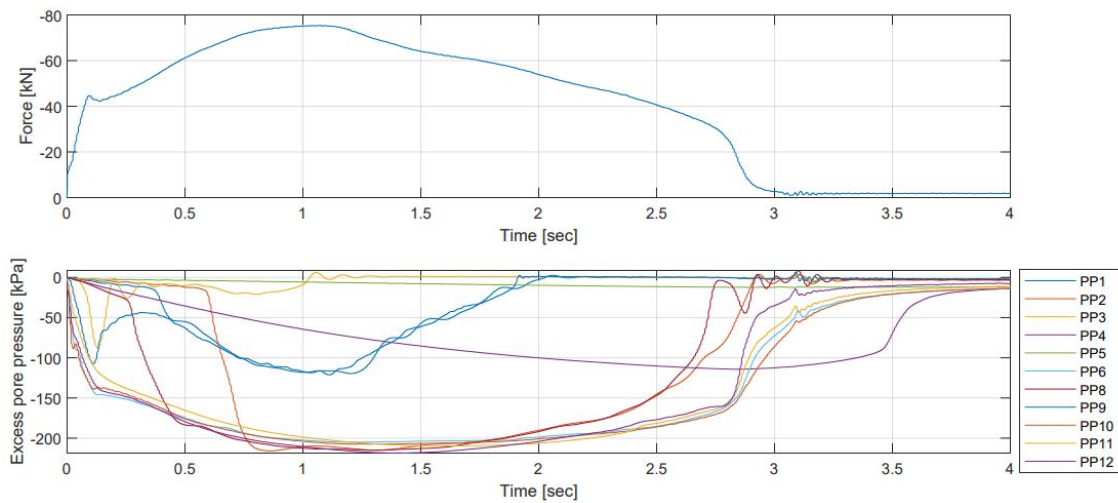


Figure C.77: Force vs time and excess PP vs time in Test D150.

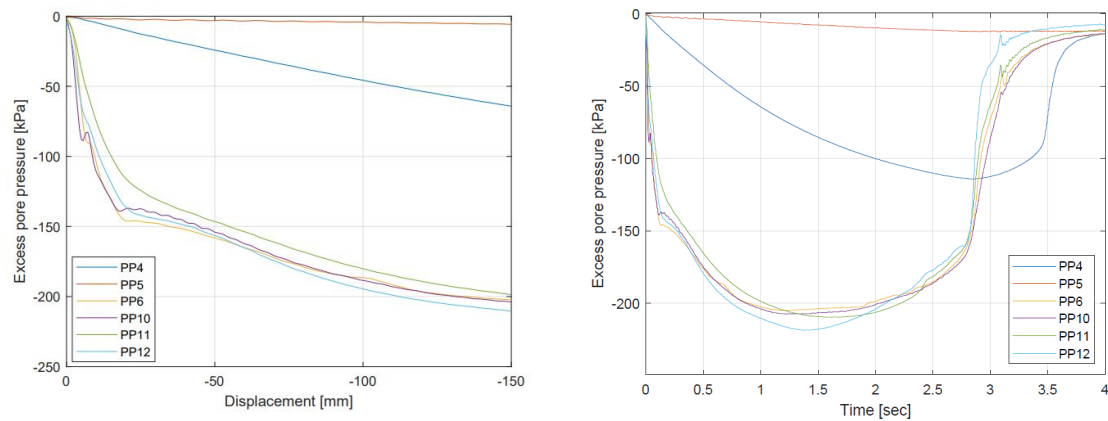


Figure C.78: Internal excess PP vs displacement in Test D150. **Figure C.79:** Internal excess PP vs time in Test D150.

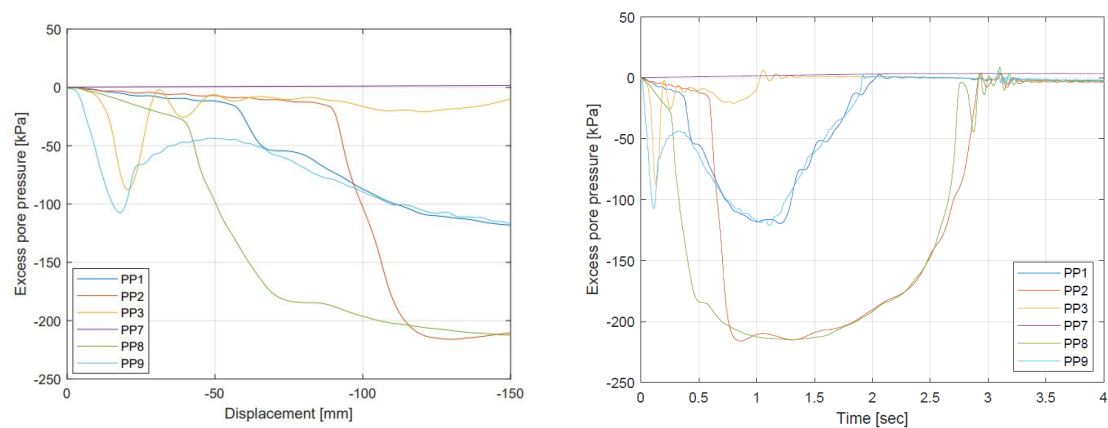


Figure C.80: External excess PP vs displacement in Test D150. **Figure C.81:** External excess PP vs time in Test D150.

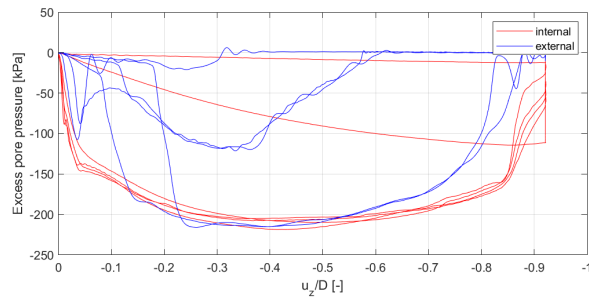


Figure C.82: Internal and external excess PP during D150

C.1.9 Test D150 without cyclic loading

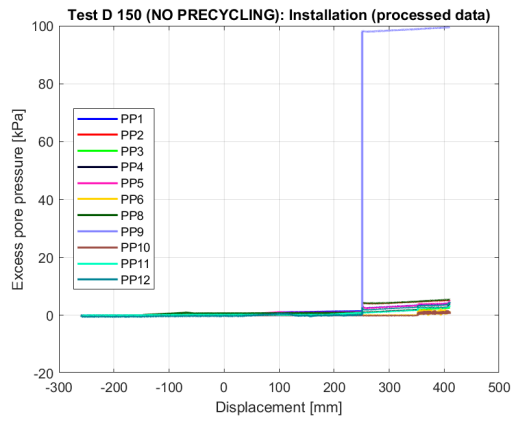


Figure C.83: Excess PP vs displacement for installation in Test D150 (NO CYC).

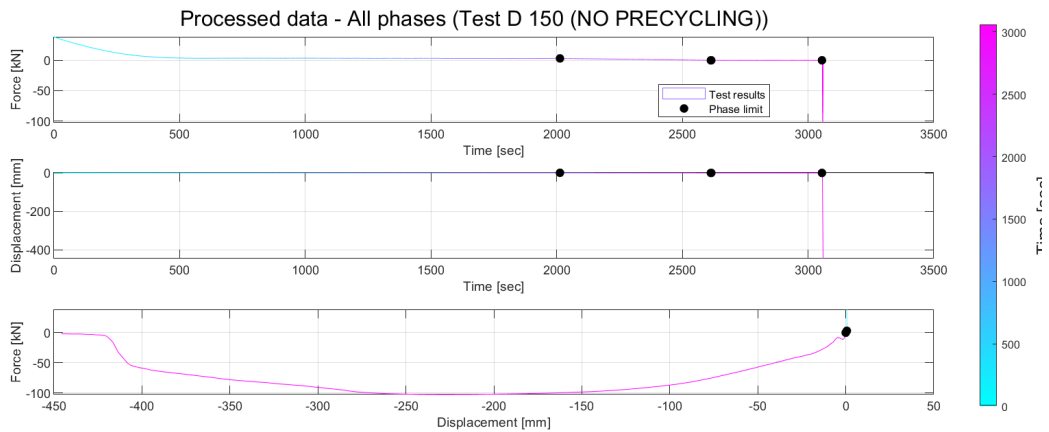


Figure C.84: Force-Time, Disp-Time, Force-Disp in Test D150 (NO CYC).

C.1 Results in High Density Sand

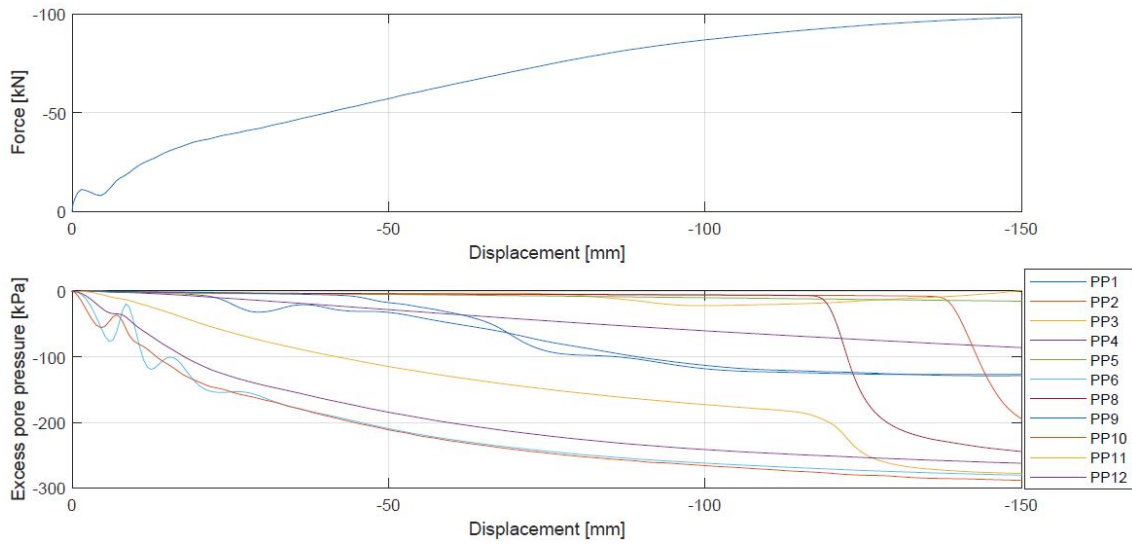


Figure C.85: Force vs displacement and excess PP vs displacement in Test D150 without cyclic loading.

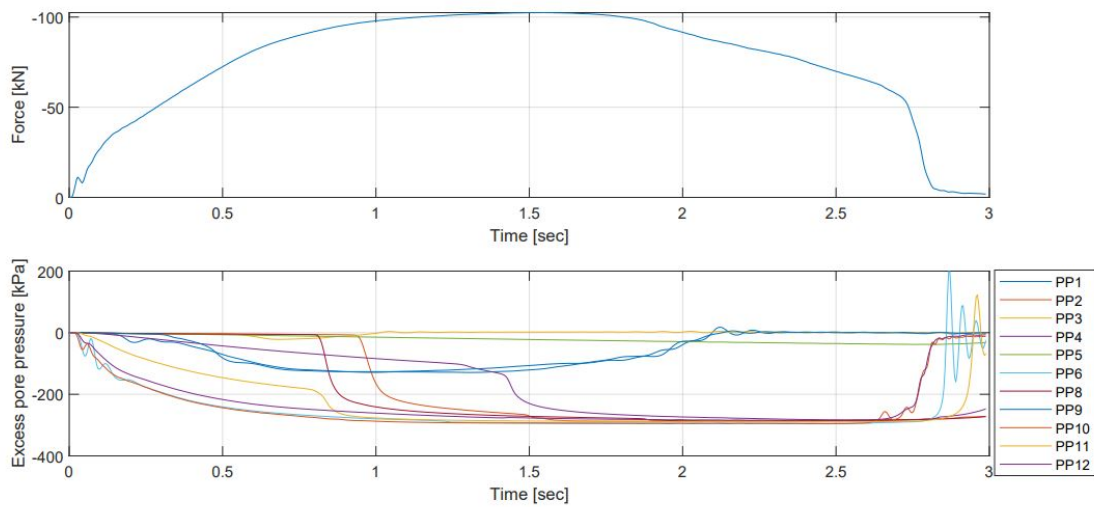


Figure C.86: Force vs time and excess PP vs time in Test D150 without cyclic loading.

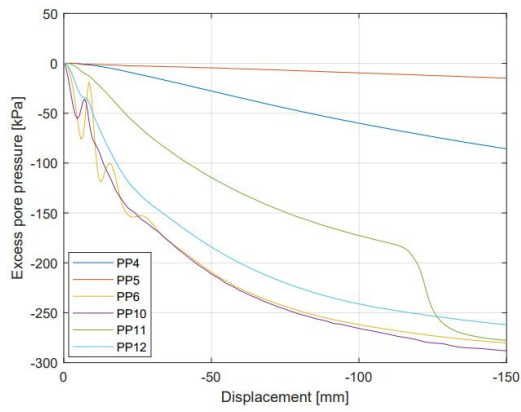


Figure C.87: Internal excess PP vs displacement in Test D150 without cyclic loading.

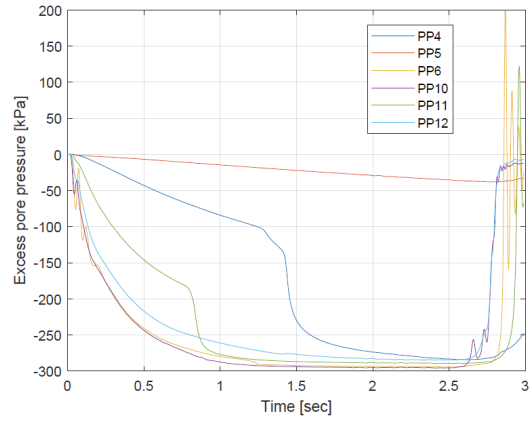


Figure C.88: Internal excess PP vs time in Test D150 without cyclic loading.

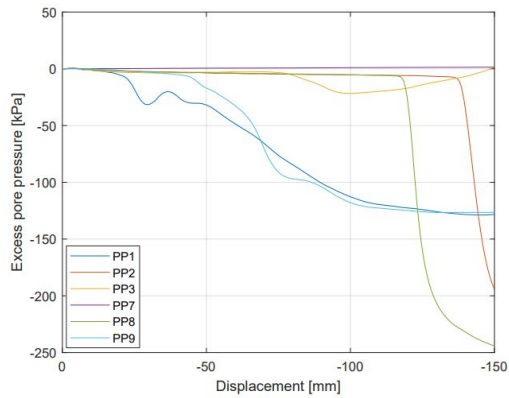


Figure C.89: External excess PP vs displacement in Test D150 without cyclic loading.

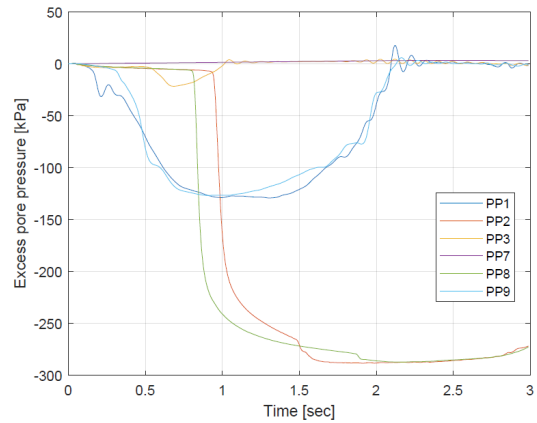


Figure C.90: External excess PP vs time in Test D150 without cyclic loading.

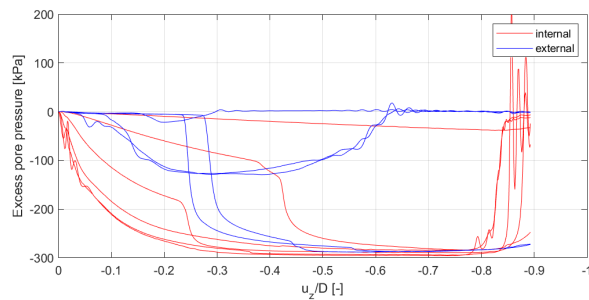


Figure C.91: Internal and external excess PP during D150 without cyclic loading

C.1.10 Test D150 Bucket B with cyclic loading

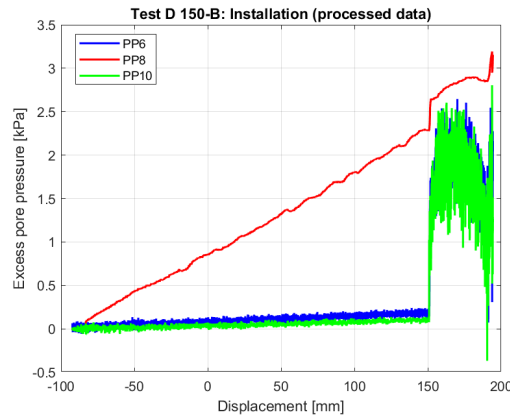


Figure C.92: Excess PP vs displacement for installation in Test D150-B.

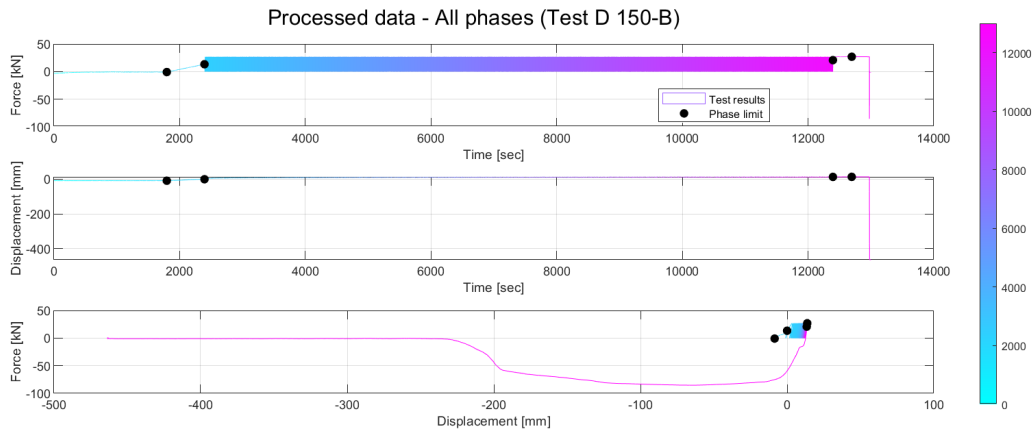


Figure C.93: Force-Time, Disp-Time, Force-Disp in Test D150-B.

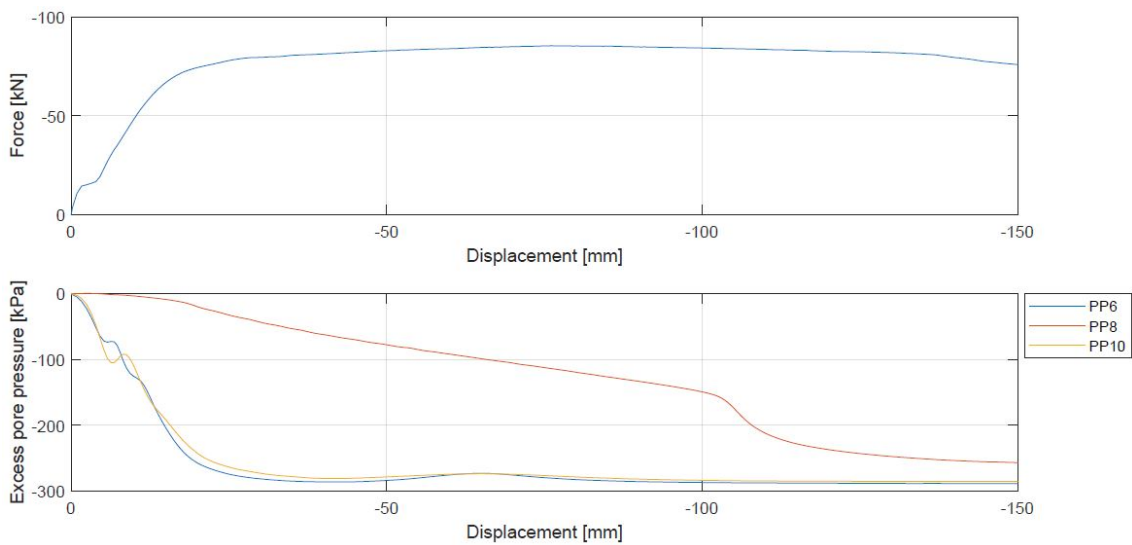


Figure C.94: Force vs displacement and excess PP vs displacement in Test D150-B with cyclic loading.

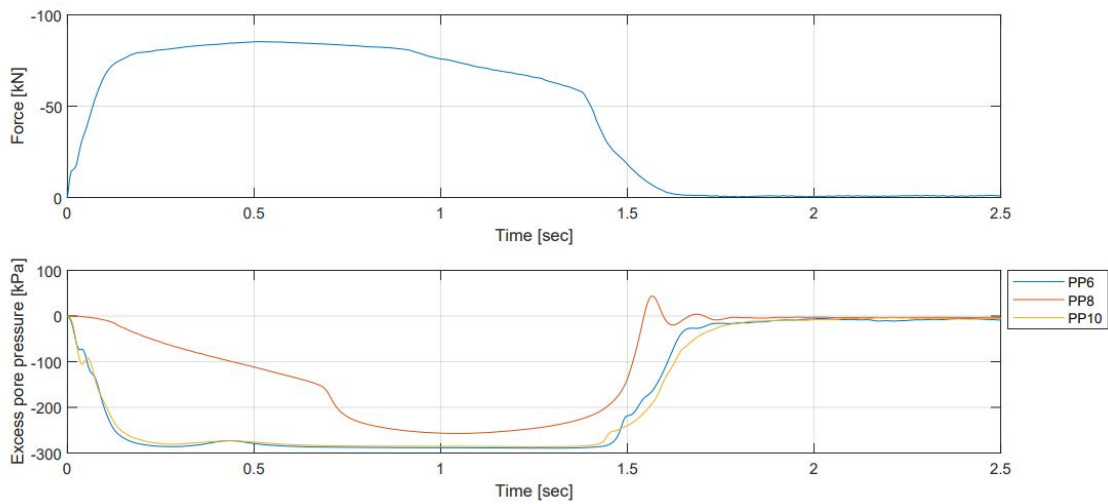


Figure C.95: Force vs time and excess PP vs time in Test D150-B with cyclic loading.

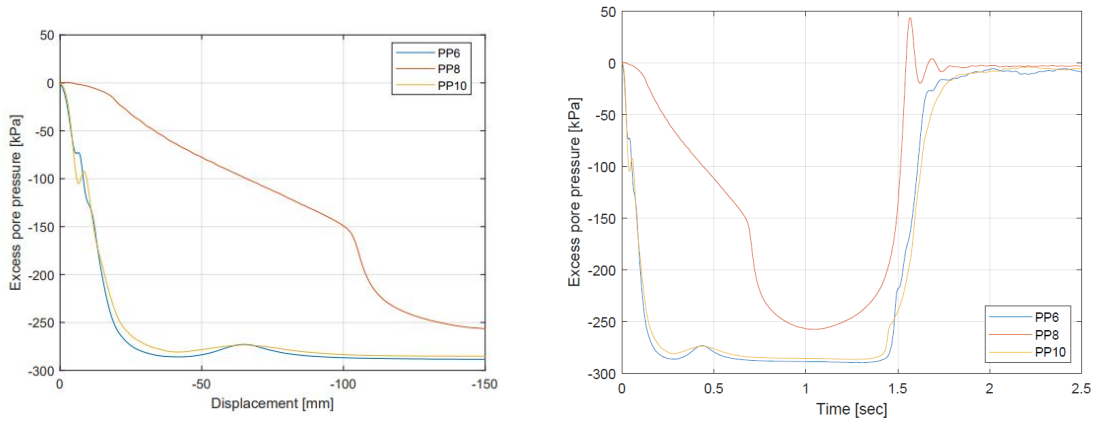


Figure C.96: Excess PP vs displacement in Test D150-B with cyclic loading. Figure C.97: Excess PP vs time in Test D150-B with cyclic loading.

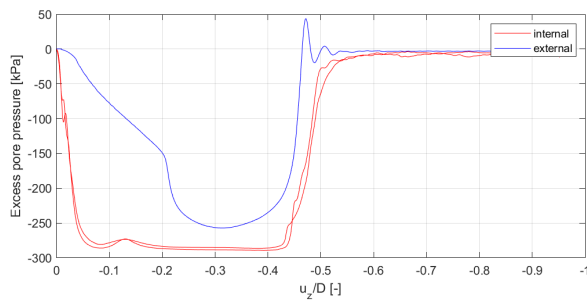


Figure C.98: Internal and external excess PP during D150-B with cyclic loading

C.1.11 Test D150 Bucket B without cyclic loading

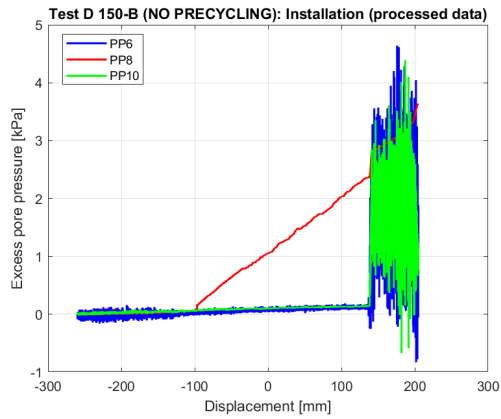


Figure C.99: Excess PP vs displacement for installation in Test D150-B (NO CYC).

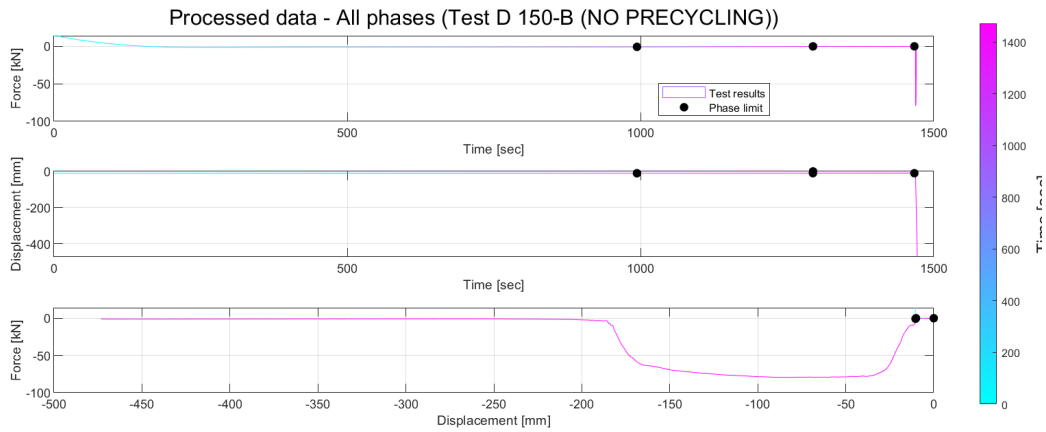


Figure C.100: Force-Time, Disp-Time, Force-Disp in Test D150-B (NO CYC).

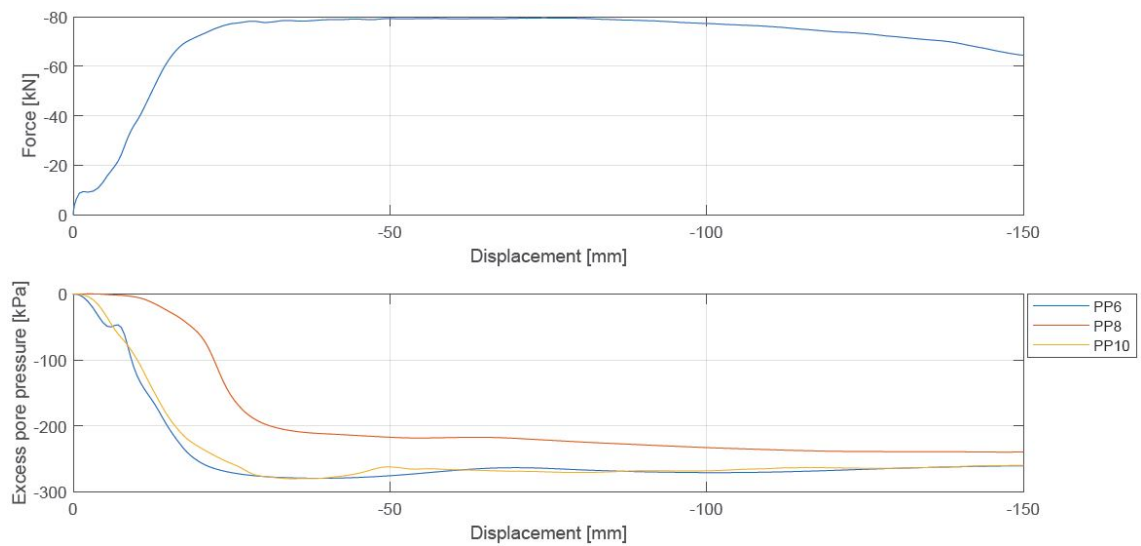


Figure C.101: Force vs displacement and excess PP vs displacement in Test D150-B without cyclic loading.

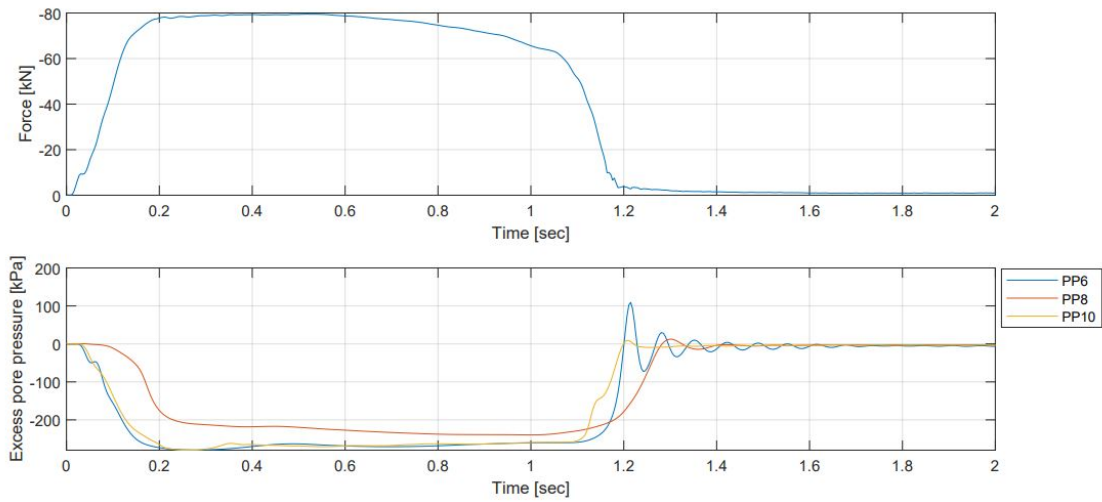


Figure C.102: Force vs time and excess PP vs time in Test D150-B without cyclic loading.

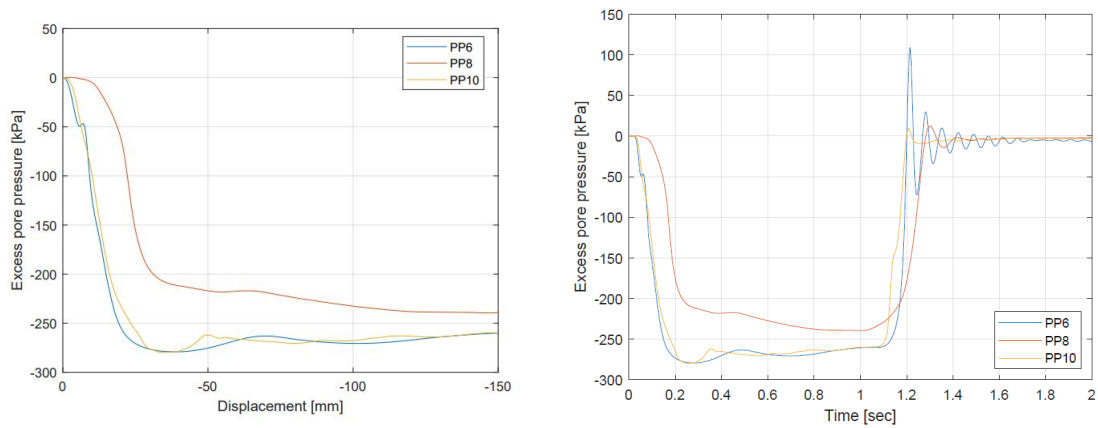


Figure C.103: Excess PP vs displacement in Test D150-B without cyclic loading.

Figure C.104: Excess PP vs time in Test D150-B without cyclic loading.

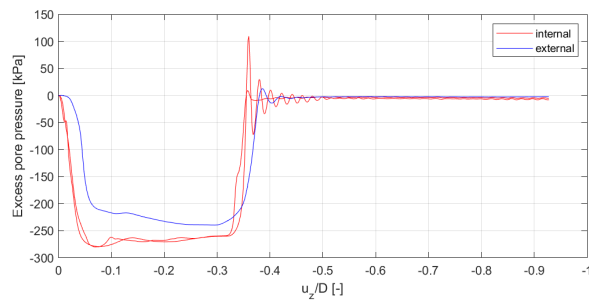


Figure C.105: Internal and external excess PP during D150-B without cyclic loading

C.1 Results in High Density Sand

C.1.12 Test D200

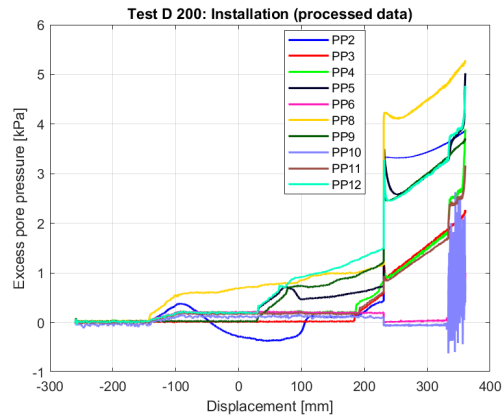


Figure C.106: Excess PP vs displacement for installation in Test D200.

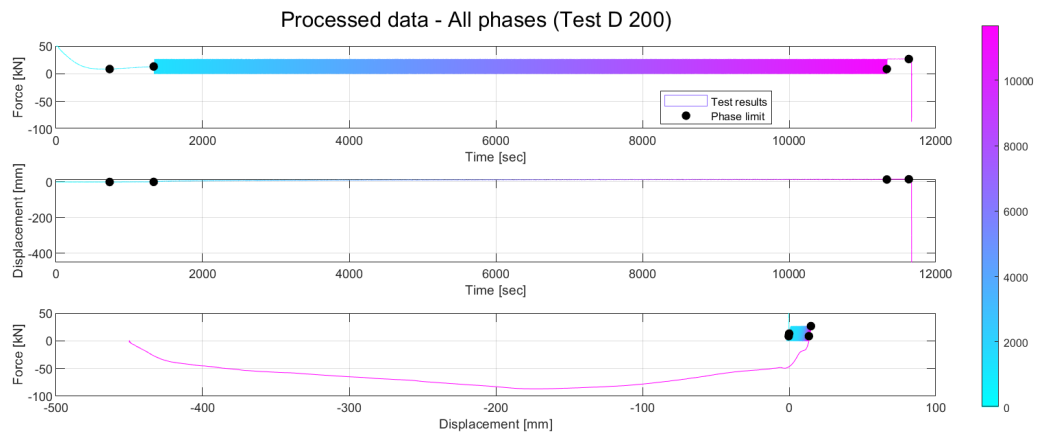


Figure C.107: Force-Time, Displacement-Time, Force-Disp in Test D200.

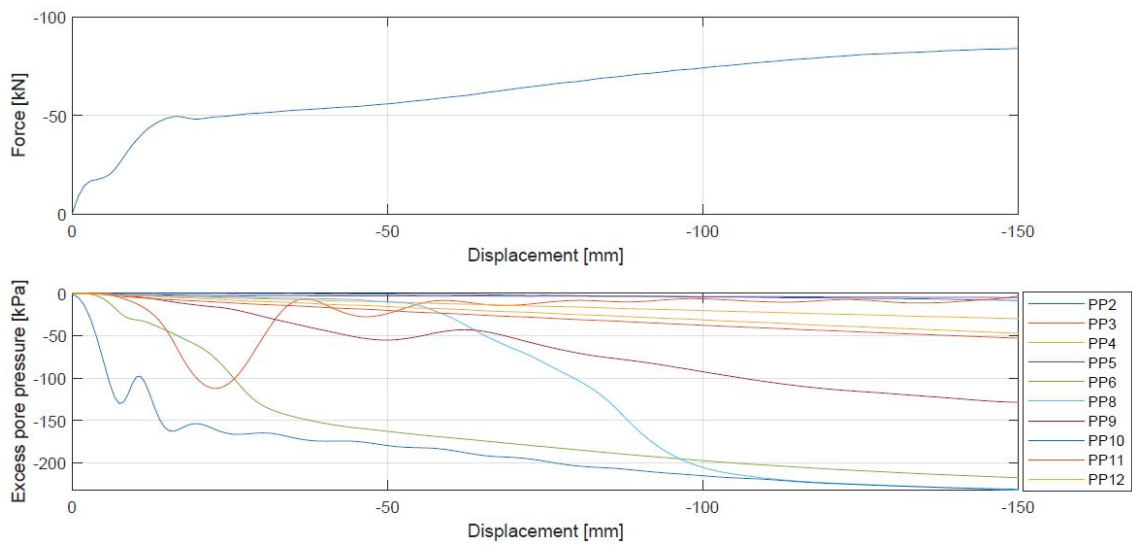


Figure C.108: Force vs displacement and excess PP vs displacement in Test D200.

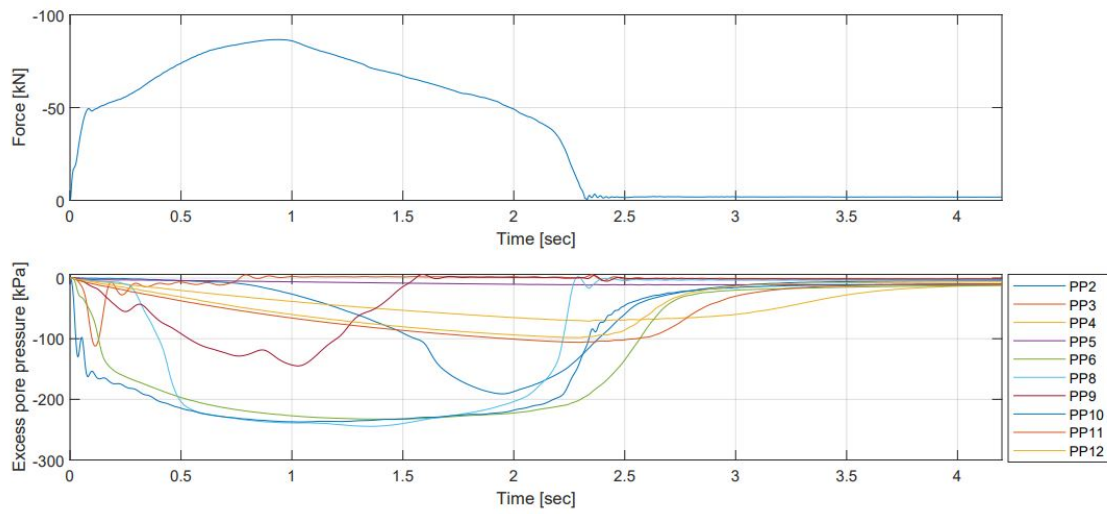


Figure C.109: Force vs time and excess PP vs time in Test D200.

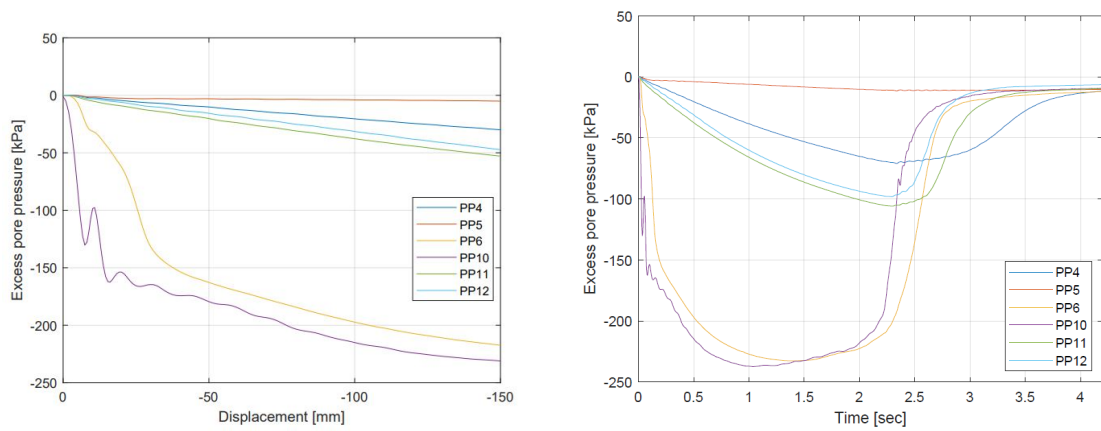


Figure C.110: Internal excess PP vs displacement in Test D200.

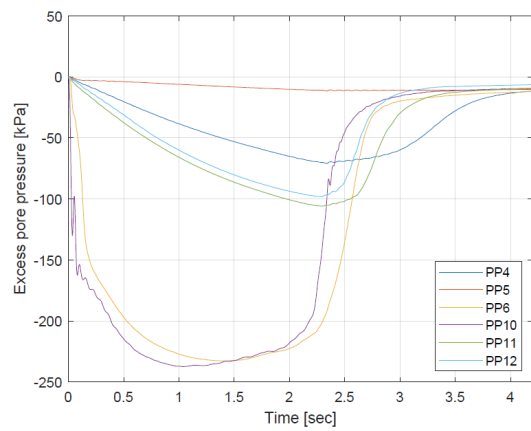


Figure C.111: Internal excess PP vs time in Test D200.

C.1 Results in High Density Sand

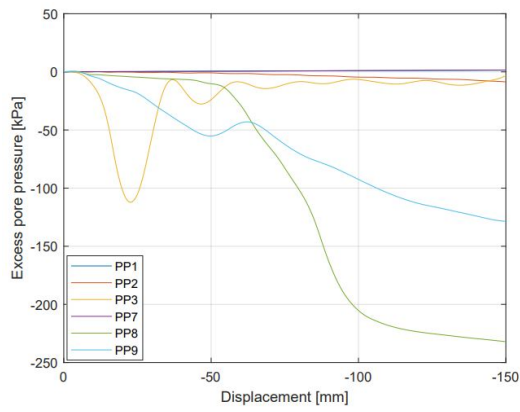


Figure C.112: External excess PP vs displacement in Test D200.

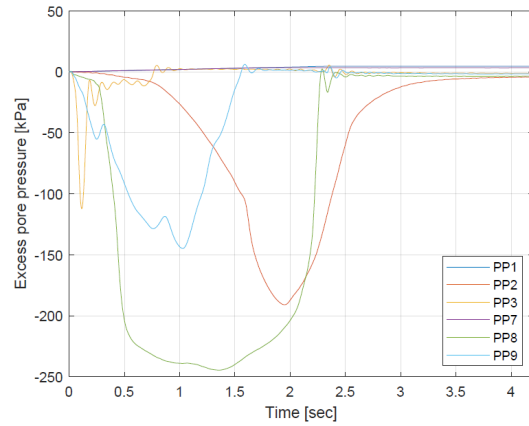


Figure C.113: External excess PP vs time in Test D200.

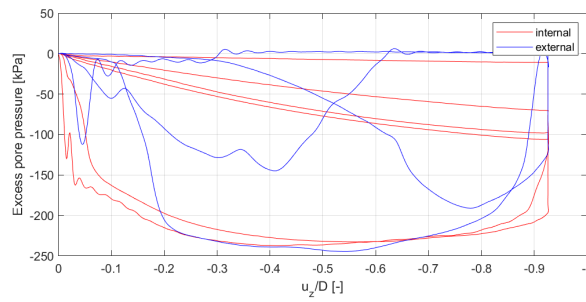


Figure C.114: Internal and external excess PP during D200

C.1.13 Test D300

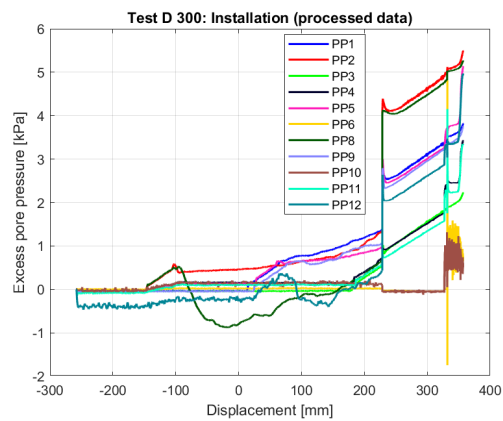


Figure C.115: Excess PP vs displacement for installation in Test D300.

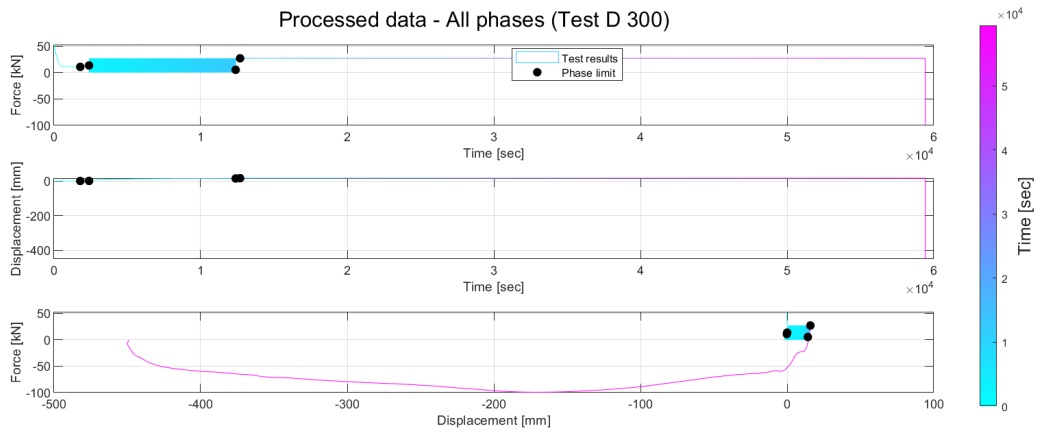


Figure C.116: Force-Time, Disp-Time, Force-Disp in Test D300.

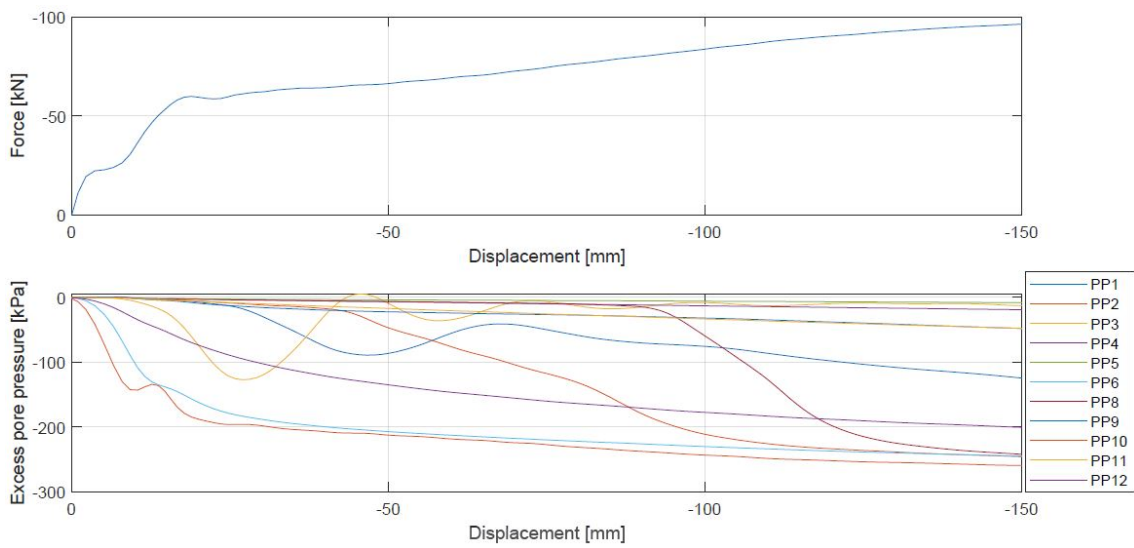


Figure C.117: Force vs displacement and excess PP vs displacement in Test D300.

C.1 Results in High Density Sand

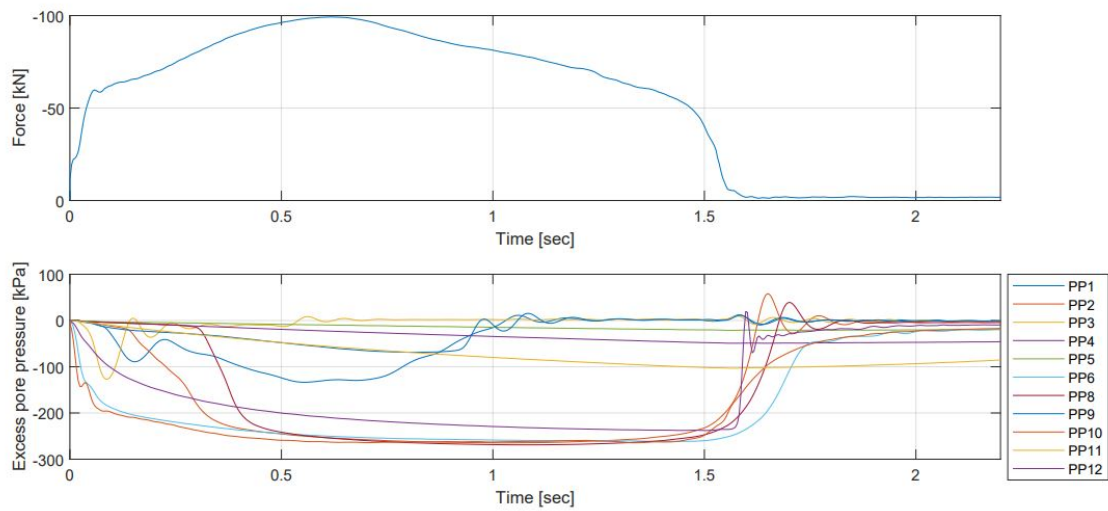


Figure C.118: Force vs time and excess PP vs time in Test D300.

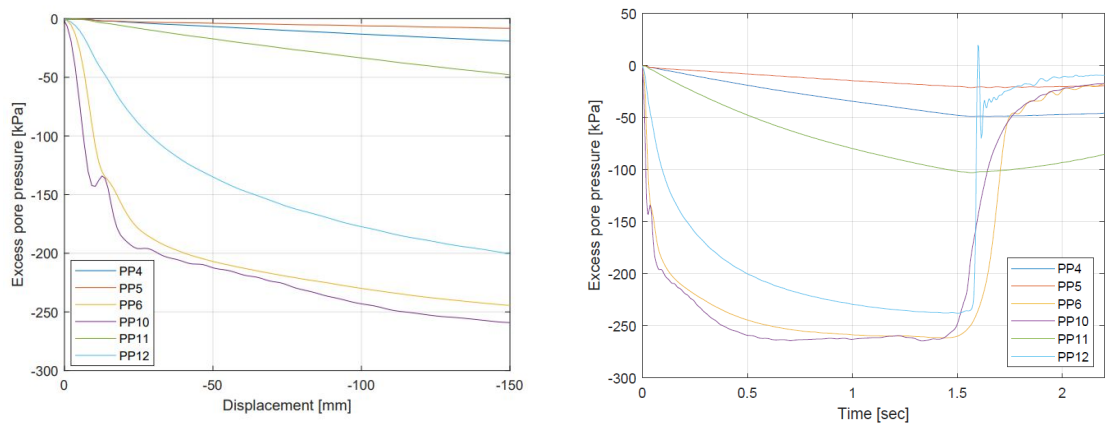


Figure C.119: Internal excess PP vs displacement in Test D300.

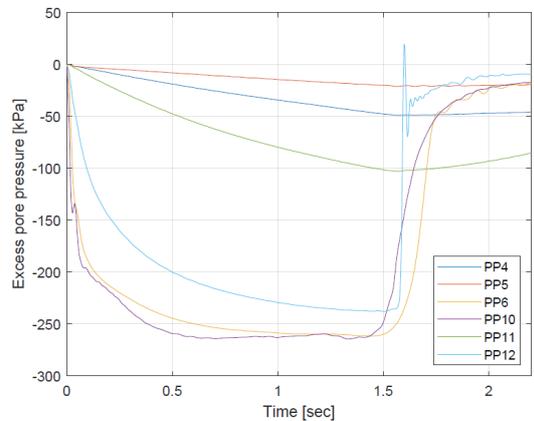


Figure C.120: Internal excess PP vs time in Test D300.

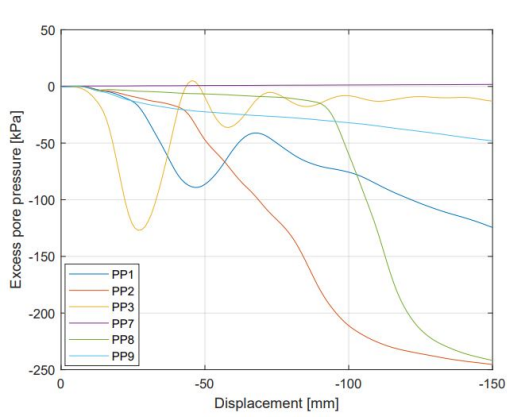


Figure C.121: External excess PP vs displacement in Test D300.

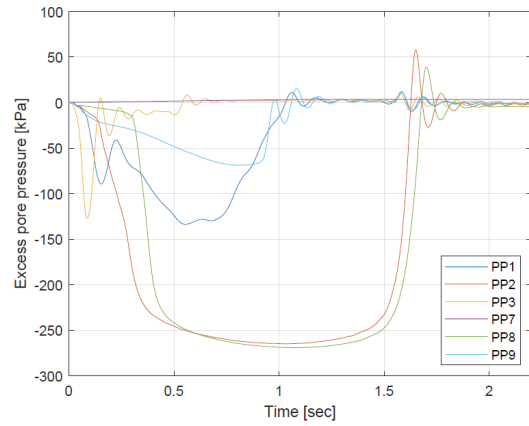


Figure C.122: External excess PP vs time in Test D300.

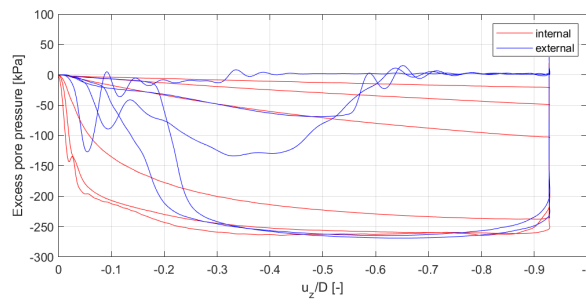


Figure C.123: Internal and external excess PP during D300

C.1.14 Test D400

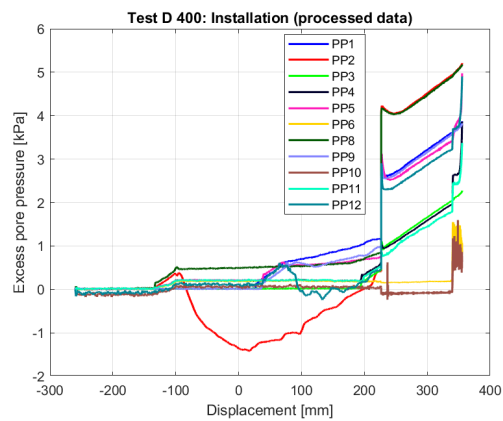


Figure C.124: Excess PP vs displacement for installation in Test D400.

C.1 Results in High Density Sand

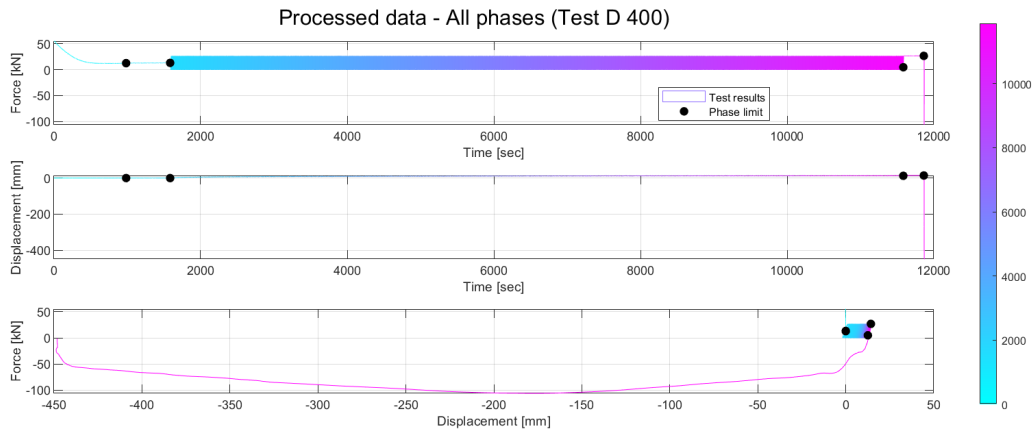


Figure C.125: Force-Time, Disp-Time, Force-Disp in Test D400.

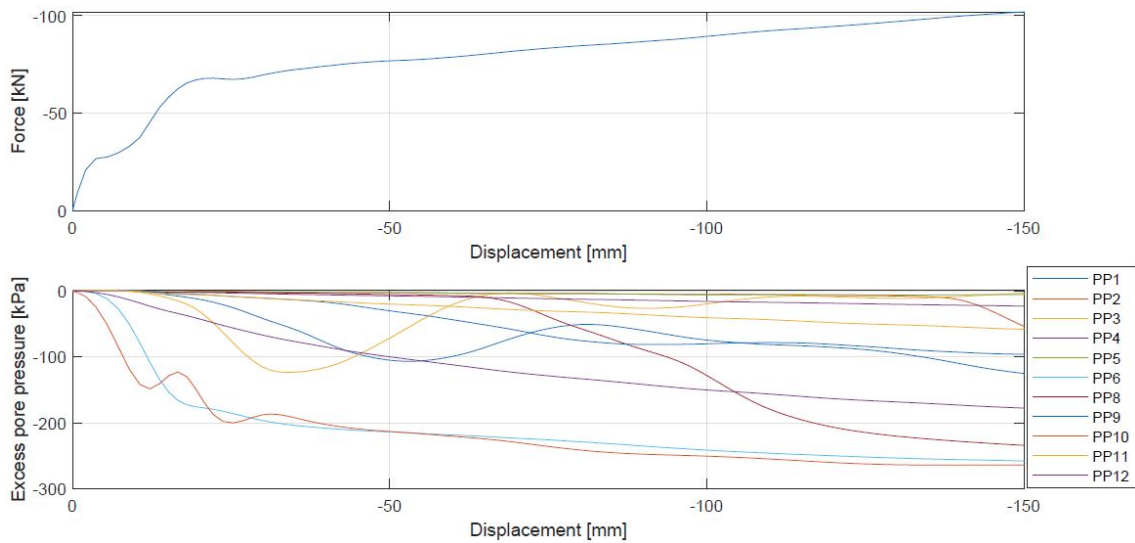


Figure C.126: Force vs displacement and excess PP vs displacement in Test D400.

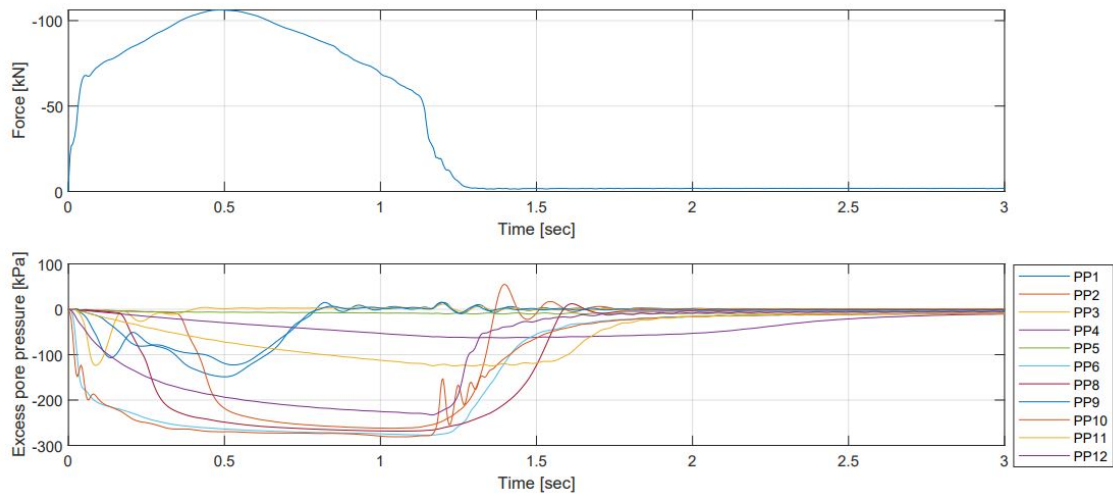


Figure C.127: Force vs time and excess PP vs time in Test D400

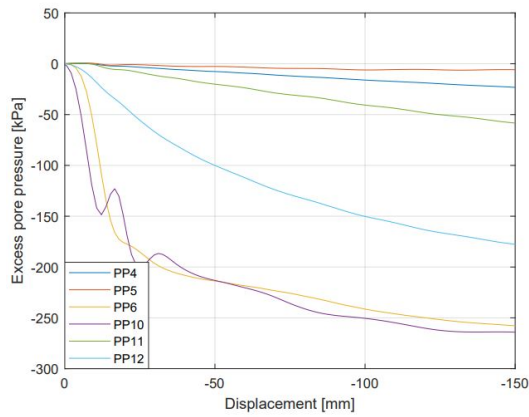


Figure C.128: Internal excess PP vs displacement in Test D400.

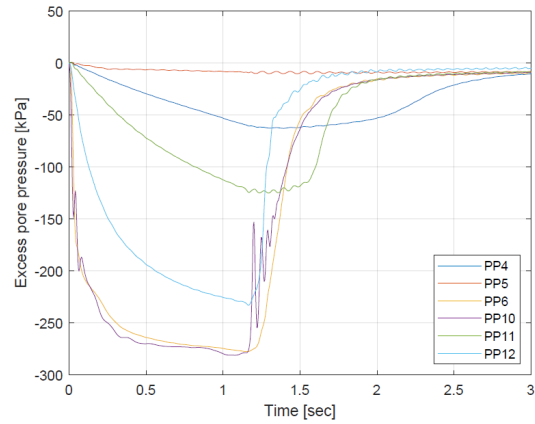


Figure C.129: Internal excess PP vs time in Test D400.

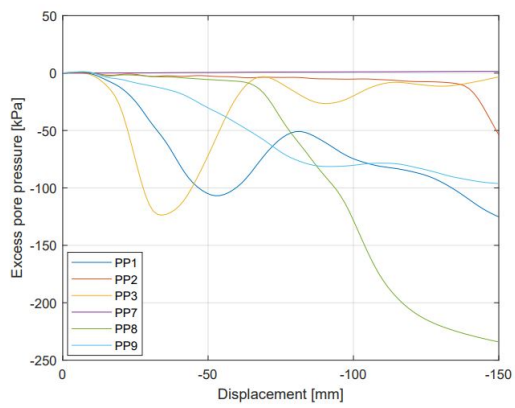


Figure C.130: External excess PP vs displacement in Test D400.

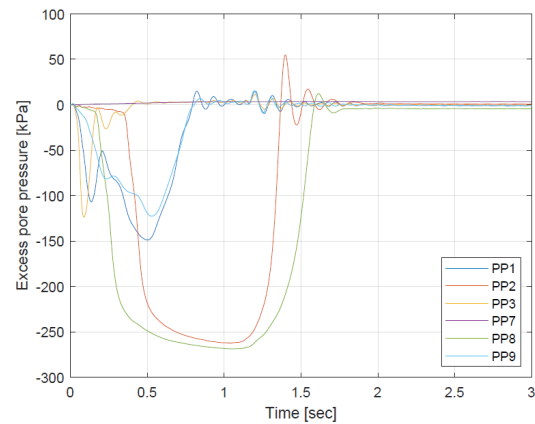


Figure C.131: External excess PP vs time in Test D400.

C.1 Results in High Density Sand

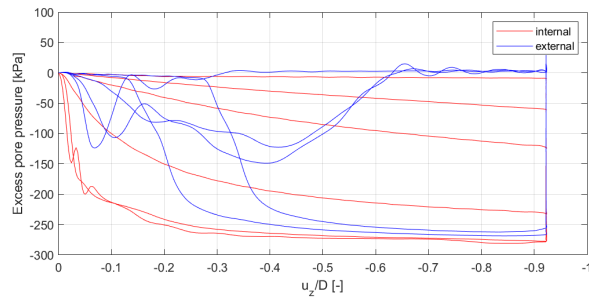


Figure C.132: Internal and external excess PP during D400

C.1.15 Test D500

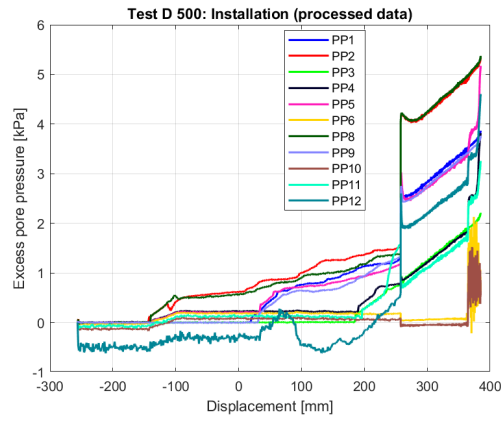


Figure C.133: Excess PP vs displacement for installation in Test D500.

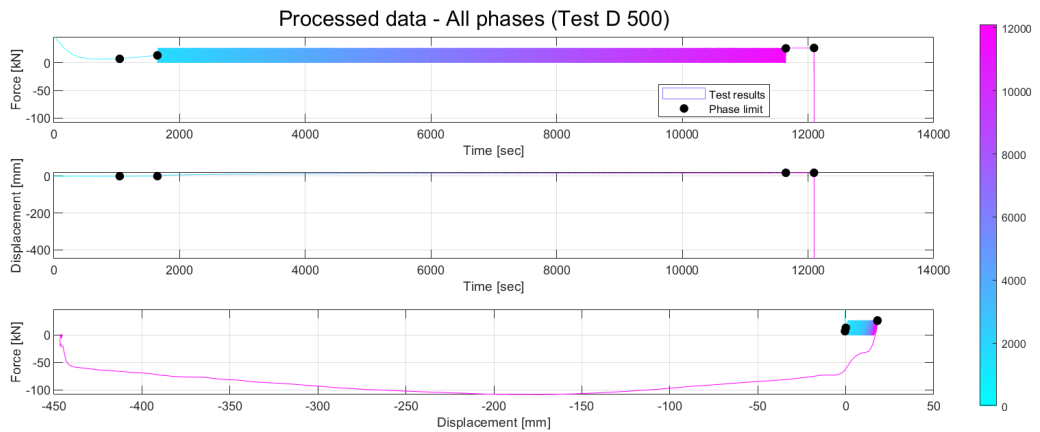


Figure C.134: Force-Time, Disp-Time, Force-Disp in Test D500.

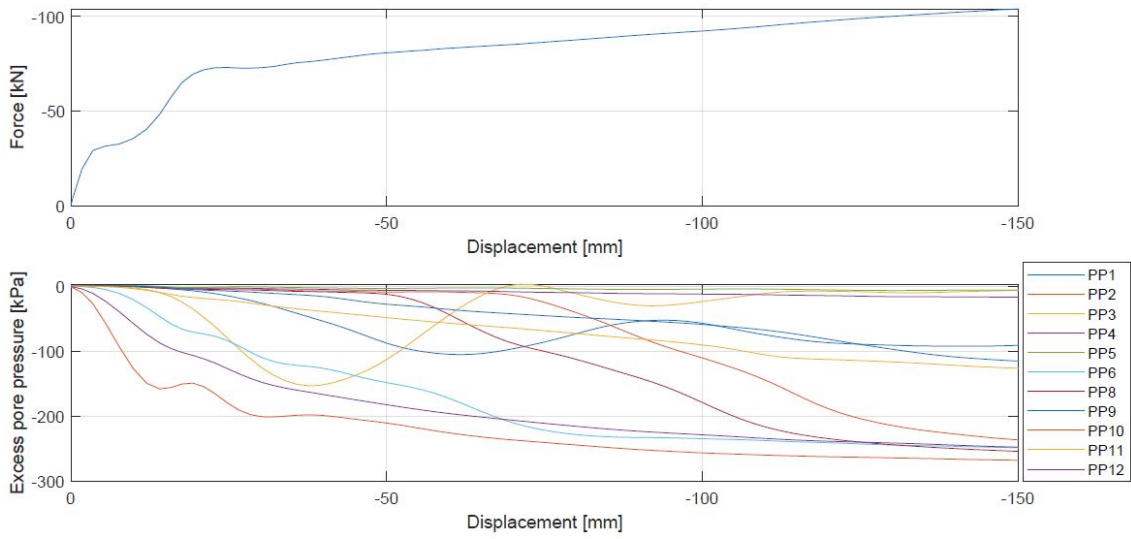


Figure C.135: Force vs displacement and excess PP vs displacement in Test D500.

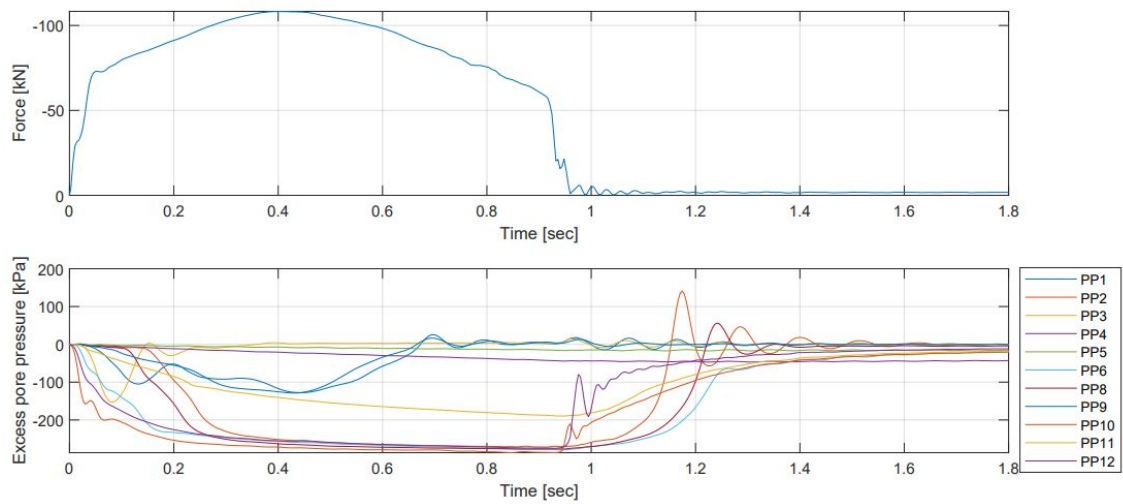


Figure C.136: Force vs time and excess PP vs time in Test D500.

C.1 Results in High Density Sand

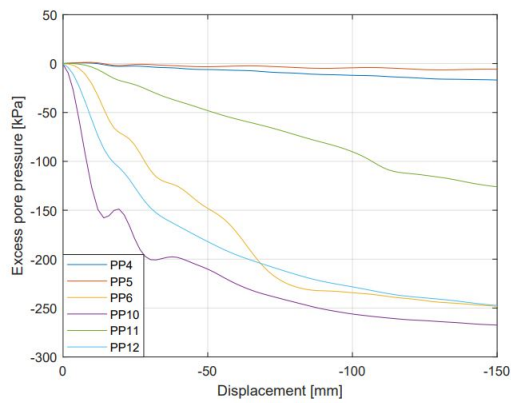


Figure C.137: Internal excess PP vs displacement in Test D500.

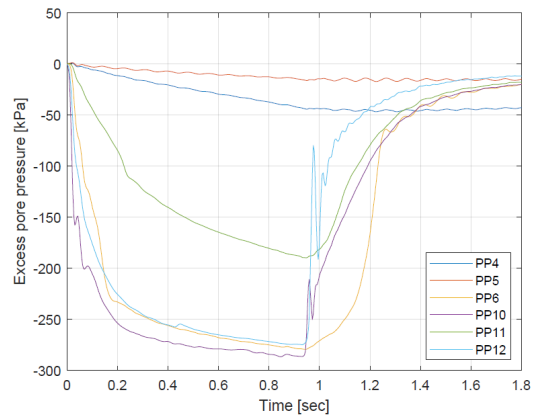


Figure C.138: Internal excess PP vs time in Test D500.

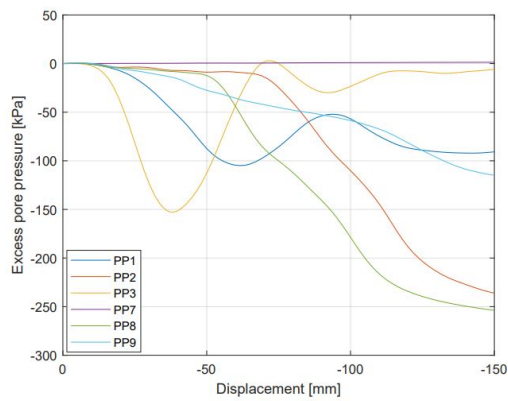


Figure C.139: External excess PP vs displacement in Test D500.

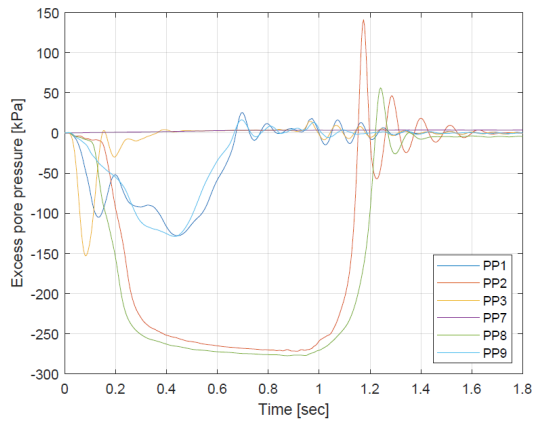


Figure C.140: External excess PP vs time in Test D500.

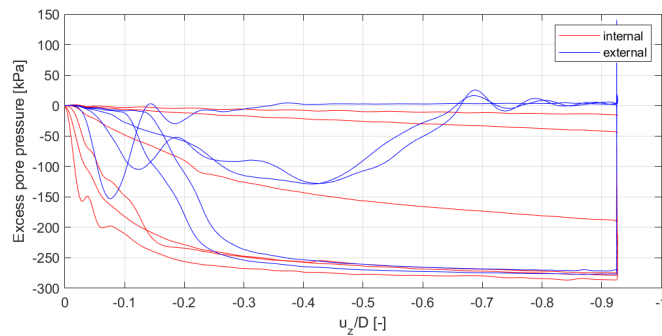


Figure C.141: Internal and external excess PP during D500

C.2 Results in Medium Density Sand

C.2.1 Test M0.05

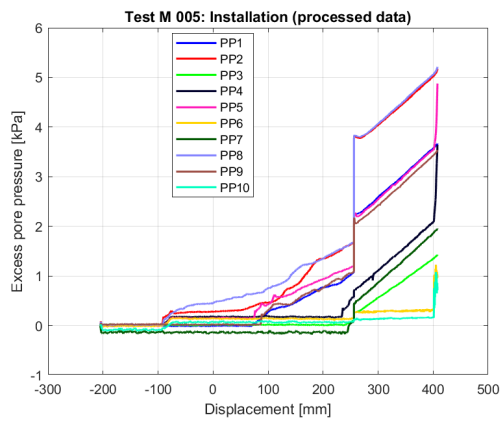


Figure C.142: Excess PP vs displacement for installation in Test M005.

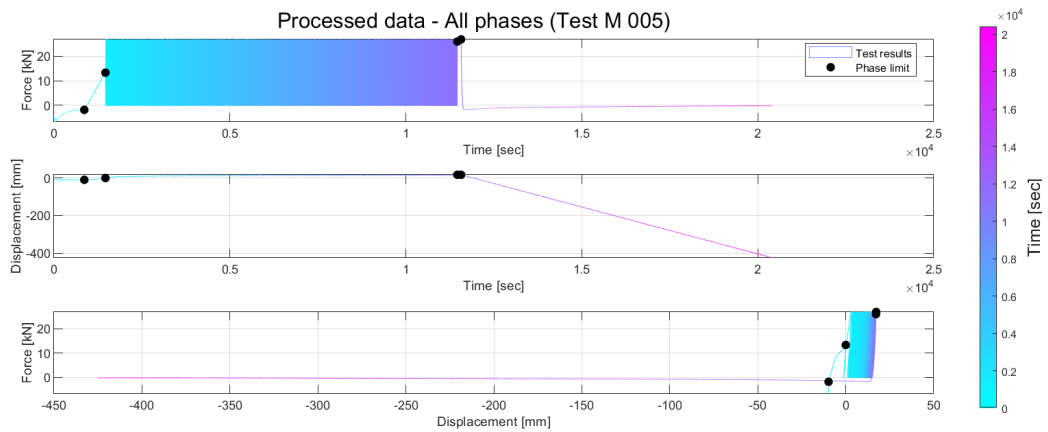


Figure C.143: Force-Time, Disp-Time, Force-Disp in Test M005.

C.2 Results in Medium Density Sand

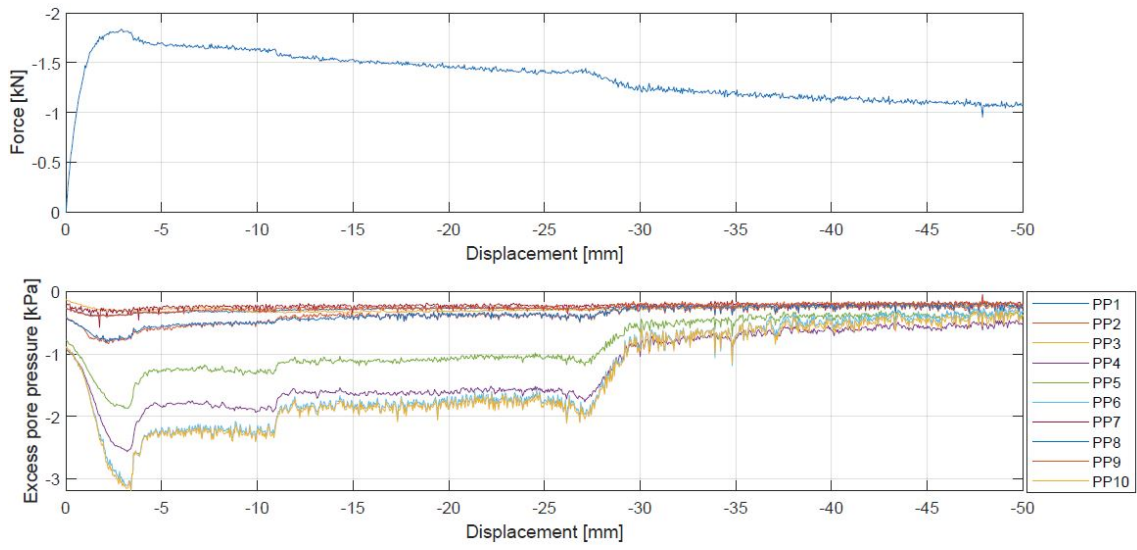


Figure C.144: Force vs displacement and excess PP vs displacement in Test M005.

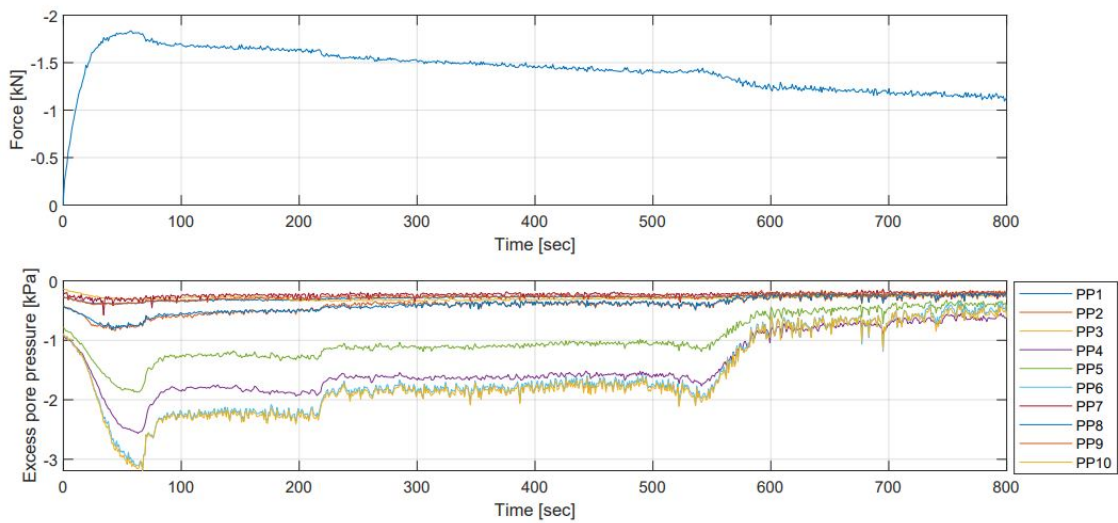


Figure C.145: Force vs time and excess PP vs time in Test M005.

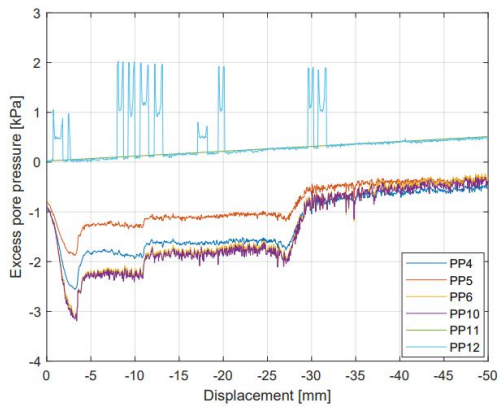


Figure C.146: Internal excess PP vs displacement in Test M005.

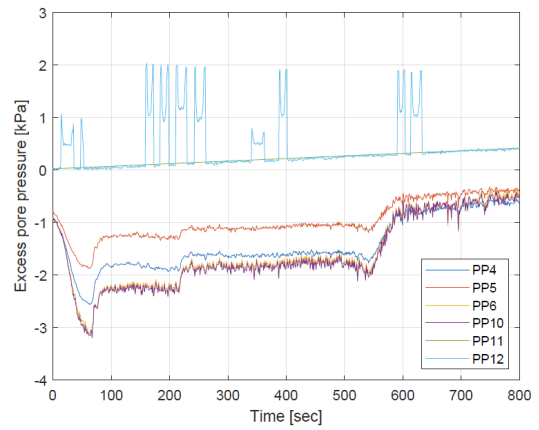


Figure C.147: Internal excess PP vs time in Test M005.

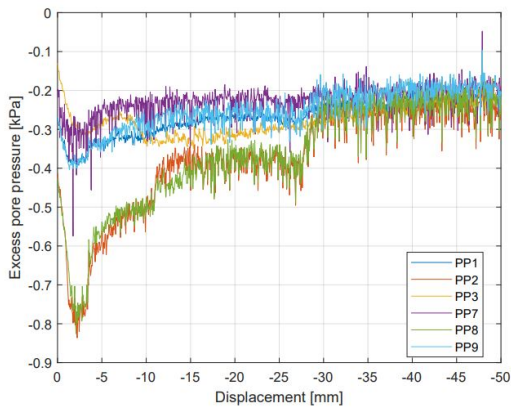


Figure C.148: External excess PP vs displacement in Test M005.

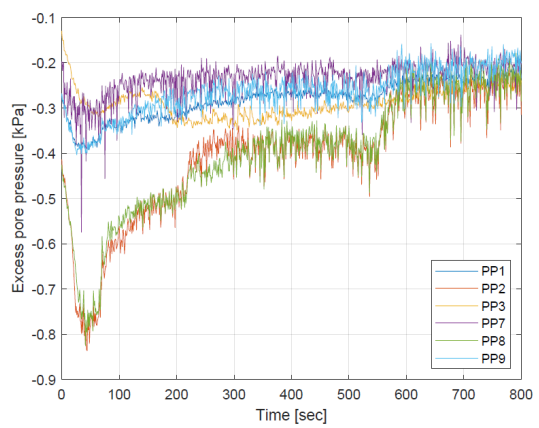


Figure C.149: External excess PP vs time in Test M005.

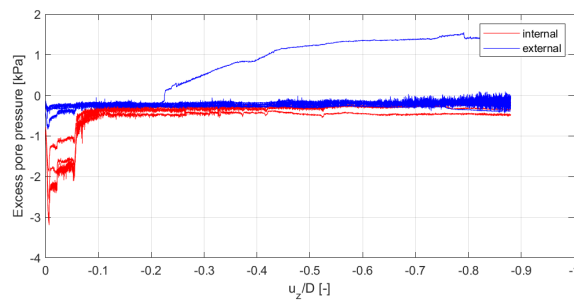


Figure C.150: Internal and external excess PP during M005

C.2.2 Test M10

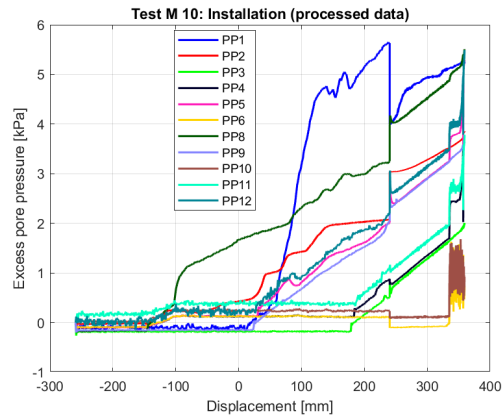


Figure C.151: Excess PP vs displacement for installation in Test M10.

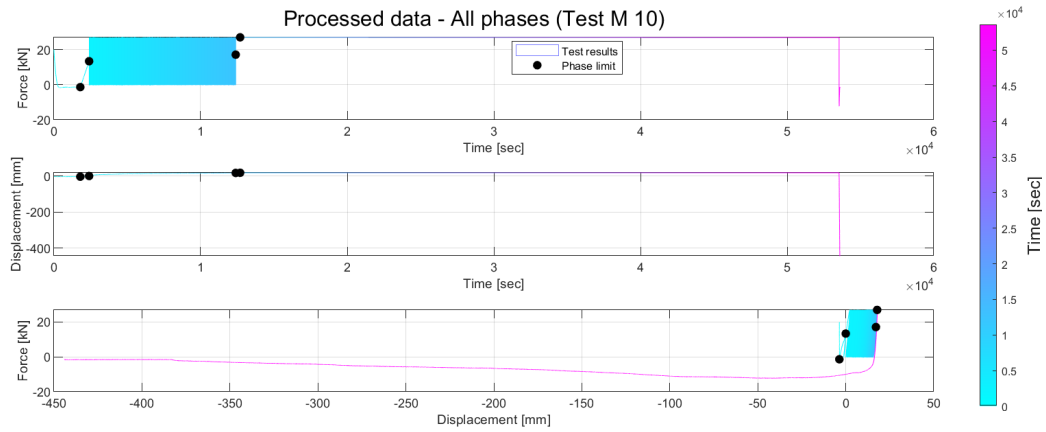


Figure C.152: Force-Time, Disp-Time, Force-Disp in Test M10.

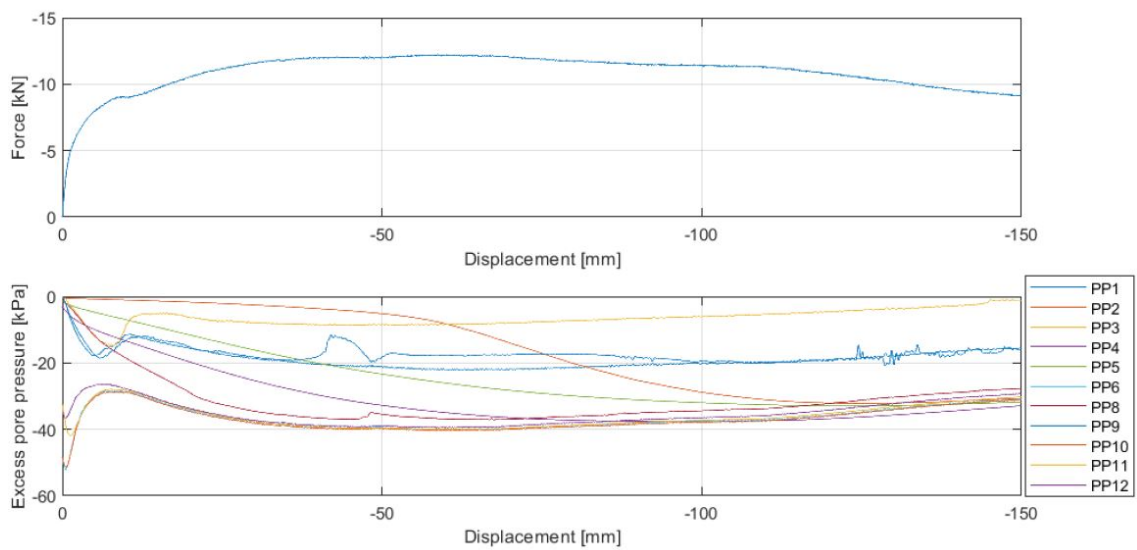


Figure C.153: Force vs displacement and excess PP vs displacement in Test M10.

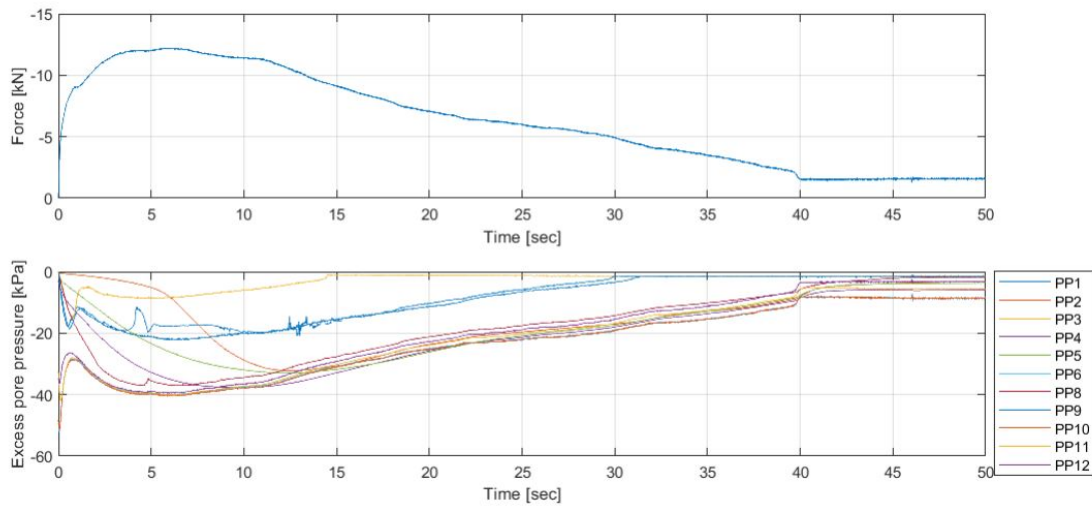


Figure C.154: Force vs time and excess PP vs time in Test M10.

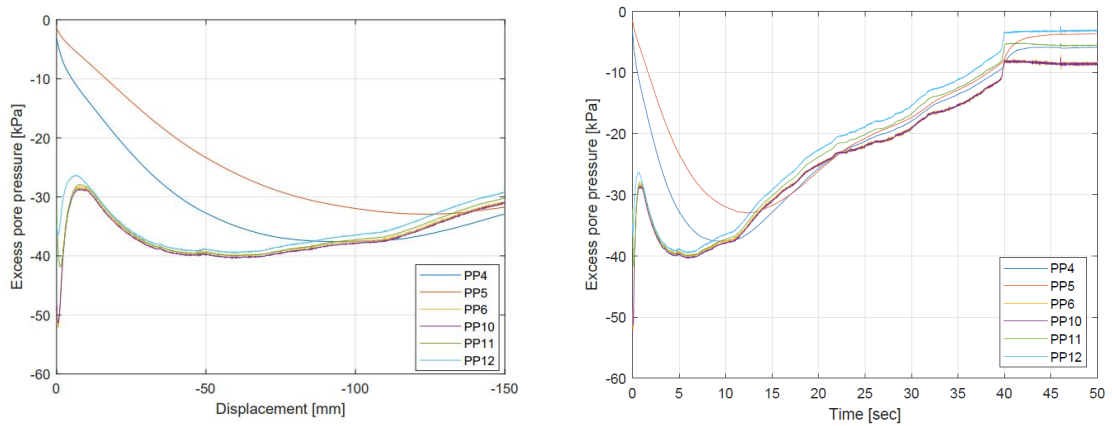


Figure C.155: Internal excess PP vs displacement in Test M10.

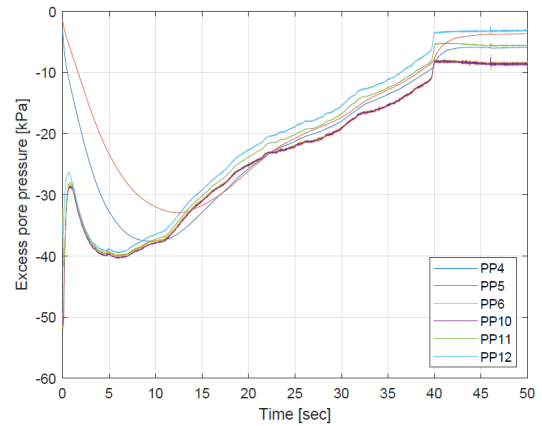


Figure C.156: Internal excess PP vs time in Test M10.

C.2 Results in Medium Density Sand

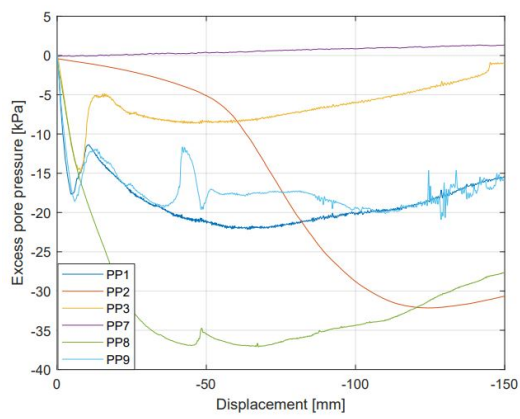


Figure C.157: External excess PP vs displacement in Test M10.

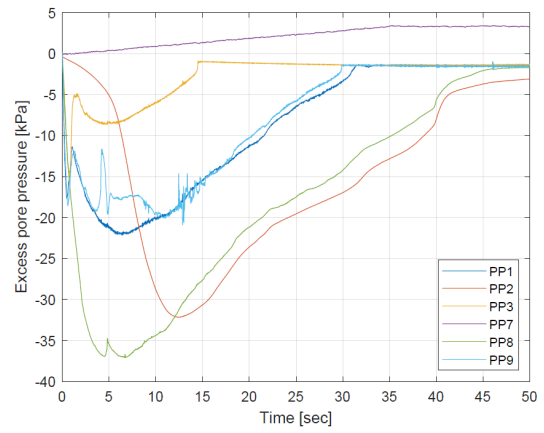


Figure C.158: External excess PP vs time in Test M10.

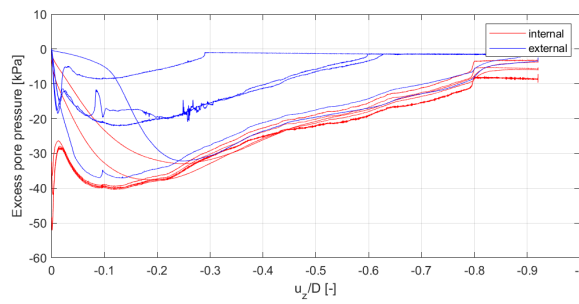


Figure C.159: Internal and external excess PP during M10

C.2.3 Test M50

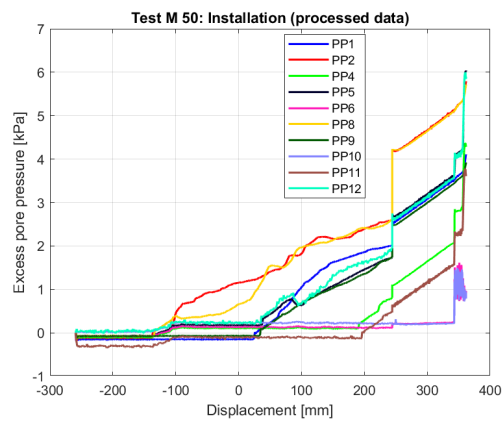


Figure C.160: Excess PP vs displacement for installation in Test M50.

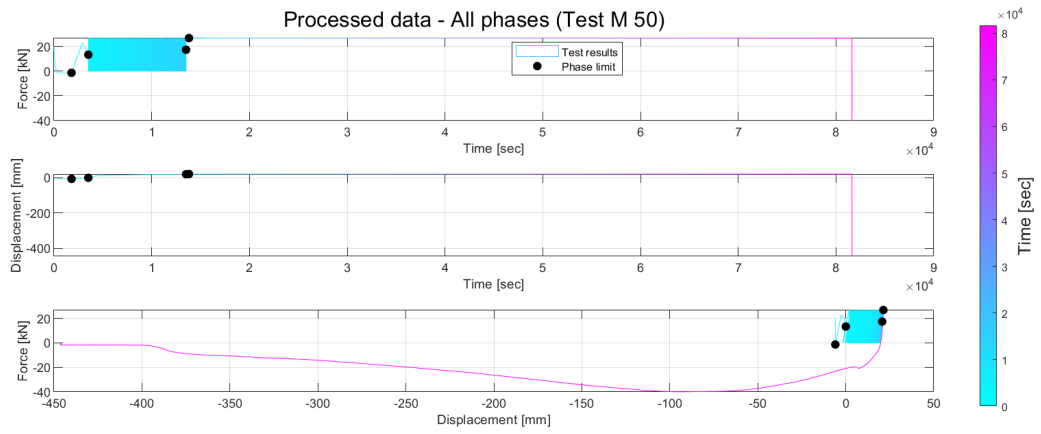


Figure C.161: Force-Time, Disp-Time, Force-Disp in Test M50.

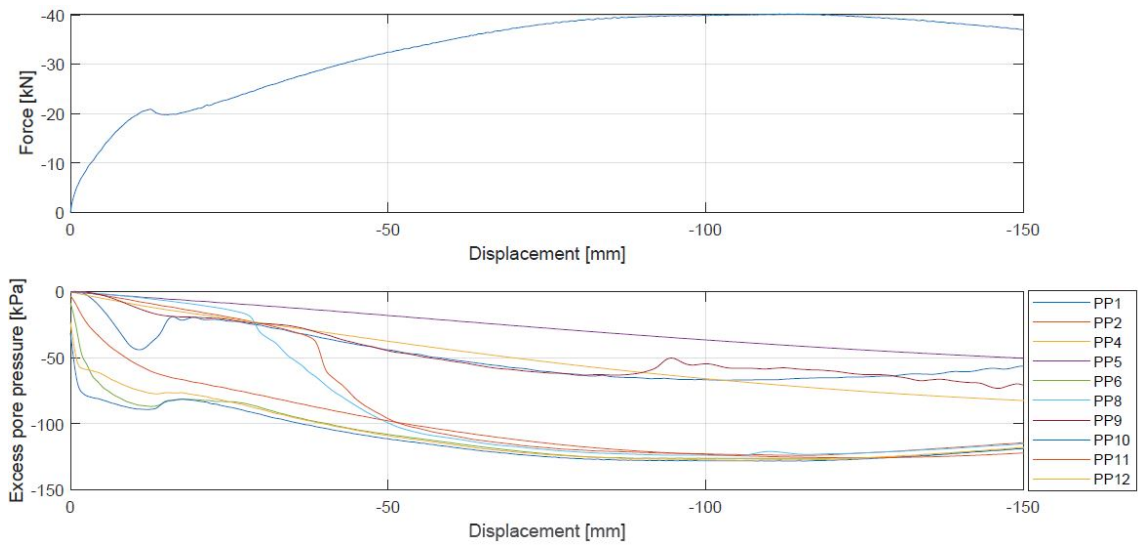


Figure C.162: Force vs displacement and excess PP vs displacement in Test M50.

C.2 Results in Medium Density Sand

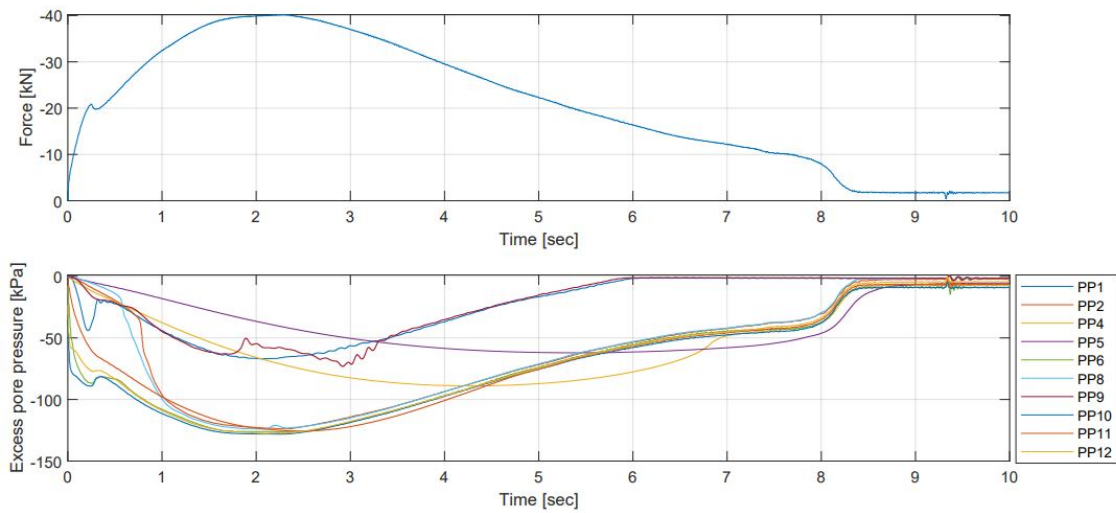


Figure C.163: Force vs time and excess PP vs time in Test M50.

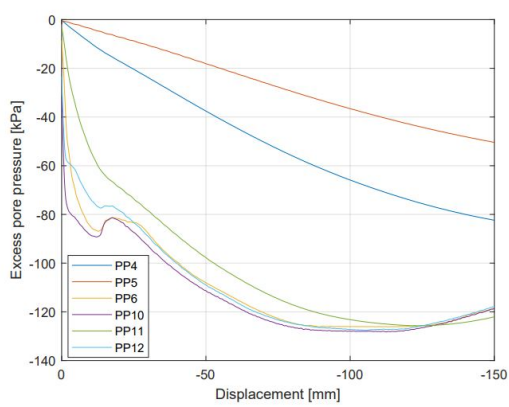


Figure C.164: Internal excess PP vs displacement in Test M50.

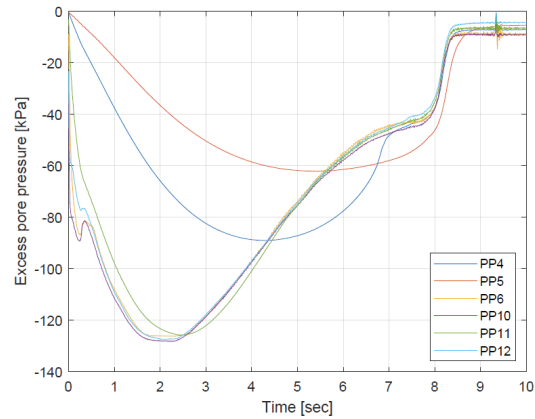


Figure C.165: Internal excess PP vs time in Test M50.

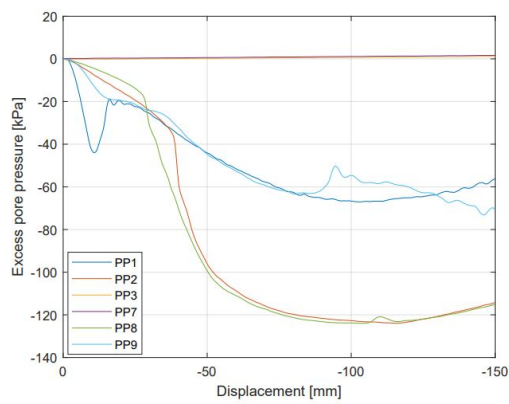


Figure C.166: External excess PP vs displacement in Test M50.

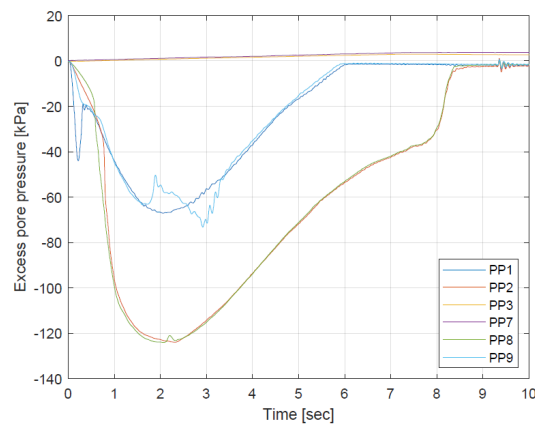


Figure C.167: External excess PP vs time in Test M50.

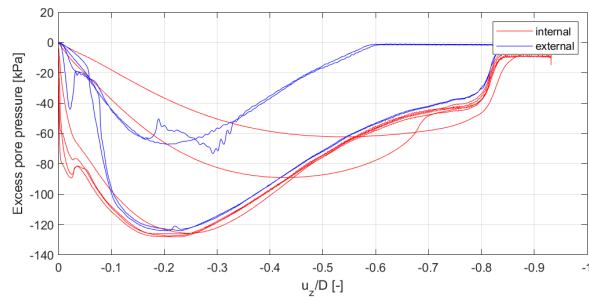


Figure C.168: Internal and external excess PP during M50

C.2.4 Test M150-1

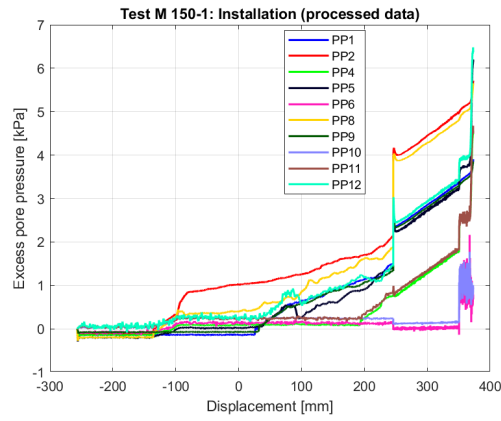


Figure C.169: Excess PP vs displacement for installation in Test M150-1.

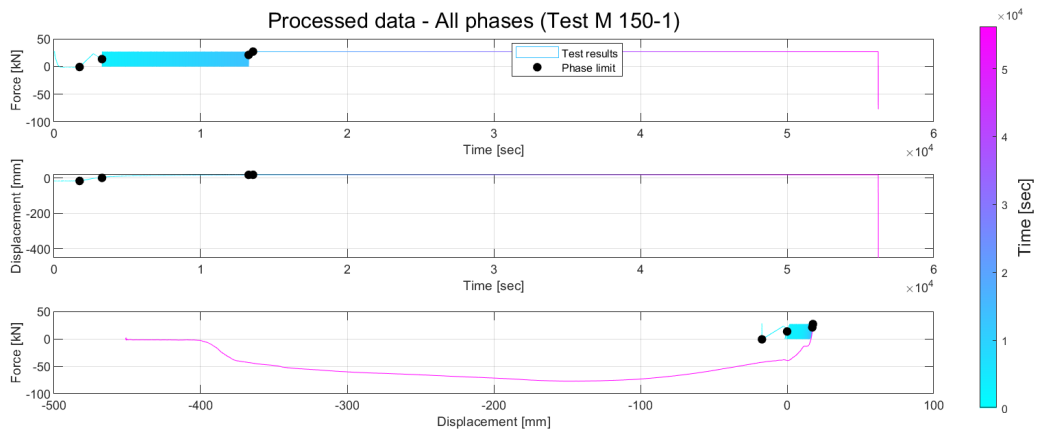


Figure C.170: Force-Time, Disp-Time, Force-Disp in Test M150-1.

C.2 Results in Medium Density Sand

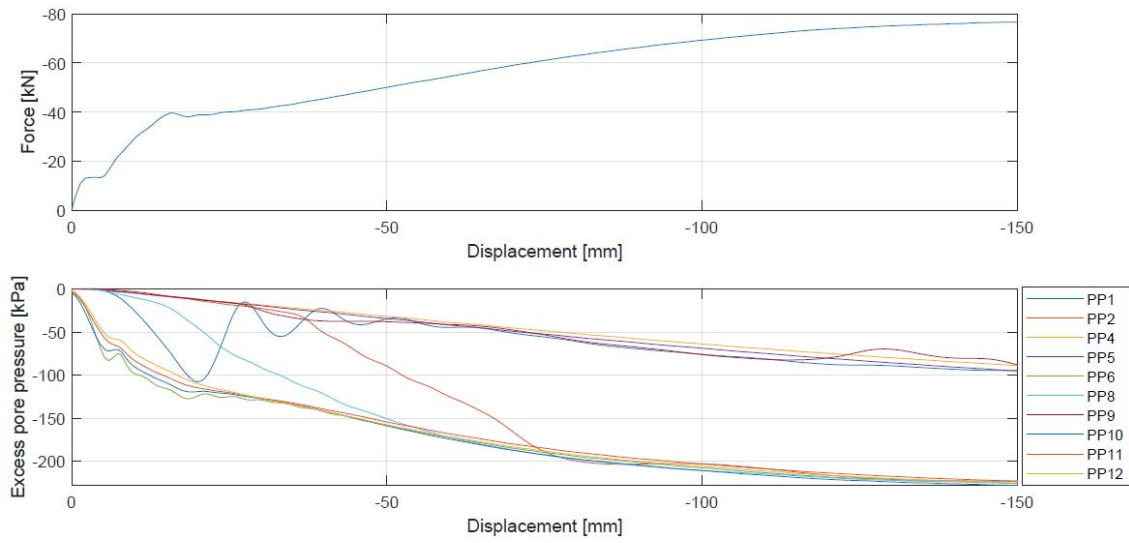


Figure C.171: Force vs displacement and excess PP vs displacement in Test M150-1.

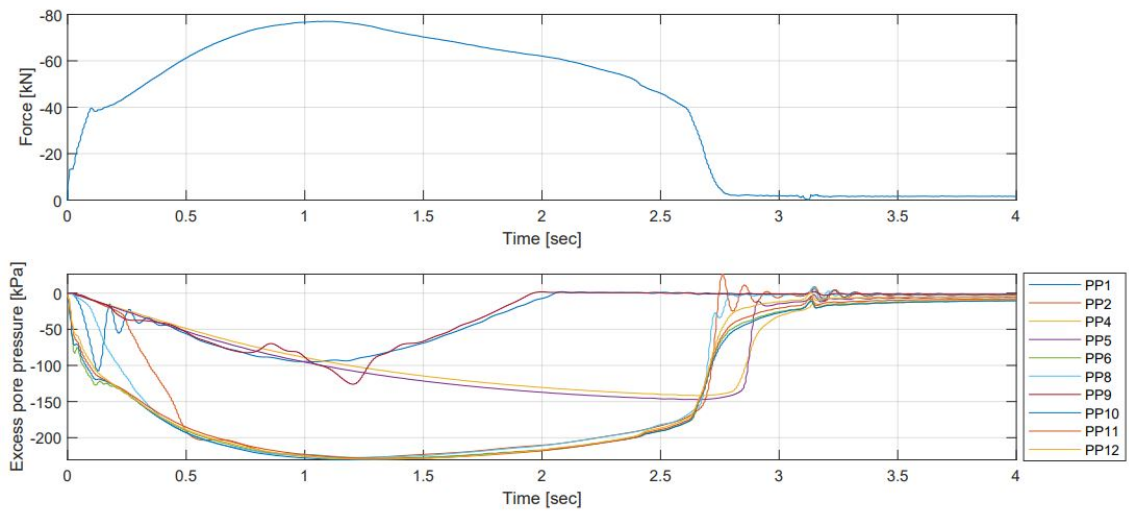


Figure C.172: Force vs time and excess PP vs time in Test M150-1.

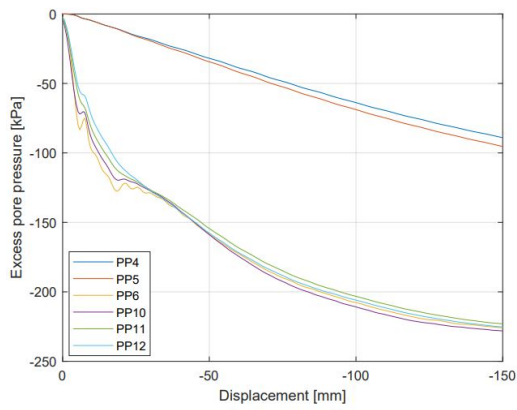


Figure C.173: Internal excess PP vs displacement in Test M150-1.

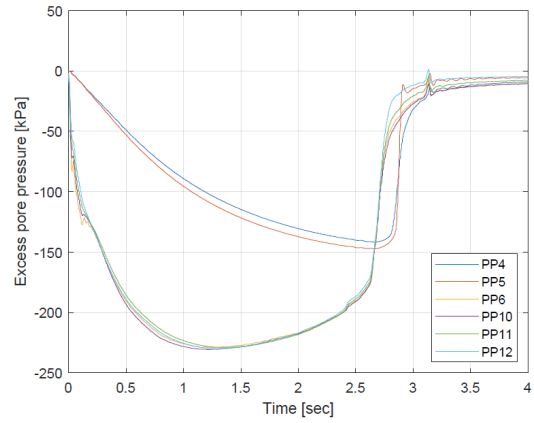


Figure C.174: Internal excess PP vs time in Test D150-1.

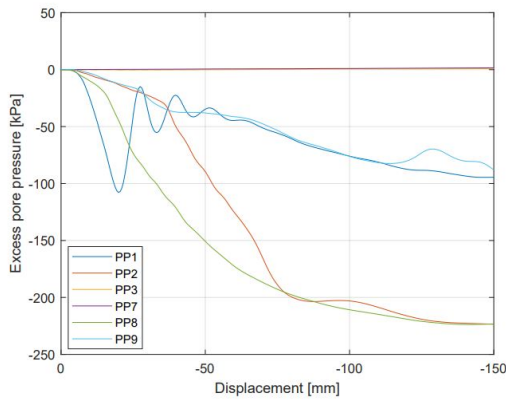


Figure C.175: External excess PP vs displacement in Test M150-1.

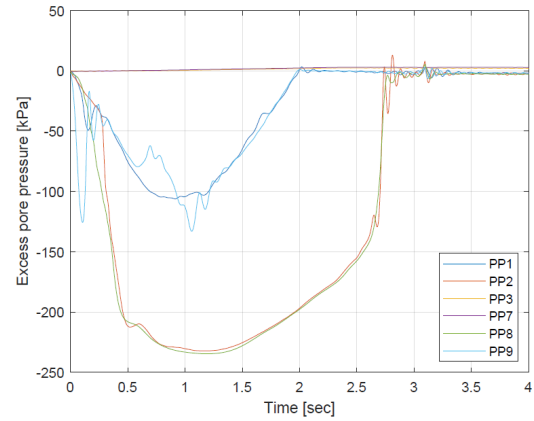


Figure C.176: External excess PP vs time in Test M150-1.

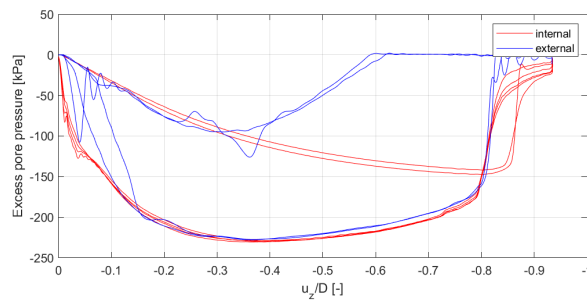


Figure C.177: Internal and external excess PP during M150-1

C.2.5 Test M150-2

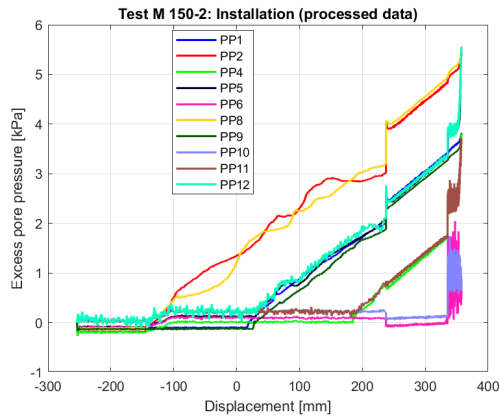


Figure C.178: Excess PP vs displacement for installation in Test M150-2.

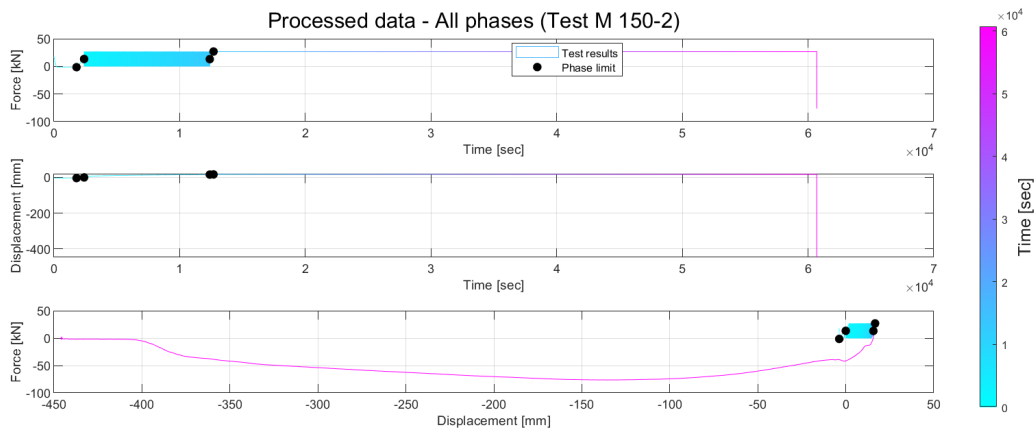


Figure C.179: Force-Time, Disp-Time, Force-Disp in Test M150-2.

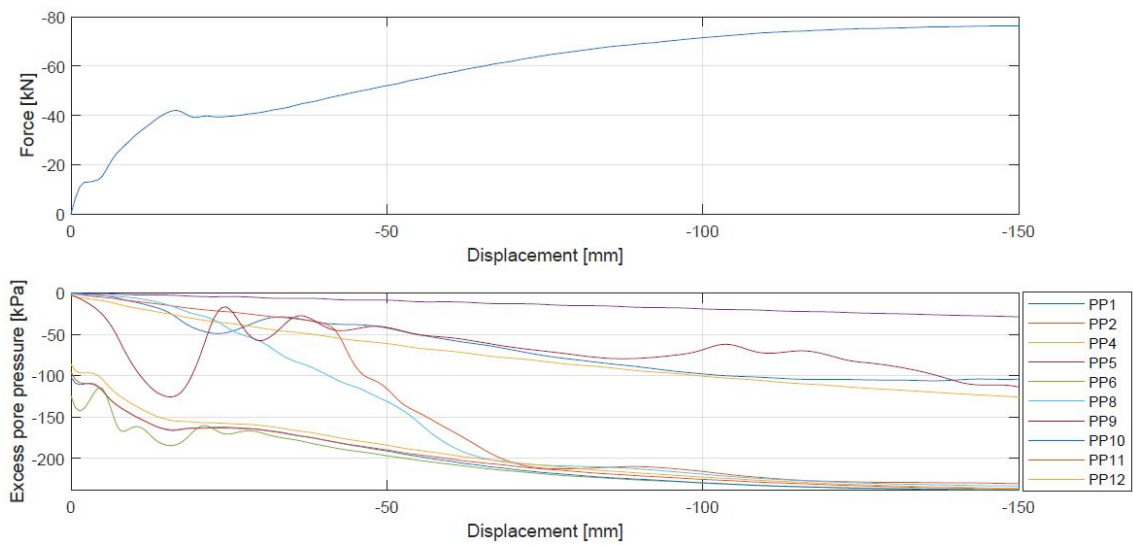


Figure C.180: Force vs displacement and excess PP vs displacement in Test M150-2.

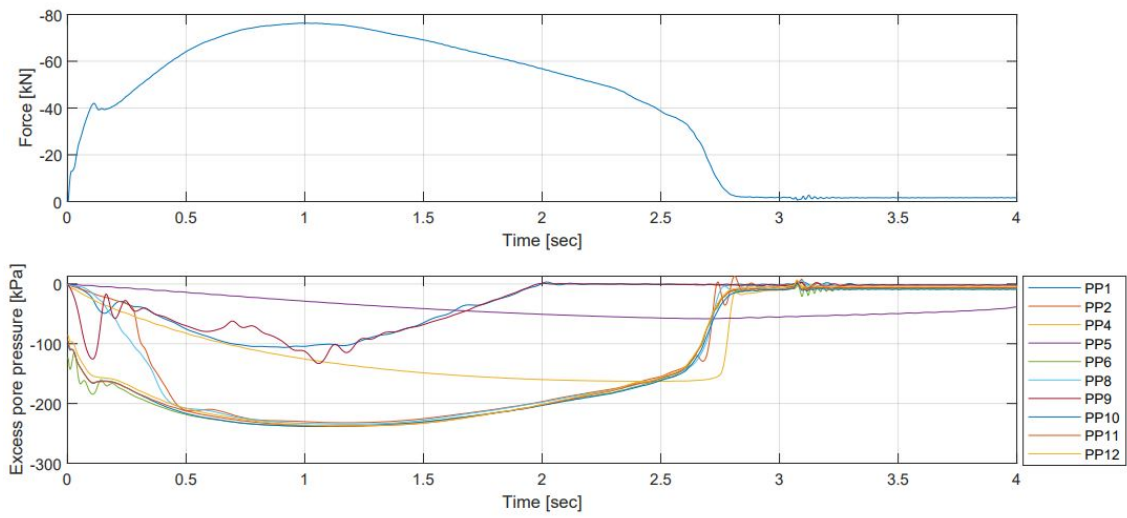


Figure C.181: Force vs time and excess PP vs time in Test M150-2.

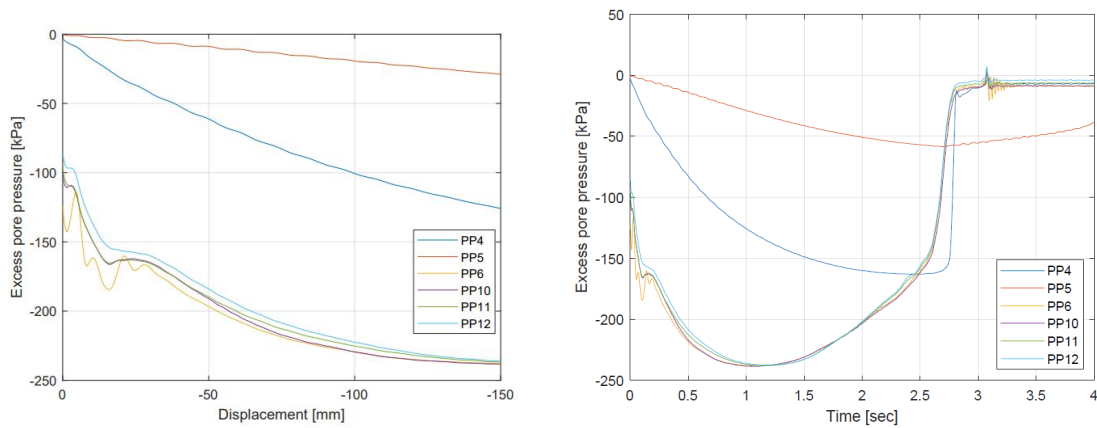


Figure C.182: Internal excess PP vs displacement in Test M150-2.

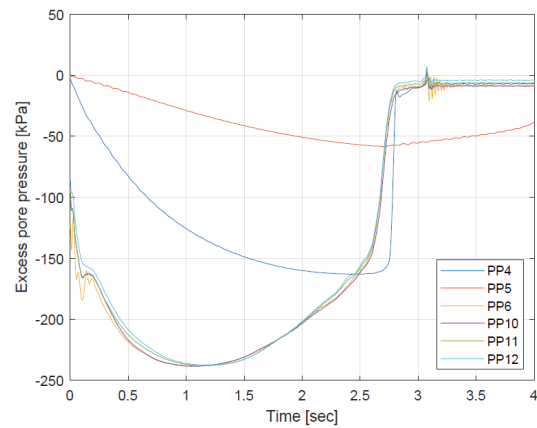


Figure C.183: Internal excess PP vs time in Test M150-2.

C.2 Results in Medium Density Sand

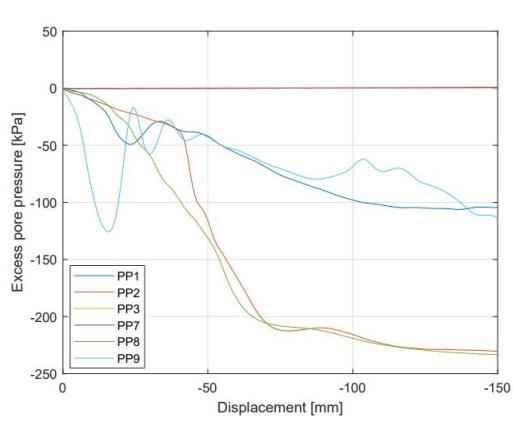


Figure C.184: External excess PP vs displacement in Test M150-2.

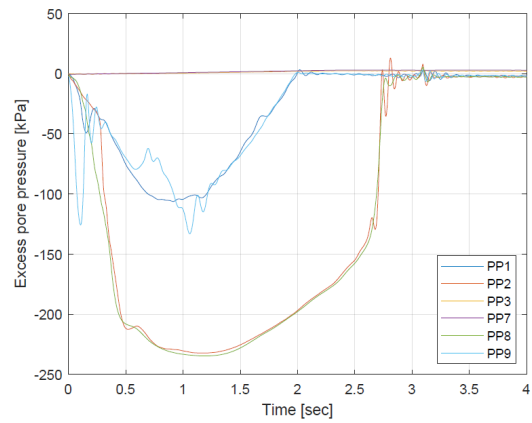


Figure C.185: External excess PP vs time in Test M150-2.

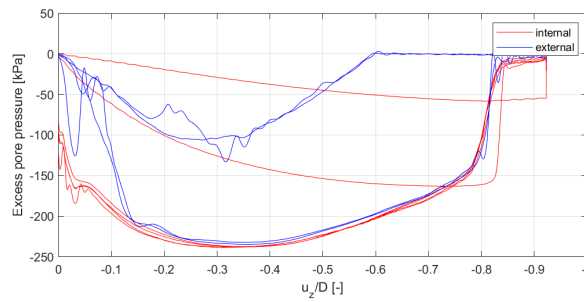


Figure C.186: Internal and external excess PP during M150-2

C.2.6 Test M500

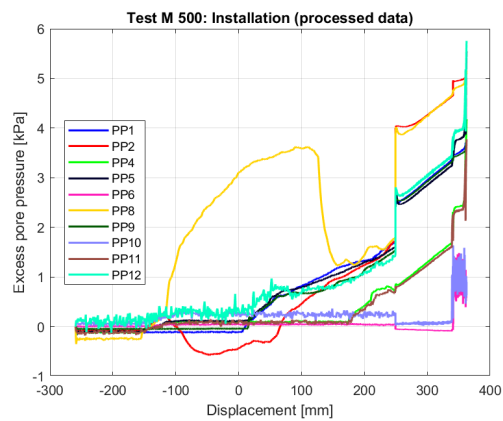


Figure C.187: Excess PP vs displacement for installation in Test M500.

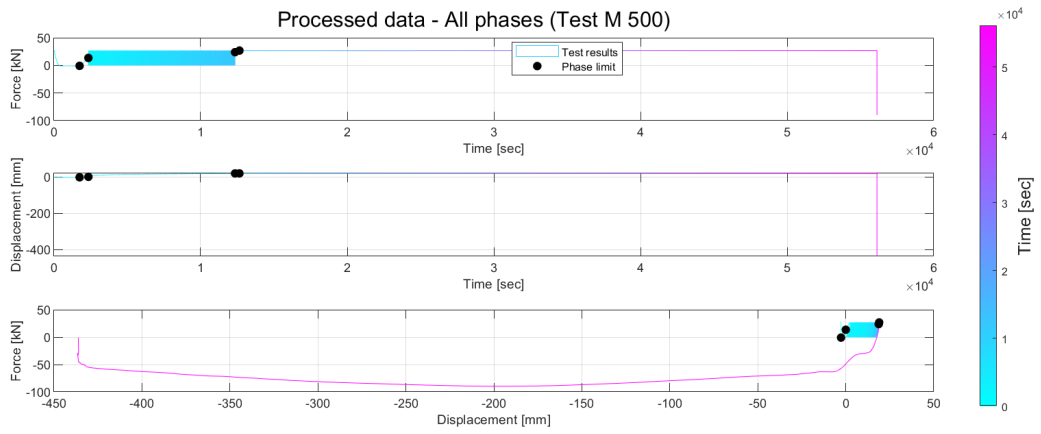


Figure C.188: Force-Time, Disp-Time, Force-Disp in Test M500.

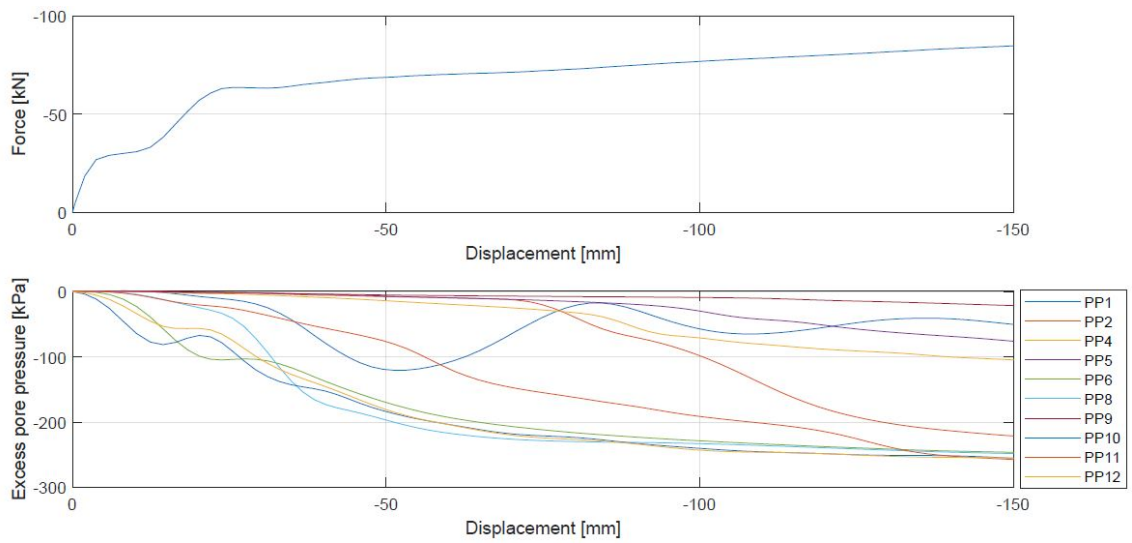


Figure C.189: Force vs displacement and excess PP vs displacement in Test M500.

C.2 Results in Medium Density Sand

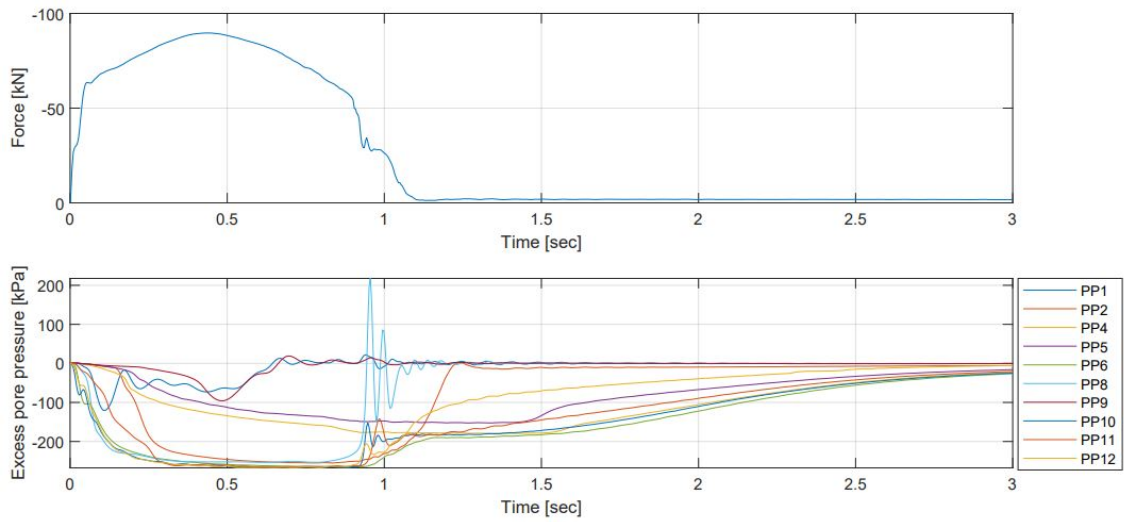


Figure C.190: Force vs time and excess PP vs time in Test M500.

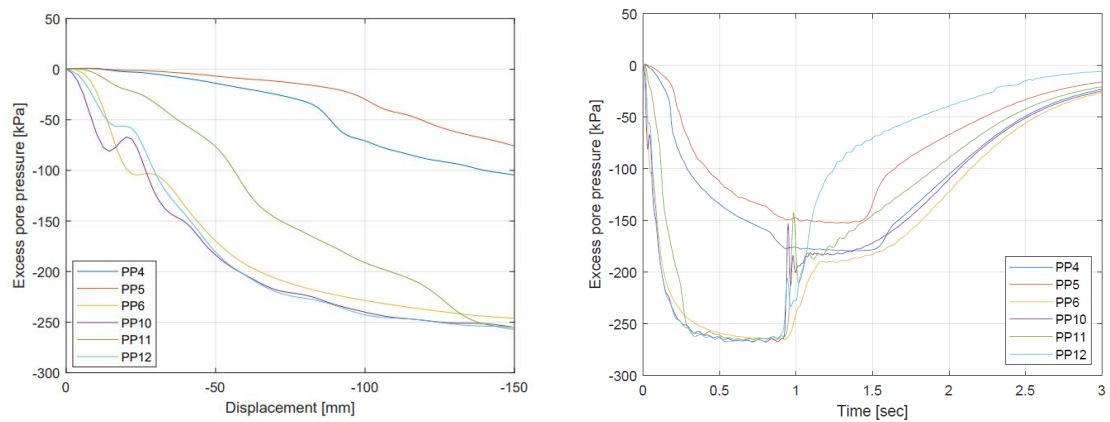


Figure C.191: Internal excess PP vs displacement in Test M500.

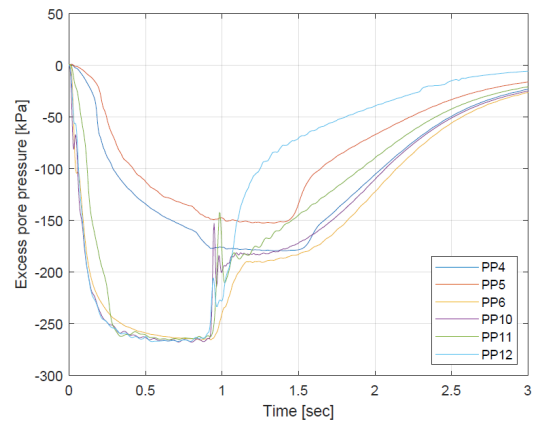


Figure C.192: Internal excess PP vs time in Test M500.

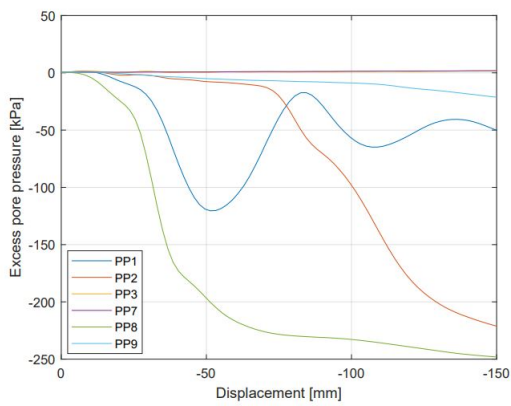


Figure C.193: External excess PP vs displacement in Test M500.

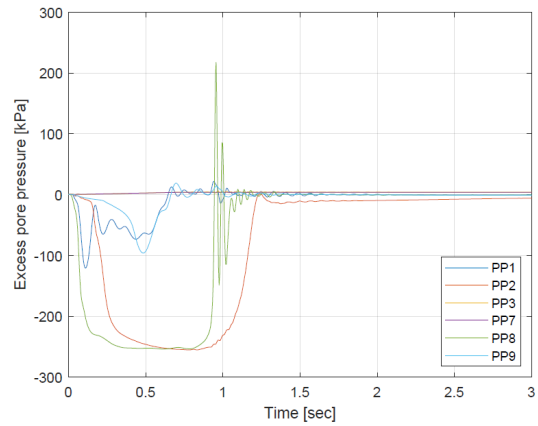


Figure C.194: External excess PP vs time in Test M500.

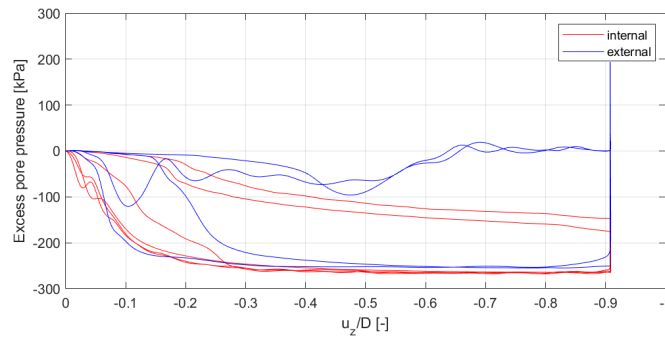


Figure C.195: Internal and external excess PP during M500

Test M 500 | Left half

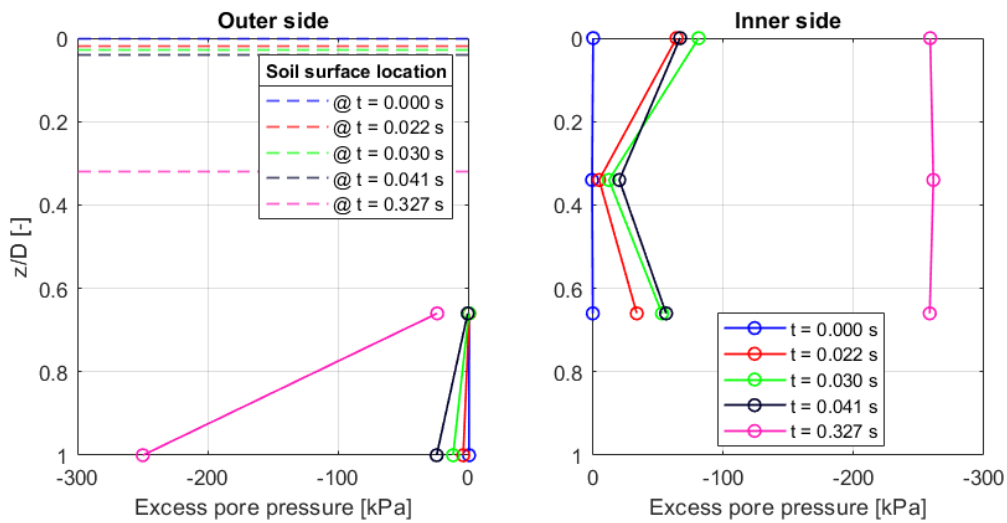


Figure C.196: Isochrones Test M500 at left side of the bucket.

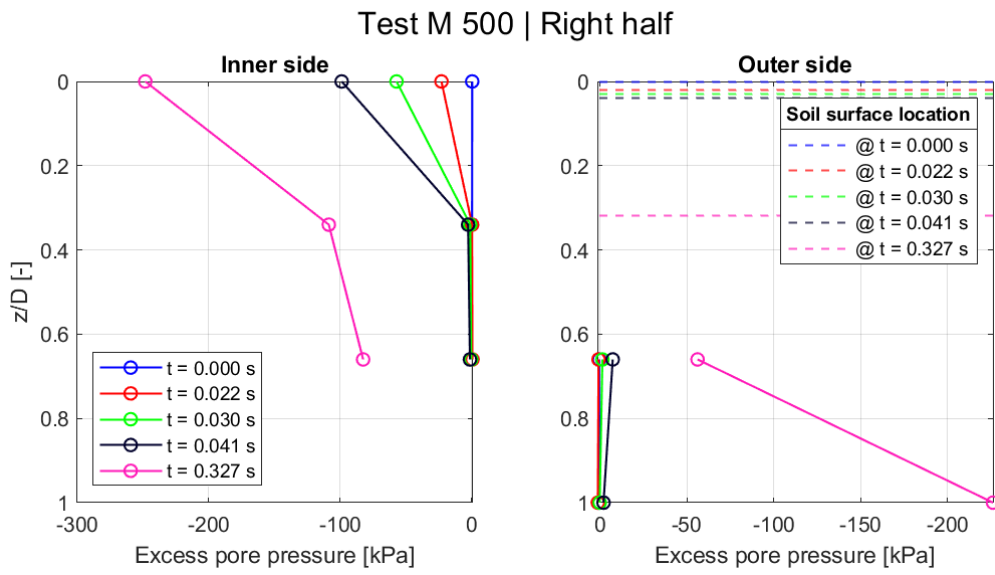


Figure C.197: Isochrones Test M500 at right side of the bucket.

C.3 Results in Low Density Sand

C.3.1 Test L0.05

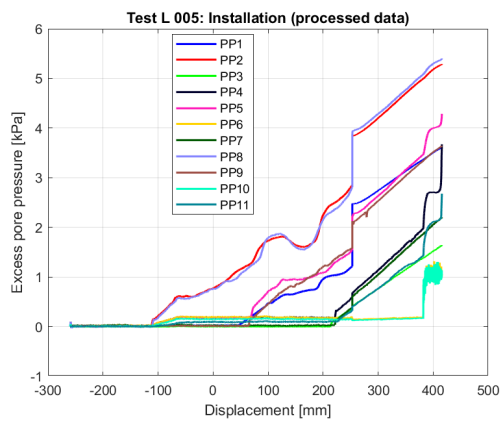


Figure C.198: Excess PP vs displacement for installation in Test L005.

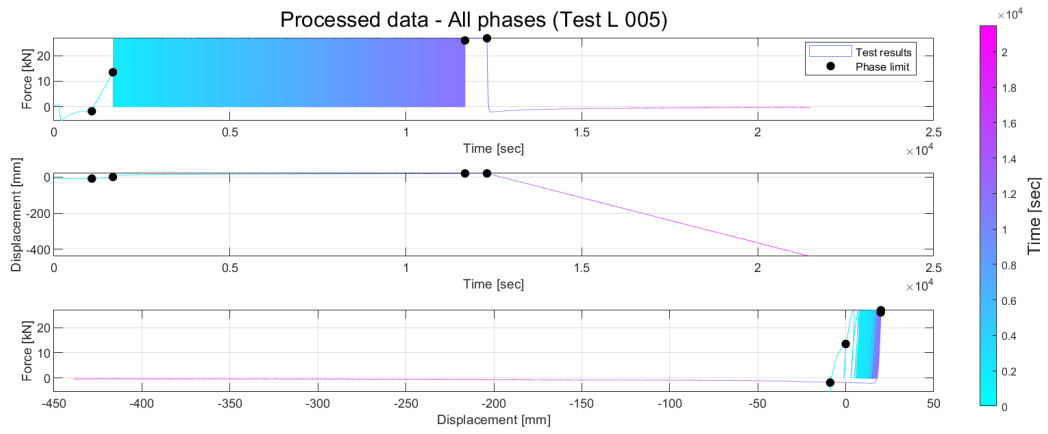


Figure C.199: Force-Time, Disp-Time, Force-Disp in Test L005.

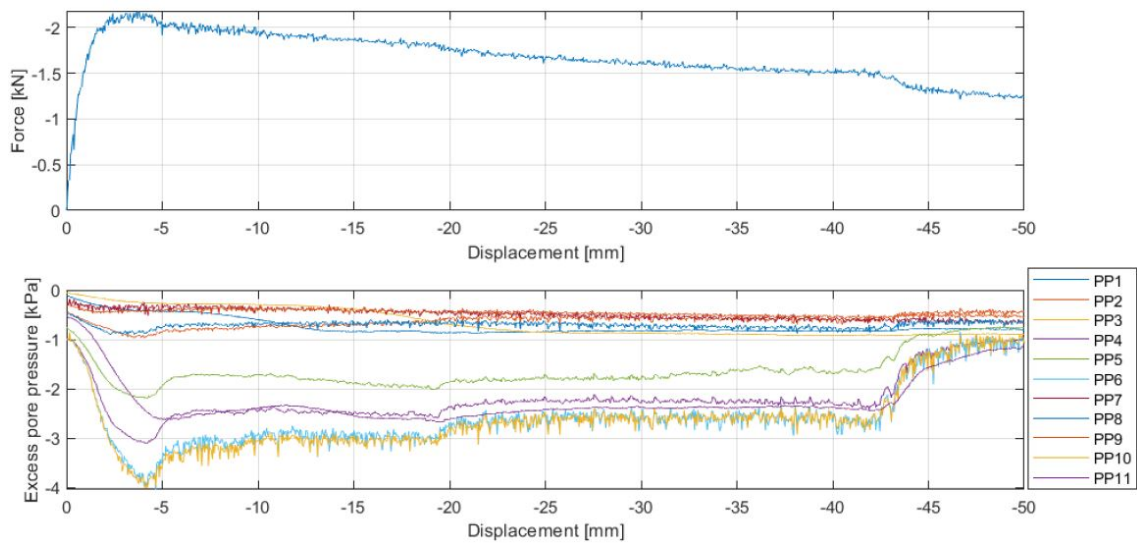


Figure C.200: Force vs displacement and excess PP vs displacement in Test L005.

C.3 Results in Low Density Sand

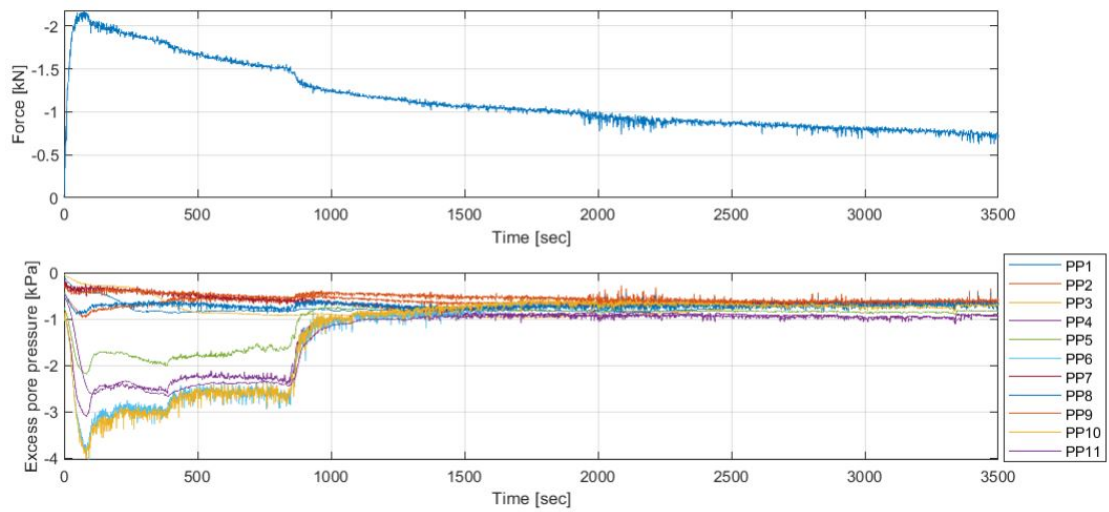


Figure C.201: Force vs time and excess PP vs time in Test L005.

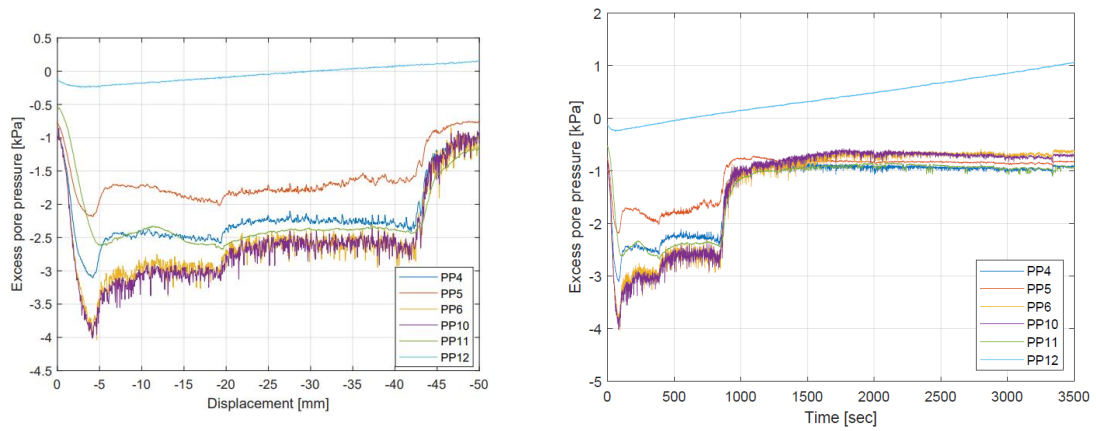


Figure C.202: Internal excess PP vs displacement in Test L005. Figure C.203: Internal excess PP vs time in Test L005.

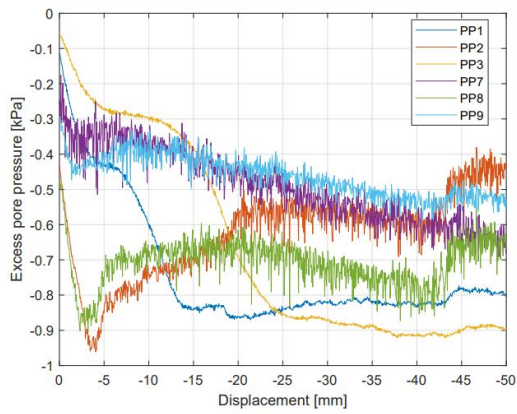


Figure C.204: External excess PP vs displacement in Test L005.

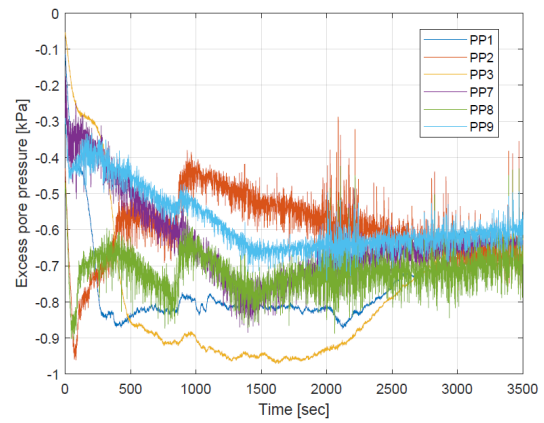


Figure C.205: External excess PP vs time in Test L005.

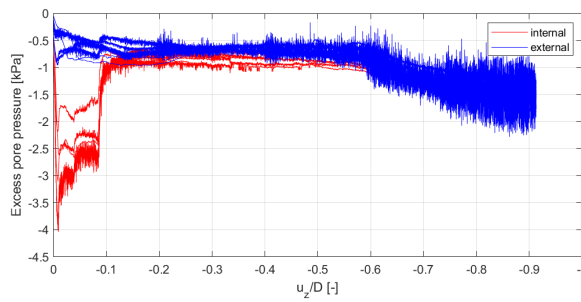


Figure C.206: Internal and external excess PP during L005

C.3.2 Test L10

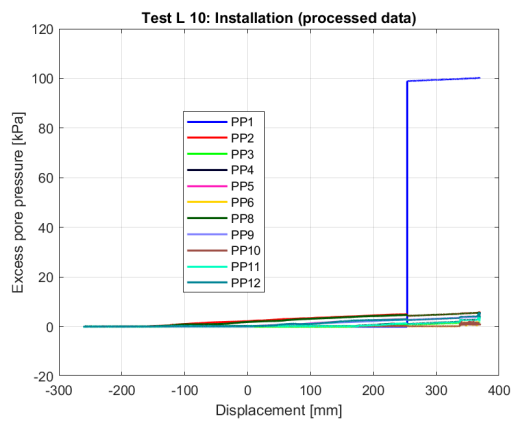


Figure C.207: Excess PP vs displacement for installation in Test L10.

C.3 Results in Low Density Sand

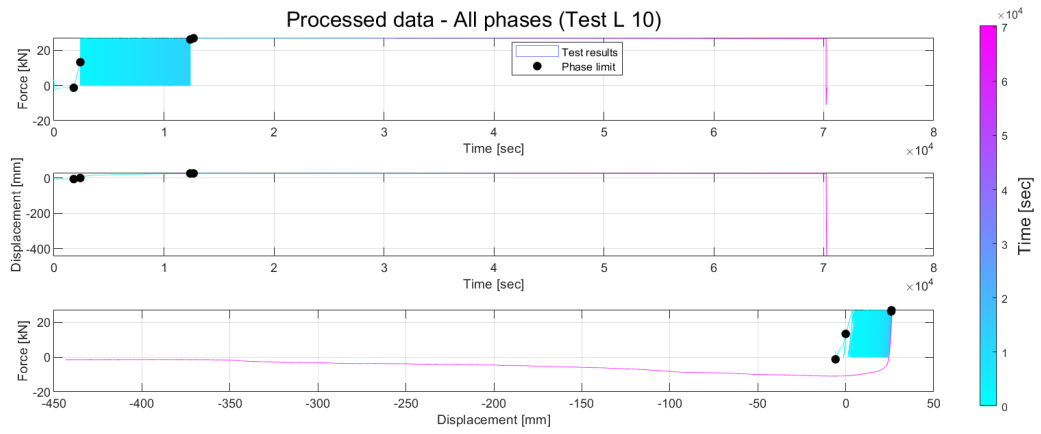


Figure C.208: Force-Time, Disp-Time, Force-Disp in Test L10.

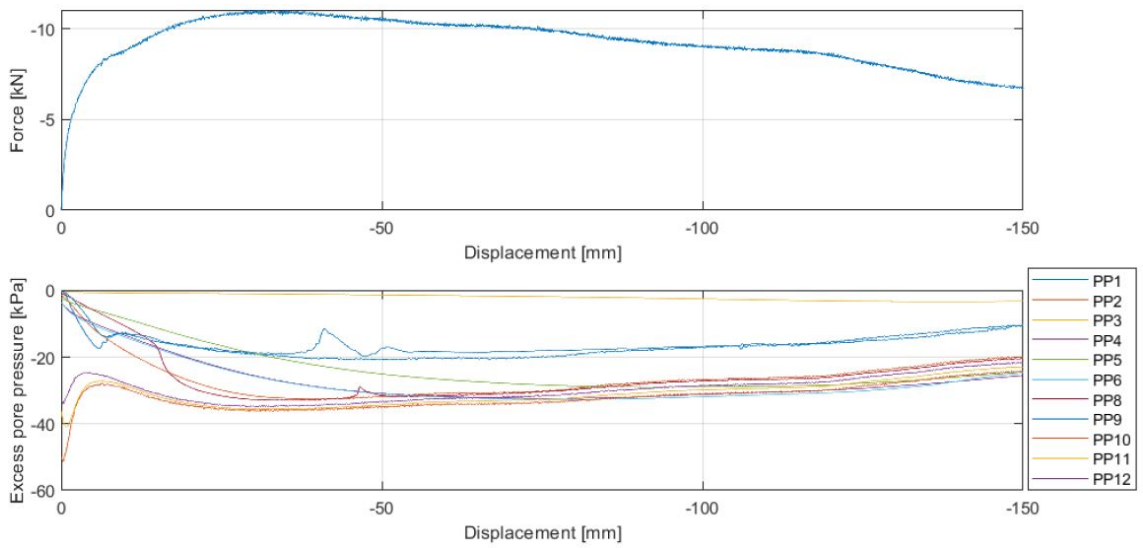


Figure C.209: Force vs displacement and excess PP vs displacement in Test L10.

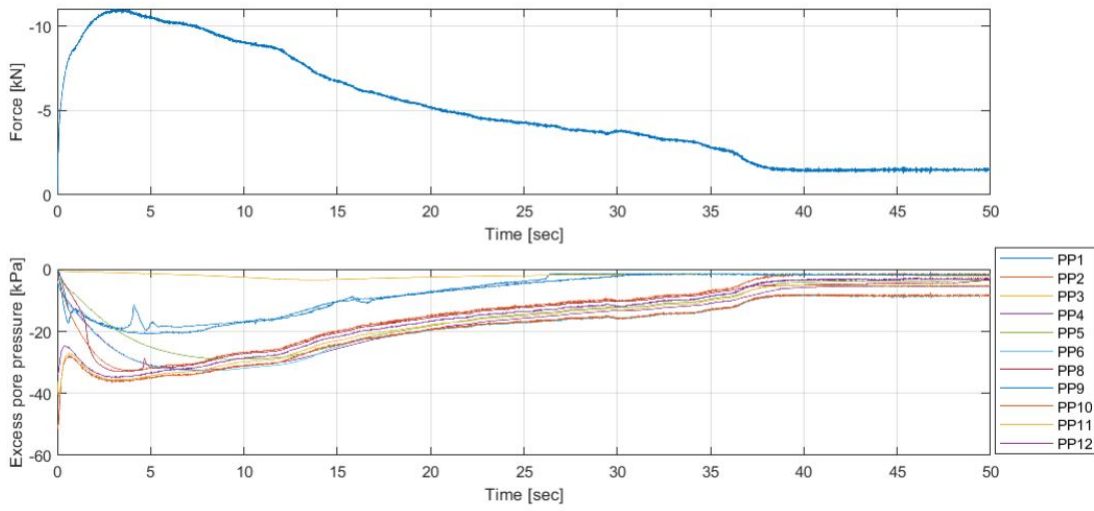


Figure C.210: Force vs time and excess PP vs time in Test L10.

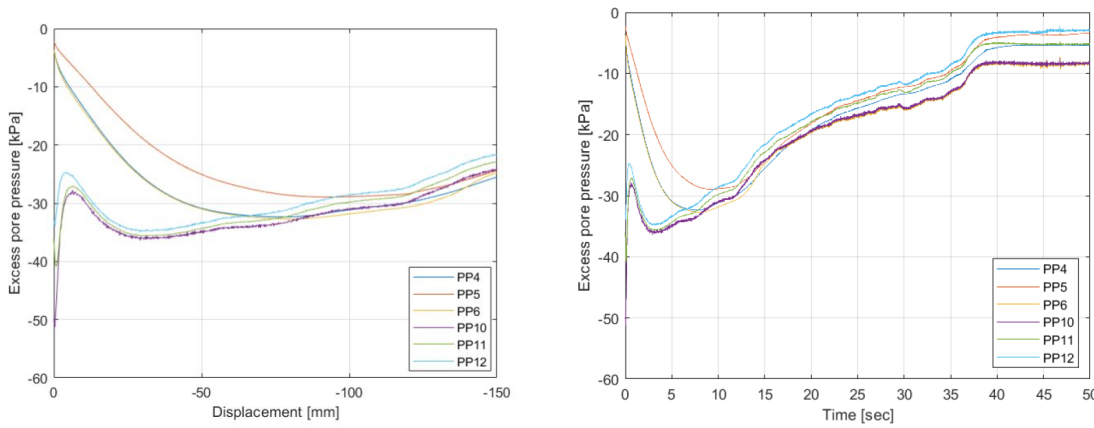


Figure C.211: Internal excess PP vs displacement in Test L10. Figure C.212: Internal excess PP vs time in Test L10.

C.3 Results in Low Density Sand

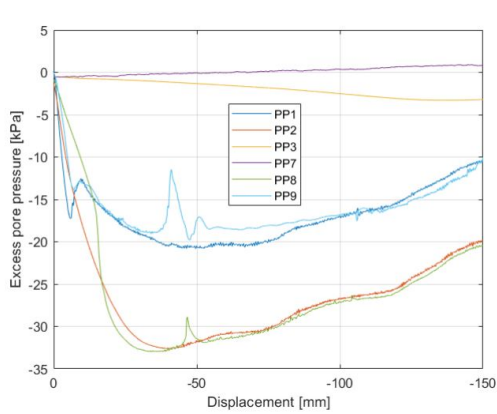


Figure C.213: External excess PP vs displacement in Test L10.

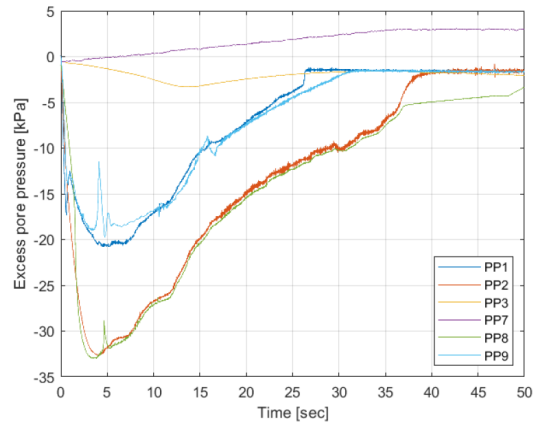


Figure C.214: External excess PP vs time in Test L10.

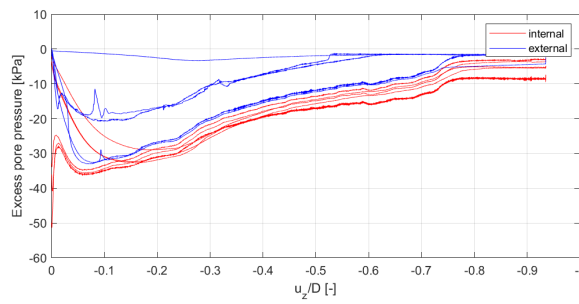


Figure C.215: Internal and external excess PP during L10

C.3.3 Test L50

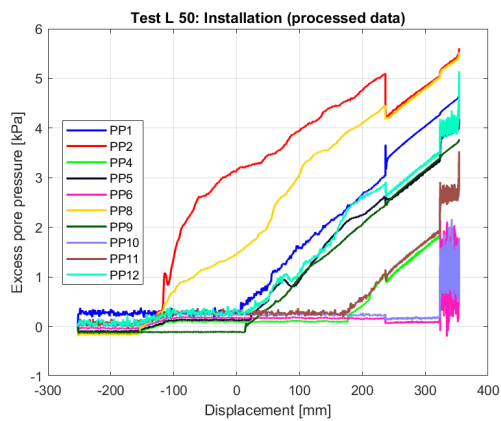


Figure C.216: Excess PP vs displacement for installation in Test L50.

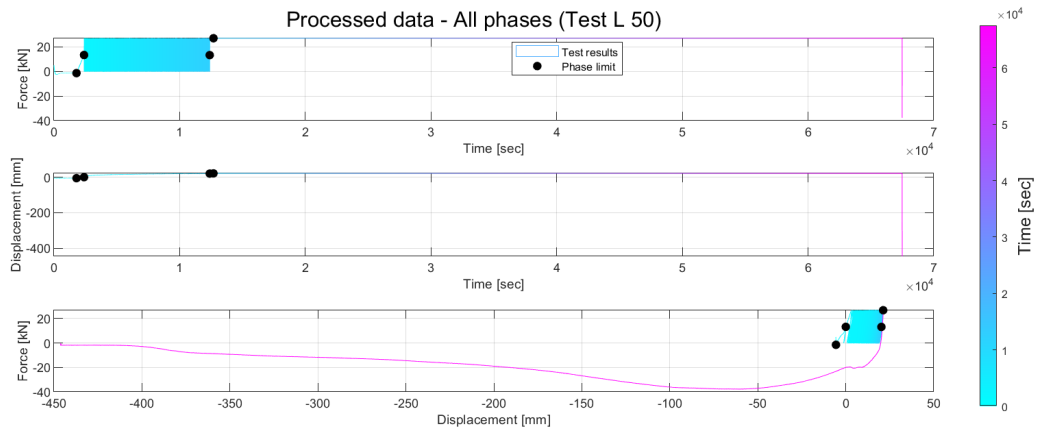


Figure C.217: Force-Time, Disp-Time, Force-Disp in Test L50.

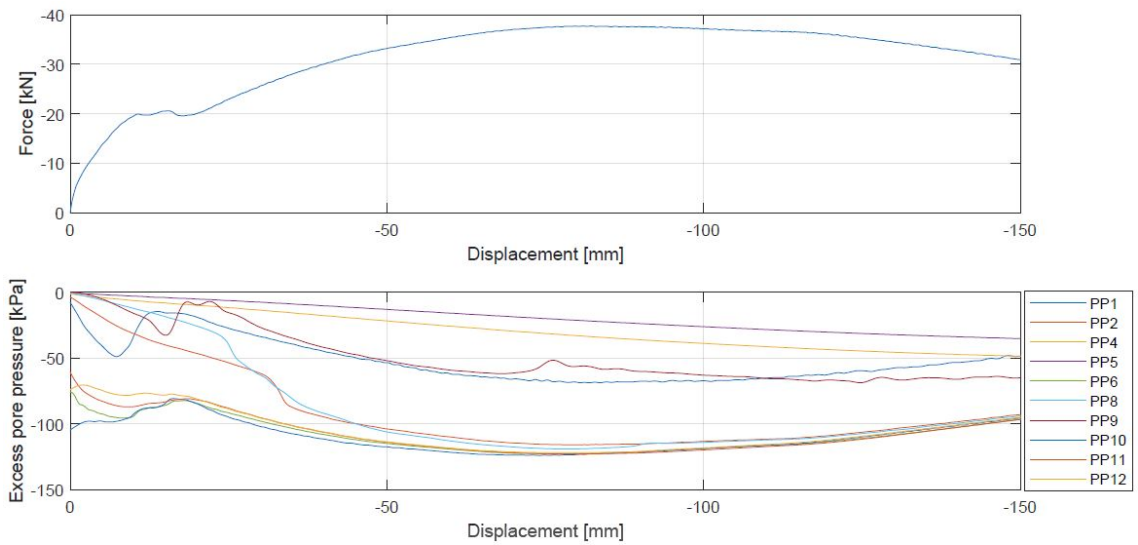


Figure C.218: Force vs displacement and excess PP vs displacement in Test L50.

C.3 Results in Low Density Sand

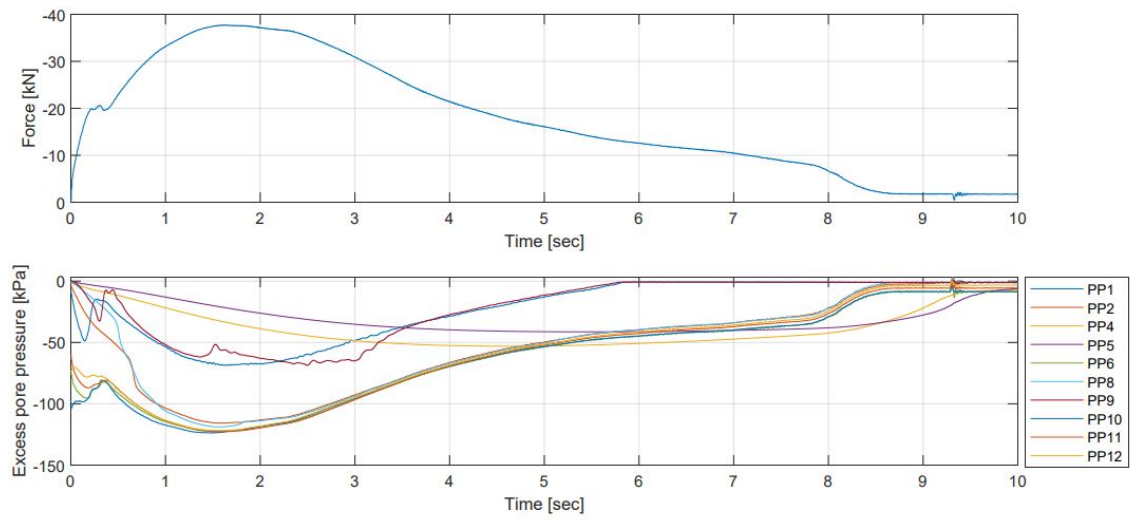


Figure C.219: Force vs time and excess PP vs time in Test L50.

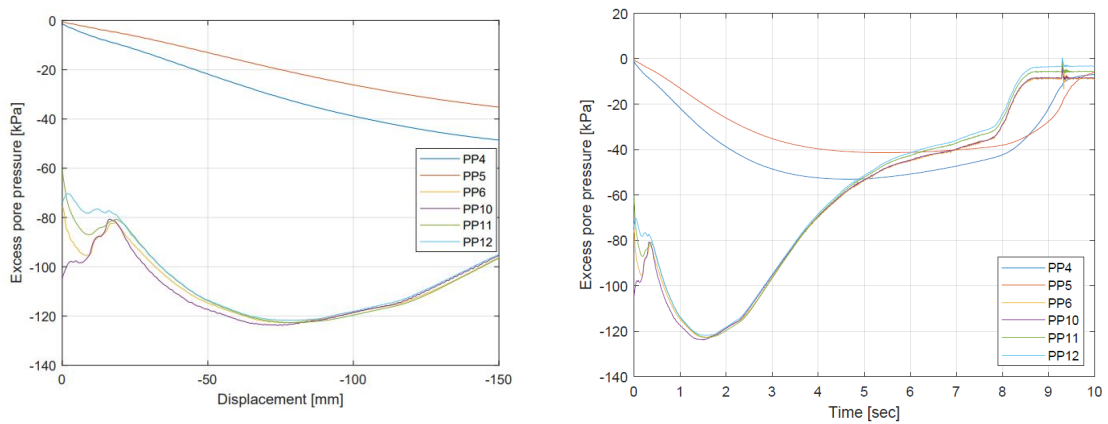


Figure C.220: Internal excess PP vs displacement in Test L50.

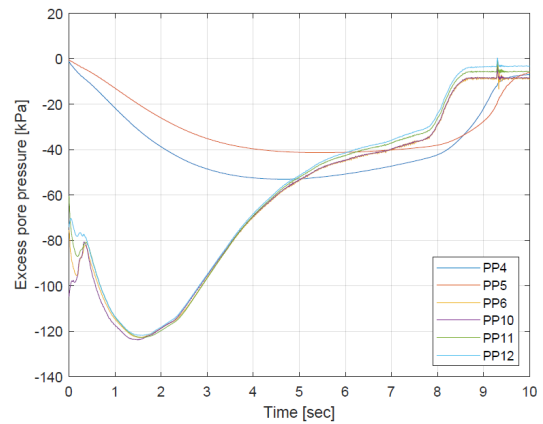


Figure C.221: Internal excess PP vs time in Test L50.

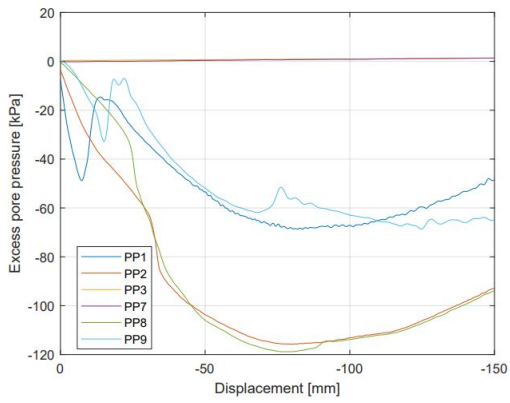


Figure C.222: External excess PP vs displacement in Test L50.

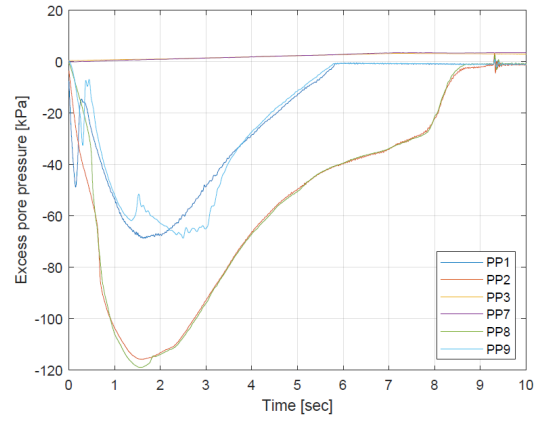


Figure C.223: External excess PP vs time in Test L50.

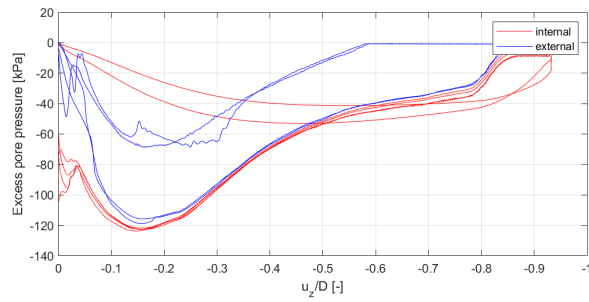


Figure C.224: Internal and external excess PP during L50

C.3.4 Test L150

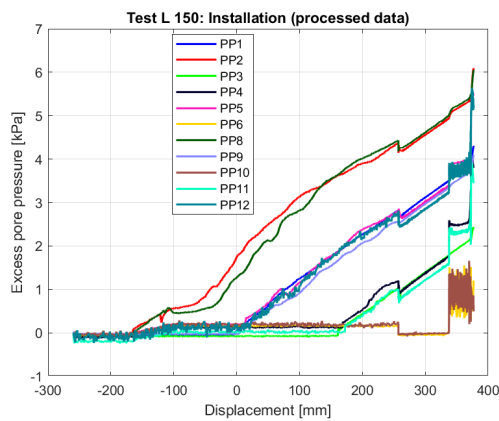


Figure C.225: Excess PP vs displacement for installation in Test L150.

C.3 Results in Low Density Sand

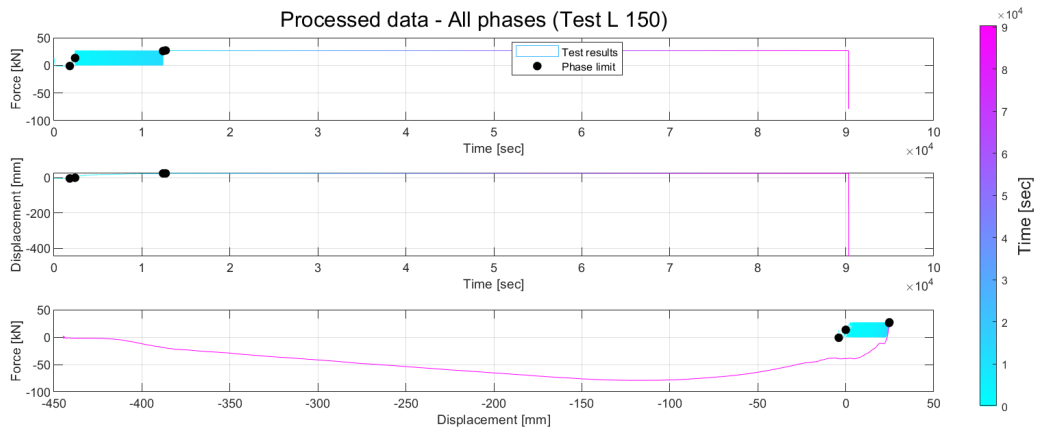


Figure C.226: Force-Time, Disp-Time, Force-Disp in Test L150.

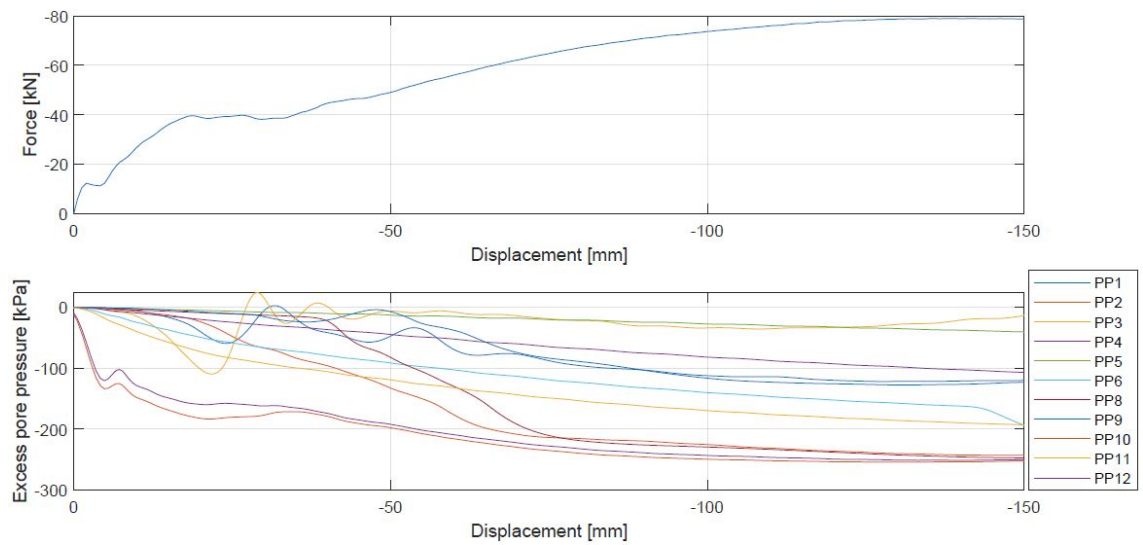


Figure C.227: Force vs displacement and excess PP vs displacement in Test L150.

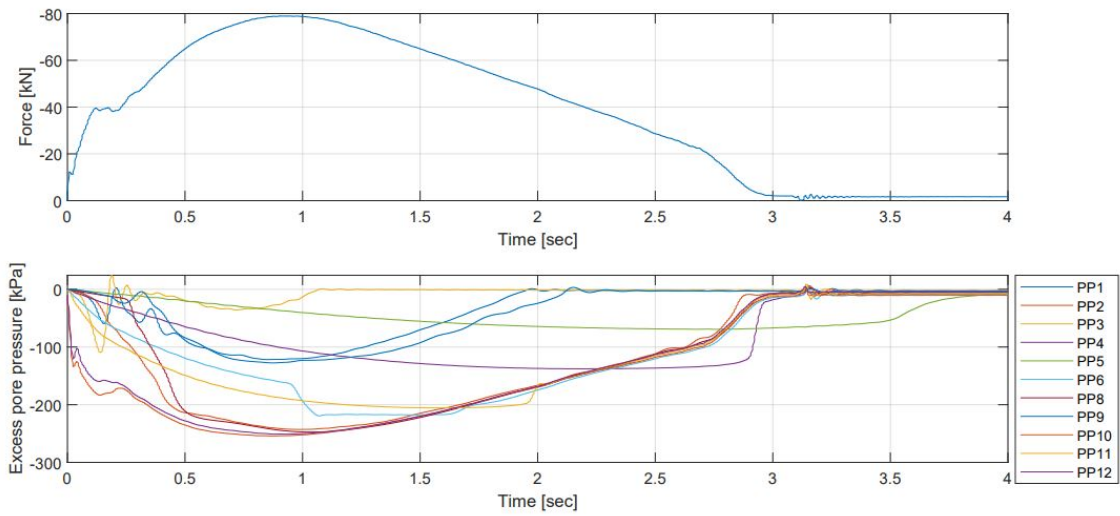


Figure C.228: Force vs time and excess PP vs time in Test L150.

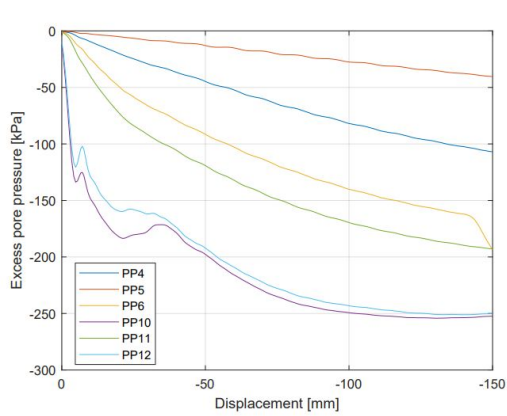


Figure C.229: Internal excess PP vs displacement in Test L150.

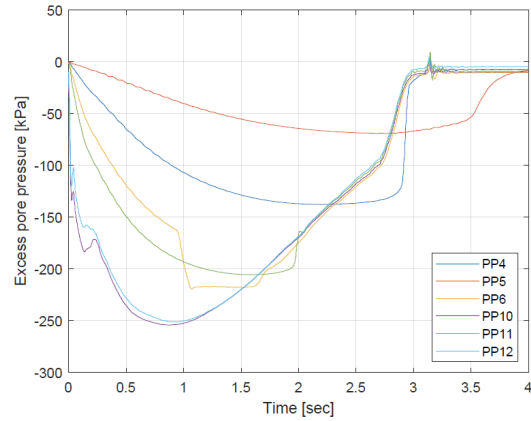


Figure C.230: Internal excess PP vs time in Test L150.

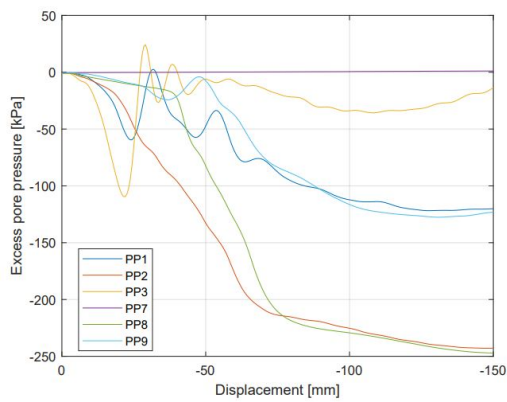


Figure C.231: External excess PP vs displacement in Test L150.

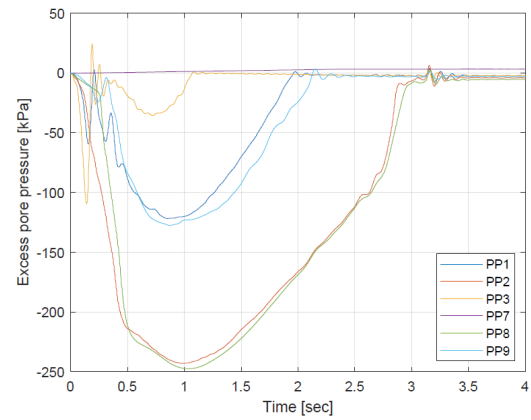


Figure C.232: External excess PP vs time in Test L150.

C.3 Results in Low Density Sand

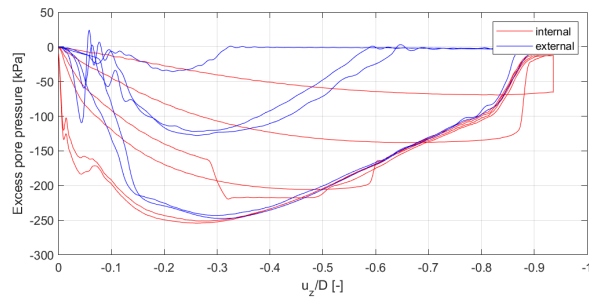


Figure C.233: Internal and external excess PP during L150

C.3.5 Test L500

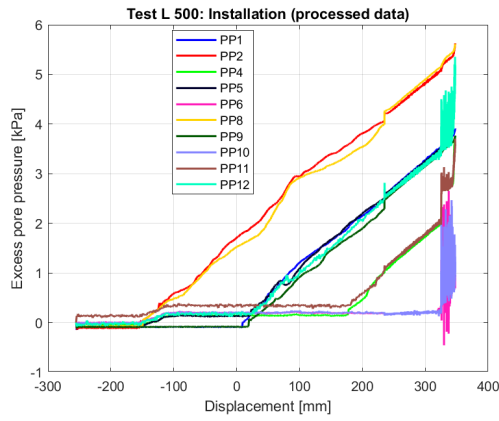


Figure C.234: Excess PP vs displacement for installation in Test L500.

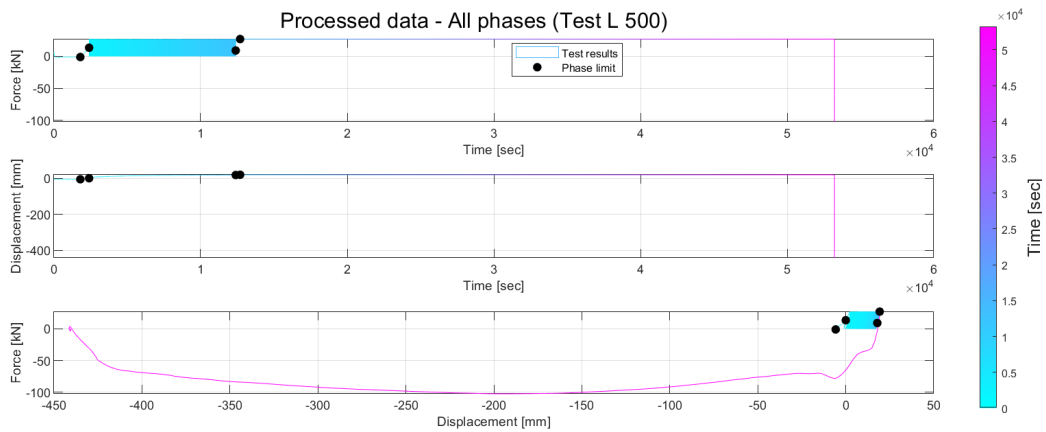


Figure C.235: Force-Time, Disp-Time, Force-Disp in Test L500.

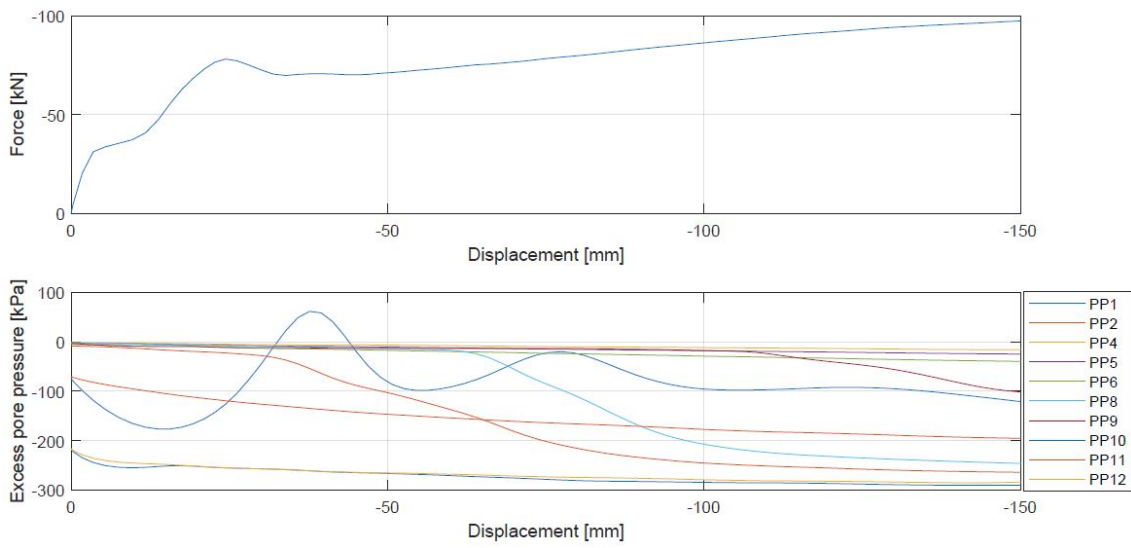


Figure C.236: Force vs displacement and excess PP vs displacement in Test L500.

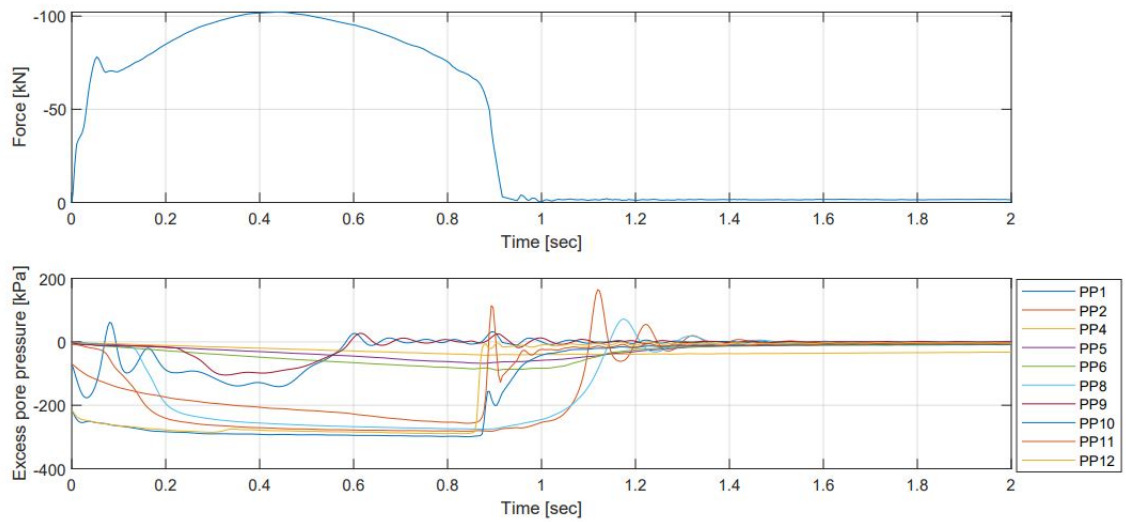


Figure C.237: Force vs time and excess PP vs time in Test L500.

C.3 Results in Low Density Sand

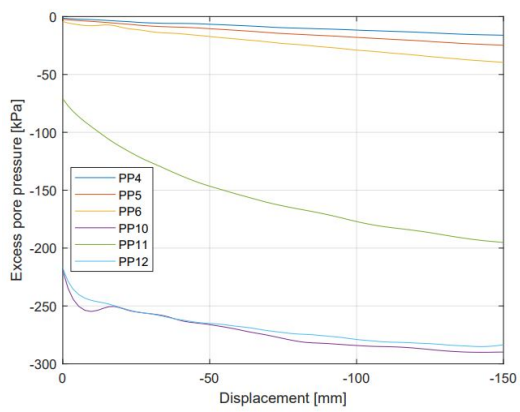


Figure C.238: Internal excess PP vs displacement in Test L500.

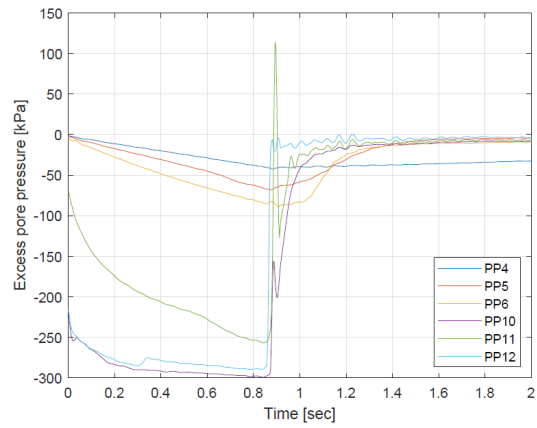


Figure C.239: Internal excess PP vs time in Test L500.

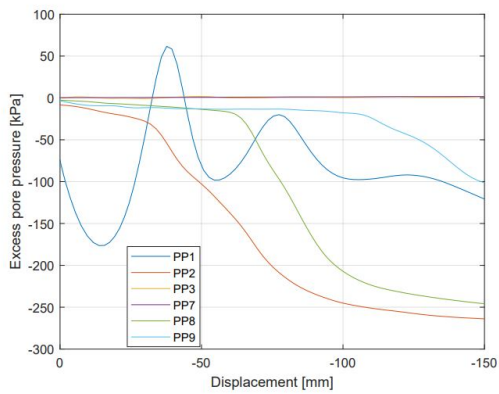


Figure C.240: External excess PP vs displacement in Test L500.

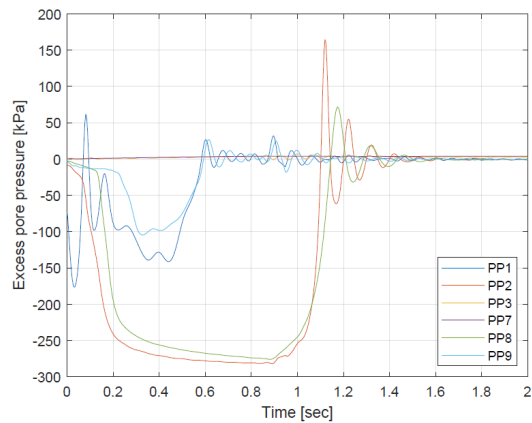


Figure C.241: External excess PP vs time in Test L500.

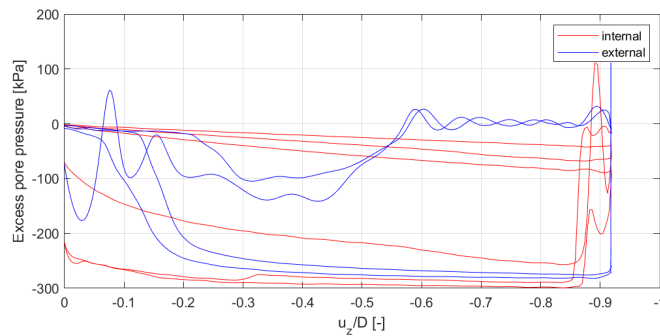


Figure C.242: Internal and external excess PP during L500

Test L 500 | Left half

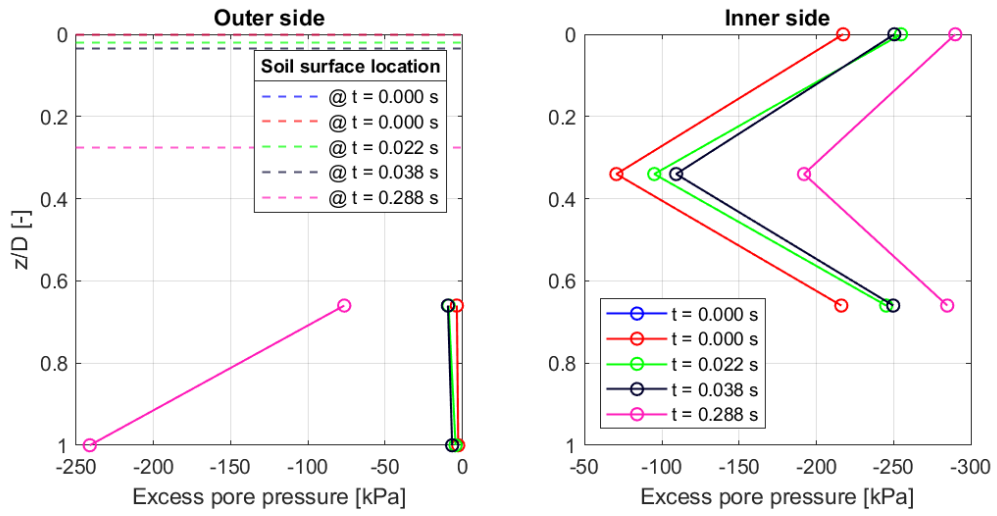


Figure C.243: Isochrones Test L500 at left side of the bucket.

Test L 500 | Right half

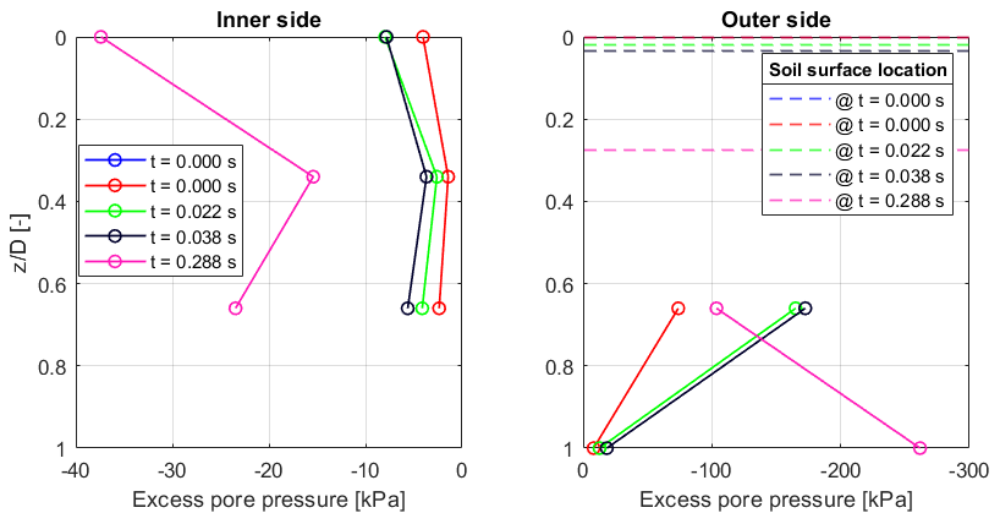


Figure C.244: Isochrones Test L500 at right side of the bucket.

